Investigating astrocyte-synapse interactions in amyotrophic lateral sclerosis

Calum Bonthron

A thesis submitted for the degree of PhD
at the
University of St Andrews

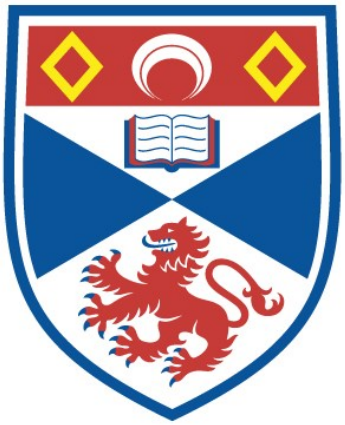

2022

"I'm not expecting to grow flowers in the desert,
but I can live and breathe and see the sun in wintertime."

Stuart Adamson, 1983

Candidate's declaration

I, Calum Bonthron, do hereby certify that this thesis, submitted for the degree of PhD, which is approximately 44,000 words in length, has been written by me, and that it is the record of work carried out by me, or principally by myself in collaboration with others as acknowledged, and that it has not been submitted in any previous application for any degree. I confirm that any appendices included in my thesis contain only material permitted by the 'Assessment of Postgraduate Research Students' policy.

I was admitted as a research student at the University of St Andrews in September 2018.

I received funding from an organisation or institution and have acknowledged the funder(s) in the full text of my thesis.

Date: 13/10/2022 Signature of candidate

Supervisor's declaration

I hereby certify that the candidate has fulfilled the conditions of the Resolution and Regulations appropriate for the degree of PhD in the University of St Andrews and that the candidate is qualified to submit this thesis in application for that degree. I confirm that any appendices included in the thesis contain only material permitted by the 'Assessment of Postgraduate Research Students' policy.

Date: 13/10/2022 Signature of supervisor

Permission for publication

In submitting this thesis to the University of St Andrews we understand that we are giving permission for it to be made available for use in accordance with the regulations of the University Library for the time being in force, subject to any copyright vested in the work not being affected thereby. We also understand, unless exempt by an award of an embargo as requested below, that the title and the abstract will be published, and that a copy of the work may be made and supplied to any bona fide library or research worker, that this thesis will be electronically accessible for personal or research use and that the library has the right to migrate this thesis into new electronic forms as required to ensure continued access to the thesis.

I, Calum Bonthron, have obtained, or am in the process of obtaining, third-party copyright permissions that are required or have requested the appropriate embargo below.

The following is an agreed request by candidate and supervisor regarding the publication of this thesis:

Printed copy

Embargo on all of print copy for a period of 2 years on the following ground(s):

- Publication would preclude future publication

Supporting statement for printed embargo request

Multiple chapters remain to be published.

Electronic copy

Embargo on all of electronic copy for a period of 2 years on the following ground(s):

- Publication would preclude future publication

Supporting statement for electronic embargo request

Multiple chapters remain to be published

Title and Abstract

- I agree to the title and abstract being published.

Date: 13/10/2022 Signature of candidate

Date: 13/10/2022 Signature of supervisor

Underpinning Research Data or Digital Outputs

Candidate's declaration

I, Calum Bonthron, hereby certify that no requirements to deposit original research data or digital outputs apply to this thesis and that, where appropriate, secondary data used have been referenced in the full text of my thesis.

Date: 13/10/2022 Signature of candidate

Abstract

Amyotrophic Lateral Sclerosis (ALS) is fatal neurodegenerative condition characterised by the loss of upper and lower motor neurons (MNs). Given that synapses and astrocytes regularly interact in the healthy spinal cord, and that pathology involving both has been reported in ALS, we posited that synaptic and astrocytic mechanisms may be intrinsically linked. One essential astrocytic function is synaptogenesis. Hyperexcitability of pre-MN networks has been observed in ALS, with a possible basis of this change being perturbed astrocytic synaptogenesis causing an early non-cell autonomous shift in excitatory : inhibitory (E:I) synaptic ratios. To look at this, we developed and validated a novel postnatal primary co-culture system of spinal astrocytes and neurons. These cultures were generated using multiple ALS mouse models bred with animals expressing a GFP tag on the postsynaptic density protein PSD95, with immunocytochemical targeting of presynaptic protein synapsin, and inhibitory postsynaptic protein gephyrin. We found that no combination of neuron or astrocyte genotypes altered E:I ratios in both $SOD1^{G93A}$ and C9BAC500 co-cultures. This lack of E:I ratio change was also seen in $SOD1^{G93A}$ spinal cords after the peak of postnatal spinal synaptogenesis, and in human ALS patient iPSC-derived MN / astrocyte cultures. Post-synapse formation, however, astrocytes also interact with mature synapses at structures called tripartite synapses. As dysfunction at tripartite synapses has previously been reported, we investigated these structures throughout disease progression in $SOD1^{G93A}$ PSD95-eGFP animals. Using multiple markers for perisynaptic astrocytic processes, the motile elements that envelop synapses, we observed consistent loss of tripartite synapses at the early symptomatic stage of 16W. Non-tripartite synapses, however, remained similar in number to controls. This was replicated in human ALS post-mortem tissue. We therefore conclude that although we find no evidence that astrocytes are driving early E:I ratio shifts,

we reveal that later in pathogenesis tripartite synapses appear to be a vulnerable fulcrum of disease in ALS.

Acknowledgements

Firstly, I would like to thank all those involved in the SPRINT MND/MS programme, the Euan MacDonald Centre, and the Chief Scientist Office for providing funding and support over the past 4 years. I am appreciative I was given the chance to complete this work.

Next, I would like to thank my supervisor Prof. Gareth Miles. I first met Gareth when I was a tiny undergrad, and am very grateful you took a chance on me when I first entered the lab at 21 to do my Laidlaw Scholarship project. Ever since, I have always felt you were there for support and guidance, especially during the many ups and downs of being a trainee. I am also appreciative that you always made time for me despite your manic Head of School duties, and I will always be grateful for your mentorship.

Thank you to Matt, who has been such a terrific role model since I started in the lab. You are genuinely fantastic to be around, and your mix of cheer and scary knowledge of all things synapses has helped me through some challenging times in the lab. You are one of the best and most enthusiastic teachers I have ever met, and I hope I can match that one day!

Thank you next to Sarah. As much as I am sure my sentimentality would garner some light teasing, the amount of times I have thought ‘thank god I work with Sarah’ during my PhD is concerning. I can say very honestly that you are the easiest person to work with, a patient teacher who very much should have left a stressed 2nd year PhD student to do his own thing, but I am grateful you stuck with me. Thank you for giving me such valuable training, I am sure the thing that will stick with me the most is that saying ‘lol’ when something goes horrendously wrong is the healthiest may to deal with lab disasters. I wish you the best, as you very much deserve it.

I would also like to thank Simon, whose knowledge of all things spinal cord continues to amaze (and slightly terrify) me. How else would I have learned that you can't patch a dead cell? I am grateful that I have gotten to learn from you and become your friend as you settled into the lab. I had a blast during our time together in Canada, and I hope this won't be the last of our stories together at conferences!

Thank you to Frankie. I was so proud when I saw you finally finish your PhD, and I could not have asked for a better friend during mine. You taught me to relax and changed how I view myself, very much for the better. You are a fantastic scientist, have offered seemingly endless support and guidance, and I couldn't have picked anyone better to enjoy the (not-so) occasional pint with.

Thank you also to the rest of the NCM lab, as well as the wonderful SMAU staff. I wanted to thank Trevor for the endless support and wonderful stories I would be told on a bad day, as well as the technicians Shaun, Sandy and Laura who were all so kind to me.

I would also like to thank my fantastic friends, who I am sure are sick of hearing about my PhD woes by now. Thank you to the wonderful Stephen, Andy and Ollie, who I adore and may be the funniest humans I have ever met. Thank you to Camillo, Ali, Mizuki, Connor, Rhia, William and my many other fabulous supportive friends. I also want to say thank you to my family; my mum, dad, sister and grandad who have helped so much along the way.

In the end, it might have even been 'so fine'…

Calum

Table of Contents

Chapter 1

Introduction

1. Amyotrophic Lateral Sclerosis – A Heterogeneous Disease

1.1. Definition

Amyotrophic lateral sclerosis (ALS) was first described as such in 1874 by prolific neurologist Jean-Martin Charcot, who noted degeneration in the anterior spinal cord resulting in muscle atrophy (hence 'amyotrophic'), in addition to scar-like lesions in the descending corticospinal axons of the lateral spinal cord (hence 'lateral sclerosis') (Kumar et al., 2011; Taylor et al., 2016). It is a progressive neurodegenerative condition, associated with the loss of multiple cell types. These include 'lower motor neurons' (LMN) (or 'true' motor neurons which project directly to muscles) in the brainstem and spinal cord, and 'upper motor neurons' (UMN) in the brain (which coordinate lower motor neuron activity to create the muscle contractions) (Hardiman et al., 2017; Purves et al., 2011). This leads to loss of muscle innervation, muscle atrophy, and death 3-5 years later, usually due to loss of diaphragm function (Brown and Al Chalabi, 2017). While this is a classical description of an ALS phenotype, in reality the disease displays a remarkable degree of heterogeneity. Such variability includes initial symptom presentation, time of onset and which genetic mutations (if any) contribute. This heterogeneiety has led to changes in the diagnosis of ALS patients over time.

1.2.Clinical Presentation

Due to a lack of available biomarkers, clinical diagnosis of ALS is reliant on detection of both LMN and UMN degeneration. The degree to which this degeneration is biased towards one or the other is not consistent between patients, however (Geevasinga et al., 2016). Thus, this is how we arrive at the classical, generalised definition of ALS mentioned previously.

But in reality, the experience of patients varies greatly, and as will become apparent in many aspects of the disease, this heterogeneous presentation creates difficulties for those trying to understand its mechanisms. The first point of variability is the area of ALS onset. The majority of ALS cases (approximately 70%) are described as 'spinal onset', whereby patients experience unilateral symptoms of muscle weakness which may occur proximally in the upper and lower limbs, or in the distal muscles (Shellikeri et al., 2017; Wijeskera and Leigh, 2009). This is accompanied by fasciculations (involuntary muscle twitching), hyperreflexia (overresponsive reflexes) and sometimes hypertonia (overly rigid / stiff muscles) (Swinnen and Robberecht, 2014). On the other hand, 20-30% of patients have 'bulbar onset' ALS, characterised by dysarthria (slow / slurred speech), dysphagia (difficulty in swallowing) and tongue fasciculations (Swinnen and Robberecht, 2014; Yunusova et al., 2019). There even exists an extremely rare subtype of respiratory onset ALS with severe breathing difficulties (Chio et al., 2011). Age of onset too is extremely variable. While most patients are diagnosed in their 50s or 60s, ALS can present early in life, with 'juvenile ALS' representing a diagnosis before the age of 25 (Sabatelli et al., 2008).

In addition to motor symptoms, there is a significant proportion of patients who also experience cognitive decline to some degree. Approximately 15% of ALS patients meet the clinical threshold for Frontotemporal Dementia (FTD), which requires deterioration of recognised behavioural characteristics as well as neuroimaging demonstrating cortical atrophy (Bott et al., 2016; Henstridge et al., 2018). FTD itself is a group of disorders broadly divided into two forms: Behavioural FTD and Language FTD. The first is associated with disinhibition, delusions, increased apathy and loss of empathy, while the latter is characterised by progressive aphasia (Young et al., 2018). With the acknowledgement that a large proportion of patients display elements of both FTD and ALS, in addition to the

discovery that *C9orf72* mutations can be a feature of both, it is now widely agreed that FTD and ALS exist on a clinical spectrum. This posits that most patients' symptoms exist between the extremes of purely cognitive and purely motor dysfunction (Balendra and Isaacs, 2019; Ferrari et al., 2011; Lillo and Hodges, 2009). This is further supported by pathological overlap between the conditions, including TDP-43 mislocalisation and taupathy (Behrouzi et al., 2016; Mackenzie and Rademakers, 2010).

1.3. Epidemiology

Studying the presentation of ALS across the world is informative in several ways. Detailed geographic information regarding incidence (i.e. the number of *new cases diagnosed*) and prevalence (i.e. the number of people *living* with a condition) aid in identifying how characteristics of these areas (e.g. race, diet, localised environmental factors) may contribute to likelihood of disease development. Current epidemiological data does suggest that there is variability in ALS incidence across the globe. Incidence is estimated to range approximately from 2-3 per 100,000 people in Europe, with Scotland reported to have a figure at the high end of this range (Couratier et al., 2015; Longinetti and Fang, 2019). However, some areas show significantly lower (e.g. region previously known as Yugoslavia) or higher (Faroe Islands) incidence rates (Alčaz et al., 1996; Joensen, 2011). Prevalence, however, is approximately 7-9 per 100,000 people, reflecting the mean 30-month life expectancy following 1st symptom onset (Hardiman et al., 2017). Outside of Europe, prospective population-based studies in South America have been limited to Uruguay, which was shown to have ALS incidence similar to a French population (believed to be due to Uruguay containing many peoples of European-origin) (Couratier et al., 2015). Studies in Asia are also distinctly limited. Some studies in the Korean peninsula and China report much lower

incidence (approximately 1 per 100,000 people) (Longinetti and Fang, 2019). This has led to the suggestion that there is a significant difference in ALS likelihood between Asian and non-Asian populations. To further this, it has been posited that ancestral origin is intrinsically linked to ALS risk. For example, native American and Alaskan peoples show a low incidence of 0.63 / 100,000, whereas countries with somewhat homogenous European ancestry (e.g. Scotland) are much higher (Gordon et al., 2013; Hardiman et al., 2017). Variability of incidence across the globe cannot be attributed solely to ancestry, however, with abnormally high figures approaching 100 times other areas of the world in the small populations of Guam (Koerner, 1952) and the Kii Peninsula of Japan (Ishiura et al., 2012). This reduced by the 1980s, with previously high incidence in Guam believed to be due (at least in-part) to defects in mineral metabolism brought about by the unique composition of the water and soil (Garruto et al., 1985). This demonstrates that epidemiological work can also help identify localised environmental factors than may contribute to ALS incidence. Together, it does appear to be the case that there is some degree of variability in ALS incidence between geographical regions. However, limitations in population-based studies, mainly variability in the success of incomplete capture estimations (Hook and Regal, 1995; Yeo et al., 2010), and a lack of evidence outside of Europe limit concrete conclusions being drawn.

1.4. Neuropathological Features

Obvious neural correlates of motor dysfunction are seen at the cellular level. A decrease in the size of the anterior (ventral) horn of the spinal cord, presumably caused by the loss of large alpha motor neurons, as well as a wider-scale reduction of other ventral interneurons is evident. In particular, alpha MNs innervating fast-twitch muscle fibres are most vulnerable to degeneration, whilst MNs in the oculomotor, abducens and Onuf's nuceli are generally

spared (Ragagnin et al., 2019). Brainstem cell loss in the lower cranial motor nuclei and loss of Betz cells in layer V of the primary motor cortex can be seen too, in addition to loss of myelinated axons in the lateral/anterior columns of the spinal cord (Saberi et al., 2015). In addition, it is common to see the presence of reactive astrocytes surrounding degenerating neurons of the ventral horn (easily identifiable by dramatic upregulation of glial fibrillary acid protein (GFAP)) (Trias et al., 2018). Reactive microglia are also a characteristic feature, with particularly prevalent microglial activation being seen in severe UMN-damaged patients (Lasiene and Yamanaka, 2011).

At the sub-cellular level, the presence of abnormal proteinopathies and RNA aggregation are present in patients, however, there does exist a degree of heterogeneity here also. Ubiquitin +ve cytoplasmic aggregates in the ventral horn cells of both sporadic (sALS) and familial (fALS) patients were an early identified pathogenic feature. Such inclusions were later found in other areas such as the frontal and temporal cortices, and in other cells types including glial cells (Saberi et al., 2015). The main component of these aggregates was found to be TDP-43, a nuclear TAR DNA-binding protein involved in splicing regulation and transcriptional control (Arai et al., 2006). These aggregates are present in 95-97% of ALS cases, and their formation appears to follow mislocalisation of TDP-43 from the nucleus to the cytoplasm (Hardiman et al., 2017; Suk and Rousseaux, 2020; Wijesekera and Leigh, 2009). There are, however, other aggregates that have been described that are less universal and appear in a subset of ALS cases, including those harbouring superoxide dismutase 1 (SOD1) mutations (Ince et al., 1998). SOD1 patients have been shown to exhibit aggregates of misfolded mutant cytoplasmic SOD1, however, recent work showed that sporadic ALS post-mortem tissue also showed diffuse staining of misfolded wtSOD1 protein (Paré et al., 2018). ALS patients with pathogenic hexanucleotide repeat expansions (HRE) of the *C9orf72* gene have structures

called ‘RNA foci’, whereby the abnormally long HRE mutant RNA strands aggregate in the nucleus, and in doing so sequester important RNA-binding proteins. Both the sense and anti-sense strands form distinct foci, interestingly generally in separate cells (Kumar et al., 2017). Figure 1 summarises the major neuropathological features of the ALS spinal cord.

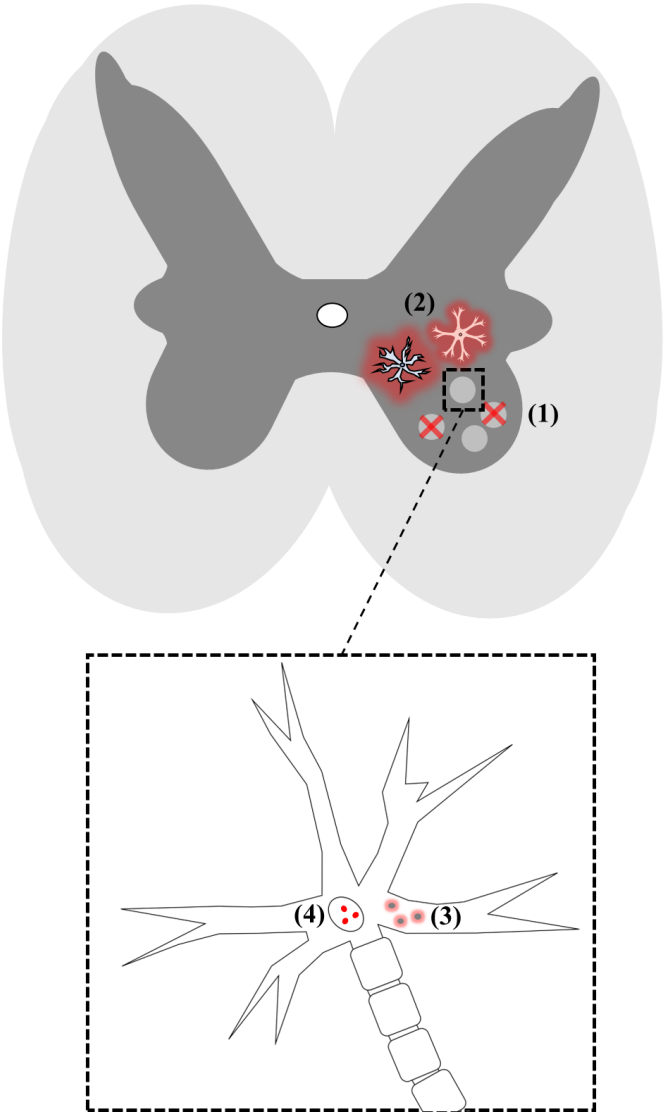

Figure 1: Schematic demonstrating key neuropathological features of ALS. These include: (1) ventral MN and interneuron degeneration, (2) reactive astrocytes and microglia, (3) cytoplasmic protein aggregation (may be TDP-43 or SOD1) and (4) C9orf72 RNA foci.

1.5.1. Genetics

When the heterogeneity of ALS is discussed, often the genetic contribution is at the forefront of conversation. The genetic contribution to ALS is complex and highly variable between patients. One of the first things to note is the distinction between 'familial' and 'sporadic' ALS, with fALS cases representing approximately 10% of the total cases, and sporadic cases sALS representing the vast majority (Alsultan et al., 2016). This presents an initial gulf between patient types, however, it should be noted that the percentage of familial cases could be underestimated to a greater or lesser degree. Multiple factors could lead to a gross underestimation of fALS cases, including no strict definition for what qualifies as 'family history' in fALS, as well as the known incomplete penetrance of many key mutations including SOD1 and *C9orf72* which may result in 'skipping' of a generation (Anderson et al., 2004; Mathis et al., 2019; Murphy et al., 2017; Turner et al., 2017). Likely partially as a result of this, sALS patients do not necessarily lack mutations, with approximately 10% of cases known to have a genetic basis (Renton et al., 2013). Twin studies have approximated sALS heritability at 60%, so it is accepted that many genetic risk factors are likely involved (Mejzini et al., 2019). This large difference between the presence of genetic mutations in sALS and estimated heritability may be due to a number of factors. Large-scale association studies such as GWAS (genome wide association studies) typically rely on high throughput short read sequencing which is ideal for identification of single-nucleotide polymorphisms (SNPs), however, not for other structural variations (e.g. deletions, insertions) which may be contributing to ALS risk. Such structural variations include long repeats, the pathogenic hexonucleotide GGGGCC C9orf72 repeat being a known example in ALS. In addition, it is possible that ALS is oligogenic (i.e. a trait influenced by multiple genes), which can be

challenging to detect when secondary mutations are rare or fail to be picked up due the previously mentioned limitations of short read sequencing (Mejzini et al., 2019).

Over 25 ALS-linked genes are currently known (Nguyen et al., 2018), with some of the most common mutations highlighted below in Table 1.

Gene (Encoded Protein)	**Basic Function**	**No. Known Mutants**	**Proportion of Patients**	
			fALS	**sALS**
C9orf72 (C9orf72)	Unclear (Implicated in endosome trafficking, RNA metabolism and autophagy)	Variable no. hexanucleotide repeats (GGGGCC)	40-50%	10%
SOD1 (superoxide dismutase 1)	Antioxidant (reduction of superoxide to $H_2O_2 + O_2$)	>185	20%	2%
TARDBP (TAR DNA-binding protein 43)	RNA-binding protein	>40	5%	<1%
FUS (FUS/TLS)	RNA-binding protein	>40	5%	<1%
OPTIN (Optineurin**)**	Autophagy	1	4%	<1%
VCP (Valosin-containing protein)	Proteasome function and autophagosome maturation	5	1-2%	<1%

Table1: Summary of some of the most prevalent ALS-linked mutations. (Balendra and Isaacs, 2019; Hardiman et al., 2017; Taylor et al., 2016; Umoh et al., 2016)

Two of the most common are SOD1 and C9orf72 mutations. SOD1 is present in healthy cells as a stable homodimer in the cytosol and mitochondrial intermembrane space, where it catalyses the conversion of the reactive oxygen species (ROS) superoxide to oxygen and hydrogen peroxide (Mathis et al., 2019). Although this suggests an obvious potential disease

mechanism, there appears to be little correlation between disease severity and enzyme activity, so instead, a toxic gain-of-function mechanism is believed to be involved. Mutations are believed to cause conformational / functional changes that may induce toxicity by various mechanisms including ER stress and mitochondrial dysfunction (Mejzini et al., 2019). In addition, insoluble SOD1 aggregates have been proposed as a mechanism of cellular stress common to both sporadic and familial ALS (Paré et al., 2018). C9orf72's healthy physiological function is still unknown , however, it is believed to aid in regulation of RNA metabolism and endosomal trafficking (Balendra and Isaacs, 2019). Abnormalities in C9orf72 is the most common genetic basis of both sALS and fALS. The presence of the hexanucleotide GGGGCC expansion may contribute to disease development in a number of ways, and it is yet to be concluded which of these suggested mechanisms contribute to disease severity, and by what degree. These include; (1) decrease in C9orf72 expression (haploinsufficiency), (2) formation of aggregated sense (G_4C_2) and antisense (G_2C_4) nuclear RNA foci and (3) formation of repeat dipeptides via repeat-associated non-ATG (RAN) translation (Gendron and Petrucelli, 2018) (see Fig. 2). In addition, changes in epigenetic regulation of gene expression have been implicated in ALS, including altered DNA methylation patterns (Bennett et al., 2019). The various ways in which these mutations may contribute to suggested disease mechanisms is discussed further in Section 2.

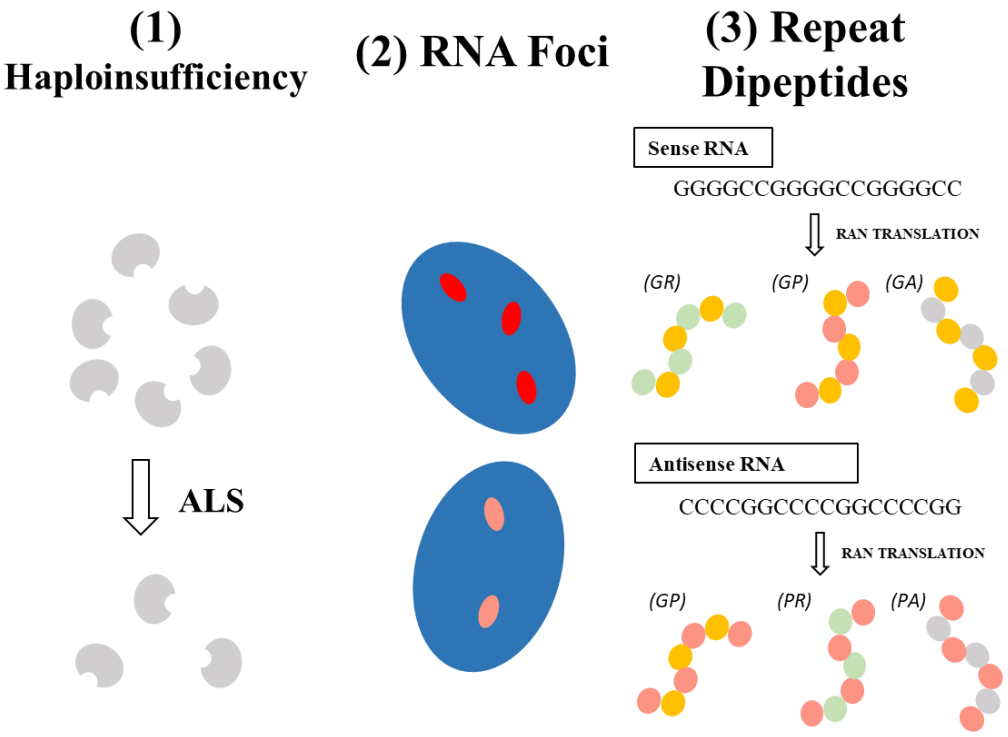

Figure 2: Schematic showing mechanisms of C9orf72 toxicity. These include: (1) haploinsufficiency of the C9orf72 protein, (2) formation of sense and antisense RNA foci and (3) formation of a number of RAN-translated repeat dipeptides. (3) also demonstrates the variety of poly (XX) proteins that can be produced from sense and antisense C9orf72 hexanucleotide repeat expansions. Repeat dipeptide schematic adapted from (Braems et al., 2020).

1.5.2. Mouse Models of ALS

More recent ALS work uses a variety of models to investigate disease mechanisms. These include the use of induced pluoripotent stem cell (iPSC)-derived MNs, which allow for the conversion of patient fibroblasts to physiologically active MNs, enabling human cells to be studied *in vitro* (Lee and Huang, 2017). Modelling fALS using mutant human genes expressed in mice is still a common way of studying ALS, however. This is due to the benefits of studying ALS in a complete spinal system during disease development, in addition to some models' ability to robustly recapitulate pathological hallmarks and motor phenotypes. Due to mutations in SOD1 being the first to be associated with ALS (Rosen et

al., 1993), development of animal models based upon this led to over 10 variations of SOD1 mutant models, including one which has been used as the standard model for ALS rodent research since. Gurney and colleagues (1994) developed and described the $SOD1^{G93A}$ mouse, with a human version of the SOD1 gene containing a guanine-to-alanine substitution at residue 93. This is randomly inserted into mouse chromosome 12 in an array of approximately 25 copies (this may vary, and copy number can be unstable between generations) (Acevedo-Arozena et al., 2011). These mice develop hind limb weakness around 85-100 days, which develops into full hind-limb paralysis, with an attenuated mean life span of approximately 120-160 days (Acevedo-Arozena et al., 2011; Bame et al., 2012; Kim et al., 2016). It should be noted, however, even when copy number is consistent, there is considerable variation in disease onset and survival rate between different background strains of mice, which further interacts with animal gender (males show shorter lifespan and earlier onset) (Heiman-Patterson et al., 2011; Pfohl et al., 2015). These animals show dramatic lumbar ventral horn neuron loss, early-onset astrogliosis and microgliosis, axonal transport deficits, mitochondrial dysfunction and end-stage TDP-43 mislocalisation (Kim et al., 2016; Philips and Rothstein, 2016; Shan et al., 2009). Due to the robustness of their phenotype, this model has been consistently used and has led to many key findings in the ALS field over the last 20+ years. More recently it has received criticism, a point of concern in particular is the gross overexpression of human protein (Acevedo-Arozena et al., 2011), with some suggesting that the observed phenotype is more the result of high protein load, and therefore is less informative regarding human disease progression.

Utilising other known ALS genes has been more of a challenge, with few other models being used to the same degree as $SOD1^{G93A}$ either due to their inability to recapitulate sufficient ALS phenotypes, or the inability to produce a model using a mutation that is present in

significant numbers of ALS patients. In 2016, characterisation of a new mouse model harbouring the human C9orf72 hexanucleotide repeat was published by Liu and colleagues (2016). The most effective model trialled was the C9BAC500 mouse which expressed one transgene copy with 500 G_4C_2 repeats. This mouse showed particular disease severity in female mice, with approximately 30-35% of females developing an 'acute' motor phenotype of limb weakness, paralysis and decreased survival between 20 and 40 weeks. Additionally, a large proportion of animals showed a more progressive phenotype, with 46% of females being symptomatic at 1 year of age. Acute end-stage animals showed reduced numbers of choline acetyltransferase (ChAT) +ve motor neurons, as well as NeuN +ve interneurons in the lateral and posterior horns. From 2 months of age, sense and anti-sense RNA foci were present throughout the CNS, including layer V of the frontal cortex and in the lumar spinal cord. Acute end-stage animals were positive for RAN dipeptide aggregation, as well as TDP-43 cytoplasmic inclusions. Whilst relatively new, it has attracted significant attention as an alternative to $SOD1^{G93A}$ that may represent a larger proportion of ALS cases. However, the phenotypic penetrance of this model appears to be variable, with some groups showing little-to-no emergence of ALS symptoms in their cohorts (Mordes et al., 2020; Nguyen et al., 2020).

2. Proposed Disease Mechanisms – Needle in a Haystack?

2.1. Review of Major Suggested Pathological Mechanisms

When causative mechanisms are discussed in ALS, it is easy to draw parallels with the difficulties of other neurodegenerative fields such as Alzheimer's Disease. A large number of cellular systems have been shown to fail to some degree (most of which have been elucidated

with the use of the SOD1^{G93A} model). It may initially be puzzling why so many systems could be involved in pathogenesis, with the range of causative genetic mutations alone encoding proteins belonging to a wide range of cellular machinery, despite the cell types dying being relatively conserved. It may be the case therefore, that heterogenous initial triggers of disease (be that a specific point mutation or the result of a wider risk factor) cause a primary effect, which may then cause resultant secondary effects and homeostatic adjustments in other cellular systems in a complex manner. Such wide-scale dysfunction spreading across cellular machinery then ultimately arrives at similar final disease pathways between patients. As a result, it is difficult to determine if the disease mechanisms discussed below are strictly causative, or simply accelerate the cell death contributed to by dysfunction in other systems. Consequently, we also cannot assume that all of these mechanisms necessarily appear in all cases of ALS (Hardiman et al., 2017; Morgan and Orrel, 2016; van Zundert et al., 2008). In addition, multiple risk factors may also interact to produce an initial trigger of disease rather than a single insult, causing downstream pathogenic cascades. With this in mind, numerous of the best studied disease mechanisms are presented here (see Fig. 3).

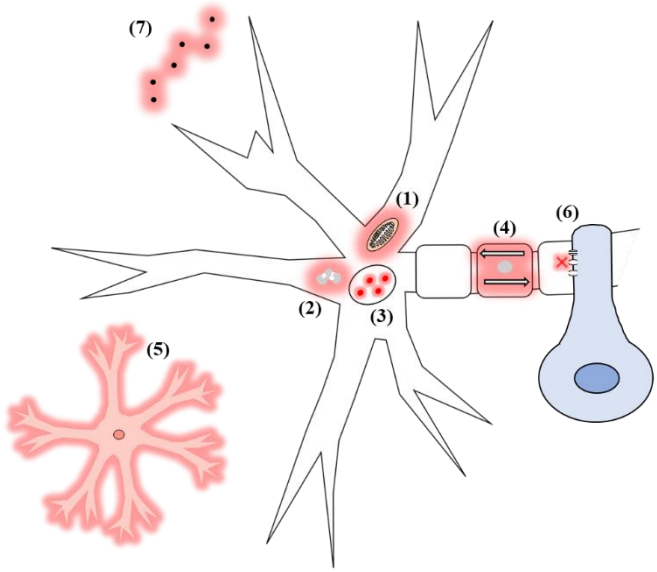

Figure 3: Schematic demonstrating proposed ALS mechanisms. These include: (1) mitochondrial dysfunction, (2) impaired protein homeostasis, (3) altered RNA metabolism, (4) defective axonal transport, (5) neuroinflammation, (6) oligodendrocyte dysfunction and (7) excitotoxicity.

2.2. Mitochondrial Dysfunction

Mitochondrial dysfunction and oxidative stress were of particular interest early in mechanistic literature, considering SOD1's role in reducing toxic ROS species. Several defects in mitochondria have been observed. Firstly, morphologically they are abnormal, appearing swollen, vacuolated and often aggregated (Hardiman et al., 2017; Smith et al., 2019). Such morphological disruption may contribute to ALS pathology as mutations in an intermembrane space mitochondrial protein (CHCHD10), which is an important regulator of mitochondrial structure, are causative in patients (Bannwarth et al., 2014; Morgan and Orrell, 2016). The activity of the electron transfer chain and resulting ATP production has also been shown to be perturbed. Mutant SOD1 entry into the mitochondria causes protein import impairments in the intermembrane space (Higgens et al., 2003) and has a major impact on electron transport chain (ETC) function, as has been demonstrated in post-mortem tissue samples (Wiedemann et al., 2002). Indeed, $SOD1^{G93A}$ animals have decreased mitochondrial respiration rates in both the brain and spinal cord, demonstrating reduced complex I and IV activity and impaired ATP synthesis (Smith et al., 2019). There is also further evidence that mitochondrial accumulation of other ALS-linked proteins causes respiratory deficits. TDP-43 mitochondrial accumulation was noted in sporadic ALS post-mortem tissue, and fibroblasts derived from patients harbouring various TDP-43 mutations showed increased mitochondrial localisation of TDP-43 versus controls (Wang et al., 2016). Indeed, it was found that this accumulation is associated with preferential binding to mitochondrial mRNA encoding complex I subunits of the ETC, inhibiting its translation and even causing complex 1 disassembly. Suppression of TDP-43 mitochondrial import abolished mitochondrial dysfunction and increased ATP production (Wang et al, 2016). Later work replicated the impact of TDP-43's effect on mitochondrial dysfunction, and showed increased production of

ROS and initiation of the mitochondrial unfolded protein response (Wang et al., 2019). To further demonstrate deficits in respiration, the C9orf72 dipeptide repeat protein poly(GR) has been shown to bind to mitochondrial ribosomal proteins and compromise mitochondrial function (Lopez-Gonzalez et al., 2016). Finally, increased ROS production appears to be present in patients, with evidence of increased oxidative damage in sALS spinal tissue and in $SOD1^{G93A}$ work (Barber and Shaw, 2010).

2.3. Impaired Protein Homeostasis

The cell has several systems at its disposal to correct misfolded proteins in the ER. When it is unable to correct these, it has further ways of disposing of them to prevent potentially pathogenic downstream effects of misfolding and aggregation (Díaz-Villaneuva et al., 2015). Chaperones within the ER ensure the correct folding of recently translated proteins, and refolding of those with exposed hydrophobic surfaces in order to prevent aggregation of misfolded proteins (Ali et al., 2010). In addition, the Unfolded Protein Response (UPR) is a tool utilised by the ER under stress (i.e. where the demand for protein folding capacity is overwhelmed, leading to the build up-of unfolded/misfolded proteins). This involves a number of processes, including upregulating the transcription of chaperones and downregulating overall mRNA translation in order to reset the proteostatic state of the ER lumen (Díaz-Villaneuva et al., 2015). When proteins are both unable to be folded properly and unable to be corrected, there exists 1) the ubiquitin proteasome system (UPS) and 2) autophagy, which act to degrade misfolded proteins. The UPS tags proteins with polyubiquitin chains which leads to their proteolysis, while autophagy involves the formation of autophagosomes, which surround the substrate and deliver them to lysosomes where they are degraded (Medinas et al., 2017).

SOD1 has been shown to perturb the proteostasis machinery at multiple stages with the use of the $SOD1^{G93A}$ mouse. Firstly, SOD1-associated inclusions are known to sequester essential chaperones such as HSP 40/70, in addition to Ub ligases which are essential in UPS function (Ruegsegger and Saxena, 2016). $SOD1^{G93A}$ animals also show reduced expression of UPS components, and mutant SOD1 can directly interact with the 19S regulatory subunits of the proteasome, inhibiting UPS activity (Webster et al., 2017). This may produce a cycle whereby limited mutant SOD1 aggregation causes significant reductions in protein degradation capacity, in turn exacerbating large-scale protein aggregation. This is of particular interest considering there is emerging data that wtSOD1 has the capacity to acquire abnormal conformation upon oxidative damage, and gains many properties of mutant SOD1 including an increased propensity to misfold (Bosco et al., 2010). Misfolded SOD1 can even cause similar axonal transport deficits to mutant SOD1, can exacerbate disease phenotypes of $SOD1^{G85R}$ animals, and has been demonstrated to show significant aggregation in sALS tissue (Bosco et al., 2010; Paré et al., 2018). It has therefore been suggested that SOD-related proteostasis perturbation may be a shared mechanism between fALS and sALS.

Multiple other ALS-linked mutations can be seen to impact integral components of the cell's proteostasis machinery. RAN translation of sense C9orf72 G_4C_2 RNA produces poly (GA) proteins, which form inclusions in patients harbouring the hexanucleotide repeat mutation. These inclusions have been shown to quickly form in neuronal culture models, and showed similar activity to the proteasome inhibitor MG-132, implying poly (GA) aggregation leads to cell death via reduced UPS activity and resulting ER stress (Zhang et al., 2014). Several other mutations are linked to proteasome dysfunction, including VCP/p97 (UPS substrate unfolding / substrate presentation) and ubiquilin-2 (UPS cargo delivery) (Barthelme et al.,

2015; Deng et al., 2011). Autophagy can be affected at all stages too, from autophagy initiation to substrate degradation. For example, C9orf72 interacts directly with the ULK-1 initiation complex, essential in autophagosome formation, suggesting that C9orf72-related haploinsufficiency may contribute to proteostasis dysregulation (Webster et al., 2016). VCP mutations, as well as affecting the UPS, also negatively affect autophagosome maturation (Ju et al., 2009). It is clear therefore that protein aggregation may occur due to several different insults to the proteostasis machinery.

2.4. Altered RNA Metabolism

In addition to alterations in protein processing and degradation, ALS mutations are also known to be associated with the presence of perturbed RNA species. In particular, RNA mechanisms of disease are associated with the C9orf72 repeat expansion, however, several key RNA-binding proteins are also known to be affected. Of the ways in which C9orf72 mutations are hypothesised to contribute to pathogenesis, 2 of the 3 main suggestions are linked to RNA perturbations (Gendron and Petrucelli, 2018).

The first is RNA derived from the GGGGCC non-coding region repeat expansion, which forms G-quadruplex structures (helical secondary structures formed by molecules rich in guanine) (Hardiman et al., 2017; Spiegel et al. 2020). This expansion is transcribed in both sense and antisense directions, producing accumulations in the nucleus called ‘RNA foci’ (Butti and Patten, 2019). These aggregations are believed to interfere with healthy RNA processing by interacting with and sequestering RNA-binding proteins, mislocating them and preventing their normal function. An example of this is a ribonuclear protein called nucleolin, which specifically binds to C9orf72 G-quadruplexes. *In vivo*, hexonucleotide repeat RNA

caused dispersion of the tight nucleolar WT expression, impairing the function of the nucleolus and resulting in decreased rRNA processing (Haeusler et al., 2014). Further mechanistic evidence for the importance of RNA foci is that there has been some success targeting RNA foci as a potential therapeutic treatment. Antisense oligonucleotides targeting the repeat expansion were used to successfully suppress sense RNA foci formation. This resulted in reduced sequestration of RNA-binding proteins and reversal of associated gene expression alterations in iPSC-derived neurons. (Donnelly et al., 2013). Antisense oligonucleotide-mediated reduction of C9orf72 RNA was shown to be well tolerated in adult mice, but there was a limited effect on associated RNA expression. It is acknowledged that such an approach would also have to target antisense RNA foci, however (Lagier-Tourenne et al., 2013). Haploinsufficiency is the second RNA mechanism by which C9orf72 mutations could contribute to ALS, whereby the presence of the hexanucleotide repeats causes a reduction in C9orf72 RNA transcription (Ling et al., 2013). There is also evidence that the mutation interferes with splicing of transcripts, as well as the suggestion that it may even disrupt promoter activity thus reducing C9orf72 expression (Gijselinck et al., 2016; Mori et al., 2013).

Production of toxic species is not the only way in which RNA may contribute to disease development. Mutant proteins which interact with RNA may also contribute. An often-cited example is the mislocalisation of TDP-43 from the nucleus to the cytoplasm. Its aggregation may cause a toxic gain of function, but its nuclear depletion may also be cytotoxic due to TDP-43's essential role in RNA processing. It controls the expression of other proteins via its roles in RNA splicing, stability-promotion and mRNA transport, with one RNA-seq study suggesting it is required for the regulation of over 200 mRNAs (Butti and Patten, 2019; Polymenidou et al., 2011). An example is the stabilisation of neurofilament light chain

mRNA via direct binding, the disruption of which leads to aggregation and MN death (Strong et al., 2007; Strong, 2010). Multiple key synaptic proteins, including structural protein Homer2 and several GABA receptor subunits are known to be regulated by the function of TDP-43. Multiple mutant models across several species have reflected such synaptic dysfunction (Butti and Patten, 2019). UNC13A, a critical synaptic protein, was recently shown to interact with TDP-43 mislocation whereby UNC13A SNPs potentiate the cryptic exon inclusion caused by loss of TDP-43 from the nucleus, resulting in loss of functional protein (Brown et al., 2022; Ma et al., 2022).

2.5. Defective Axonal Transport

Microtubules are vast polymers of tubulin, consisting of heterodimers of α- and β-tubulin. They are polarised, where the faster growing 'plus' end towards the axon tip is exposed, and such polarity determines the directional movement of associated 'molecular motors' (Millecamps and Julien, 2013). These molecular motors, of which kinesins mainly control anterograde transport (towards the cell body) and cytoplasmic dyneins mainly control retrograde transport (away from the cell body), enable cargoes to be moved down the microtubule tracks. The cellular contents being transported are varied, including vesicular cargoes (e.g. mitochondria and lysosomes), filamentous cargoes (e.g. neurofilaments) and cytoplasmic proteins (De Vos and Hafezparast, 2017; Millecamps and Julien 2013). It is clear, due to the variety of cargoes essential for cell function, that disruption of such molecular machinery could contribute to dysfunction of the neuron as a whole.

Amongst those to first notice axonal transport deficits was Sasaki and colleagues (1990), who noted that the distal initial segments of motor neuron axons in ALS patients were swollen and

enriched with accumulations of mitochondria, lysosomes and intermediate filaments, suggesting defective axonal transport. Since then, transport deficiencies of various types of cellular cargo have been investigated further. Some work suggested that mitochondrial transport deficits may create a perturbation in the distribution of these organelles due to a shift in the balance of anterograde / retrograde transport, potentially resulting in depletion of axonal mitochondria (De Vos et al., 2007). Altered MN axonal mitochondrial distributions have been noted in both the $SOD1^{G37R}$ and $SOD1^{G85R}$ models (Vande Velde et al., 2011). Further non-SOD ALS mouse models including those expressing mutant VAPB and TDP-43 have also demonstrated mitochondrial transport issues (Magrané et al., 2014; Mórotz et al., 2012). While this represents an encouraging hypothesis behind defective axonal transport-based neuronal death, further studies have disputed the idea that this is a major event in ALS pathological progression. One such study depleted axon-targeted syntaphilin, a mitochondria-specific docking receptor, in order to reduce immobilisation of mitochondria. This failed to alter disease progression in $SOD1^{G93A}$ animals (Zhu and Sheng, 2011).

Phosphorylated neurofilaments are considered a pathological hallmark of ALS, and the reduction in functional transport of neurofilaments may contribute to transport-based ALS pathology (De Vos and Hafezparast, 2017). Activation of p38 and CDK5-p25 kinase (which can occur due to the presence of glutamate, linking to excitotoxic mechanisms) causes neurofilament phosphorylation, preventing binding to kinesin (Millecamps and Julien, 2013). Such phosphorylation of the NF-M and -H (middle and heavy, respectively) side chains in rat cortical neurons exposed to glutamate caused slowing of anterograde transport (Ackerly et al., 2000). Neurofilament transport vulnerability is given further credence by several reports of mutations in the phosphorylation repeat domain of the NFH-encoding gene NEFH, potentially causing abnormal phosphorylation (Al-Chalabi et al., 1999; Figlewicz et al.,

1994). Glutamate-triggered activation of kinases may have a further role in disrupted axonal transport, as glutamate exposure also activates c-Jun N-terminal kinase (JNK). In combination with previously mentioned p38 and CDK5-p25 kinase, JNK can act to phosphorylate both kinesin heavy and light chains, inhibiting kinesin's binding to microtubules and other cargo (Millecamps and Julien, 2013).

It is clear that there is a wide variety of cargo affected in ALS-linked axonal transport deficiencies. However, dissecting how depletion of specific cargos contribute to ALS pathogenesis, and the molecular mechanisms behind these alterations, is a topic of continued debate.

2.6. Neuroinflammation

Neuroinflammation involves complex changes in phenotype from a variety of cell types, and is typically associated with neuronal loss. This includes astrocyte and microglial activation, infiltration of T lymphocytes and inflammatory cytokine overproduction (Liu and Wang, 2017). This 'activated' phenotype varies depending on cell type, and is context dependent. Astrocyte activation is characterised by changes in basic morphology, developing thicker processes and enlarged cell bodies, concomitant with GFAP and aldehyde dehydrogenase 1 (ALDH1L1) upregulation (Philips and Robberecht, 2011). Microglia activation meanwhile is diverse, with a shift to an amoeboid-like morphology. They can first secrete proinflammatory factors such as TNFα, with the goal of clearing potential threats, but can also be neurotoxic as a result. Their second phenotype, however, involves the release of anti-inflammatory and trophic factors, which limit inflammation and promote tissue repair. These are sometimes referred to deleterious (M1) and benign / protective (M2) phenotypes respectively, and

selection is dependent on the states of neighbouring inflammatory T-cells and astrocytes (Tang and Le, 2016).

Microglial activation has been reported in multiple studies, from presymptomatic $SOD1^{G93A}$ animals to ALS patients in PET studies (Corcia et al., 2012; Philips and Robberect, 2011). The factors that may be triggering this include detection of misfolded SOD1 from injured MNs and astrocytes, as well as extracellular ATP release (Liu and Wang, 2017). The latter is detected by microglial P2X receptors, which are upregulated in ALS post-mortem spinal tissue and $SOD1^{G93A}$ mice. Triggered neuroinflammation appears to contribute to ALS severity to some degree, as deletion of $P2X_7$ receptors in end-stage $SOD1^{G93A}$ animals aggravated symptoms, whilst use of a $P2X_7$ antagonist at the late presymptomatic stage was neuroprotective (Apolloni et al., 2013; Apolloni et al., 2014). This is likely due to the dual action of the receptor, possibly reflecting a switch from the M2 to M1 phenotype with disease progression, with modulation of either having an effect on ALS pathogenesis.

Related to this, T lymphocytes appear to alter disease phenotypes due to their interactions with microglia. Restoration of CD4+ T cells (known more generally as 'helper T cells') using bone marrow transplants prolonged survival in animals both harbouring the $SOD1^{G93A}$ mutation and lacking T and B lymphocytes ($SOD1^{G93A}$ x RAG2 KO mouse). A CD4+ KO mouse when bred with G93A animals had reduced survival similar to the $SOD1^{G93A}$ x RAG2 KO mouse, indicating the presence of CD4+ cells is neuroprotective in disease (Beers et al., 2008). This link to microglia is suggested due to significantly decreased microglial activation being observed when T cells were ablated using T cell receptor β (TCRβ) null mice (Chiu et al., 2008). Endogenous regulatory T cells (Tregs) too appear to be beneficial, as they were increased in early-progressive $SOD1^{G93A}$ spinal cords which was associated with increased

M2 microglial activation, and then decreased as disease progression rapidly accelerated. Passive transfer of Tregs from early stage mice increased the numbers of M2 microglia and prolonged survival (Beers et al., 2011). Together with evidence that the number of Tregs is lower in rapidly progressing ALS blood, and that those that are present are dysfunctional, it appears that multiple T lymphocyte cell types interact with microglia to modulate disease severity (Beers et al., 2017). However, as it is clear that there is significant crosstalk between astrocytes and microglia (Matejuk and Ransohoff, 2020), it is likely that T lymphocyte – microglia interactions represent only part of the story of neuroinflammatory insults in ALS.

2.7. Oligodendrocyte Dysfunction

Oligodendrocytes are essential in the function of neurons under healthy physiological conditions by providing the myelin sheath required for saltatory conduction along axons. During the development of the spinal cord, oligodendrocyte progenitor cells (OPCs), which eventually differentiate into mature oligodendrocytes, begin as migratory cells occurring in multiple waves beginning at E12.5 and continuing postnatally (Michalski and Kothary, 2015). They can proliferate, and as shown in the brain, a significant number remain in the adult animal. They occupy their own non-overlapping domains, and in healthy brains, are able to replace naturally dying mature oligodendrocytes and generate replacement myelin in order to maintain white matter tracts (Hughes et al., 2013; Michalski and Kothary, 2015). Indeed, this has been shown to be a potential pathogenic route, as $SOD1^{G93A}$ OPCs have the ability to rapidly proliferate, but fail to mature and cause progressive MN axon demyelination (Kang et al., 2013).

The insulating properties of myelin are not the only important function of oligodendrocyte – neuron contact. They also provide essential metabolic support through the transport of lactate, pyruvate and ketone bodies. This is enabled by monocarboxylate transporter 1 (MCT1) expression on oligodendrocytes and MCT2 expression on axons (Lee et al., 2012). Indeed, Fünfschilling and colleagues (2012) investigated these transporters in disease with the use of a mutant mouse which expressed an impaired ETC complex IV in oligodendrocytes, and therefore relied on anaerobic glycolysis for ATP production, thus forming excess lactate. Mature oligodendrocytes survived, and magnetic resonance imaging confirmed that there was lactate build up in the brain, which was only detectable under anaesthesia. This implied that the lactate was being metabolised due to neuronal activity in the active animal. Lactate is clearly important for neuron survival to some degree, as MCT1 knockdown with glucose deprivation caused concentration-dependent MN loss in a spinal culture model, which could be prevented with exogenous lactate application. When ALS post-mortem tissue is examined for MCT-1 expression, there is a dramatic 50% reduction, which was replicated in early / late stage $SOD1^{G93A}$ mice (Lee et al., 2012). Later work using oligodendrocytes derived from both iPSC and iNPC (induced neural precursor cells) verified this. Cells from multiple sporadic patients, as well as those harbouring various ALS mutations including SOD1, TARDBP and C9orf72 showed that co-cultures of diseased oligodendrocytes and WT mouse MNs induced MN death (Ferraiuolo et al., 2016). The intra- and extracellular contents of all ALS oligodendrocytes tested *except* those derived from C9orf72 patients showed reduced lactate, and addition of lactate could not rescue the effect of conditioned medium from C9orf72 patient oligodendrocytes on MNs (Ferraiuolo et al., 2016). It appears therefore that ALS oligodendrocyte dysfunction can cause deficits in MN survival, but through a different pathway in C9orf72 patients.

2.8. Excitotoxicity

Currently, the only reliable drug used to treat ALS (modestly improving lifespan by approximately 3 months) is riluzole. While it is not fully understood how it functions mechanistically, it is widely believed it is successful at least partially due to its modulation of excitotoxicity (Van Den Bosch et al., 2006; Dharmadasa and Kiernan., 2018). Excitotoxicity refers to cell death caused by excessive exposure to excitatory neurotransmitters, usually glutamate, resulting in a toxic influx of ions (particularly Ca^{2+}). (Dong et al., 2009) (see Fig. 4). The reduction of excitotoxicity by riluzole gives credence to this mechanism of disease, and as such it is amongst the most heavily studied. Section 3 will therefore examine in detail the various proposed sources of excitotoxicity, including several gaps in our knowledge that will be pursued in the remainder of this thesis.

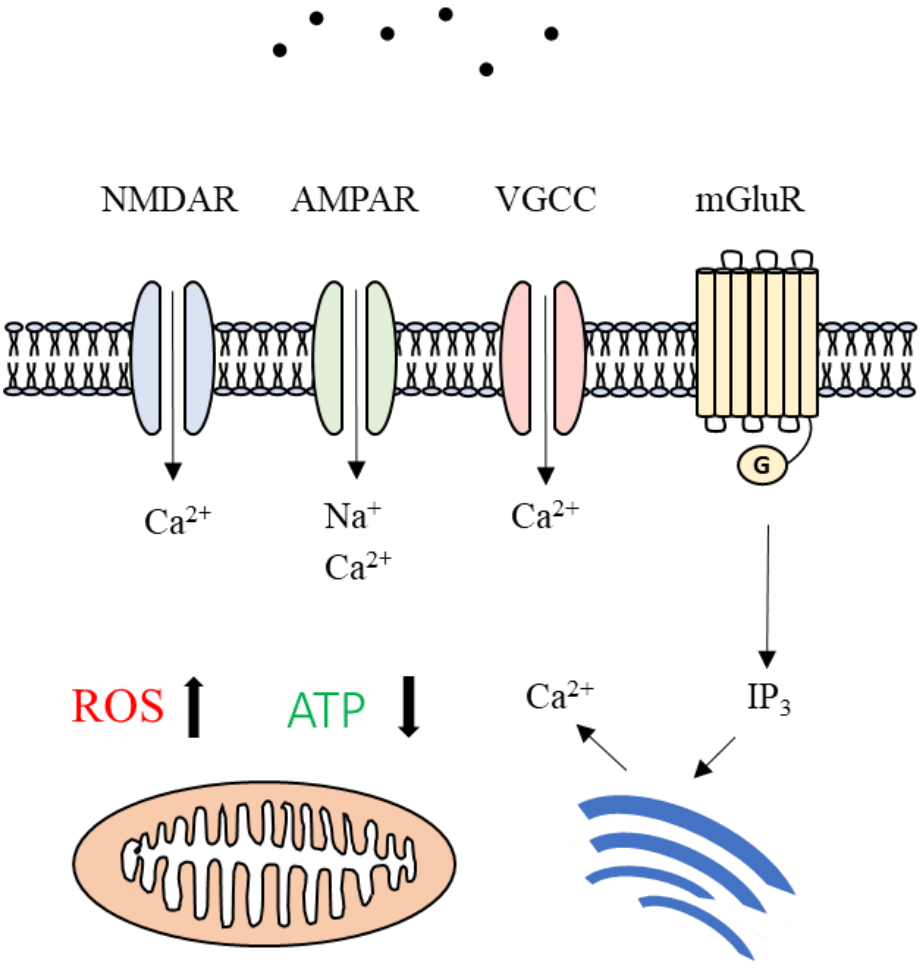

Figure 4: Mechanism of glutamate-mediated excitotoxicity. Glutamate results in Ca^{2+} influx through NMDA receptors and AMPA receptors, with activation of metabotropic glutamate receptors (mGluRs) causing further increases in Ca^{2+} concentration due to release from the endoplasmic reticulum via the inositol triphosphate (IP_3) pathway. Voltage-gated Ca^{2+} channels (VGCC) also contribute to Ca^{2+} intake. This can lead to excessive Ca^{2+} entry into the mitochondria, causing increases in ROS and reduction of ATP production. It may also result in the release of cytochrome C, triggering apoptotic pathways. Pathways described in Dong et al., 2009 and Mattson, 2019.

3. Sources of ALS Excitotoxicity

3.1. Intrinsic Hyperexcitability – Presymptomatic Disease Mechanism or Red Herring?

Of the mechanistic insights that we have gained with the use of $SOD1^{G93A}$ model, one which has received the most scrutiny is the idea of 'intrinsic hyperexcitability'. This refers to the production of excessive output of a neuron in response to the same input, thus being referred to as 'hyperexcitable'. This excessive excitability is then thought to lead to excitotoxicity of MNs, as well as other neurons in the motor circuitry (LoRusso et al., 2019). One of the first to report this was Kuo and colleagues (2004), who utilised both organotypic neonatal slice cultures and embryonic neural cultures derived from $SOD1^{G93A}$ animals. As will become a point of discussion later, the electrophysiological parameters used to define whether a neuron is over- or under- excitable is variable and may contribute to confusion in the field. Two parameters which are reported here are the rheobase, or minimum current required to elicit spiking, and the frequency-current relationship (F-I), more specifically the gain of the slope produced when the frequency of AP production at various levels of current injection is plotted (see Fig. 5). A further source of variability in the field comes from how the F-I relationship is calculated, as some groups utilise increasing current steps, whilst others use slow current ramps. In the study by Kuo and colleagues (2004), rheobase was not different in either culture type when cells contained the $SOD1^{G93A}$ mutation vs controls. However, analysis of the F-I relationship revealed disease-related changes in the F-I slope, meaning that the same current injection produced more firing in $SOD1^{G93A}$ cells vs controls.

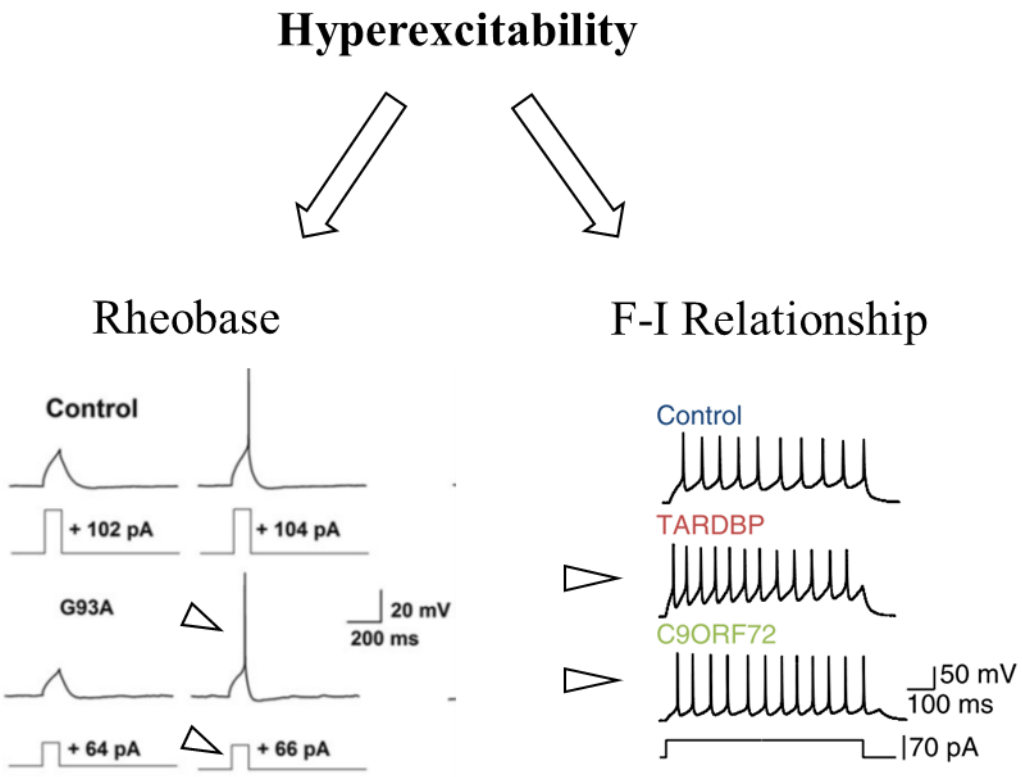

Figure 5: Measures used to describe hyperexcitability of a neuron in ALS. (*Left*) shows an example of a lower rheobase value in SOD1^{G93A} mice. Arrows annotate the lower current injection required to elicit an AP versus controls (adapted from Saba et al., 2015). (*Right*) shows an example of increased firing frequency in response to the same current injection in iPSC-derived MNs (arrows annotate ALS traces). Such frequencies are used to plot F-I relationships and assess excitability changes (adapted from Devlin et al., 2015).

Later embryonic neuron culture work attempted to target currents behind this reported hyperexcitability. Once again, Kuo and colleagues (2005) reported a significant increase in F-I gain in SOD1^{G93A} cells. However, when cells were divided according to high and low input conductance (proportional to neuronal soma size), it was noted that only high conductance cells showed a significant difference in F-I. Use of slow triangular current ramps revealed a persistent inward current (PIC), which could be blocked with voltage-gated Na^+ channel blocker TTX. This PIC_{Na} was significantly larger in SOD1^{G93A} cells. However, an opposing TTX-insensitive persistent current ($PC_{TTX\text{-}ins}$), which likely represented a net outward current

and acted to *decrease* excitability, was also increased in SOD1^{G93A} cells. The total PC amplitude is defined by the size of PIC_{Na} and $PC_{TTX\text{-}ins}$, and when high conductance cells were compared to low conductance ones, it was found that PIC_{Na} was always larger irrespective of conductance, whereas $PC_{TTX\text{-}ins}$ was only significantly larger in low input conductance cells. This created an offset in larger, high conductance cells and potentially explained their increased excitability.

Moving from *in vitro* analyses to *ex vivo* brainstem and spinal slice work, van Zundert and colleagues (2008) looked at the vulnerable population of hypoglossal MNs innervating the tongue. SOD1^{G93A} MNs showed increased firing frequency relative to current injection vs non-transgenic littermates in a current step protocol. When riluzole (inhibits PIC_{Na} with minor effect on inactivating Na^+ current) and TTX were added during slow triangular current ramps, the previously reported PIC_{Na} could be abolished, and once again, it was noted that PIC_{Na} was increased in SOD1^{G93A} MNs. Such a PIC_{Na} increase was also noted in spinal MNs (Quinlan et al., 2011). Total PIC, as well as specifically PIC_{Na}, was increased between the binarised age groups of P0-5 and P6-10. The presence of the SOD1^{G93A} mutation also increased both total PIC and PIC_{Na}. These authors did note some evidence of increased excitability. They showed that both the normal developmental: A) *decrease* in the time constant of the afterhyperspolarisation (AHP) and B) *increase* in the rate of AP rise / fall were enhanced in SOD1^{G93A} MNs. They did not observe alterations in the F-I slope or rheobase, however (Quinlan et al., 2011). Such acceleration of this maturation in electrophysiological parameters led to the conclusion that ALS may be a condition of expedited development, whereby increased early excitability quickens the onset of normal age-related motoneuron degeneration.

Finally, wild-type rat neuron cultures demonstrated decreased survival of SMI 32 +ve MNs when exposed to $SOD1^{G93A}$ astrocyte conditioned media (ACM). Analysis of persistent inward currents again revealed increased PIC_{Na} in cells exposed to $SOD1^{G93A}$ ACM. These cells showed increased firing frequency in response to increasing current pulses (although a F-I relationship was not generated). It should be noted, however, that it is challenging to select only MNs in a mixed neuron culture. The authors noted several voltage-sensitive Na^+ channel blockers including riluzole (although this is a 'dirty' drug and has effects on other currents) prevented SMI 32 +ve MN death induced by the ACM, therefore concluding the PIC_{Na}-drived hyperexcitability was a cause of cell death (Fritz et al., 2013).

While this picture of MN hyperexcitability initially seems clear, more recent work has revealed ALS-related excitability changes are less simple than initially thought. MNs can be divided into two types based on their physiological properties: delayed firing and immediate firing. This refers to their behaviour in response to a square current pulse at rheobase. Delayed firing MNs do not immediately fire, and upon firing onset do so with increasing frequency, whilst immediate firing MNs spike immediately and continue to do so with a relatively constant frequency. Dye labelling of recorded MNs in combination with immunohistochemistry for markers expressed in MNs innervating slow-twitch motor units (S-type MNs) and fast contracting / fatigable motor units (F-type MNs) allowed for correlation of firing behaviour and identification of motor unit type. Immediate firing MNs were revealed to be S-type MNs (resistant in ALS), whilst delayed firing MNs are F-type MNs, including those innervating vulnerable fast / fatigable (FF) motor units (Leroy et al., 2014). Authors found decreased rheobase values in P6-10 $SOD1^{G93A}$ MNs in immediate, but not delayed firing MNs. This was seen using both current step and triangular current ramp protocols. Immediate firing $SOD1^{G93A}$ MNs showed no differences in their F-I relationship

versus wild-type. In delayed firing cells, F-I gain was difficult to measure due to issues finding a linear primary range (presumably due to their accelerating firing frequencies at a set current). This was instead measured using firing frequency only 0.5s after recruitment, but it should be noted this is not the same measurement of F-I gain described in other work. This was not significantly different to wild-type. (Leroy et al., 2014). The authors therefore concluded that there was only evidence of early hyperexcitability in a MN subtype *not* vulnerable in ALS.

Up to this point, most work focussed on early hyperexcitability in embryonic primary culture and neonatal tissue. However, later work went on to investigate this in older tissue which was closer to symptom onset in the $SOD1^{G93A}$ model. In a population of MNs from animals aged P34 to P82, there was no measured difference in rheobase or F-I gain (Delestrée et al., 2014). It was noted, however, that a fraction of $SOD1^{G93A}$ MNs were unable to repetitively discharge during a triangular current ramp, a significantly higher proportion than WT. When restricted to P34-60 (preceding / just at the initial stages of NMJ denervation), all WT MNs could repetitively fire, but 35% of SOD1 MNs could not (thus were referred to as *hypoexcitable*). A compensation for increased input conductance in MNs is increased inward PIC_{Na}, which acts as a subthreshold depolarising current to aid sustained firing. The authors noted increased peak input conductance of SOD MNs, and provide evidence that there was a concomitant reduction in PIC_{Na} in cells that were hypoexcitable (Delestree et al., 2014). Further work doing intracellular MN recordings whilst measuring force at the tendon of the triceps surae muscle allowed motor unit type to be identified based on their contractile properties in response to MN stimulation (Martínez-Silva et al., 2018). Excitability measures of MNs in P46-60 $SOD1^{G93A}$ animals using slow triangular current ramps again showed a subset of cells were unable to fire repetitively in response to the ramp, but interestingly could

still activate their muscle fibres when injected with single current pulses. Using their motor unit characterisation, it was established that of the MNs that couldn't fire repetitively, most belong to FF motor units, followed by the largest of the fast fatigue resistant (FR) motor units. All slow-twitch (S) motor units could fire repetitively. It appears therefore that the most vulnerable MN types in ALS are those which develop hypoexcitable properties at later stages of disease, and as these are still able to activate muscle fibres, such hypoexcitability appears to precede denervation of the NMJ (Martínez-Silva et al., 2018).

This apparent dichotomy makes it challenging to draw clear conclusions about pathogenic intrinsic excitability changes in ALS. Although more recent work has cast doubt over the possibility of hyperexcitability being a major causative presymptomatic disease mechanism, it may simply be the case that observed excitability changes from hyperexcitable to hypoexcitable are part of downstream homeostatic mechanisms in response to cell dysfunction. Some work in human iPSC-derived MNs harbouring ALS-causing C9orf72 and TARDBP mutations showed expected early hyperexcitability (increased F-I gain) at 2-6W (weeks), which then switched to hypoexcitability at 7-10W, where the number of cells able to fire APs in response to current steps reduced (Devlin et al., 2015). More recent work, again utilising iPSC-derived MNs, showed further evidence of age-related excitability shifts (Sommer et al., 2022). Indeed, some mechanisms discussed earlier may give insight as to why this is the case. Early hyperexcitability may be transient, partially as a result of the often described increase in PIC_{Na} (Kuo et al., 2005; van Zundert et al., 2008; Quinlan et al., 2011; Fritz et al., 2013). At later time points, hypoexcitability is often noted (Delestrée et al., 2014; Martínez-Silva et al., 2018) , however an important difference observed is the increased input conductance of $SOD1^{G93A}$ MNs (Quinlan et al., 2011). A primary compensation for higher conductance is increased PIC_{Na}, which aids in sustained firing by providing subthreshold

depolarising currents. As there is evidence that cells that are hypoexcitable have decreased PIC_{Na} (Delestrée et al., 2014), it has been suggested that the switch in excitability states is seen when cells' compensatory upregulation of PIC_{Na} fails. The upregulation of PIC_{Na} therefore initially causes *hyperexcitability*, the failure of which later in life may leave the cell unable to compensate for increased input conductance, then causing *hypoexcitability* (Delestree et al., 2014).

Equally it should be noted that although mechanistically there are suggestions as to why this switch may occur, there are also inconsistencies in how changes in excitability are reported. For example, exactly which properties must be changed to describe a cell as hyperexcitable (i.e. rhoeobase, F-I gain or both) is not agreed upon. Equally, what is considered hypoexcitable (unable to fire repetitively vs unable to fire at all) is not consistent (Delestrée et al., 2014; Devlin et al., 2015). Together with variable specificities of MN subtype investigated and differences in controls utilised (e.g. non-transgenic littermates vs WTSOD1 vs a mix of both), reported inconsistencies are expected and the literature needs to be considered wholistically in an attempt to draw conclusions about changes in intrinsic MN excitability changes.

Finally, excitability of neurons other than MNs may also be altered. Superior colliculus interneurons which input to the hyperexcitable hypoglossal MNs mentioned previously also show hyperexcitability at P10-P12. Related to this, overall pre-MN network hyperexcitability was noted as spontaneous AMPA- and GABA-mediated PSC frequencies were significantly higher in $SOD1^{G93A}$ animals (van Zundert er al., 2008). Jiang and colleagues (2009) performed spinal ventral root recordings in later stage animals (P50, P90 and P120). Use of picrotoxin and strychnine to suppress inhibitory transmission produced synchronised

bursting, which is therefore mediated by excitatory pre-MN circuitry. The proportion of $SOD1^{G93A}$ animals which showed bursting was significantly higher. During these bursting episodes, there were 'sub-bursts', which likely represented multiple incidences of burst initiation. These too were increased in $SOD1^{G93A}$ animals, showing increases in both metrics of pre-MN network excitability at P90 and P120. Later work in P50-90 animals showed evidence of reduced system-wide short-term depression and increased frequency of MN oscillating EPSPs (polyEPSPs which acted continuously with multiple peaks, appearing oscillatory) (Jiang et al., 2017). Both represent evidence of overall hyperactivity of the pre-MN network, rather than just the MNs themselves.

3.2. Altered Synaptic Input – Cell Death by Hyperexcitation?

Beyond changes to intrinsic properties of MNs resulting in hyperexcitability, alterations in the synaptic input to either MNs or across the whole pre-MN network could be a source of excitability changes. This may occur due to changes in the ratio of excitatory : inhibitory (E:I) synaptic inputs onto MNs (or throughout the pre-MN circuitry), resulting in excessive excitation and subsequent excitotoxicity. For clarity, although there is considerable evidence of synaptic pathology in the brain also (Fogarty et al., 2015; Fogarty et al., 2016; Henstridge et al., 2018), only spinal synaptic changes will be discussed here as we aim to assess their contribution to lumbar excitability changes.

Early post-mortem work, although limited in specificity of synapse-type targeted (only using generic presynaptic markers), revealed pronounced synaptic pathology. Several pieces of work looked at presynaptic loss by targeting synaptophysin, an integral protein expressed in the overwhelming majority of presynaptic vesicles (Glantz et al., 2007). This work showed consistent loss of synaptophysin immunoreactivity in the ventral horn (Ince et al., 1995;

Matsumoto et al., 1996; Sasaki and Iwata, 1995; Sasaki and Maruyama, 1994). Immunoreactivity was directly correlated with the degree of neuronal loss, as is to be expected at late-stage disease with significant MN and interneuron loss (Sasaki and Maruyama, 1994). Interestingly, there was also evidence of synaptic loss in the intermediate and dorsal horn (Ince et al., 1995). Early post-mortem work likely did not consider confounding variables controlled for in modern human anatomy studies, such as post-mortem delay and fixation time, both of which can influence immunohistochemical outcomes (Lundström et al., 2019). Work using the same marker was done in $SOD1^{G93A}$ mice, quantifying immunopositive synaptophysin puncta contacting retrogradely labelled α and γ MNs. The number of co-localised presynaptic puncta was reduced by P90, approximately the age of symptom onset reported by other groups, although this work failed to correlate synaptic changes with measures of motor impairment such as rotarod testing (Zang et al., 2005; Pfohl et al., 2015). These studies provided a starting point to explore further synaptic changes, however, the lack of specificity in synaptic subtype targeted limits the information that can be drawn from them.

Immunohistochemcial studies using more specific markers to target excitatory and inhibitory synapses provide more information about potential changes in synaptic-input. Hossaini and colleagues (2011) showed a reduction in both glycinergic (GlyT2) and GABAergic (GAD65/67) presynaptic markers in end-stage low-copy number $SOD1^{G93A}$ mice (these animals show a reduced severity of disease onset compared to standard $SOD1^{G93A}$ mice), while GAD65/67 loss was present earlier in the symptomatic stage. In a binary division splitting the grey matter into just the ventral and dorsal horn, this synaptic loss was only noted in the ventral horn. In a standard $SOD1^{G93A}$ model at the transition to early-symptomatic stages (3 m.o.), there was a reported increase of VGLUT2 (vesicular glutamate

transporter 2, presynaptic glutamatergic marker) punta apposing fluorogold-labelled hypoglossal MNs. There was a simultaneous loss of VGAT (vesicular GABA transporter, a presynaptic GABAergic / glycinergic marker) (Sunico et al., 2011). This implies a shift in the E:I ratio onto these MNs to favour excitability.

Chang and Martin (2009) also looked at levels of inhibition specifically onto MNs, and noted reduced GlyT2 puncta apposition at the presymptomatic time point of 8W, which worsened with disease progression until end-stage. One defined source of glycinergic input onto MNs is that of Renshaw cells, which constitute a negative feedback circuit for MNs, receiving inputs from MN collaterals and forming inhibitory inputs back onto them (Moore et al., 2015). By 12 weeks using calbindin as a marker, Renshaw cell numbers were significantly reduced. Although it appears some of the loss of glycinergic input was due to Renshaw cell death, it cannot be solely attributed to this as the loss of glycinergic input precedes significant cell loss (Chang and Martin, 2009). Other groups report Renshaw cell loss, but not until 4 months in $SOD1^{G93A}$ animals (Wootz et al., 2013). Further evidence of glycinergic loss was reported in embryonic Hb9-eGFP x $SOD1^{G93A}$ MN primary culture, where glycine receptor (GlyR) puncta were reduced along both the dendrites and on the soma (Chang and Martin, 2011). A chimeric model of ALS, in which iPSC-derived spinal progenitors from sporadic ALS patients were implanted into the spinal cord of mice, also demonstrated inhibitory loss (Qian et al., 2017). The majority of these progenitors differentiated into human astrocytes, thus providing a novel way to model sporadic disease using mice. These animals developed expected motor symptoms, such as reductions in grip strength and changes in stride, at 9 months post-grafting of tissue. At this symptomatic stage, authors noted a significant reduction of GAD65 puncta onto ChAT +ve MNs (Qian et al., 2017). More recent work has demonstrated that vulnerable F MNs receive more input from glycinergic V1 interneurons

compared to S MNs, and that in SOD1^{G93A} animals these MNs show dramatic loss of V1 glycinergic input presymptomatically from P45, which continued to P84. Concurrent VGLUT2 staining revealed no differences in glutamatergic input in this time frame (Allodi et al., 2021).

While most evidence points towards a bias in excitatory transmission, usually due to a loss of opposing inhibitory transmission, not all of the literature is consistent with this. Schültz (2005) used two glutamatergic presynaptic markers (VGLUT1 and VGLUT2), both of which are known to be expressed throughout the grey matter (Todd et al., 2003). In addition, an inhibitory presynaptic marker called vesicular inhibitory amino acid transporter (VIAAT) was used, which is found at both glycinergic and GABAergic synapses (Juge et al., 2009). At the beginning of symptom onset in SOD1^{G93A} mice (P110, approx. 3.5 months), it was found there was a loss of VGLUT1 and VGLUT2 appositions to vesicular acetylcholine transporter (VACHT) +ve surviving MNs, whilst VIAAT co-localisation was not significantly changed. An embryonic organotypic spinal culture of SOD1^{G93A} animals showed a consistent overall synapse density in ventral regions vs wild-type at DIV (*days in* vitro) 14. However, when the density of excitatory vs inhibitory synapses was quantified using electron microscopy, SOD1^{G93A} cultures showed both fewer excitatory synapses and more inhibitory synapses (Avossa et al., 2006). Both studies therefore demonstrate an E:I shift biased towards increased inhibition.

Beyond immunohistochemical evidence of synaptic changes in ALS, another good measure of changes in synaptic input is quantification of ‘minis’, or miniature postsynaptic potentials / currents (mPSPs / mPSCs). These are the result of non-Ca^{2+}-dependent release of vesicles from synaptic boutons, therefore they are independent of presynaptic action potentials (APs).

Changes in amplitude represent changes in postsynaptic receptor function / expression, while a change in frequency can represent presynaptic changes (Choi and Lovinger, 1997). These may be a change in presynaptic release probability, or a change in the density of synapses contacting the cell measured. Glycinergic mIPSCs were investigated in primary MN culture by exposure to TTX (which inhibits AP firing and therefore Ca^{2+}-dependent neurotransmitter release), as well as CNQX (AMPAR antagonist), APV (NMDAR antagonist) and bicuculine (GABAR antagonsist) (Chang and Martin, 2011). The frequency of glycinergic mIPSCs was reduced by nearly 50%, however, failed to reach statistical significance (P=0.09).

Taken together, drawing a concise takeaway from the literature discussing changes in synaptic innervation in ALS is challenging. Synaptic pathology is clear from cruder early post-mortem work, however, defining changes in particular synapse types in a precise timeframe has proven difficult as a result of large variations in methodology. Although the $SOD1^{G93A}$ mouse has been consistently used, variation in how time points are defined can make precise comparisons between studies difficult (i.e. stating a disease timepoint in months rather than postnatal days). Another issue is a lot of work looks at MN input specifically, usually using ChAT +ve or VAChT +ve immunofluorescence to define the area of the MN. It is clear, however, that these markers only stain the soma and some large proximal processes of the MNs (Schutz, 2005; Chang and Martin, 2009). Thus, if co-localisation is defined by overlap with a presynaptic marker, it will fail to capture all the synaptic input to the cell. This may also introduce a source of bias towards inhibitory synaptic loss, as generally more inhibitory synapses are thought to be located on the soma and larger dendritic shaft than excitatory synapses (Boivin and Nedivi, 2018). In addition, the knowledge that some inhibitory spinal synapses can co-release glycine and GABA (Gamlin et al., 2018) may make interpretation of studies which attempt to separate them challenging. Despite this, there does

appear to be a body of evidence supporting loss of inhibitory input in ALS. Why these inputs may be more vulnerable is uncertain. There is evidence that inflammatory microglia can phagocytose synapses (Henstridge et al., 2019). For example, depletion of TDP-43 in microglia resulted in increased microglial ingestion of synapses (Paolicelli et al., 2017). Combined with the knowledge that their lipopolysaccharide activation can cause a selective microglia-mediated removal of inhibitory synapses (Chen et al., 2014), it may be the case that inhibitory synapses are more vulnerable to phagocytic loss, however, this is unknown.

As much of the evidence does not look at the balance between excitatory and inhibitory synapses, and much of it focusses solely on MNs, which has its caveats as described earlier, a more thorough examination of E:I ratios across the wider spinal circuitry is vital to better understand putative synaptic changes in ALS.

3.3. Astrocytic Synaptogenesis and Altered E:I Synaptic Ratio

Beyond loss of specific types of synapses driving potential alterations in E:I ratio in ALS, there is an alternative hypothesis that instead ALS may be a developmental disorder, whereby unknown mechanisms drive pathological shifts in E:I balance during development (Kiernan et al., 2019). A key cell type involved in modulating synapse formation during development is astrocytes (Risher and Eroglu, 2020). Astrocytes are a type of glial cell found abundantly in the CNS, and are broadly divided into two subtypes, described as ‘fibrous’ and ‘protoplasmic’ (Hochstim et al., 2008; Sun and Jakobs, 2012). Fibrous astrocytes are mainly located in the white matter, with few process and an extended morphology, where they are known to contact local blood vessels as well as the nodes of Ranvier on extended axonal tracts (Sofroniew and Vinters, 2010, Vasile et al., 2017). Protoplasmic astrocytes on the other

hand are mainly found in the grey matter, where they exhibit a bush-like extended morphology with 5-10 primary processes radially projecting from the soma, terminating in extremely fine perisynaptic astrocytic processes (PAPs) (Allen and Eroglu, 2017; Sun and Jakobs, 2012; Tabata, 2015). These intricate networks of PAPs allow for ensheathing of up to 2,000,000 synapses, where they form structures called 'tripartite synapses' (Allen and Eroglu, 2017). At these dynamic structures (evidence suggests they can move in a sub-1hr timescale), they have a diverse set of functions including promotion of synapse stability (Bernardinelli et al., 2014; Henneberger et al., 2020), and importantly when considering putative changes in E:I ratios, synaptogenesis.

The role of astrocytes in synaptogenesis was first noted in cultured retinal ganglion cells, where recorded spontaneous PSCs were greatly increased when neurons were grown with glia. This effect was mimicked when only glial conditioned media was added (Pfrieger and Barres, 1997). Subsequent microscopy work confirmed that the increase in spontaneous activity did indeed reflect an increase in the number of formed synapses (Ullian et al., 1997; Christopherson et al., 2005). Further studies went on to show that this is not isolated to retinal ganglion cells, but astrocyte-modulated synaptogenesis is also seen in other areas of the CNS. Hippocampal neurons formed increased numbers of excitatory synapses *in vitro* when cultured alongside astrocytes (Hama et al., 2004; Shen et al., 2016). Crucially for our interest in ALS, astrocytic presence also promotes synapse formation in spinal neurons (Garrett and Weiner, 2009).

Evidence from the brain suggests that the peak of excitatory synaptogenesis appears to be in postnatal weeks 2 and 3 (Chung et al., 2015; Risher and Eroglu, 2020). How astrocytes modulate this process appears to be the result of both secreted factors, and contact-dependent

factors. Beginning with secreted synaptogenic agents, the first protein family to be identified in astrocyte conditioned media was the thromospondins (TSPs) (Christopherson et al., 2005). These include five mammalian isoforms (TSP1-5), all of which are synaptogenic, although it appears they may be differentially expressed by different astrocyte subtypes (Eroglu et al., 2009). TSP1/2 expression peaks in the first postnatal week before decreasing in the adult brain. However, other members of the TSP family may be expressed to a higher degree in the mature CNS, and TSP1/2 is known to be upregulated after CNS injury to support further synapse formation (Christopherson et al., 2005; Liauw et al., 2008; Risher and Eroglu, 2012). Another secreted protein called hevin is expressed during development, peaking in postnatal weeks 2-3 and continuing into adulthood (Chung et al., 2015; Kucukdereli et al., 2011). Hevin has also been shown to promote excitatory synaptogenesis. However, in this case a related astrocytic protein called SPARC can antagonise the synaptogenic effect of hevin, providing a modulatory pair of proteins that can downregulate, as well as upregulate, synapse formation (Kucukdereli et al., 2011). Further evidence suggests that the synaptogenic effects of hevin may specifically act to promote healthy synapse development in certain CNS regions (Risher et al., 2014). It should be noted that electrophysiological validation of newly formed synapses induced by TSP and hevin alone indicate that they are postsynaptically silent due to a lack of AMPAR expression. Alternative components of the ACM called Glypicans 4 and 6 are required to increase surface level AMPAR expression and clustering, allowing for recordable glutamatergic activity (Allen et al., 2012). Many other secreted factors likely interact to modulate excitatory synapse formation and maturation, for example astrocytic cholesterol is known to promote synaptogenesis and strengthen presynaptic function (Gortiz et al., 2005).

Astrocytic contact with neurons via adhesion molecules appears to also be important in synaptogenesis. A family of neuronal adhesion proteins called γ-protocadherins are also expressed at the PAPs of protoplasmic astrocytes (Garrett and Weiner, 2009). It has been shown that contact-dependent mechanisms are critical for excitatory and inhibitory synapse formation *in vitro* and appropriate synapse development *in vivo* (Garrett and Weiner, 2009). Other contact-dependent factors include Ephrins and Eph receptors, a bidirectional signalling system between astrocytes and neurons (Risher and Eroglu, 2020). Koeppen and colleagues (2018) noted that astrocytic knockout of ephrin-B1 resulted in an increase in the number of excitatory VGLUT1+ve glutamatergic synapses in the hippocampus, implying it's presence acts to negatively regulate synapse formation. This result was replicated, and the inverse shown when astrocytic ephrin-B1 was overexpressed, causing a reduction in VGLUT1+ve synapses (Nguyen et al., 2020a). Finally, it was concluded that during a period of synapse formation and maturation in the hippocampus (P14-28), alteration of ephrin-B1 expression acts to modulate the overall E-I balance. As noted before, knockout caused increased glutamatergic synapse formation, in addition to enhanced AMPAR and NMDAR EPSCs, while EPSCs were reduced in overexpressing mice (Nguyen et al., 2020b). However, it was also noted that knockout mice showed loss of inhibitory synapses, along with a reduced number of parvalbumin +ve inhibitory interneurons, which is likely to at least partially explain this synapse loss (Nguyen et al., 2020b). It appears therefore that modulation of ephrin-B1 expression can alter E:I ratios in developing circuits by affecting both excitatory and inhibitory synapses. Parvalbumin +ve interneurons are a subset of fast-spiking GABAergic interneurons with a unique set of properties. Importantly for analysis of E:I ratios in ALS, these interneurons are also known to be populous in the spinal cord (Booker and Wyllie, 2017; Nahar et al., 2021; Petitjean et al., 2015).

It is clear therefore that there are multiple mechanisms by which astrocytes can influence synapse formation during development. There is also a considerable body of evidence that supports astrocytes being involved in disease pathogenesis and contributing to neuronal death in a non-cell autonomous manner (Valori et al., 2014). There is therefore the potential for astrocytes to undergo aberrant synaptogenic processes. As changes in network-wide excitability have been noted in the ALS spinal cord (Jiang et al., 2009; Van Zundert et al., 2008), it has been suggested that this may be the result of excessive excitatory input either to MNs, or across the network as a whole (Martin and Chang, 2012; Kiernan et al., 2019). As changes in excitability have been noted at early postnatal stages, there is even the possibility that a developmental bias in synapse formation 'primes' the network towards hyperexcitability, leading to excitotoxic cell death. When taken together, it is possible that in ALS network-wide alterations in E-I balance shift the excitability of the spinal network as a whole towards cell death, and that this shift in synaptic formation may be modulated by aberrant astrocytic synaptogenesis. It is this hypothesis that will be investigated in Chapter 4 of this thesis.

3.4. Astrocytic Dysfunction at the Tripartite Synapse

Although astrocytes have important roles in synapse formation, they are also essential components of mature synapses post-formation, where they dynamically wrap around synaptic boutons at the tripartite synapse (Garrett and Weiner, 2009). Here they are involved in the glutamate-glutamine cycle, whereby expression of glutamate transporters allow excess glutamate to be internalised and subsequently broken down into glutamine. This can then be transported back to neurons for use in the production of further glutamate, thus sustaining future synaptic activity (Uwechue et al., 2012; Tani et al., 2014). Such glutamate transport is

mainly handled by excitatory amino acid transporter 2 (EAAT2), accounting for over 90% of clearance in the brain (Pajarillo et al., 2019). This is crucial not just for allowing glutamate recycling to occur, but it also prevents excessive glutamate being retained in the synaptic cleft, which may cause postsynaptic excitotoxicity both locally and extrasynaptically via diffusion (Allen and Eroglu, 2017; Pajarillo et al., 2019). Astrocytes also directly modulate synaptic function in a process called 'gliotransmission'. For example, spinal astrocytes are able to directly respond to local neuronal glutamate, causing the release of astrocytic ATP which is subsequently broken down to adenosine. This then acts at neuronal A_1 adenosine receptors, reducing activity of the central pattern generator (CPG) circuitry (Broadhead and Miles, 2020; Witts et al., 2011). This direct manipulation of neuronal circuitry by astrocytes has also been noted in the brain (Matos et al., 2018).

First, before we discuss the mechanisms by which dysfunction at the tripartite synapse may drive ALS pathogenesis, the reported effects of the astrocyte 'secretome' should be noted (Zhao et al., 2020). Multiple studies have shown that beyond the effects of astrocytic contact, undefined secreted factors in the ACM have been shown to result in MN toxicity *in vitro* (Fritz et al., 2013; Nagai et al., 2007; Ramírez-Jarquín et al., 2017). Although this is the case, dysfunction at the tripartite synapse has been one of the most discussed ALS mechanisms. This is the case due to early reports of EAAT2 loss in disease. Rothstein and colleagues (1996) demonstrated *in vivo* that EAAT2 is responsible for the majority of glutamate clearance at the synapse. This is of note, as work in post-mortem tissue from ALS patients showed a substantial loss (up to 90%) of EAAT2 protein expression at the time of death (Rothstein et al., 1995). Work in a $SOD1^{G93A}$ rat model showed loss of EAAT2 immunoreactivity just prior to symptom onset, which progressed to an even more pronounced loss at end-stage (Howland et al., 2002). Work in multiple mouse models ($SOD1^{G93A}$ and

SOD1^{G85R}) confirmed loss of EAAT2 by end-stage, although this protein loss was only noted in the symptomatic stages of disease progression (Bendotti et al., 2001; Bruijn et al., 1997). It should be noted, however, that Howland et al. (2002) looked just prior to symptom onset in rats, whilst Bendotti et al. (2001) only measured EAAT2 expression at broad time points (8W presymptomatic, 14W early symptomatic). A presymptomatic loss could have emerged in this large gap between timepoints when animals weren't tested. One thing to note, however, is that although EAAT2 protein loss is consistent, it was shown that there was no concurrent loss of EAAT2 mRNA (Bendotti et al., 2001). Later work using immunoblotting showed that a presymptomatic loss of EAAT2 was present, together with the concurrent appearance of a band corresponding to truncated EAAT2 (Boston-Howes et al., 2006; Gibb et al., 2007). This was shown to be to the result of EAAT2 being cleaved by caspase-3, as in the presence of oxidative stress, SOD1 mutants showed significantly more caspase-3 activation, and resulting decreases in EAAT2-mediated glutamate uptake (Boston-Howes et al., 2006). It may be the case therefore, that loss of EAAT2 at late-presymptomatic stages is due to cleavage of translated protein rather than alterations in EAAT2-mRNA production. Together with evidence that drug-induced upregulation of EAAT2 can prolong survival in ALS mouse models (Ganel et al., 2006; Rothstein et al., 2005), it appears that dysfunctional modulation of glutamate at the tripartite synapse likely contributes to cell death in ALS.

Beyond modulation of glutamate transport, perturbations in gliotransmission provide another avenue by which dysfunction at the tripartite synapse may drive ALS pathogenesis. As described earlier, astrocytes are able to react to local glutamate release and produce ATP, which then degrades to adenosine. This then acts on neuronal CPG A_1 adenosine receptors to inhibit neuronal activity (Broadhead and Miles, 2020; Witts et al., 2011). It is feasible therefore that disruption of this bi-directional signalling mechanism could result in excessive

excitability of the network. Indeed, ALS patient cerebrospinal fluid shows increased levels of adenosine (Yoshida et al., 1999), in addition to post-mortem tissue showing increased expression of the excitatory A_{2a} receptor (Ng et al., 2015). This study also showed that pharmacological inhibition of A_{2a} receptors delayed disease progression of $SOD1^{G93A}$ mice, so it is possible that an imbalance of gliotransmission could bias circuitry towards excitatory transmission.

Astrocytes have been repeatedly implicated in ALS pathogenesis (Valori et al., 2014), and their multitude of essential functions at the tripartite synapse give them the potential to be a vulnerable fulcrum of disease. Their modulation of excitatory signalling via glutamate transport and gliotransmission make them important structures to investigate in ALS. This is particularly the case as evidence of widescale changes in the excitability of spinal circuitry implicates possible changes in tripartite synapses throughout the grey matter. Therefore, investigating tripartite properties at different stages of disease is essential, as they represent a target for reducing excitotoxic cell death in clinical trials (Rosenblum and Trotti, 2017).

Taken together, we hope to investigate 2 potential toxic mechanisms of astrocyte-synapse interactions in ALS (see Fig. 6):

1. We hypothesise that ALS could be a developmental disorder, in which astrocytes aberrantly undergo synaptogenic processes resulting in increased E:I ratios.
2. We hypothesise that the tripartite synapse may be a vulnerable fulcrum of disease in ALS, and could represent a site of future intervention.

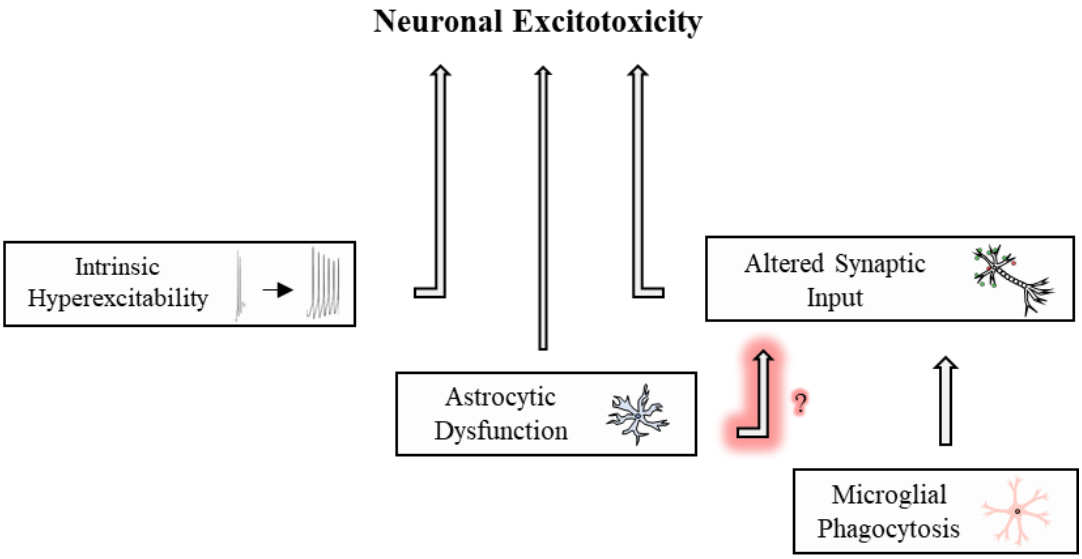

Figure 6: Schematic describing possible mechanistic sources of ALS hyperexcitability and subsequent excitotoxicity. Intrinsic hyperexcitability of the neurons may be the route cause. In addition, alterations in E:I ratios could lead to excess excitability. This may be the result of a number of mechanisms including aberrant microglial synaptic phagocytosis or potentially an astrocyte-derived synaptogenesis perturbation in development, potentially resulting in excitotoxic cell death. Finally, astrocytic dysfunction at the tripartite synapse may also cause such toxicity.

Chapter 2

Materials and Methods

1. Animals and Ethics

1.1. Animal Breeding

All procedures performed on animals were performed in accordance with the UK Animals (Scientific Procedures) Act 1986 and approved by the University of St Andrews Animal Welfare and Ethics Committee. $SOD1^{G93A}$ and PSD95-eGFP animals were maintained on a C57bl/6 background, while C9BAC500 animals were maintained on an FVB background. Both heterozygous ALS mouse lines were bred with $PSD95\text{-}eGFP^{+/+}$ animals to produce offspring that all expressed $PSD95\text{-}eGFP^{+/-}$. As C9BAC500 animals were on a different background strain, all C9BAC500 PSD95-eGFP animals used were first generation FVB/C57bl/6 crosses. Both $SOD1^{G93A}$ and C9BAC500 lines were provided by Dr. Richard Mead (University of Sheffield), whilst the PSD95-eGFP line was obtained from Prof. Seth Grant (University of Edinburgh).

1.2. Phenotype Monitoring

ALS motor phenotypes were monitored using a 0-4 scoring system; 4 showed no motor phenotype, 3 showed hind-limb splay and tremors when lifted by the tail, 2 showed gait abnormalities when freely moving, 1 showed hind limb dragging and 0 showed the inability to self-right after being placed on their back for 30s. Mice were euthanised when they reached a phenotypic score of 2 or lower.

2. Polymerase Chain Reaction (PCR)

2.1. PCR Protocol

Neonatal progeny of either SOD1$^{G93A\ +/-}$ x PSD95-eGFP $^{+/+}$ or C9BAC500 $^{+/-}$ x PSD95-eGFP $^{+/+}$ were tail-sampled (with local topical anaesthetic) 1 day before sacrifice for genotyping. Tail samples approx. 2mm in length were added directly to 75µl alkaline lysis reagent (all reagent recipes listed in section 2.2) and heated at 95^{o}C for 30 minutes, before agitation to ensure complete tissue breakdown. This extracted DNA solution was then cooled at 4^{o}C for 10 minutes, before addition of 75µl neutralisation solution. After thorough mixing, a PCR master-mix was then made using the following primers for SOD1^{G93A} or C9BAC500 samples:

SOD1^{G93A}

Forward: 5'-CAT CAG CCC TAA TCC ATC TGA-3'
Reverse: 5'-CGC GAC TAA CAA TCA AAG TGA-3'
Forward Control: 5'-CTA GGC CAC AGA ATT GAA AGA TCT-3'
Reverse Control: 5'-GTA GGT GGA AAT TCT AGC ATC ATC C-3'

C9BAC500

Forward: 5'-TCG AAA TGC AGA GAG TGG TG-3'
Reverse: 5'-CTT CCT TTC CGG ATT ATA TGT G-3'
Forward Control: 5'-CTG TCC CTG TAT GCC TCT GG-3'
Reverse Control: 5'- AGA TGG AGA AAG GAC TAG GCT ACA-3'

Following thorough mixing, 2µl of DNA solution was added to 23µl of master-mix for each sample, mixed, and placed in the thermocycler undergoing the following sequence:

1. 94ºC, 3.00 (min.secs)
2. 94ºC, 0.15
3. 65ºC, 0.15
   -0.5ºC per cycle
4. 68ºC, 0.01
5. GO TO step 2, 10x
6. 94ºC, 0.15
7. 60ºC, 0.15
8. 72ºC, 0.01
9. GO TO step 6, 28X
10. 72ºC, 1.00
11. 14 ºC, hold

An agarose gel was prepared (Sigma Aldrich, 1.5%) in 1x tris borate EDTA (TBE) (Sigma Aldrich) running buffer. 5µl RedSafe DNA Stain 20000x (Chembio) was added to the agarose solution, which was left to set for 25 minutes. PCR samples were removed from the thermocycler, then 5µl of TriTrack loading dye (6X) (Thermo Scientific) added to each sample. 10µl of this final solution was then pipetted into the wells of the agarose gel, which had already been placed in a gel tank and submerged in 1x TBE running buffer. A voltage of approximately 156V was applied for 20 minutes and DNA bands were visualised under UV light to identify sample genotype. Positive and negative control samples were always run alongside experimental samples to confirm results (see Fig 7).

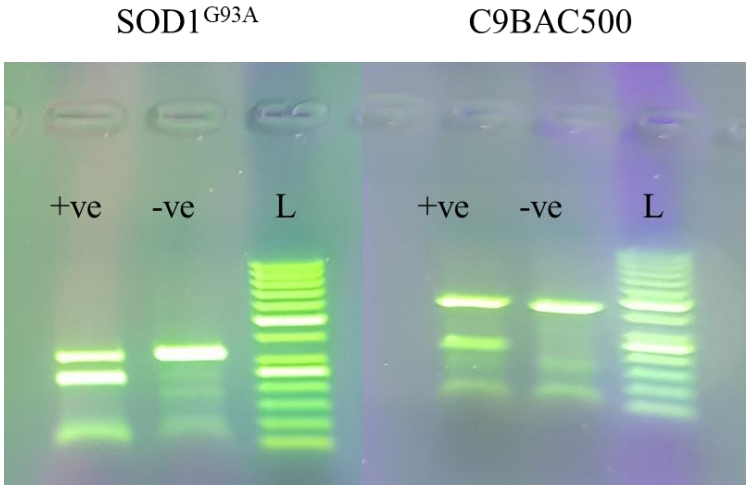

Figure 7: Example images of electrophoresis gels used in PCR protocol to identify genotype. (*Left*) From left to right: $SOD1^{G93A}$ +ve sample (double band), $SOD1^{G93A}$ -ve sample (single control band) and DNA ladder (L). (*Right*) From left to right: C9BAC500 +ve sample (double band), C9BAC500 -ve sample (single control band) and DNA ladder (L).

2.2. PCR Reagents

Alkaline Lysis Reagent:

0.5g NaOH (25mM)
0.03722g Na^2-EDTA $2H_2O$ (0.2mM)
Dilute up to 500ml w. dH_2O, pH approx. 12

Neutralisation Solution:

3.152g Tris-HCl (40mM)
Dilute up to 500ml w. dH_2O, pH approx. 5

PCR Master-Mix

Component	Final Concentration	Per Sample
PCR-Grade H_2O	Up to 25 µl	9.8µl
5x KAPA 2G HS Buffer $MgCl_2$ FREE	1x	5µl
25mM $MgCl_2$	2.5mM	2.6µl
10mM dNTP KAPA	0.2mM	0.5µl
10µM F Primer	0.5µM	1.25µl
10µM R Primer	0.5µM	1.25µl
10µM F Control Primer	0.5µM	1.25µl
10µM R Control Primer	0.5µM	1.25µl
5KAPA 2G HS Taq Polymerase 5U/µl	0.5U	0.1 µl

3. Primary Cell Culture

3.1. Neonatal Spinal Cord Tissue Collection (Primary Culture)

Animals were cervically dislocated, decapitated, and had their spinal cords dissected free-floating in 'Tissue Collection Solution' (TCS), part of the NeuroCult Enzyme Dissociation Kit for Adult CNS Tissue (Stemcell Technology). Free spinal cords were trimmed at the thoracic and sacral boundaries to isolate the lumbar cord. Next, their DRGs, roots and meninges were removed. All cords were dissected in genotype-specific petri dishes to prevent crossover of tissue and kept on ice to promote tissue health. Cords were then diced with sterile scalpels and transferred to falcon tubes with approximately 4-5ml of TCS.

3.2. Mouse Spinal Primary Neuron Cultures

See Fig. 8 for a simplified schematic. One day before DIV 0, non-etched coverslips sterilised with 100% ethanol were coated in a 0.22µm-filtered 1:20 poly-D-lysine (PDL) (Sigma-Aldrich) solution overnight at 37^{o}C in the incubator. The following morning, the PDL solution was removed, and coverslips washed twice in dH_2O. Laminin (Sigma-Alrich) was utilised as a secondary coating, with 350µl of 0.22µm filtered 1µg/35µl laminin solution being applied to the coverslips for 2 hours at room temperature. Dissections were carried out, and just before transport to the cell culture hood, papain latex (Sigma-Aldrich / Stemcell Tech) solution was thawed at 37^{o}C in the water bath. TCS was removed, before addition of 1.5ml papain latex solution to the diced tissue (whilst changing falcons to maintain sterility). This was incubated at 37^{o}C for 20 minutes, agitating every 5-10 minutes. After incubation, the papain latex solution was removed and replaced with fresh 1.5ml papain latex before a further 20 min water bath incubation.

Tissue was then washed 3x with 3ml Neurobasal A^+ (NBA^+) growth medium, again changing tubes to stop the action of any remaining papain present in the falcon. The 3rd wash was removed, and using a 5ml stripette, 2ml of NBA^+ was used to stripette up and down 50-60 times in order to triturate the spinal tissue, before topping up with a further 2ml NBA^+. This was then left to settle for 5 minutes at 37^{o}C. 2ml of the solution above the tissue was removed and placed in a dedicated falcon for single-cell solution. The process of media addition, trituration, settling and single cell solution transfer was repeated 2 more times, however on the 3rd trituration step, a further 15 resuspensions with a P1000 pipette were conducted to ensure complete tissue dissociation. Single-cell solutions for both positive and negative genotypes were placed in a centrifuge for 4min at 200 RCF (Relative Centrifugal Force)

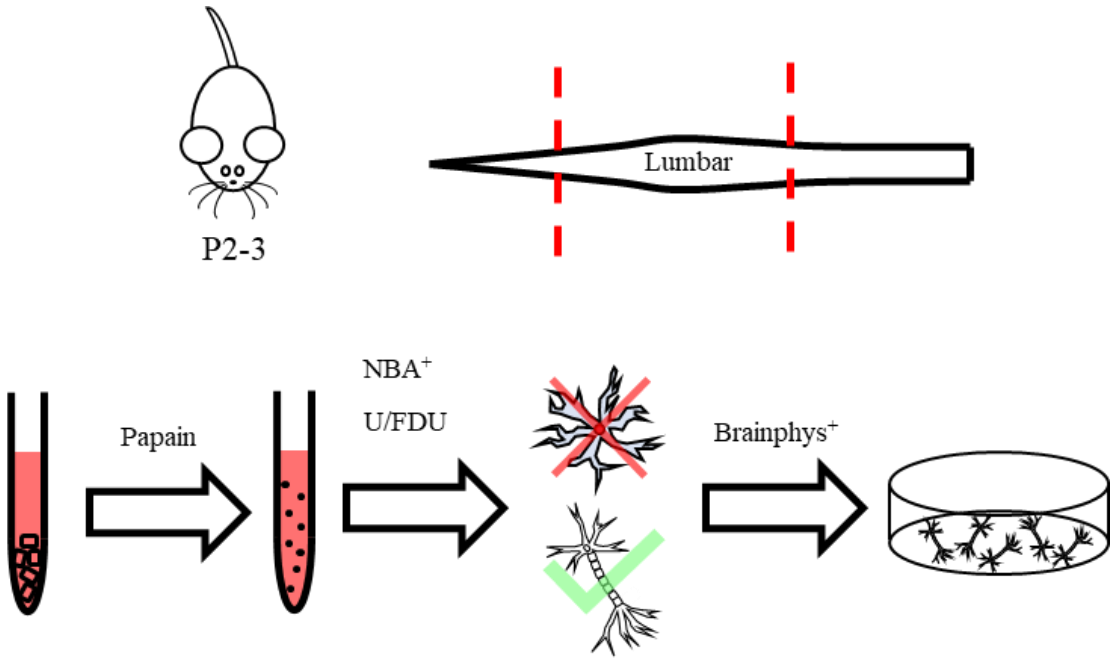

Figure 8: Methodology for producing postnatal spinal neurons. Lumbar spinal sections were isolated from postnatal day (P)2-3 mice and mechanically dissociated. Papain is used to preserve neuron viability, with U/FDU treatments post-plating removing mitotic astrocyte populations.

before removal of the supernatant. Pellets were resuspended in 1ml NBA^+, before counting using a haemocytometer. Cells were plated at 300,000 cells per well and left for 1 hour at 37°C to allow neurons to settle. After this, cells were washed twice with 500ml NBA (Gibco) to remove dead cells, before addition of 500ml NBA^+ w. uridine / fluorodeoxyuridine (U/FDU, both Sigma-Aldrich) at 1:10000 in order to stop the growth of mitotic astrocytes. Cells received a full feed of 500ml NBA^+ U/FDU 2-3 days later, before moving to $Brainphys^+$ half-feeds every 2-3 days following this.

3.3. Mouse Spinal Astrocyte Cultures

See Fig. 9 for a simplified schematic. The day prior to DIV 0, 75ml flasks were coated with 1:100 PDL solution and left in the incubator at 37°C. The next day, flasks were washed twice with 10ml dH_2O and left to dry. During the final stages of dissection, the proprietary

‘Inhibition Solution’ and ‘Dissociation Enzyme’ were warmed to room temperature (NeuroCult Enzyme Dissociation Kit for Adult CNS Tissue, Stemcell Technology). After isolation of the cords, the TCS was removed and 1.5ml of ‘Dissociation Enzyme’ was added whilst transferring to a new 15ml falcon to minimise contamination risk. Falcons were incubated strictly for 3 minutes in a water bath at 37^{o}C. After incubation, 1.5ml of ‘Inhibition Solution’ was added, and after allowing the tissue to settle, all 3ml was removed. The tissue was transferred to another fresh 15ml tube with astrocyte media. A further 2 washes (total of 3) were conducted, allowing the tissue to settle between each. The final wash was removed, and the tissue resuspended in 2ml of astrocyte media. A 5ml stereological stripette was then used to agitate the tissue, moving the solution up and down 30-40 times. A further 2ml of media was added and the falcon placed in a water bath at 37^{o}C for 5 min. 3ml of the solution was removed and added to a new falcon for our single-cell solution. The agitation step was repeated as before, this time 4ml was removed and added to the single cell tube. A final resuspension was conducted by adding 1ml and triturating using a 1000µl pipette tip to aid in breaking up the remaining tissue. 1ml more astrocyte media was added, before a final 5-minute 37^{o}C incubation to allow any debris / surviving meninges to settle at the bottom of the falcon. The solution was then transferred to the single cell tube except for the last approx. 250µl of solution in order to avoid transfer of debris resting at the bottom. The single-cell solution was stripetted up-and-down to aid in de-clumping of cells, before being added to the coated flask containing 5ml of astrocyte media.

When flasks reached near-100% confluency (approx. 10 days), flasks were washed with PBS to remove any serum in the astrocyte media which could later inhibit TrypLE. 3ml of TrypLE (Gibco) was added to each flask and incubated at 37^{o}C for 10 minutes. This acted to free the cells from the flask coating. Flasks were gently agitated in order to dislodge any cells still

stuck down. 5ml of media was added to neutralise the TrypLE, and the flask contents were moved to a 15ml falcon. Another 5ml of astrocyte media was used to spray down each flask to collect any remaining cells. The single cell solution was centrifuged at 300 RCF for 5 minutes. The supernatant was removed, and cell pellets were resuspended in 1ml of astrocyte media before counting using a haemocytometer. Astrocytes were plated at 100,000 cells per well in a 24 well plate, with sterilised coverslips coated in 1:100 PDL solution.

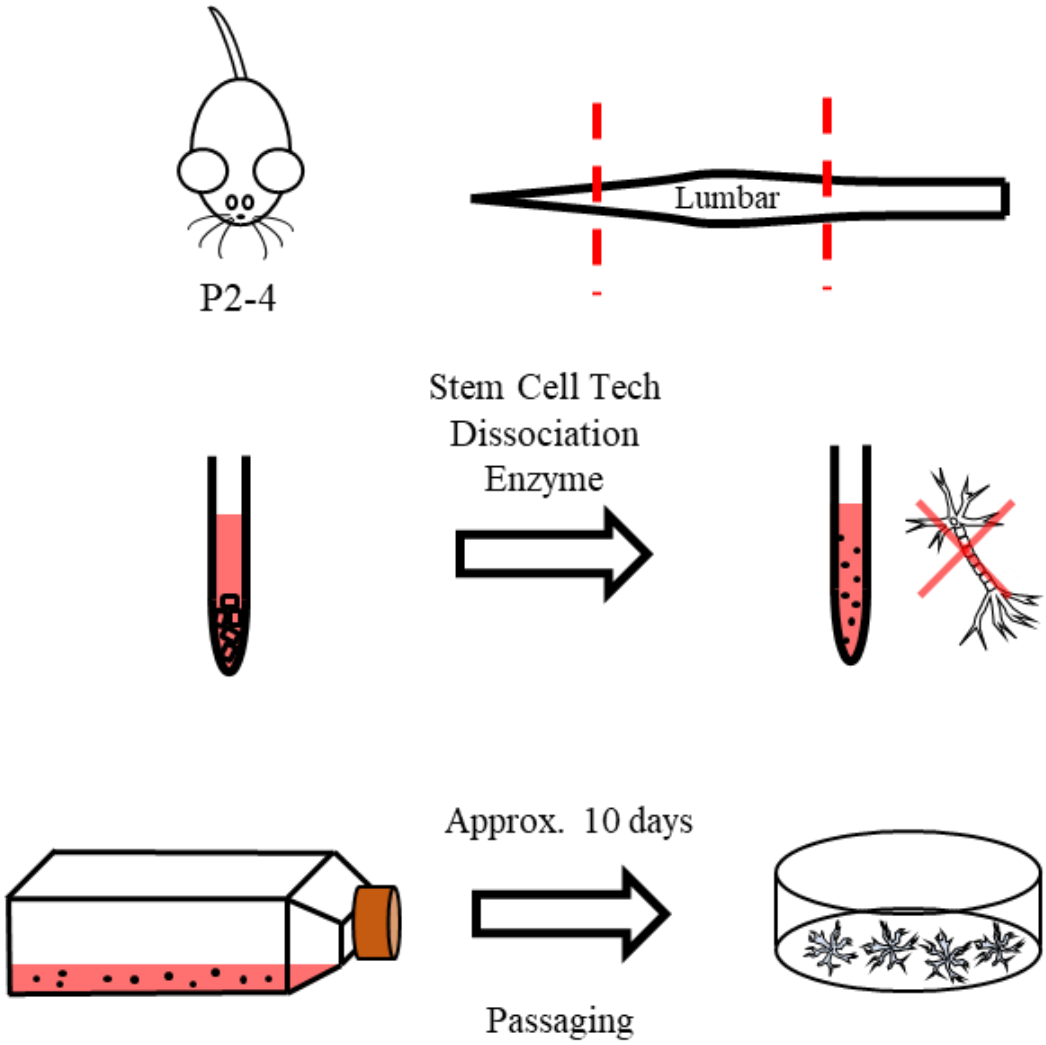

Figure 9: Methodology for producing postnatal spinal astrocytes. Lumbar spinal sections were isolated from P2-4 mice and mechanically dissociated. Tissue was incubated in Stem Cell Tech's proprietary dissociation enzyme before further mechanical agitation. Suspended cells were separated from spinal debris and grown until confluency at approx. 10 days, before replating.

3.4. Mouse Spinal Co-Cultures

Astrocytes were found to be confluent between 9 and 13 days. When this was the case, astrocytes were replated and maintained. Neurons were plated (as described previously) on top of astrocytes from DIV 14 onward, with the astrocytes being washed with NBA prior to neuron plating to remove any astrocyte media. Co-cultures were grown with the same feeding schedule as neurons, including the 2 pulses of U/FDU to ensure astrocytes from the neuron platedown did not significantly proliferate.

3.5. Primary Cell Culture Reagents

PDL: 1:20 (neurons) or 1:100 (astrocytes) PDL solutions were made by diluting 2mg/ml stock in dH_2O, before running through a 0.22µm filter.

Laminin Solution: Stock solution (1-2mg/ml) was diluted with NBA, for a total of 350µl solution per well containing 10µg of laminin. In a 1mg/ml stock, this would simply be 10µl of laminin stock in 340µl NBA. Batch variability was taken into account however, and the total volume of stock solution to be diluted was adjusted to ensure there was 10µg of laminin per well (e.g. if one batch = 1.2mg/ml, 8.33µl contains 10µg). This was then 0.22µm filtered.

Papain Latex Solution: Lyophilised powder contains approx. 10 units/mg. Batch variability was taken into account to ensure consistent concentrations, as a single papain bottle contains 1000 units (e.g. if 13 units/mg, 1000/13 = 76.92mg was used). This was added to a bottle containing 45mg L-Cysteine (Sigma-Aldrich) and 18.917mg kynurenic acid (Sigma-Aldrich), before 100ml TCS was added. The papain latex was dissolved by periodically warming at 37^{o}C in a water bath for 2 minutes. Once dissolved, this solution was 0.22µm filtered to sterilise.

NBA$^+$: 96.75ml of Neurobasal A media was mixed with 2ml of B27 neuronal supplement (Gibco), 0.25ml of Glutamax (Gibco) and 1ml Antibiotic-Antimycotic (Anti-Anti) (Gibco) to create our initial neuronal growth medium. This was then 0.22µm filtered to sterilise. NBA$^+$ was stored at 4^{o}C and used for up to 1 week.

Brainphys$^+$:19.4ml of Brainphys neuronal media (Stemcell Technology) was mixed with 0.4ml 2% Neurocult SM1 supplement (Stemcell Technology) and 0.2ml Anti-Anti. The mixture was 0.22µm filtered to sterilise. Could be stored for up to 1 month at 4^{o}C.

Astrocyte Media: 500ml of DMEM + Glutamax, low glucose, pyruvate (Gibco) was mixed with 50ml 10% FBS (Gibco) and 5ml 1% Anti-Anti. This was then 0.22µm filtered to sterilise and could be stored at 4^{o}C for up to 1 month.

4. iPSC Culture

4.1. iPSC Differentiation and MN Maturation

Day 0: iPSCs were dissociated using TrypLE, collected and washed with KO DMEM (Gibco), before being spun down for 5min @ 200-250 RCF. Supernatant was aspirated, before resuspension in Day 0 Differentiation medium. This consisted of Differentiation Base medium supplemented with: Rock inhibitor (Tocris, 10µM final), SB-431542 (Tocris, 20µM final), LDN-193189 (Sigma-Aldrich, 0.1µM final), CHIR-99021 (Tocris, 3µM final) and ascorbic acid (AA, Sigma-Aldrich, 10µM final). Cells were plated at 2x10^5 cells/ml on ultra-low attachment plates.

Day 2: Neurospheres were spun down @ 200 RCF for 3 mins, before resuspension in Differentiation Base medium supplemented with: Rock inhibitor (10µM final), SB-431542 (20µM final), LDN-193189 (0.1µM final), CHIR-99021 (3µM final) and AA (10µM final), retinoic acid (RA, Sigma-Aldrich, 100nM final) and smoothened agonist (SAG, Millipore 500nM final).

Day 4: Repeat day 2.

Day 7: Cells were spun down @ 200 RCF for 3 mins. Resuspended in Differentiation Base medium supplemented with: AA (10µM final), RA (100nM final), SAG (500nM final) and brain-derived neurotrophic factor (BDNF, R&D Systems, 0.01 µg/ml).

Day 9: Neurospheres were resuspended in Differentiation Base medium supplemented with: AA (10µM final), RA (100nM final), SAG (500nM final), BDNF (0.01µg/ml) and DAPT (Tocris, 0.01mM).

Day 11: Repeat day 9.

Day 14: Neurospheres were resuspended in Differentiation Base medium supplemented with: AA (10µM final), RA (100nM final), BDNF (0.01µg/ml), DAPT (0.01mM) and glial-derived neurotrophic factor (GDNF, R&D Systems, 0.01µg/ml).

Day 15: Day before dissociation, coverslips were coated with Matrigel Matrix (Corning) in KO DMEM @ 1:30 (stock = 10mg/ml).

Day 16 (Dissociation): Neurospheres were collected and washed in PBS. 0.05% trypsin (Gibco) + DNase (Sigma-Aldrich) was added, before a brief 15 min incubation at 37^{o}C. Trypsin was inhibited with FBS + DNase, before addition of 5ml Maturation Base medium. Supernatant was removed before dissociation of neurospheres with a P1000, which was repeated a 2nd time, adding single cell solutions to a separate falcon. Cells were centrifuged @ 200-250 RCF for 5 min. Supernatant was removed before resuspension in Maturation Platedown medium (Maturation Base medium + GDNF (1:100), BDNF (1:1000), insulin-like growth factor (IGF-1, R&D Systems, 1:1000), ciliary neurotrophic factor (CNTF, R&D Systems, 1:1000), GluE (Sigma-Aldrich, 1:1000), RA (1:10,000) and AA (1:1000)). Cells were counted and plated on 24 well plates @ 120,000 cells per well.

Cells were subsequently half-fed every 2-3 days in Maturation Platedown medium w.o. GluE.

4.2. iPSC Media

Differentiation Base Medium (Day 0-15):

94.8ml Advanced DMEM/F12 (Gibco)
94.8ml Neurobasal medium
2ml Anti-Anti
2ml 1X Glutamax
0.4ml 100µM β-mercaptoethanol (β-ME, Gibco)
4ml B27 supplement
2ml N2 supplement (Gibco)

Maturation Base Medium (Day 16-28):

480ml Neurobasal medium
5ml 1X Glutamax
5ml Non-essential Amino Acids (NEAA) (Gibco)
2ml 100µM β-ME
4ml B27 supplement
2ml N2 supplement
5ml Anti-Anti

5. Mouse Spinal Tissue Processing

5.1. Spinal Cord Tissue Collection (Fixed Tissue)

Adult mice were transcardially perfused with 4% paraformaldehyde (diluted w. dH_2O from 16% stock) (PFA, Alfa Aesar), before the spinal cord was removed and placed in aliquots of PFA for a further 4 hours. Cords were then washed in PBS, before being left in 30% sucrose solution overnight at 4^{o}C. Finally, they were incubated in an equal mixture of sucrose sol. / OCT (optimal cutting temperature) embedding compound (Scigen) for 2 hours. The tissue was then placed in embedding moulds w. OCT compound and frozen at -80^{o}C. Embedded blocks were sliced at approx. 20µm using a Leica CM1860 cyrostat onto Superfrost Gold Plus glass slides (VWR).

6. Immunocytochemical / Immunohistochemical Techniques

6.1. Immunocytochemistry Primary Culture

Coverslips were washed in Dulbecco's Phosphate-buffered Saline (DPBS, containing Cl^- and Mg^{2+}, Gibco) and fixed for 25 minutes in 4% PFA, before 3 further washes in DPBS. Cells were then permeabilised in DPBS w. 0.1% Triton X100 (TriX) for 10 minutes. Following this, DPBS w. 5% bovine serum albumin (BSA) / 0.1% TriX was added, and cells were blocked for 1 hour. Primary antibodies were diluted in this solution, using a combination of the following antibodies depending on the study:

Rb anti-β-III Tubulin (1:1000, Abcam), **Rb anti-Connexin-43** (1:500, Sigma-Aldrich), **Rb anti-EAAT2** (1:500, Bioss Inc.), **Gt anti-Ephrin-B1** (1:500, Biotechne), **Ms anti-Gephyrin** (1:500, Synaptic Systems), **Ch anti-GFAP** (1:500,

Aves Labs Inc.), **Ms anti-Glutamine Synthetase** (1:500, ProteinTech), **Rb anti-Oligodendrocyte Specific Protein** (1:500, Abcam), **Rb anti-pEzrin** (1:500, Abcam), **Ms anti-PSD95** (1:500, Abcam), **Ms anti-SMI-32** (1:1000, Biolegend), **Rb anti-Synapsin** (1:500, Cell Signalling) and **Rb anti-TMEM119** (1:500, Abcam)

This incubation was done overnight. Following this, 3 5-minute washes in DPBS w. 0.1% TriX were performed. Again, DPBS w. 5% BSA / 0.1% TriX was used to dilute secondary antibodies in, which included:

Dk anti-Gt Alexa Fluor 488 (1:1000, Invitrogen), **Gt anti-Rb Alexa Fluor 488 Plus** (1:1000, Invitrogen), **Dk anti-Ms Alexa Fluor 555** (1:1000, Invitrogen), **Gt anti-Ch Alexa Fluor 647 Plus** (1:1000, Invitrogen), **Dk anti-Rb Alexa Fluor 647 Plus** (1:1000, Invitrogen)

Coverslips were incubated in secondary antibody solution for 1 hour, before being washed 3 times in DPBS. Finally, coverslips were incubated in 1:5000 DAPI solution (Stock = 5mg/ml, Sigma-Aldrich) for 10 minutes. Following a DPBS wash, coverslips were mounted face down onto microscopy slides with Vectashield Vibrance (Vector Labs) mounting media.

6.2. Immunocytochemistry iPSC-derived Neurons

Immunocytochemistry was performed as described in Section 6.1. Primary antibodies used included:

Gt anti-GAD65 (1:500, Abcam), **Ms anti-Gephyrin** (1:500, Synaptic Systems), **GP anti-PSD95** (1:500, Synaptic Systems), **Rb anti-Synapsin** (1:500, Cell Signalling) and **Rb anti-VGAT** (1:500, Protein Tech)

Secondary antibodies used included:

Dk anti-Gt Alexa Fluor 488 (1:1000, Invitrogen), **Gt anti-Rb Alexa Fluor 488 Plus** (1:1000, Invitrogen), **Dk anti-Ms Alexa Fluor 555** (1:1000, Invitrogen), **Gt anti-GP Alexa Fluor 647** (1:1000, Abcam) and **Dk anti-Rb Alexa Fluor 647 Plus** (1:1000, Invitrogen)

6.3. Immunohistochemistry Spinal Tissue

Slides were removed from -80ºC storage, placed in a closed slide box and left at 37ºC for 30min in an incubator to allow the mounting PBS / condensation to evaporate and improve tissue adhesion to the slides. These were then washed in PBS (Gibco) 3 times. The slides were dried around the tissue, and a hydrophobic pen used to circle around slices. 25µl of PBS w. 3% BSA / 0.25% TriX solution was added to each tissue sample and incubated in a covered container for 2 hours. Primary ABs were diluted in PBS w. 1.5% BSA / 0.125% TriX and incubated with tissue for 2 nights. These were as follows:

Ch anti-ChAT (1:250), Rb **anti-EAAT2** (1:500, Bioss Inc., **Gt anti-Ephrin-B1** (1:250, Biotechne), **Ms anti-Gephyrin** (1:500, Synaptic Systems), **Rb anti-GFAP** (1:500, DAKO), **Ms anti-Glutamine Synthetase** (1:500, ProteinTech), **Rb anti-Oligodendrocyte Specific Protein** (1:500, Abcam), **Rb anti-pEzrin** (1:500, Abcam),

Rb anti-Synapsin (1:500, Cell Signalling), **Rb anti-TMEM119** (1:500, Abcam) and **Ms anti-VGLUT2** (1:500, Abcam)

Primary antibody solution was then removed, and slides washed 5 times in PBS for 10 minutes each. Secondary ABs were prepared in PBS w. 0.1% TriX. These included:

Gt anti-Ms FITC (1:200, Jackson), **Dk anti-Gt Alexa Fluor 488** (1:500, Invitrogen), **Dk anti-Rb Cy3** (1:200, Jackson), **Dk anti-Ms Alexa Fluor 555** (1:500, Invitrogen), **Dk anti-Rb Alexa Fluor 594** (1:200, Abcam), **Gt anti-Ch Alexa Fluor 647** (1:250, Invitrogen) and **Dk anti-Rb Alexa Fluor 647 Plus** (1:500, Invitrogen)

If DAPI (Sigma Aldrich) was being applied, a 1:5000 dilution was added for 10 mins. Slides were finally washed once in dH_2O and were mounted in Mowiol with 13mm coverslips.

6.3.1. Mowiol

2.4g of Mowiol (Millipore) was slowly added to 6g of glycerol (Sigma-Aldrich) whist mixing over the course of 1 hour. 5ml of dH_2O was added, mixing for 1 min and left at room temperature overnight, covered. The next day, 12ml of 0.2M Tris (pH 8.5) heated to 50^oC was added, mixing for 1 hr. The mixture was then centrifuged at 3850 RCF for 15min. The supernatant was then removed, leaving 0.5ml to exclude residue. 2.5g/100ml DABCO (Sigma-Aldrich) was then added, before inversion to mix. Solution was cooled to 4^oC and allowed to settle, so air bubbles could rise and be excluded. This final solution was then aliquoted and stored at -20^oC.

6.4. Immunohistochemistry Human Post-Mortem Tissue

Human spinal cord sections were obtained from the Edinburgh Brain and Tissue Bank, with the help of Prof. Colin Smith. Ethical approval was provided by the East of Scotland Research Ethics Service REC 1 (16/ED/0084). ALS spinal sections were obtained from patients who died of the condition and harboured mutations in the *C9orf72* (5 cases, all male, av. age = 57.6 years) or SOD1 gene (4 cases, all male, av. age = 54 years), with age matched control sections obtained from patients who died of natural causes (6 cases, 5 male / 1 female, av. age = 57.2 years). Protocol was adapted from Curran et al. (2021). 4µm sections were provided fixed and paraffin embedded. These were de-paraffinised using sequential washes of Xylene (Sigma-Aldrich), 100% ethanol, 95% ethanol, 70% ethanol and 50% ethanol, before an antigen retrieval step. This was done using a citric acid solution (pH 6.0), whereby sections were submerged and steamed for 20 min at 95^{o}C to aid in the reveal of epitopes. This was followed by 3 washes in PBS, before incubation with 1x Tris-buffered Saline (TBS) w. 5% BSA / 0.2% TriX for 2 hours at room temperature. Primary antibodies were diluted in TBS w. 3% BSA / 0.2% TriX, and sections were incubated in this at 4^{o} C for two nights. The primary antibodies used were:

Rb anti-pEzrin (1:250, Abcam) and **GP anti-PSD95** (1:500, Synaptic Systems)

This was followed by 5 TBS w. 0.2% TriX washes. Secondary antibody solutions were then prepared in TBS w. 0.2% TriX, and tissue incubated with these for 3 hours at room temperature. The secondary antibodies utilised were as follows:

Gt anti-Rb Cy3 (1:250, Life Tech) and **Gt anti-GP Alexa Fluor 647** (1:500, Abcam)

5-6 washes in PBS w. 0.2% TriX were conducted, before a single dH_2O wash, drying and mounting with Mowiol.

6.5. Imaging Strategy and Data Collection

High resolution imaging was conducted on a Zeiss Axio Imager M2 Microscope equipped with an Apotome 2.0. Illumination was provided by a HXP120 bulb, and images were acquired at x63 magnification using a digital MRm camera. Super-resolution imaging was conducted on a Leica SP8 SMD g-STED microscope at the Edinburgh Super-Resolution Imaging Consortium hosted by Heriot Watt University. Excitation was provided by a CW super-continuum white light laser source at 488nm, with depletion provided by 594 and 774nm lasers. Images were acquired with a x100 magnification STED objective lens. During all imaging, exposure times and illumination settings were kept consistent within datasets.

Cell culture imaging involved pseudo-random capture of 10 images per coverslip to account for variability across different areas of the sample. If multiple coverslips were available in one condition per platedown, images across all coverslips were averaged to give the mean value for that platedown. In the case of co-culture imaging, as neurons were not abundant across all of the coverslip, imaging was guided in the synapsin channel without switching to postsynaptic channels in order to avoid unconscious bias towards excitatory or inhibitory synapse capture.

Spinal cord hemi-sect imaging involved creation of a ROI, whereby x63 magnification images were captured encompassing the whole hemi-section and subsequently stitched. One hemi-section per mouse was obtained.

6.6. Data Analysis and Statistics

Astrocyte Quantification

Analysis was conducted using CellProfiler (McQuin et al., 2018) in order to consistently analyse large numbers of images in a high-throughput manner. Multi-channel images were split into single channels and fed into custom pipelines. For quantification of % cells expressing GFAP or GS, DAPI +ve nuclei were identified as primary objects, as were GFAP and GS +ve areas. GFAP and GS masks could be overlayed onto the DAPI primary objects. The number of nuclei co-localising with these markers was then calculated as a % of total nuclei. For quantification of EAAT2, Cx43 and ephrin-B1, images were fed into the 'EnhanceOrSuppressFeatures' module to subtract background signal before subsequent identification of primary objects from this output. This was used to create a mask, which was overlayed onto the raw images of each marker. The 'MeasureObjectIntensity' module then calculated integrated intensity values of identified objects for each marker. In the case of EAAT2 and Cx43 during initial astrocyte characterisation, only the integrated intensity values of objects within GS +ve masks were calculated to ensure quantification strictly in astrocytes. As >99% of cells expressed GS, however, this was deemed unnecessary during ephrin-B1 quantification.

Synaptic Quantification

Quantification of synapses was performed in Fiji is just ImageJ (FIJI) (Schindelin et al., 2012). For all *in vitro* work (primary co-culture and iPSC-derived MNs), images were processed using background subtraction and gaussian smoothing to increase clarity of synaptic puncta. For detection of synapsin, Moments-based thresholding was utilised, while for PSD95 and gephyrin Otsu-based thresholding was used. Typically, a degree of manual adjustment was required, however. The experimenter was blinded to genotype conditions during imaging and analysis to avoid unconscious bias during this step. Minimum and maximum size thresholds were set to avoid detection of both very dim structures, as well as large supra-synaptic sized objects that were likely lipofuscin aggregates or other debris. Thresholding produced binarised images, with the co-localisation of pre- and postsynaptic objects (by at least 1 pixel) being interpreted as a synapse. This was determined to be the case, as the maximum resolution of the Zeiss system (approx. 320μm) would not allow for accurate observation of the gap at the synaptic cleft (approx. 25μm) (Zuber et al., 2005), and instead we would expect to see overlap of both markers. This is exacerbated by the size of the primary-secondary antibody complex (single ABs approx. 10μm in length (Reth, 2013)), meaning the fluorophore is further from the antigen. When taken together, 1 pixel or greater overlap was deemed sensible for synaptic analysis.

Immunohistochemical work in mouse and post-mortem human spinal tissue was done similarly. Delineation of Rexed's laminae was completed using a standard mouse spinal cord anatomical atlas as reference (Watson et al., 2009). For clarity, lamina 8 contains a heterogenous population of ventral neurons including the medial MN pool, whilst lamina 9 contains the lateral MN pool. Thresholding was completed on a lamina-by-lamina basis in

these data sets in order to accurately detect all structures within each region without variability of expression between laminae causing dimmer puncta to be missed.

Statistics

Data processing was performed in Microsoft Excel. Statistical analysis and graph preparation were performed in both Excel and Prism 9 (Graphpad). Data was assessed for normality using the Shapiro-Wilk test, and when applicable for two-way ANOVAs, Geisser-Greenhouse corrected values were calculated as sphericity was not assumed. For datasets that contained missing values in a time course study (Chapter 3: Fig. 11 and 12), Prism 9 provides an alternative to a multi-factorial two-way ANOVA (which does not tolerate missing values and instead removes all values in that platedown). This is called a mixed effects analysis and was deemed as the most appropriate statistical test to maximise power with the data available. Two-way ANOVAs were conducted for all normalised synapse counts (Chapter 4: Fig. 18, 19 and 23), tissue E:I ratio quantification (Chapter 4: Fig. 21), synaptic mapping (Chapter 4: Fig. 21, Chapter 5: Fig. 29 and 30), tripartite mapping (Chapter 5: Fig. 29 and 30) and ephrin-B1 quantification (Chapter 4: Fig. 20). Multiple comparisons testing was done using either Šídák or Tukey corrections as recommended depending on the number of comparisons conducted. One-way ANOVAs were used for primary culture E:I ratios (between-subjects, Chapter 4: Fig. 18 and 19), post-mortem non-tripartite and tripartite synapse densities (between-subjects, Chapter 5: Fig. 31) and PSD properties of different synaptic subtypes (within-subjects, Chapter 5: Fig. 27). Unpaired T-tests were used for comparisons of iPSC-derived MN E:I ratios and adjusted E:I ratios (Chapter 4, Fig. 23), ALS MN quantification (Chapter 5, Fig. 28) and post-mortem PSD densities when ALS cases were considered one group (Chapter 5, Fig. 31). Statistical significance is denoted as follows: * = <0.05, ** = <0.01, *** = <0.001, **** = <0.0001.

6.7. Antibody Negative Controls

All presented immuno images were conducted alongside no primary negative controls in order to assure secondary antibodies were binding to their desired epitopes. Fig. 10 shows accompanying -ve controls for all demonstrated antibodies, which are white-matched within FIJI to their corresponding positive images to provide a representative level of fluorescence.

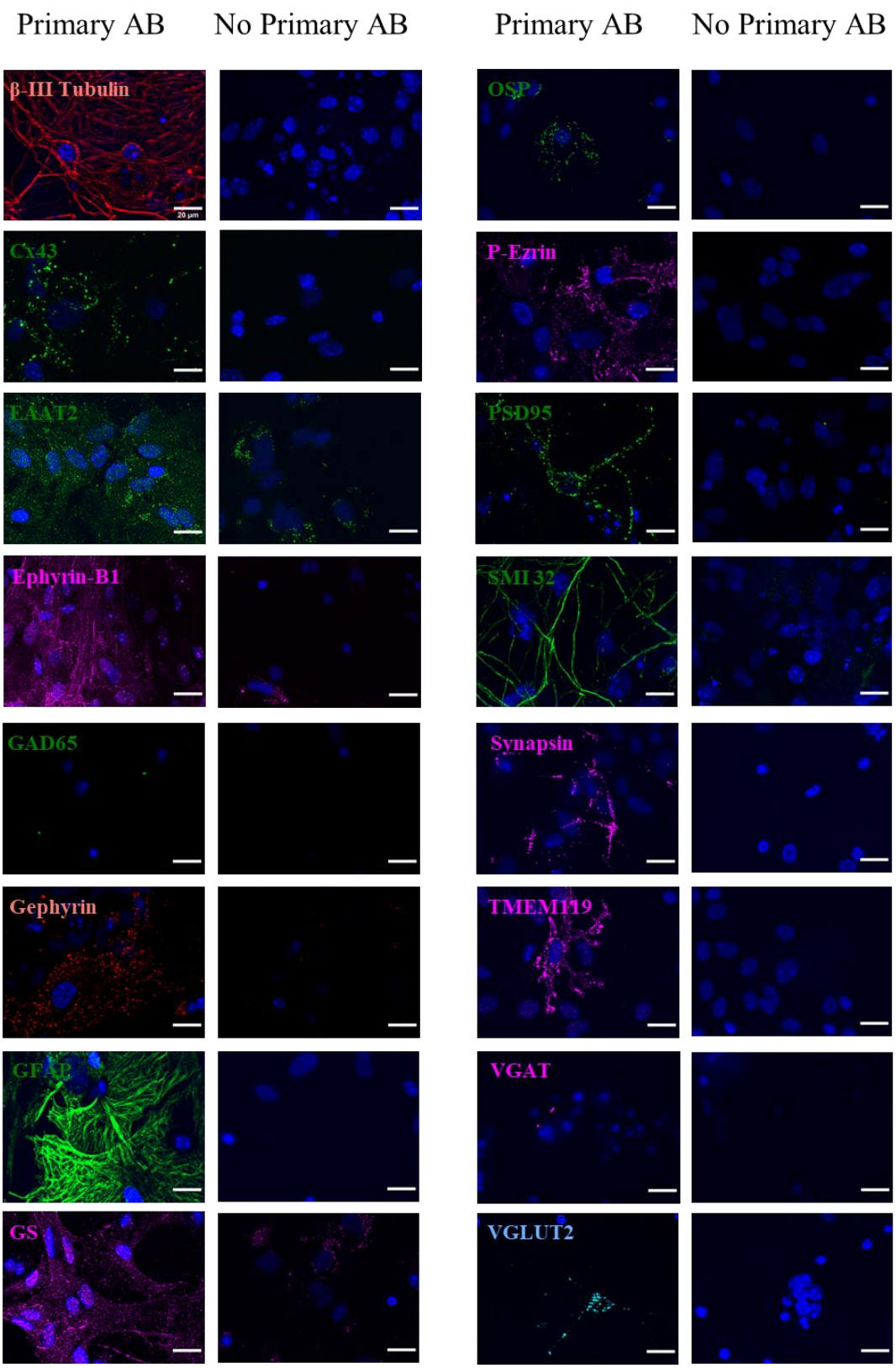

Figure 10: Images showing markers used, alongside no primary antibody controls *in vitro*. Images were taken in their relevant culture types (Primary Neurons: β-III Tubulin, Gephyrin, PSD95, Synapsin, SM1 32 and VGLUT2. Primary Astrocytes: Cx43, EAAT2, Ephrin-B1, GFAP, GS, OSP, P-Ezrin and TMEM119. iPSC-derived MNs: GAD65 and VGAT).

7. Electrophysiology

7.1.Whole-Cell Patch-Clamp Recordings

Coverslips were placed in a recording chamber with oxygenated artificial cerebral spinal fluid (aCSF) which was circulated at room temperature. Patch electrodes were pulled using a Sutter P-97 horizontal puller (Sutter Instrument Company) from borosilicate glass capillaries (World Precision Instruments), with accepted electrodes having a range of approximately 5-8MΩ resistance values. These were filled with Internal Recording solution before being placed on the rig. Cells were visualised using an Olympus upright BX51WI microscope equipped with a x40 submersion lens. Signals were amplified and filtered using a MultiClamp 700B amplifier (Axon Instruments) and acquired using a Digidata 1440A analogue-to-digital board with pClamp (Axon Instruments). In voltage clamp mode, whole-cell capacitance, input resistance and resting membrane potential were calculated using the seal test within pClamp. Clampfit 11 was used to visualise traces and aid in manual analysis.

7.2. Whole-Cell Patch-Clamp Solutions

aCSF:

NaCl (0.127M)
KCl (0.003M)
NaH_2PO_4 (0.00125M)
$MgCl_2$ (0.001M)
$CaCl_2$ (0.002M)
$NaHCO_3$ (0.026M)
Glucose (0.01M)

Equilibrated w. 95% O_2 and 5% CO_2, pH 7.45, osmolarity approx. 310mOsm.

Internal Recording Solution:

$KMeSO_4$ (0.14M)
NaCl (0.01M)
$CaCl_2$ (0.001M)
HEPES (0.01M)
EGTA (0.001M)
Mg-ATP (0.003M)
Sucrose (0.0025M approx.)
GTP (0.0004M)

pH 7.2-7.3, adjusted w. KOH, osmolarity adjusted to approx. 300mOsm w. sucrose.

Chapter 3

Novel Methodology for Producing Postnatal Spinal Co-Cultures of Astrocytes and Neurons for Use in the Study of ALS

Work within this chapter was completed with contribution from Dr. Sarah Burley and Dr. Vanya Metodieva

1. Introduction

As previously mentioned, a potential source of ALS-linked excitotoxicity is a shift in the ratio of excitatory : inhibitory synapses in the motor circuitry biasing it towards excessive excitation. We also know, however, that astrocytes have roles in synapse formation and maturation, and are actively associated with disease pathogenesis (Hama et al., 2004; Garrett and Weiner, 2009; Zhao et al., 2020). Taken together, it is conceivable that the roles of astrocytes may be perturbed in ALS in a way that could drive biases in E:I synaptic ratios. Investigating the progress of neurodegeneration in the whole spinal cord gives us a complete system with which we can monitor changes in different cell types. What is more challenging, however, is the ability to manipulate certain properties of particular cell types in a controlled environment. In the context of disease research, this includes investigating non-cell autonomous effects by altering the characteristic of one cell type and monitoring its effects on another. To probe this, we need to be able to separately manipulate the genotype of both astrocytes and neurons in order to understand if any synaptic changes which we may see are due to the neurons alone, or are due to the presence of ALS astrocytes. Due to our access to multiple ALS mouse lines ($SOD1^{G93A}$ and C9BAC500), spinal primary culture is a promising tool with which to investigate these putative changes.

Embryonic tissue has long been relied upon as a source of viable spinal neurons *in vitro*. This is due to challenges in dissociating spinal neurons postnatally and ensuring their survival in culture, as these cells seem to be particularly vulnerable to cell death (Ransom et al., 1977; Mikhailova et al., 2019). Culturing postnatal spinal cells, however, has some key advantages over embryonically derived tissue. These include 1) preservation of the mother (who can go on to produce more pups thus reducing animal use), 2) ability to genotype pups before beginning the protocol, thus allowing for easy culturing of separate genotypes, 3) ease of

dissection of larger animals, improving quality of utilised tissue and 4) cultured cells are intrinsically more ‘mature’ from a postnatal animal, and are derived from animals at an age when many key cellular changes have been observed in ALS mouse models (Van Zundert et al., 2008; Quinlan et al., 2011). This last point is of particular interest, as it allows for data produced from such a model to be directly comparable to established neonatal ALS literature.

Culturing postnatal spinal cells has been described previously, with a multitude of caveats and varying degrees of success in yields and specificity. Adult lumbar sensory neurons derived from the DRGs of 6 month and 2 year-old mice were successfully cultured for up to 29 days, aided by the concentration-dependent neuroprotective effects of nerve growth factor (Jiang and Smith, 1993). Other than producing primary cultures of these peripheral cells, other early efforts to produce spinal cultures involved production of organotypic preparations. Lumbar slice cultures from P8 rat pups have been successfully produced, being kept for up to 3 months. Such a culture allows for survival of both small dense neurons in the dorsal horn, and large ChAT +ve MNs in the ventral horn (Rothstein et al., 1993). A similar protocol has been used to maintain slice cultures from P1/2 mice, with the aid of a cocktail of neurotrophic factors used to increase MN viability (Rakowicz et al., 2002). The obvious caveat of such a preparation is that it does not allow for the isolation of specific cell types, and instead, allows for the maintenance of a semi-physiological representation of the lumbar spinal cord (depending on the survival of individual cell types). This limits the ability to pursue questions regarding non-cell autonomous effects of disease.

Isolation of individual spinal neurons has been attempted also. Kehl and colleagues (1997) successfully dissociated and cultured cervical spinal cord cells from P15/16 rats. Cultures could be maintained for up to 28 days, and neurons were confirmed with the presence of the

neuron specific tubulin isoform, β-III tubulin (Sullivan, 1988). These were found in addition to astrocytes, tagged with GFAP. This showed that isolation of postnatal spinally derived neurons is possible, however, isolation of individual cell types was not achieved which is required for investigation of cell non-autonomous effects. This protocol also required the use of media conditioned by separate cultures of astrocyte-rich foetal cortical monolayers, which is additionally labour intensive.

Later work has attempted to separately culture postnatal spinal neurons and glia. In particular, efforts have been made to culture MNs specifically. A protocol by Milligan and Gifondorwa (2011) used anesthetised P30 mice to collect the lumbar spinal cord. Such a protocol shares a few details with our final methodology, such as choice of dissociation enzyme (papain) and removal of nerve roots and meninges to aid purification of the final cell types. This method, however, relies on use of an Optiprep density gradient with three centrifugation steps, prolonging total dissociation time and potentially reducing cell viability. Production of ChAT +ve MNs was achieved, but cell yield was very low, producing just 10000-40000 cells per adult spinal cord. A later protocol successfully produced higher yields of MNs using considerably older mice (5 m.o) (Beaudet et al., 2015). This protocol also used an anti-mitotic agent, in this case arabinosylcytosine (AraC) to eliminate excess proliferating astrocytes in their neuronal cultures. Use of such an anti-mitotic agent was replicated in our optimised protocol to aid in the purification of spinal neural cultures. While isolation of pure MN cultures is a useful tool for studying single-cell properties and MN-specific perturbations, these cultures lack a more heterogenous spinal neuron population that is desired for investigation into formation of E:I bias in the spinal circuitry as a whole.

Finally, a couple of groups have attempted to produce more mixed neuronal populations. Freeman and colleagues (2015) successfully cultured mixed spinal neurons from P2-3 mice, relying on isoflurane exposure before decapitation. Again, an optiprep density gradient was used to isolate the neurons with AraC being added to prevent astrocytic replication. Cells were only maintained for 7-10 days, however, so longer-term viability was not validated. Eldeiry and colleagues' (2017) protocol shares many similarities with an isofluorane kill, use of papain for cell dissociation, multiple trituration steps and reliance on an optiprep gradient with multiple centrifugation steps. The authors only state neurons are considered 'mature' at 7 days, and again do not show their capability to be maintained over longer experimental durations.

Our aim therefore, was to produce cultures of both postnatal astrocytes and mixed spinal neurons, avoiding some of the drawbacks of previous protocols. We aimed to create a methodology which:

1. Does not involve the use of isoflurane during animal sacrifice, which reduces total protocol length, improves animal welfare and avoids known electrophysiological changes induced by anaesthetic administration (De Sousa et al., 2000).
2. Is as rapid as possible, allowing for same-day genotyping of an experimental litter.
3. Does not rely on a density gradient with multiple centrifugation stages, which adds significant time to the protocol and may reduce neuron viability.
4. Produces neuron cultures which can be maintained for multiple weeks, allowing production of functionally and structurally mature cells which can be used in time-course studies.

2. Results

2.1. Primary Astrocyte Cell Purity Verification

Our first goal was to validate the production of both astrocytes and neurons, before confirming we can combine them to produce our desired co-culture model. First, we aimed to characterise our astrocyte cultures in multiple ways; A) by checking for expression of validated astrocyte-specific proteins, and B) by investigating markers indicative of the functional maturity of the astrocytes produced. This characterisation was done over 2-6 weeks DIV, with 2W being the earliest astrocytes became confluent enough in flasks to be passaged and replated onto coverslips, and 6W being a time point beyond which astrocytes became too dense and regularly peeled off coverslips.

Qualitatively, when observed down a standard compound microscope, cells could be broadly divided into two known morphologies described previously. The majority of cells displayed a flat, round morphology indicative of protoplasmic astrocytes, while there was also those with a more elongated morphology which were likely fibrous astrocytes (Sofroniew and Vinters, 2010). To verify they were indeed astroglia, two common immunocytochemical markers for astrocytic identity were used. GFAP is an intermediate filament expressed almost exclusively in astrocytes (Hol and Pekny, 2015; Liddelow and Barres, 2017), while glutamine synthetase (GS) is an enzyme critical in the recycling of glutamate and is thought to be the most general astrocyte marker, being expressed by all astroglial subtypes (Anlauf and Derouiche, 2013). To check these cells are likely functionally mature and reflective of their *in vivo* counterparts, we also tracked expression of two key proteins which are known to be upregulated after birth and are key to astrocytes being able to fulfil their physiological roles in the spinal cord. These include excitatory amino acid transporter 2 (EAAT2), which transports excess glutamate

from the synaptic cleft into the cell to be recycled, and Connexin 43 (Cx43), a component of the astrocytic gap junction enabling the formation of the astrocyte network (Yang et al., 2013) (see Fig. 11A). As ALS has been suggested to be a disorder in which accelerated maturation could drive disease pathogenesis (Quinlan et al., 2011), we also investigated whether there may be differences in developmental expression of these functional proteins in cells harbouring the C9BAC500 insertion.

GFAP showed the expected fibrillar expression, producing networks of complex elongated structures. Fluorescence intensity was slightly variable, likely a result of differential levels of astrogliosis between cells, in addition to potential differences in astrocytic subtypes (Hol and Pekny, 2015). GS showed a much more diffuse expression throughout the cell, punctuating cell boundaries in a fashion similar to that described previously (Anlauf and Derouiche, 2013) (see Fig. 11B). The proportion of cells expressing GFAP at 2-6W was analysed in C9BAC500 versus control using a mixed effects analysis (see Materials and Methods) (see Fig. 11C). No significant main effect of genotype was found ($F(1,6)=0.1589$, $P=0.70$), indicating the presence of the C9orf72 repeat expansion did not affect the proportion of GFAP +ve cells present. There was, however, a significant main effect of time ($F(2.168, 11.93)=9.668$, $P=0.0028$). Cells at 2W showed a higher proportion of GFAP +ve cells compared to 3W ($P=0.0057$), 4W ($P=0.0455$) and 6W ($P=0.0242$), with another slight peak at 5W (5W vs 3W ($P=0.0216$), 5W vs 4W ($P=0.0293$) and 5W vs 6W ($P=0.0258$). The highest proportion at 2W may be due to it being closer to the day of dissection which likely induced a large amount of reactive astrocyte activation during tissue dissociation, thus producing more cells with a detectable GFAP expression level.

A

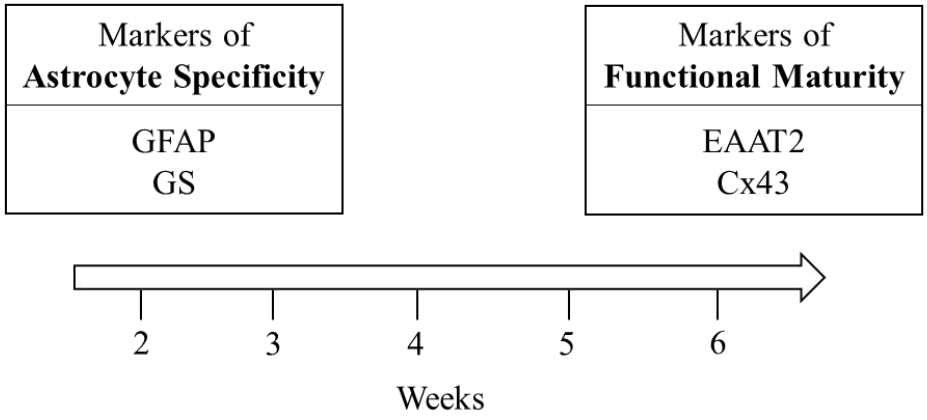
Markers of
Astrocyte Specificity
GFAP
GS
Markers of
Functional Maturity
EAAT2
Cx43
2
3
4
5
6
Weeks

B

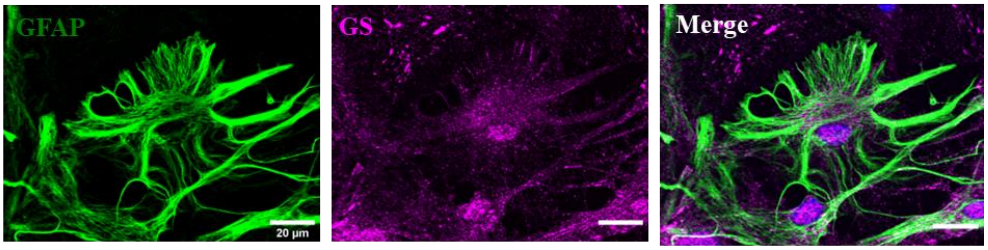
GFAP
GS
Merge
20 µm

C

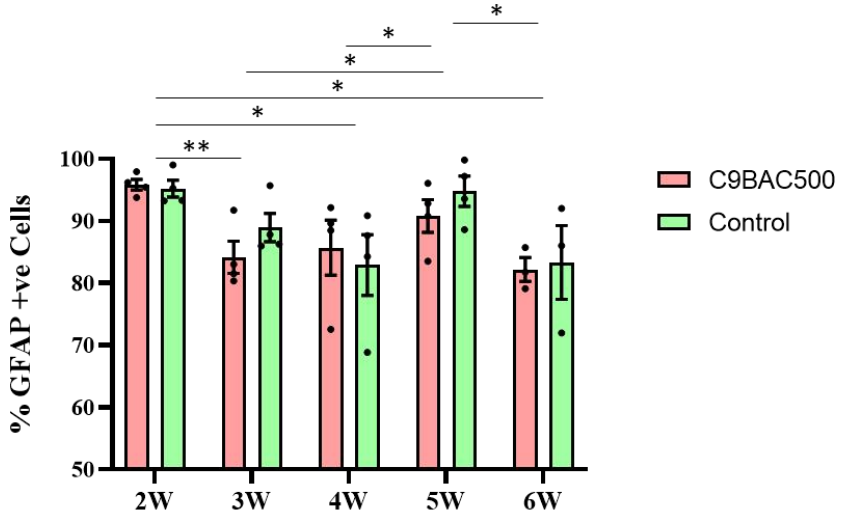
% GFAP +ve Cells
100
90
80
70
60
50
2W
3W
4W
5W
6W
C9BAC500
Control

D

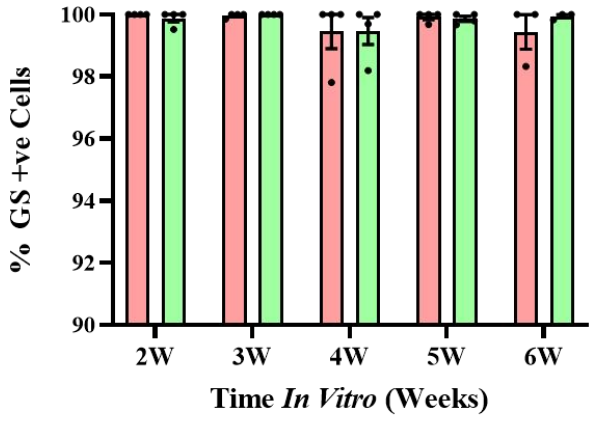
% GS +ve Cells
100
98
96
94
92
90
2W
3W
4W
5W
6W
Time *In Vitro* (Weeks)

Figure 11: **A**) Schematic demonstrating characterisation of primary astrocytes from 2-6W. This includes quantification of astrocyte specificity, and multiple markers of functional maturity required for normal physiological function. **B**) Images showing expression of 2 specific astrocyte markers, GFAP and GS, along with DAPI in the merged image. **C**) Graph demonstrating % cells +ve for GFAP from 2-6W in cells derived from C9BAC500 mice vs control littermates (N=3-4). **D**) Graph demonstrating % cells +ve for GS from 2-6W in cells derived from C9BAC500 mice vs control littermates (N=3-4). **NOTE** Astrocyte protocol initially based on different brain methodology kindly shared by Dr. Vanya Metodieva.

GS expression meanwhile was consistently seen in the vast majority of cells, showing very little variability and providing further evidence that it is likely the most robust marker of all astrocyte subtypes. In a mixed effects analysis, there were no significant effects of genotype ($F(1,6)=0.1585$, P=0.70) or time ($F(1.706,9.385)=1.429$, P=0.28) (see Fig. 11D). Taken together with evidence from both markers, we conclude that our glial cultures are highly enriched in astrocytes (82-95% GFAP +ve, >99% GS +ve) and contain an appropriate proportion with which to study their non-cell autonomous effects on neurons.

2.2. Primary Astrocyte Functional Maturity Marker Analysis

Next, we assessed the development of essential functional markers of maturity: Cx43 and EAAT2. Cx43 is a component of astrocytic gap junctions, and shows expression consistent with this, forming large punctate structures seen across the surface of the cell (see Fig. 12A). Expression was quantified using integrated intensity as a measure, which gives the sum of the pixel intensity for all pixels in an identified object. This therefore gives us a measure of total protein expression in an identified object, as it takes into account object size as well as fluorescence intensity (a measure of protein 'concentration' at a set point). Immunohistochemical quantification has been shown to provide a reliable measure of protein expression and has been successfully correlated with other techniques, including western blot and ELISA (Guirado et al., 2018). Expression of Cx43 is evident from our earliest 2W timepoint, and there is no significant difference across our developmental timescale ($F(1.630, 8.967)=3.007$, P=0.11), however, there does appear to be a trend towards lower expression at 2W. There was also no effect in expression as a result of the presence of the C9orf72 expansion ($F(1,6)=0.1969$, P=0.67) (see Fig. 12B).

A

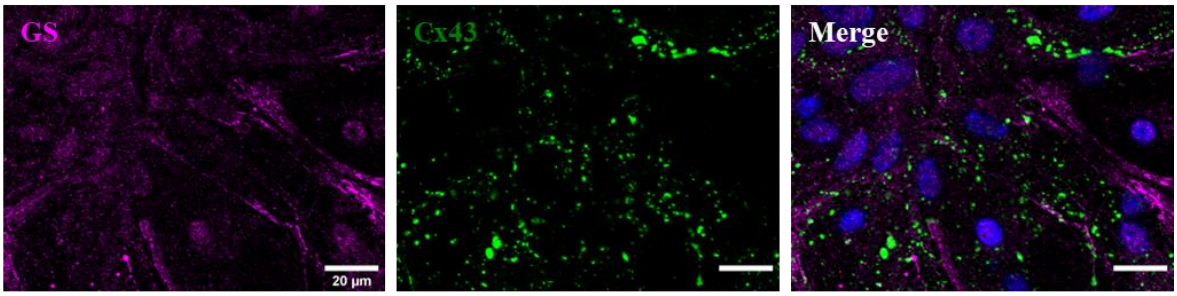
GS
Cx43
Merge
20 µm

B

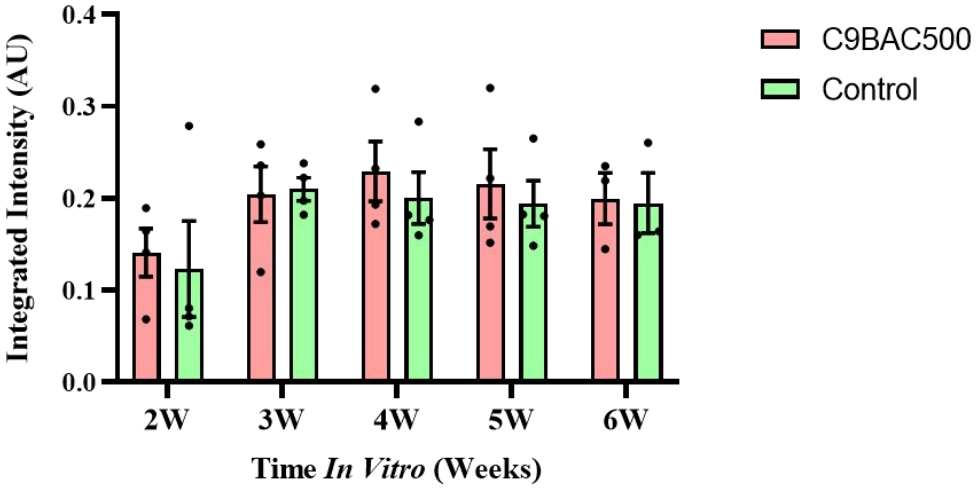
Integrated Intensity (AU)
0.4
0.3
0.2
0.1
0.0
2W
3W
4W
5W
6W
Time *In Vitro* (Weeks)
C9BAC500
Control

C

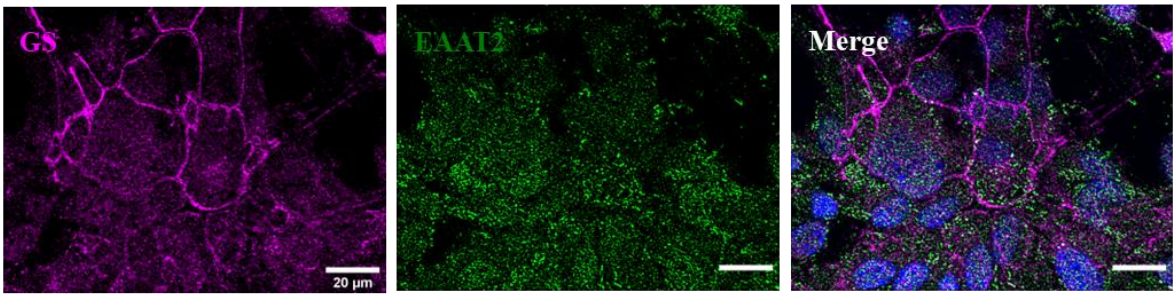
GS
EAAT2
Merge
20 µm

D

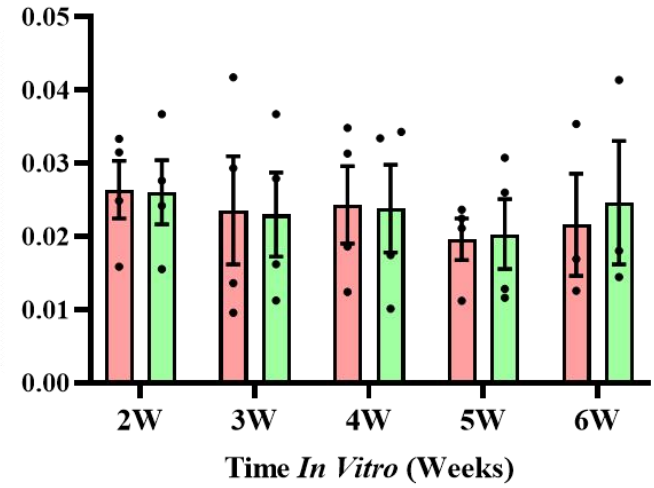
0.05
0.04
0.03
0.02
0.01
0.00
2W
3W
4W
5W
6W
Time *In Vitro* (Weeks)

Figure 12: **A**) Images showing expression of GS in primary astrocyte culture, along with functional marker of maturity Cx43. DAPI shown in merged image. **B**) Graph demonstrating integrated intensity of Cx43 in primary astrocytes from 2-6W derived from mice harbouring the C9BAC500 insertion vs control littermates (N=3-4). **C**) Images showing expression of GS in primary astrocyte culture, along with functional marker of maturity EAAT2. DAPI shown in merged image. **D**) Graph demonstrating integrated intensity of EAAT2 in primary astrocytes from 2-6W derived from mice harbouring the C9BAC500 insertion vs control littermates (N=3-4).

EAAT2 meanwhile shows a more diffuse expression throughout the cell (see Fig. 12C). Both EAAT2 and GS appear to display some nuclear staining in addition to their expected expression patterns. Both primary antibodies were validated in spinal tissue (see Chapter 5, Fig. 24C). GS also shows clear morphological features that would not be present in random binding, and primary astrocyte nuclear localisation has been noted using both markers previously (Anlauf and Derouiche, 2013; Varini et al., 2012). Therefore, while this may represent some non-specific nuclear binding, future work could use western blotting to definitively confirm fluorescence reflects true protein expression. Quantification revealed reasonably invariable expression across our time points ($F(1.767,9.717)=2.605$, P=0.13), again showing consistent expression of a key functional marker from 2W DIV. Once again, cells cultured from our C9BAC500 mice showed no difference in expression when compared to those cultured from control littermates ($F(1,6)=0.004004$, P=0.95) (see Fig. 12D). From these analyses, we can deduce that our primary postnatal astrocytic cultures express markers indicative of physiological maturity from 2W, allowing for subsequent plating of neurons in a flexible timeframe. This aids in the practicality of the protocol, as variable breeding timescales can result in litters being born slightly outside of expected dates. In addition, we see no evidence of altered maturation of astrocytes in our C9BAC500 cultures, providing no evidence of developmental shifts in this mouse model of ALS.

2.3. Analysis of Contaminating Glia in Astrocyte Cultures

Although we have validated that the vast majority of cells in our glial cultures were indeed astrocytes, we wanted to further characterise these by looking for the presence of other common CNS glia. In particular, we aimed to look for the presence of oligodendrocytes and microglia. In order to do this, we selected appropriate markers known to be selectively expressed by these cell types. In the case of oligodendrocytes, we selected oligodendrocyte-

A

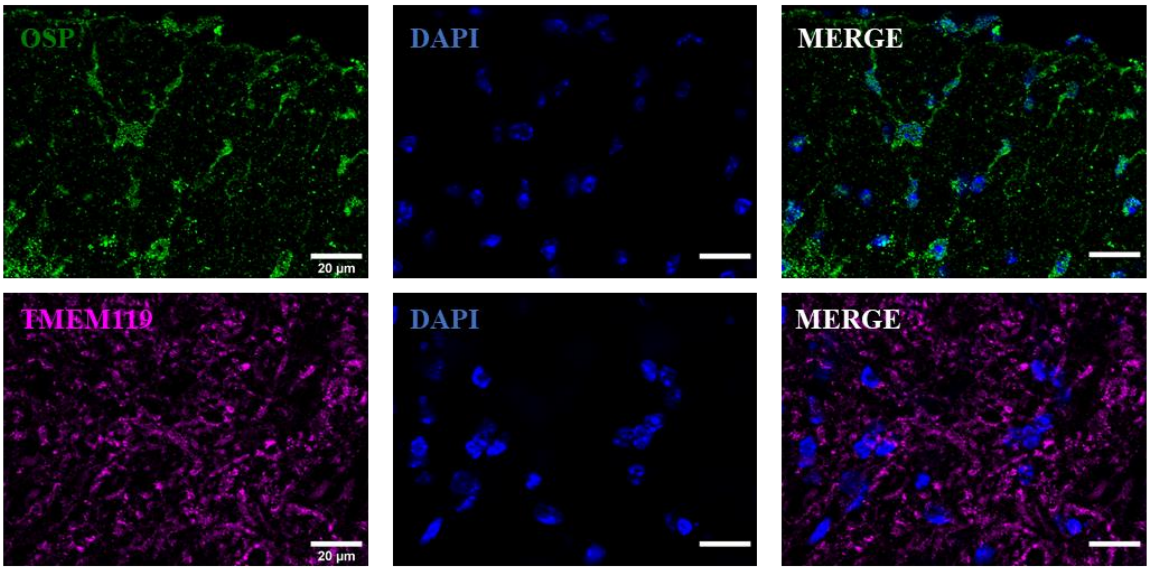

B

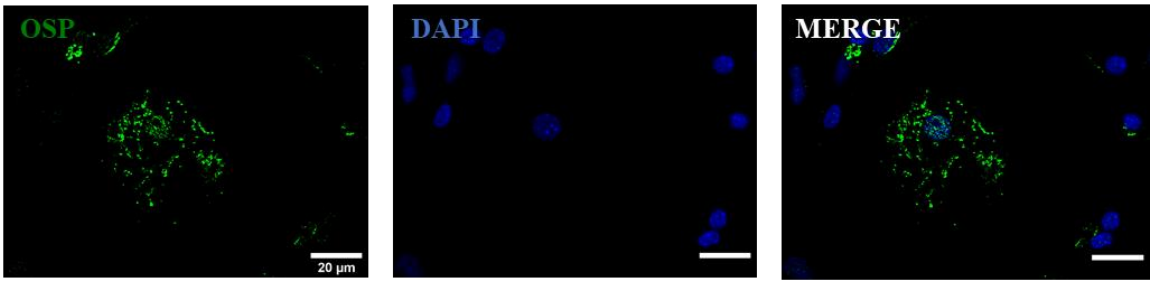

Oligodendrocyte Marker	% Positive Cells	% Error +/-
OSP	0.6	0.6

C

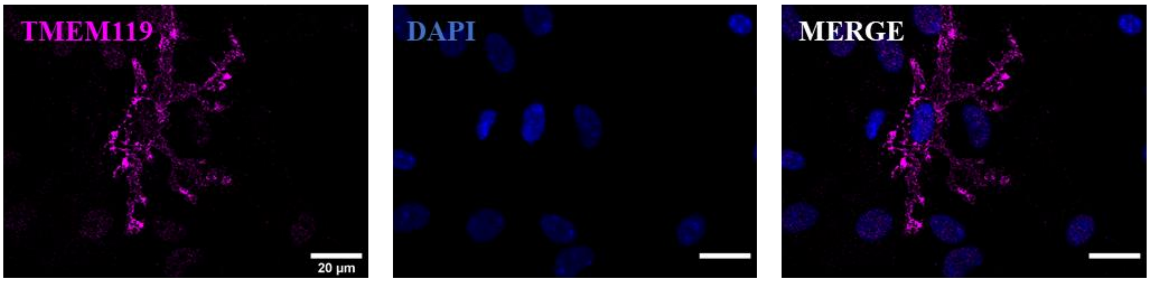

Microglia Marker	% Positive Cells	% Error +/-
TMEM119	2.9	1.2

Figure 13: **A**) Positive control images for OSP and TMEM119 in 3–4-month-old mouse spinal tissue. OSP imaging is focussed on the white matter, whilst TMEM119 is seen clearly throughout the grey matter. **B**) Example image of OSP +ve cell in 6W glial culture, along with quantification of +ve cell frequency (N=3 plate downs). **C**) Example image of TMEM119 +ve cell in 6W glial culture, with quantification of +ve cell frequency (N=3 plate downs).

specific protein (OSP), a protein known to be selectively expressed in mature oligodendrocytes which shows strong co-localisation with other classical oligodendrocyte markers such as myelin basic protein (Bronstein et al., 1996; Michalski et al., 2018). For microglia, we selected TMEM119, a validated, robustly expressed microglial marker which has the advantage of not being expressed by other immune cells such as macrophages (Bennett et al., 2016).

Due to our finding that astrocytic cultures are greatly enriched in our desired cell type, it was suspected that oligodendrocytes and microglia would be infrequent. In order to be certain that this infrequency was genuine, and was not simply a result of unreliable antibodies, we first used spinal tissue as a positive control to validate the binding of our antibodies. For oligodendrocytes, we focussed on the white matter as this is where we would expect them in high frequency. We observed numerous OSP +ve cells with branched, elongated morphologies throughout the white matter (see Fig. 13A). Microglia meanwhile were targeted in the grey matter where they are frequent. Here we observed robust TMEM119 staining with branching, blob-like morphologies (see Fig. 13A).

Satisfied that our antibodies were functional, we analysed oligodendrocyte and microglia frequencies in enriched astrocyte cultures at 6W, assuming any contaminating cell types would be at their highest frequency at our latest time point due to microglia's proliferative ability (Tan et al., 2022). OSP +ve cells were incredibly infrequent (0.6% $\pm$ 0.6% SE), with only 1 of 3 plate downs showing any clear immunocytochemically tagged putative oligodendrocytes (see Fig. 13B). It should be noted, however, that only cells with clear oligodendrocytic morphology were counted in this quantification, with some cells showing small fluorescent puncta that could have been lipofuscin. The cells that were identified

showed a branched web-like morphology as described by other protocols attempting to create pure cultures of mature oligodendrocytes (Amaral et al., 2015). It is possible, however, that surviving postnatal OPCs are present, which would not be tagged by our antibody due to OSP only being expressed by mature myelinating oligodendrocytes (Bergles and Richardson, 2016; Michalski et al., 2018). Therefore, it could be the case that the small punctate structures highlight developing oligodendrocytes, upregulating OSP after changing from OPCs. TMEM119 +ve putative microglia were slightly more common than oligodendrocytes, representing 2.9% $\pm$ 1.2% of cells counted. These cells showed expected blob-like, branched morphologies as can be seen in Fig. 13C. Together, we can conclude that oligodendrocyte and microglial populations are negligible in our postnatal primary glial cultures.

2.4. Primary Neuron Culture Characterisation

Next, we moved onto our postnatal spinal neuron cultures. This protocol is designed to be used in co-culture to look at astrocytic effects on synaptogenesis throughout the spinal circuitry, so we aimed to produce a mixed lumbar neuronal population, and not just one containing MNs. There are several things we wanted to verify in these cultures; A) we wanted to validate that we have a relatively pure neuronal population, B) that some of these cells are MNs, C) that they express synaptic markers and D) that they are physiologically functional.

When viewed down a compound microscope, cells show long processes and tend to aggregate into clumps, indicative of neurons in culture. β-III tubulin, an isotype of the β-tubulin protein that forms dimers with α-tubulin to produce microtubules, is a specific marker used extensively to visualise mature neurons (Sullivan, 1988). This was utilised on our primary neural cultures, revealing large amounts of β-III tubulin +ve processes. SMI 32 is a

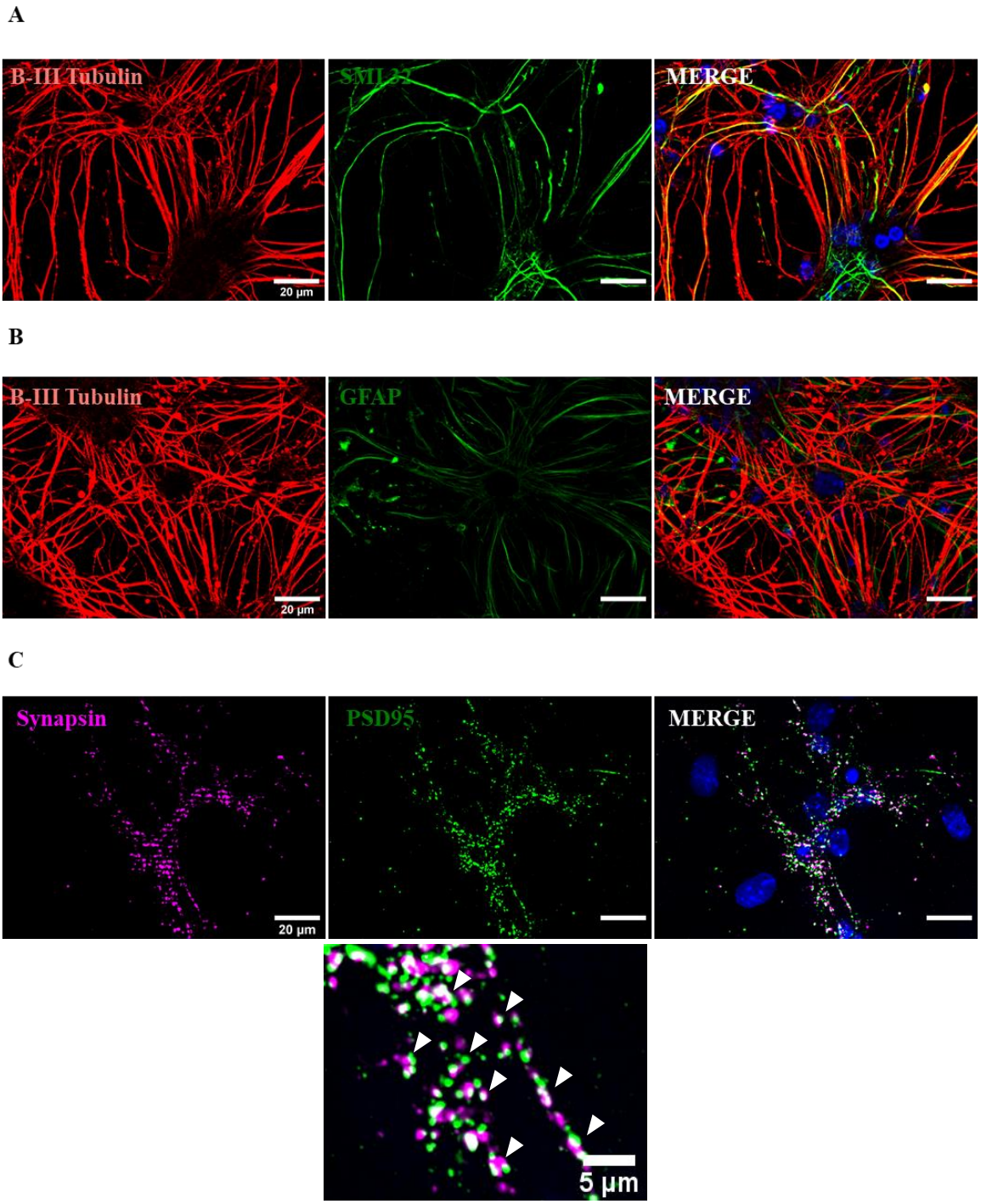

Figure 14: **A**) Images showing postnatal spinal neuronal cultures at DIV 2-3W. B-III tubulin +ve mixed neuron populations are clear, whilst SMI 32 +ve putative MNs are also present. **B**) Images showing the same cultures, with dense B-III tubulin +ve neurons present, as well as the presence of sparse GFAP +ve astrocytes. **C**) Images showing neuronal cultures tagged with the presynaptic marker synapsin and postsynaptic density marker PSD95 (AB). Significant numbers of co-localised puncta show areas of dense synapses, notated with white arrows. **NOTE**: Dissociations displayed here were completed jointly by Calum Bonthron and Dr. Sarah Burley. Immunocytochemistry and imaging were conducted by Calum Bonthron.

marker of non-phosphorylated neurofilament H, and is known to be enriched in spinal MNs (Carriedo et al., 1996; Tsang et al., 2000). A subset of cells showed SM1 32 +ve processes, which strongly co-localised with β-III +ve cells and represented putative MNs (see Fig. 14A).

In addition to this, we wanted to check that the number of contaminating astrocytes in our neuronal cultures was relatively low. Down a compound microscope, comparatively infrequent large astrocytes (showing large flat morphologies indicative of protoplasmic astrocytes as described earlier) could usually be observed in the background. When GFAP was used to identify astrocytes in our neuronal culture, usually in a x63 magnification field of view there would be 1-3 astrocytes (mean = 2.2 astrocytes in 10 fields of view) (seen here at 2W, see Fig. 14B). These showed extended GFAP +ve processes which did not co-localise with β-III tubulin +ve processes. This is typical of astrocytes at very low densities, as they are able to extend their cell boundaries, producing wide, web-like GFAP expression (see Fig. 11B for comparison of dense astrocytic culture). It was noted during development of this protocol that astrocytes were unable to be removed completely due to excessive U/FDU treatment also causing neuronal toxicity (Hui et al., 2016), and due to their ability to proliferate. However, as the goal was to create a co-culture of neurons plated on top of a dense layer of astrocytes in order to control the genotype of both separately, we find it unlikely that the few remaining astrocytes would have a significant effect on neuronal properties being investigated, as the monolayer astrocytes vastly outnumber these and should produce clear non-cell autonomous effects if they are present.

As we aim to use this protocol to investigate non-cell autonomous effects of astrocytes on synapse formation, we looked for expression of pre- and postsynaptic markers. Synapsin-I,

hereon referred to as simply ‘synapsin’, is a presynaptic bouton protein found in the vast majority of neurons where it has roles in synapse formation and modulation of neurotransmitter release (Mirza and Zahid, 2018). PSD95 is a major scaffolding protein found at the postsynaptic density (PSD), where is acts to aid organisation of essential neurotransmitter receptors, amongst other PSD proteins (Keith and El-Husseini, 2008). Immunocytochemical targeting of these proteins revealed abundant expression of synapsin and PSD95. What was key, however, is that they often showed a degree of co-localisation. As we are visualising proteins at the pre- and postsynaptic densities, these regions of overlap can be interpreted as synapses. (see Fig. 14C).

We can conclude therefore that we have produced enriched neural cultures which contain a subset of SMI 32 +ve MNs, and that these neurons show structural evidence of excitatory synapse formation. However, we also wanted to validate that our cells are physiologically indicative of neurons, in addition to showing expression of protein markers we would expect. To do this, we grew spinal neuron cultures for multiple weeks and conducted whole-cell patch-clamp recordings on them to validate a number of physiologically relevant parameters (data described here derives from 3 plate downs). Although cells could be patched at 2W, we found they did not reliably fire action potentials (APs) in response to current steps, and often lacked significant Na^+- and K^+-mediated currents. At 3W, however, they more reliably produced evidence of electrophysiological activity. All subsequent data described is therefore from this time point.

First, passive properties of our neuronal cultures were investigated (see Fig. 15A). Properties indicative of cell size include capacitance (directly proportional to cell size) and resistance (inversely proportional to cell size). Mean capacitance was 32.07 $\pm$3.08pF, whilst mean

A

Passive Property	Value	Error
Capacitance	32.07 pF	+/- 3.08 pF
Membrane Resistance	378.45 MΩ	+/- 69.76 MΩ
Resting Membrane Potential (RMP)	-53.84 mV	+/- 2.81 mV

B

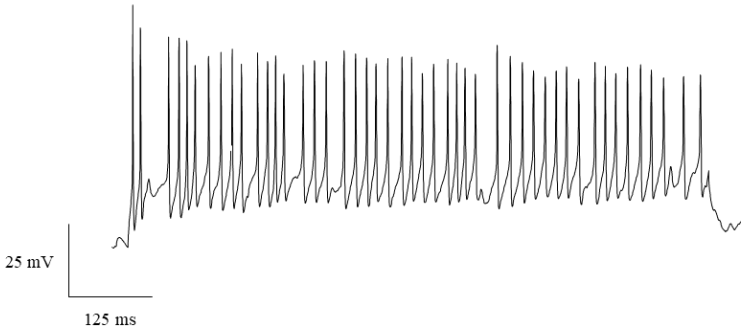

C

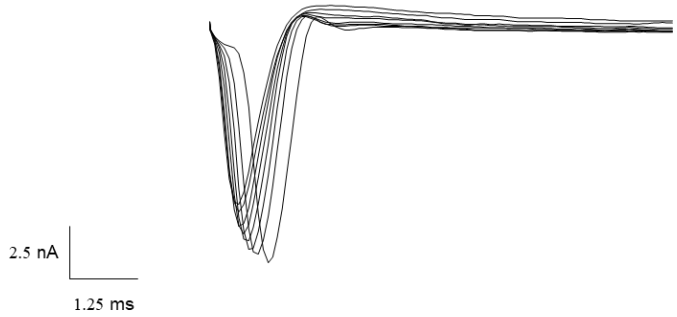

D

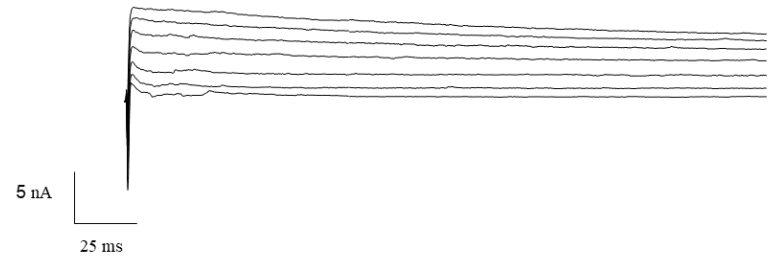

E

F

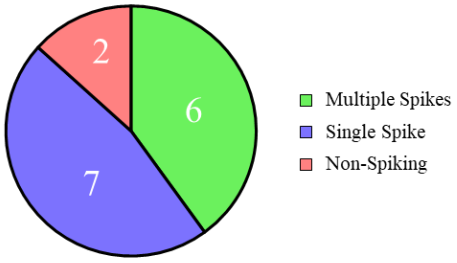

G

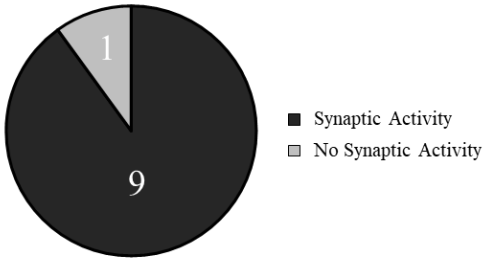

Figure 15: **A**) Passive properties of neuronal monocultures at DIV 3W (N=16). **B**) Whole-cell patch-clamp recording showing example trace of APs elicited by 1s current pulse. **C**) Example of voltage-gated recording showing Na^+-mediated currents. **D**) Example of voltage-gated recording showing K^+-mediated currents. **E**) Example of spontaneous synaptic activity recorded in voltage-clamp mode. **F**) Pie chart demonstrating the proportion of cells which could fire either multiple spikes, single spikes, or no spikes in response to increasing current pulses (N=15). **G**) Pie chart demonstrating the proportion of cells receiving spontaneous synaptic input versus no clear synaptic input in a 120s gap-free recording in voltage-clamp mode (N=10). **NOTE**: Dissociations were completed jointly by Calum Bonthron and Dr. Sarah Burley. Whole-cell patch-clamp recordings conducted by Sarah Burley. Analysis performed by Calum Bonthron.

membrane resistance was 378.45 ± 69.76MΩ. Resting membrane potential (RMP) showed a physiologically appropriate value of -53.84 ± 2.81mV (N=16 cells). Next, we wanted to assess our neurons' ability to fire APs. A current step protocol in which cells were held at -60mV and 1s current pulses (10-50pA depending on behaviour of cell) were applied allowed us to investigate their firing behaviour. An example of spiking behaviour can be seen in Fig. 15B. The maximum firing activity seen in our cultures was 47 Hz.

The majority of cells could fire one or more APs, with only 2/15 cells (13.3%) being unable to do so. 7/15 cells (46.7%) fired a single spike, whilst 6/15 (40%) were able to fire multiple (see Fig. 15F). Related to spiking activity, key currents involved in the generation of APs include Na^+- and K^+-mediated currents. In voltage-clamp mode, these currents can be assessed using a protocol whereby cells are held at a range of voltages and the resultant currents observed. In the case of Na^+-mediated currents, cells were held for 10ms, moving from -10mV to 80mV with increments of 2.5mV. Fig 15C demonstrates an example of fast-inactivating Na^+-mediated inward currents. The vast majority of cells displayed Na^+-mediated currents in excess of 1nA (14/16 cells, 87.5%). The cells which had very low inward currents also failed to fire APs in response to current injection. The protocol to reveal persistent, outward, likely K^+-mediated currents utilised 500ms voltage steps from -10mV to 100mV, with increments of 10mV. An example of K^+-mediated currents is demonstrated in Fig 15D. Of the cells measured, 14/15 cells (93.3%) showed large K^+-mediated currents in excess of 1nA. Together, the high proportion of cells showing these essential currents in combination with equally high numbers being able to fire at least 1 AP in response to stimuli gives us confidence that our neurons are capable of being physiologically active *in vitro*.

Of significant interest was also evidence of synaptic activity in these cultures. As mentioned in Fig. 14, we see expression of synaptic proteins in our neural cultures. However, we also wanted to provide physiological evidence that these cultures have active synapses *in vitro*. To do this, we recorded for 120s in voltage-clamp mode holding the cells at -60mV for evidence of spontaneous synaptic activity, indicated by the presence of postsynaptic currents (PSCs). The majority of inputs are likely excitatory, indicated by downward deflections as can be seen in Fig. 15E. As the number of PSPs can be affected by multiple factors including; synapse density, neuron survival (and therefore density) and overall activity of the network, we chose to define the presence of synaptic input in a binary fashion (i.e. evidence of any PSPs during the duration of 120s recording). Of the 10 cells recorded, we observed some evidence of spontaneous synaptic activity in 9 (90%) (see Fig. 15G).

When considered together, we have shown that our cultures express proteins indicative of a neural identity, but have also characterised their functional properties. Considering that the majority of cells recorded showed the ability to fire action potentials in response to current input, had significant Na^+- and K^+-mediated currents, and received some form of spontaneous synaptic input, we consider our neurons functionally mature and are confident in their identity. As we begin to see reliable evidence of synaptic transmission at 3W, these data also indicate that this is an appropriate time point in our subsequent study to investigate E:I ratio changes in the context of disease.

2.5. Primary Neuron / Astrocyte Co-Culture Validation

After we were confident we had characterised our individual cell types, we next wanted to show we could co-culture them together. Neurons were plated on top of an astrocytic monolayer typically at DIV 2-3W (as shown earlier, astrocytes display suitable expression of

functional proteins in a wide timescale). These were then immunocytochemically tagged for neuron-specific marker β-III tubulin and astrocyte-specific marker GFAP. Z-stacks were then taken, descending through the Z-dimension to capture neurons atop the astrocyte layer. Although in some cases astrocytes had been in culture for up to 6 weeks, so extensive proliferation meant they no longer existed in perfect monolayers and began to grow on top of each other, Z-stacks demonstrated bright β-III tubulin +ve neurons with faint GFAP +ve processes present in a lower focal plane. As we descended, neural processes became faint as the dense GFAP +ve astrocytic layer came into focus (see Fig. 16A). We were therefore confident the vast majority of astrocytes seen in our co-cultures belonged to the original plated monolayer.

As discussed earlier, the aim of developing this culture system was to use it to look at astrocytic non-cell autonomous effects on synaptogenesis, in particular looking for changes in the ratio of excitatory : inhibitory synapses. Neuronal validation already showed that in monoculture, they express the generic presynaptic marker synapsin, as well as glutamatergic postsynaptic density protein PSD95. Although traditionally referred to as ‘symmetric synapses’ due to a lack of an obvious EM-dense PSD, more recent work has indicated that inhibitory synapses indeed contain a thin postsynaptic sheet structure also, with a key molecular scaffolding protein called gephyrin. Here it acts to anchor and cluster GABA and glycine receptors, as well as interacting with a multitude of signalling molecules (Bai et al., 2021; Tyagarajan and Fritschy, 2014). As such, it is an ideal candidate for a postsynaptic marker we can use to quantify inhibitory synapse density. Figure 16B demonstrates a co-culture, whereby we see expected dense punctate expression of our presynaptic marker synapsin, as well as our glutamatergic postsynaptic marker PSD95. Gephyrin shows a similar expression, abundantly present down neuronal processes and onto what appears to be the

soma. Synapsin shows considerable co-localisation with both our excitatory and inhibitory postsynaptic markers, demonstrating that our neurons in co-culture appear to form both synapse types in abundance, making our model appropriate to use in the investigation of non-cell autonomous E:I changes in ALS.

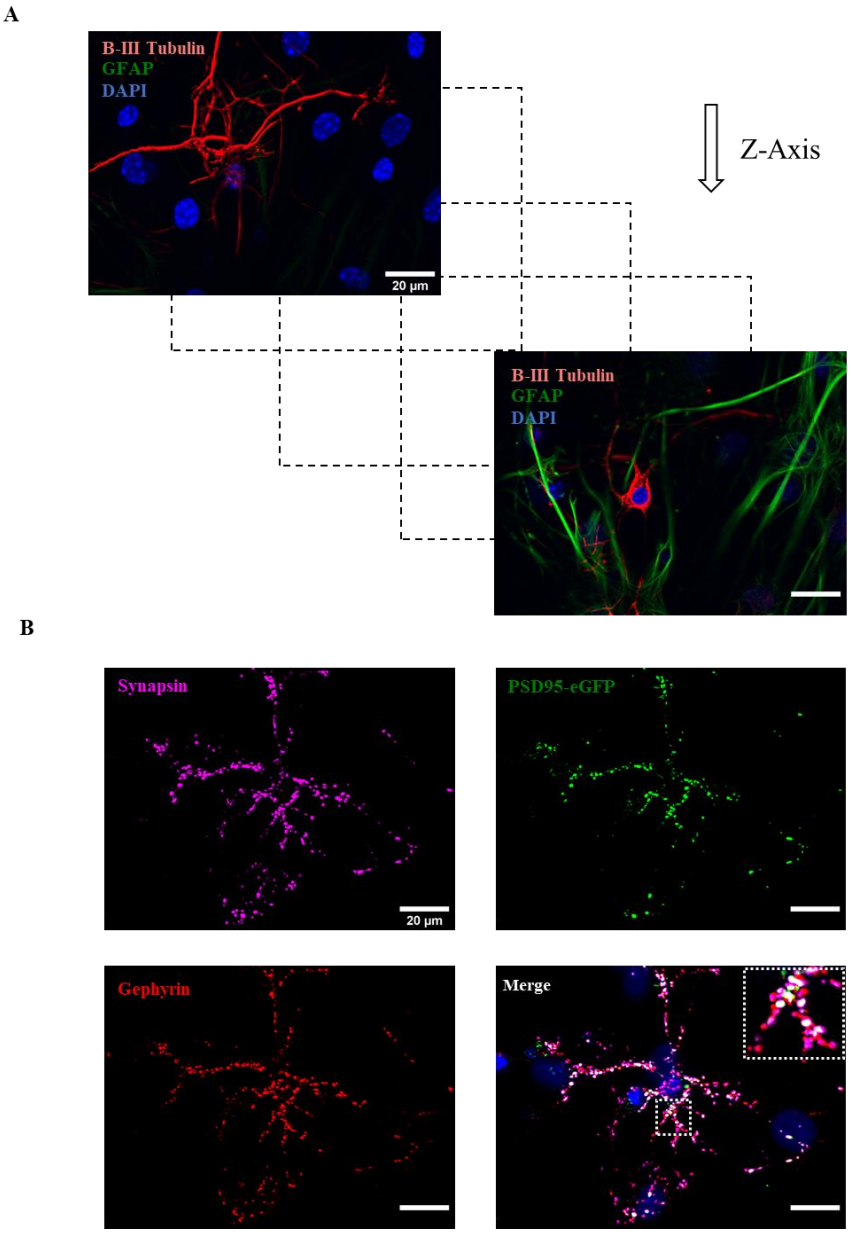

Figure 16: **A**) Images at multiple points of a Z-stack in a neuron / astrocyte co-culture. Demonstrates presence of DIV 3W β-III +ve neuron with GFAP +ve astrocytic staining faint in the background. As we progress down the Z-stack, we see fading of β-III +ve processes and an increase in intensity of GFAP, indicating we are moving towards our astrocytic layer. **B**) Images showing abundant expression of presynaptic marker (synapsin) as well as postsynaptic excitatory (PSD95-eGFP) and inhibitory (gephyrin) markers. Neurons DIV 3W.

3. Discussion

Creation of protocols to quickly and reliably generate enriched spinal astrocyte and neuron monocultures from postnatal mice was desirable to enable the study of non-cell autonomous effects on E:I synapse formation. Titration of these protocols to ensure optimum cell survival and purity of these desired cell types resulted in astrocytic and neuronal monocultures that can be combined to control the genotype of each cell layer. First, postnatal spinal glial cultures could be produced that were enriched in cells of appropriate astrocytic morphology, and the vast majority of which expressed specific astrocyte markers GFAP and GS. These cells also expressed proteins required for mature astrocytic function (Cx43 and EAAT2) from the earliest time point measured post-passaging. Although accelerated development has been discussed as a potential mechanism underlying neuronal hyperexcitability in ALS (Quinlan et al., 2011), the presence of an ALS-liked mutation (C9BAC500 hexanucleotide insertion) had no effect on the developmental expression pattern of astrocytic maturation markers. Our astrocyte-enriched cultures showed very low numbers of contaminating microglia and oligodendrocytes, so we can be further confident our cultures are relatively pure in the cell type we desire. Our neuron-enriched cultures meanwhile expressed β-III tubulin as expected, and showed a subset of cells which expressed the MN marker SMI 32. U/FDU treatment left minimal numbers of contaminating astrocytes in these cultures, and the neurons were validated physiologically using whole-cell patch clamp recordings, where the vast majority showed the ability to fire APs and received spontaneous synaptic input. Finally, we validated that these monoculutres could be plated together and expressed key markers of excitatory and inhibitory synapses, showing this model is appropriate for use in the study of non-cell autonomous effects on E:I synaptic ratios in ALS.

Postnatal spinal astrocyte cultures are generally considered easier to achieve than their neuronal counterparts as they are both proliferative in culture, and appear to be much less vulnerable to insults. Other groups have successfully produced postnatal spinal astrocyte cultures of approximately the same purity (85-90% GFAP +ve), although these usually rely on the use of a gradient during dissociation (Agalave et al., 2020; Kerstetter and Miller, 2012). Our protocol does not rely on this and dissociation of astrocytes into tissue culture flasks is very rapid (within 1 hour post-dissection). Interestingly, authors of other spinal astrocyte protocols also noted a decrease in GFAP expression with extended periods in culture (Kerstetter and Miller, 2012). This may be due to increased astrogliosis as a result of being closer in time to the initial dissection (our highest expression was seen at 2W DIV), with GFAP expression being increased in reactive astrocytes (Sofroniew, 2015). Astrocytes would be expected to be more reactive as a result of the insults undergone during the dissection and dissociation, which may decrease with time in culture. GS expression was found in over 99% of cells at all time points, and appeared to be expressed in more of our population than GFAP. This is consistent with previous observations that GS likely represents the most general marker of the astroglial family, and in the brain is expressed by astrocytes which appear to lack GFAP staining (Anlauf and Derouiche, 2013). This likely explains the slight variation in proportions of immuno-positive cells for the two markers. Together, however, it appears that we have highly enriched astrocytic cultures at 2-6W *in vitro*.

After validating the cell specificity of our astrocyte cultures, we also wanted to quantify their expression of key molecular markers of astrocytic maturity to find if; A) there was developmental changes in expression *in vitro* that would mean neuronal plating on top would be optimal at a certain time point, B) our astrocytic cultures provide evidence they can

perform key functions they would *in vivo* and C) the presence of an ALS-linked mutation altered the developmental expression pattern of these proteins. The first marker looked at was Cx43, a connexin subunit of gap junction hemichannels which connect to form the astrocytic network. Here, spinal astrocytes form a complex network allowing for exchange of ions and metabolites, which is essential for, amongst other things, calcium wave propagation and K^+ / glutamate buffering (Xing et al., 2019). As a result, they are able to communicate and aid in modulation of synaptic transmission of the greater neuronal network (Pannasch et al., 2012). Unpaired hemichannels are also able to release gliotransmitters, acting as a further mechanism to alter the activity of surrounding neurons (Retamal et al., 2014). Immunocytochemical characterisation of our astrocytic cultures at 2-6W *in vitro* demonstrated that at all time points, there was clear Cx43 expression. Expression quantified using the integrated intensity revealed no significant difference between any time point, although indicated a trend. While this could be an indication that the cells are slightly more immature this early in plating, it should be noted that gap junctions form at points of cell-cell contact (Liu et al., 2020). Astrocyte cultures are initially grown in tissue-culture flasks before being replated onto coverslips when confluent (approx. DIV 10 days). It could be the case therefore that there is less cell-cell contact at the 2W time point as astrocytes are still proliferating and extending their cell boundaries after being transferred to coverslips, and hence potentially have a slightly lower density of Cx43 +ve hemichannels.

EAAT2, our other marker of astrocytic maturity due to its role as a glutamate transporter at the synaptic cleft (Guo et al., 2002), showed a remarkably consistent developmental pattern of expression. Together with the developmental pattern of Cx43, it appears that there is little variation in expression of these markers at the time points measured. Therefore, neurons are able to be plated onto mature astrocytes at a range of time points, which practically is

beneficial if there is a delay in the birth of subsequent litters from which neurons will be dissociated.

As discussed previously, intrinsic neuronal hyperexcitability in neonatal neurons has been suggested to reflect a pathological 'accelerated development' in ALS (Quinlan et al., 2011). The function of mature astrocytes is essential in the development and activity of surrounding neural circuitry (Allen and Eroglu, 2017). As such, it was hypothesised that such an acceleration of neuronal development could be mirrored in astrocytic molecular markers of maturity. This was not the case however, with the presence of the C9BAC500 mutation having no impact on expression of Cx43 or EAAT2 at the time points investigated. Astrocytes derived from $SOD1^{G93A}$ embryonic spinal glial restricted precursor (GRP) cells have previously been shown to have elevated expression of Cx43 after just 1W in culture, an effect which was replicated in iPSC-derived human astrocytes harbouring C9orf72 mutations when cultured for a similar time-scale post-differentiation (Almad et al., 2016; Almad et al. 2022). It should be noted, however, that such an elevation was not noted in $SOD1^{G93A}$ spinal cord tissue until end-stage (P120-P140) (Almad et al., 2016). Evidence showing EAAT2 protein expression changes appears to be more restricted to late presymptomatic / symptomatic stages rather than early-stage *in vitro* work. As discussed in Chapter 1, $SOD1^{G93A}$ animal models show evidence of EAAT2 loss either presymptomatically or at the point of symptom onset (Bendotti et al., 2001; Howland et al., 2002). This loss has also been observed in ALS patient post-mortem tissue (Rothstein et al., 1995).

Although Almad and colleagues (2016) observed changes in Cx43 expression at just 1W post-differentiation from GRPs, there is a variety of possible reasons why we did not observe such an increase in expression. It should be noted that in addition to the tissue culture models

utilised being very different, the C9BAC500 mouse shows a considerably different phenotypic timescale to the $SOD1^{G93A}$ mouse model, with acute-onset animals (see Chapter 1, Section 1.5.2. for details) not developing motor phenotypes until 20-40 weeks, while our $SOD1^{G93A}$ colony developed motor deficits by approximately 12/13 weeks (Liu et al., 2016). In addition, although the $SOD1^{G93A}$ model has been questioned for its ability to accurately recapitulate the majority of human ALS cases (Acevedo-Arozena et al., 2011), the C9BAC500 model presents with its own flaws. In our hands, no mice developed acute motor phenotypes, despite maintaining adult mice of both sexes well into the described phenotypic timeframe. Our experimental animals were PCR-genotyped with relevant positive controls, in addition to showing the presence of RNA-foci, a key molecular hallmark of C9orf72-related ALS (Broadhead et al., 2022), so their expression of the C9orf72 hexanucleotide repeat was verified. Other groups have also described the very low phenotypic penetrance of this model (Mordes et al., 2020; Nguyen et al., 2020). Current evidence suggests housing environment may have a significant impact on the emergence of symptoms, in addition to the suggestion that drawbacks of the FVB/N mouse background used to develop the model (including susceptibility to seizures) could have caused false interpretation of ALS phenotypes in the original study (Liu et al., 2016; Mordes et al., 2020).

In the process of validating the purity of our astrocyte cultures, we looked at the proportion of cells expressing mature oligodendrocyte and microglia markers. OSP +ve cells were very infrequent in our astrocytic cultures. As mature oligodendrocytes do not significantly proliferate, it is common to culture populations of OPCs that can then be differentiated, something that has been shown to be particularly challenging in mouse primary culture (Chen et al., 2007; Yang et al., 2016). Oligodendrocyte survival *in vitro* has also been shown to be strongly dependent on the presence of neurons (Barres et al., 1993). As, by definition, our

astrocyte cultures lack neurons, it is likely we have poor oligodendrocyte survival by DIV 6W when OSP +ve cells were quantified. If OPCs are not maintained in our cultures too, then it is perhaps unsurprising our OSP +ve population is small. We also report low numbers of TMEM119 +ve microglia in our astrocyte cultures. This low level of microglial contamination is expected. Mature microglia proliferate slowly to maintain their population in the adult CNS (Tan et al., 2022). Beaudet and colleagues (2015) successfully developed a methodology to culture adult spinal microglia from 5 m.o. mice. They noted, however, that postnatal microglia would often take 1 month before beginning to proliferate, and even then this was in media developed to promote their growth. It is understandable therefore that at DIV 6W in astrocytic media, we would produce low numbers of microglia using our astrocytic protocol.

Next, characterisation of our neurons confirmed the presence of β-III tubulin +ve processes, in addition to SMI 32 +ve putative MNs. It is clear that these cultures are not MN-enriched, and contained a mixed population of spinal MNs and interneurons. Although the obvious avenue of investigation in ALS is to pursue solely MN pathology, evidence of widescale pre-MN spinal hyperexcitability (van Zundert et al., 2008; Jiang et al., 2009) shows that analysis of the greater motor network is key to understanding ALS disease mechanisms. This is of particular interest as our model has been initially designed to look at network imbalances in E:I ratios and the putative role astrocytes may have in shifting this, thus it was deemed critical that our neuronal populations were mixed. We do not know the precise identity or proportions of the interneuron populations present in our cultures. Future work using *in situ* hybridisation to target specific markers such as parvalbumin could help further define our neuronal populations. Use of U/FDU, an effective anti-mitotic agent, effectively eliminated the vast majority of proliferating astrocytes. This agent has been used to effectively isolate

primary neuronal cultures previously, and has been shown to facilitate greater neuronal survival versus other more toxic alternatives such as AraC (Hui et al., 2016; Lamas et al., 2014). Although it has been reported that neuronal survival can be reduced if neurons are exposed to FDU for an extended time (Hui et al., 2016), we still noted the expression of key neuronal and synaptic proteins. However, as a result of the concern over signficantly reduced neuronal health in response to U/FDU treatment, we felt it necessary to also show our neurons are capable of being physiologically active.

Electrophysiological validation of our postnatal spinal neurons verified both their identity, and their possession of relatively mature functional properties. Comparison with other protocols is challenging here, as often validation is done only using immunocytochemical methods (Beaudet et al., 2015; Eldeiry et al., 2017). IPSC-derived MNs are another commonly used culture model in the study of ALS, and have been characterised more thoroughly. Our neurons showed an average capacitance of 32.07 +/- 3.08 pF, a measure which is proportional to cell size. Our neurons show approximately 3 times the capacitance value of iPSC-derived MNs at a similar timepoint *in vitro* (Devlin et al., 2015). Our neurons also showed a more hyperpolarised RMP, being closer to the RMP of week 1-3 MNs in spinal slice, however, as expected they still do not reach these values (approx. -58 to -67mV) and are considerably smaller than neurons *ex vivo* (approx. 250-500pF) (Delvin et al., 2015; Sharples and Miles, 2021). The vast majority of cells had sufficient Na^+- and K^+-mediated currents and were capable of firing APs. In addition to this, most received some form of spontaneous synaptic input, giving further evidence along with expression of synaptic markers that these cultures form neuronal networks *in vitro*.

Following plating of these neuronal monolayers on top of our astrocytic layers, our measurement of spontaneous synaptic activity was supported by the expression of the general presynaptic marker synapsin, as well glutamatergic postsynaptic marker PSD95 and GABAergic/glycinergic postsynaptic marker gephyrin. Taken together, our validated monocultures, when combined, are suitable for the study of non-cell autonomous E:I ratio changes in ALS. In addition, validation of their electrophysiological activity also makes this methodology an ideal model for investigating astrocyte-neuron interactions in other mechanisms of disease underlying ALS. Returning to our original aims, we have shown:

1. We can produce neural cultures without relying on anesthetising our animals, thus avoiding effects on electrophysiological function.
2. We can rapidly produce neurons, allowing for genotyping and dissociation within a single day.
3. Produced neurons are viable, without the use of density gradients in our methodology.
4. Cultures can be maintained for at least 3W, producing cells with mature physiological properties and appropriate protein markers.

Chapter 4

Probing Putative Astrocyte-Mediated Shifts in Excitatory : Inhibitory Synaptic Ratios in ALS

Work within this chapter was completed with contribution from Dr. Matthew Broadhead and Dr. Sarah Burley

1. Introduction

As discussed in Chapter 1.3, hyperexcitability of motor networks, either from changes to the MNs themselves or the pre-MN circuitry, is a regularly reported phenomena in ALS. Although much work has looked at early stage intrinsic hyperexcitability of MNs, a less discussed mechanism that may lead to excitotoxicity is insufficient inhibition within the motor network. As the excitability of a neuron is partially dictated by the balance of excitatory to inhibitory input, an imbalance of this ratio has the potential to elicit pathogenic hyperexcitability. Martin and Chang (2012) presented an argument as such, that frequent observation of insufficient inhibition, either onto the MNs themselves or within pre-MN networks, leads to ALS-associated neuronal death. Evidence from patients goes some way to reinforce this. A study looking to behaviourally assess recurrent inhibitory pathways (modulated by glycinergic Renshaw cells) using a 'H-reflex technique' showed marked reductions in recurrent inhibition in ALS patients (Raynor and Shefner, 1994). Post-mortem, glycine receptor density is significantly reduced in the ventral horn of spinal samples from ALS patients (Hayashi et al., 1981). In mouse models of ALS, as discussed earlier, evidence of loss of glycinergic input to MNs is observed presymptomatically, which was seen alongside evidence of Renshaw cell loss slightly later (Chang and Martin, 2009). Further evidence of inhibitory loss specifically onto MNs has also been reported in ALS mouse models (Allodi et al., 2021; Qian et al., 2017), whilst evidence of widescale inhibitory synapse loss in the grey matter is also present (Hossaini et al., 2011).

Whilst it has been posited that there is a shift in E:I ratios, likely due to inhibitory loss during disease pathogenesis (Martin and Chang, 2012), there is an alternative hypothesis for the basis of this change. Kiernan and colleagues (2019) suggested that instead of a later shift

towards excitation due to synaptic loss, there may in fact be a developmental alteration in ALS that biases the system towards excitation from early life. Although neurodegenerative conditions are not classically thought of as such, ALS could be considered a developmental disorder if this is the case, as is seen in other neurological conditions such as schizophrenia and autism spectrum disorders (Nelson and Valakh, 2015). Evidence of hyperexcitability in the wider spinal network has been noted from neonatal stages through to symptomatic stages in the $SOD1^{G93A}$ model (van Zundert et al., 2008; Jiang et al., 2009). Such an early developmental bias in E:I ratios throughout the spinal circuitry could explain these observations.

There are multiple mechanisms by which this may occur. The first is a delay in the developmental shift of GABAergic synapses from excitatory to inhibitory signalling. High intracellular chloride concentrations, and thus more depolarised reversal potentials in immature neurons, results in GABA depolarising neurons, resulting in excitatory transmission (Kiernan et al., 2019; Wang and Kriegstein, 2009). This shift occurs in the first to second postnatal week and is dictated by changes in expression of the K^+-Cl^- co-transporter 2 (KCC2) and Na^+-K^+-$2Cl^-$ co-transporter 1 (NKCC1), the balance of which modulates intracellular Cl^- concentrations (Furukawa et al., 2017; Jean-Xavier et al., 2007). A delay in this shift likely causes long-lasting neuronal insults and contributes to a bias in excitability, thus eventually causing excitotoxic cell death (Kiernan et al., 2019).

Another mechanism by which developmental biases in E:I ratios could emerge is a pathological change in astrocytic synaptogenesis. Like GABAergic changes, astrocyte-mediated synaptogenesis occurs postnatally, occurring maximally in weeks 2 and 3 in the brain, and showing a similar pattern in the spinal cord which appears to peak entering week 3

before declining (Risher and Eroglu, 2020; Weber and Stelzner, 1980). As discussed earlier, astrocytes promote synapse formation in a complex manner, utilising both secreted factors such as TSPs and hevin, as well as contact-dependent factors such γ-protocadherins and ephrin-B1 (Chung et al., 2015; Risher and Eroglu, 2020). Although much of this work has focussed on excitatory synapse formation, astrocytes are also directly involved in inhibitory synaptogenesis. Ephrin-B1 in the hippocampus can directly modulate E-I balance by increasing glutamatergic and decreasing inhibitory synapse numbers (Nguyen et al., 2020b). Transforming growth factor beta 1 (TGF-β1) is found in the conditioned media of both human and mouse astrocytes, and as well as being involved in excitatory synaptogenesis, was also found to promote GABAergic synapse formation in cortical neurons (Diniz et al., 2012; Diniz et al., 2014). This was replicated *in vivo* with intraventricular injection of TGF- β1 (Deniz et al., 2014). Glycinergic synaptogenesis is also reliant to some degree on astrocytes, as cultured spinal neurons showed significantly impaired glycinergic transmission when cultured without astrocytes (Cuevas et al., 2005). It is clear therefore that astrocytes have complex signalling mechanisms which allow them to modulate both excitatory and inhibitory synapse formation.

Astrocytic involvement in disease is believed to be multifaceted, with implications ranging from perturbed glutamate transport to release of toxic factors (Valori et al., 2014). With their clear involvement in synaptogenesis in the developing CNS, in addition to the proposal that ALS may be a developmental disorder in which the system is biased towards excessive excitation from a very young age, it is possible perturbation of synaptogenesis could represent another astrocytic ALS mechanism. As spinal network-wide hyperexcitability has been reported (van Zundert et al., Jiang et al., 2009), pathological alterations in astrocytic synaptogenesis could cause early changes in the E:I ratio of the pre-MN network and / or

synaptic input onto MNs. Such changes biasing excitatory transmission may then lead to later excitotoxic events as a result of hyperexcitability. This astrocyte-mediated shift in E:I ratios is a phenomenon which will be pursued in this chapter, in an effort to elucidate whether non-cell autonomous shifts in synapse formation could contribute to excitotoxic cell death in ALS. We will therefore use a variety of models, including our novel primary culture methodology, to investigate whether the presence of ALS mutations causes shifts in E:I ratios.

2. Results

2.1. Validation of ALS x PSD95-eGFP Mouse Crosses

In order to accurately visualise the PSD of glutamatergic synapses in our co-cultures of spinal neurons and astrocytes, we took advantage of a PSD95-eGFP $^{+/+}$ mutant mouse. PSD95 is a key molecular organiser at the PSD. Part of the membrane-associated guanylate kinase (MAGUK) family, it recruits and binds essential transmembrane proteins required for the function of the PSD, including NMDARs and AMPARs. It does this via binding of intermediate proteins such as stargazin, as well as other transmembrane AMPAR regulating proteins (Hafner et al., 2015). The protein itself consists of three PDZ domains, in addition to one SH3 and GK domain, which together form one SH3-GK (Src homology 3-guanlyate kinase) module. A GFP tag is inserted after these domains in the open reading frame of Dlg4 (PSD95-encoding gene) at the 3' end, immediately before its stop codon via a Gly-Gly-Gly-Ser linker sequence (Fernández et al., 2009; Hafner et al., 2015; Zhu et al., 2018). A schematic of the edited Dlg4 gene can be seen in Fig. 17A. As this is inserted into the endogenous murine gene, this model is described as a 'knock-in' mutant mouse. These animals were initially created using a C57bl/6 background strain and are homozygous for the PSD95-eGFP mutation.

These animals were bred with our two ALS mouse models, producing both SOD1$^{G93A\ +/-}$ and C9BAC500 $^{+/-}$ animals (plus their respective control littermates) which also expressed PSD95-eGFP $^{+/-}$. As all progeny contained a copy of the PSD95-eGFP gene, we could therefore visualise the PSDs of both disease and control neurons. To verify that the

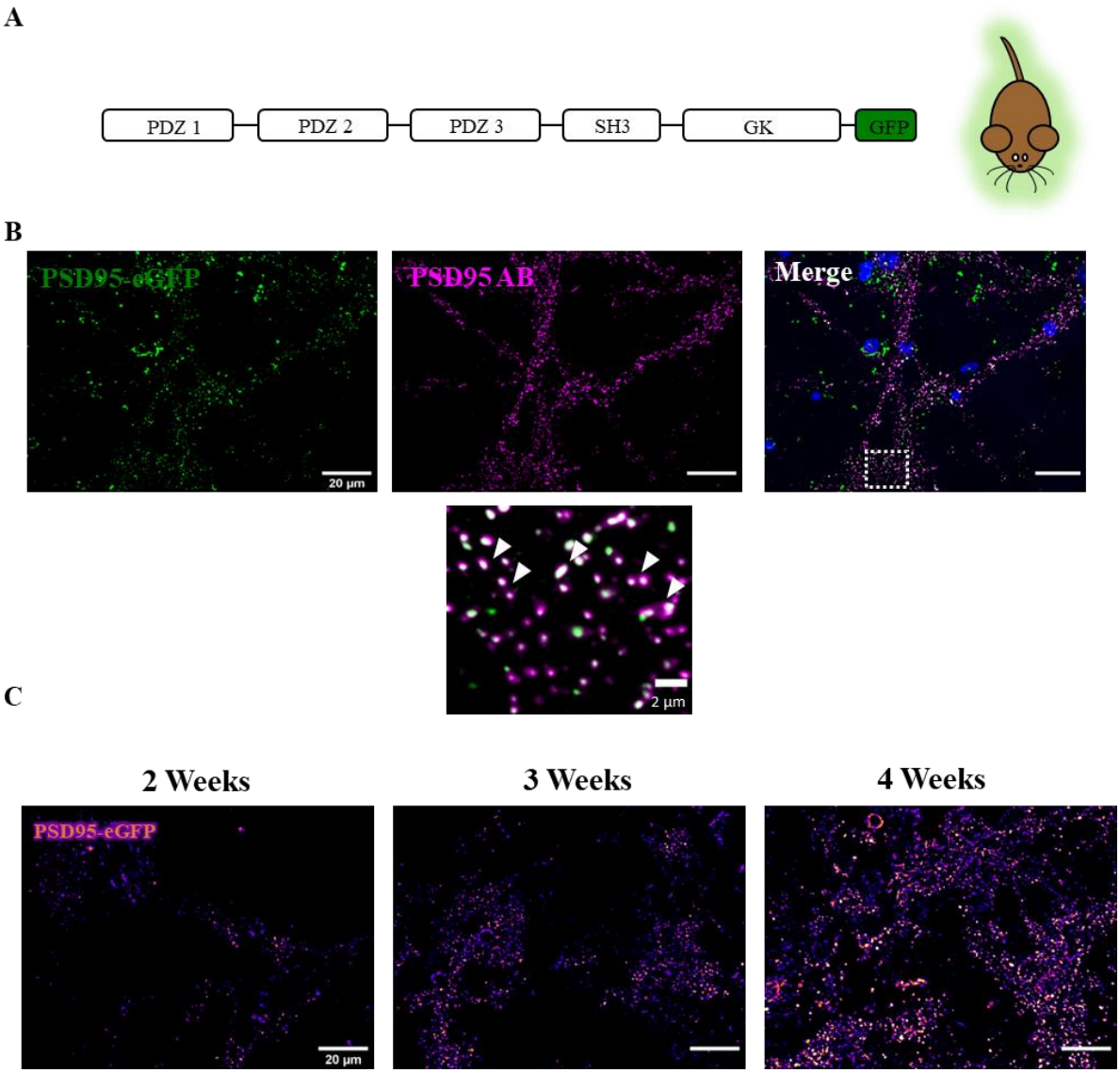

Figure 17: **A**) Schematic demonstrating the structure of PSD95 with the GFP tag insertion in the PSD95-eGFP mouse. **B**) Validation images in C9BAC500$^{+/-}$ PSD95-eGFP$^{+/-}$ neuron cultures stained with an anti-PSD95 antibody (PSD95 AB). White arrows indicate clear co-localisation between GFP and PSD95 AB. **C**) Images showing PSD95 expression in C9BAC500$^{+/-}$ PSD95-eGFP$^{+/-}$ neuron cultures from DIV 2-4W. PSD95 expression is present from 2W and appears to increase as cells mature.

GFP fluorescence we saw in our neuronal cultures was at the PSD, we also applied a PSD95 antibody. Our PSD95-eGFP signal showed expected punctate expression, with some infrequent large objects which were likely autofluorescent dead cells or lipofuscin aggregates. Importantly, our PSD95-eGFP signal showed excellent co-localisation with our PSD95 antibody, which gave us confidence that it was a reliable method of imaging excitatory synapses (see Fig. 17B).

Finally, we wanted to use the strength of the PSD95-eGFP tag to visualise PSD95 expression across development in our neurons. As can be seen in Fig. 17C, from DIV 2W, PSD95 expression is present in C9BAC500 x PSD95-eGFP neuronal monocultures. Qualitatively it seemed clear that at 3W this level of expression had increased, which was further evident at 4W. It should be noted, however, that when neurons were grown to 4W in co-culture, the astrocytic layer could be up to DIV 7W, and it was common to lose these cultures due to astrocytic peeling. Such an increase of PSD95 at DIV 3W is in line with our electrophysiological characterisation (see Chapter 3, Fig. 15), as neurons reliably fired APs in response to current injection and displayed spontaneous synaptic activity. Together, this provides evidence that neurons at DIV 3W is a 'sweet spot' for future E:I analysis, as in monoculture they have prominent PSD95-eGFP expression in addition to robust electrophysiological activity, whilst also minimising the risk of astrocytic peeling.

2.2. Investigation of Non-Cell Autonomous Effects on E:I Ratios in ALS Co-Cultures

As we were confident in using our ALS x PSD95-eGFP crosses, we proceeded to utilise these in co-cultures with the aim of looking at non-cell autonomous effects on E:I ratios. Our first

study utilised the classical SOD1^{G93A} model, bred with our PSD95-eGFP mice to produce SOD1$^{G93A\ +/-}$ PSD95-eGFP $^{+/-}$ mice, along with their SOD1$^{G93A\ -/-}$ PSD95-eGFP $^{+/-}$ littermates. As described in Chapter 3, we first produced astrocyte monocultures. Neonates were genotyped prior to dissection, so cultures +ve and -ve for the SOD1^{G93A} mutation could be grown separately. Typically, 2-3W later, neurons +ve or -ve for the SOD1^{G93A} mutation were plated on top and cultured until DIV 3W, before fixation and staining. Neurons in our co-culture, as mentioned previously, showed appropriate punctate expression of synapsin, PSD95-eGFP and gephyrin (see Fig. 18A). Importantly, we saw significant co-localisation of pre- and post-synaptic markers, which allowed us to quantify the ratio of excitatory (synapsin-PSD95) to inhibitory (synapsin-gephyrin) synapses.

As E:I ratios were calculated within an image, no normalisation of this metric was required. Both excitatory and inhibitory synapse counts came from the same cells in that field of view, introducing no other sources of variation that needed to be accounted for, such as inter-image cell count variability. Synapses were counted in the entire field of view, with pseudo-random selection (guided by synapsin) accounting for potential variability caused by imaging distal versus proximal dendrites. For brevity, +N and +A refer to neurons and astrocytes, respectively, which are +ve for the SOD1^{G93A} mutation. -N and -A refers to these cell types generated from -ve SOD1^{G93A} littermates. This produced 4 conditions which allowed us to probe non-cell autonomous effects on E:I ratios (+N/+A, +N/-A, -N/+A, -N/-A) (see Fig 18B). We found, however, that there was no significant difference in the ratio of excitatory to inhibitory synapses in these cultures ($F(3,12)=0.9431$, $P=0.45$). There appears to be a bias towards inhibitory transmission in our co-cultures, with mean E:I ratios ranging from 0.62-0.74 between conditions.

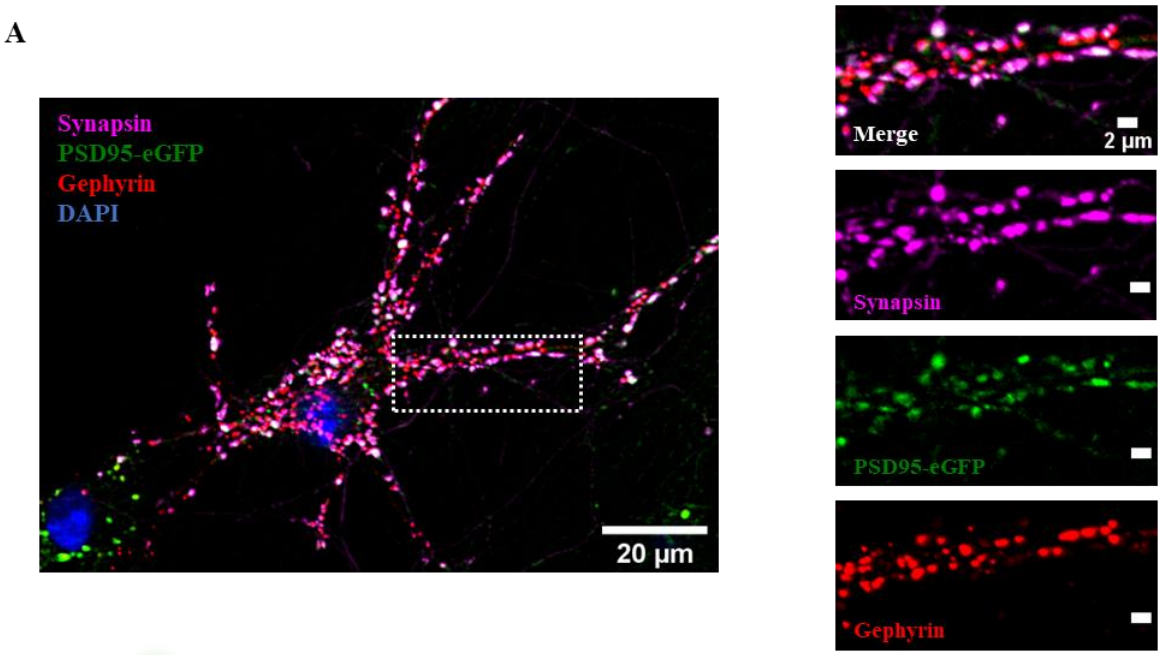
A
Synapsin
PSD95-eGFP
Gephyrin
DAPI
20 µm
Merge
2 µm
Synapsin
PSD95-eGFP
Gephyrin

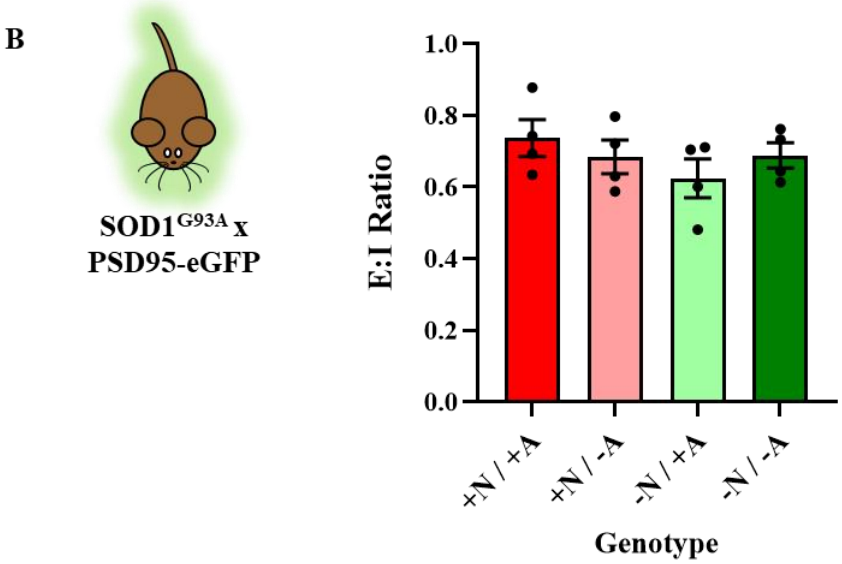
B
SOD1G93A x
PSD95-eGFP
E:I Ratio
1.0
0.8
0.6
0.4
0.2
0.0
+N / +A
+N / -A
-N / +A
-N / -A
Genotype

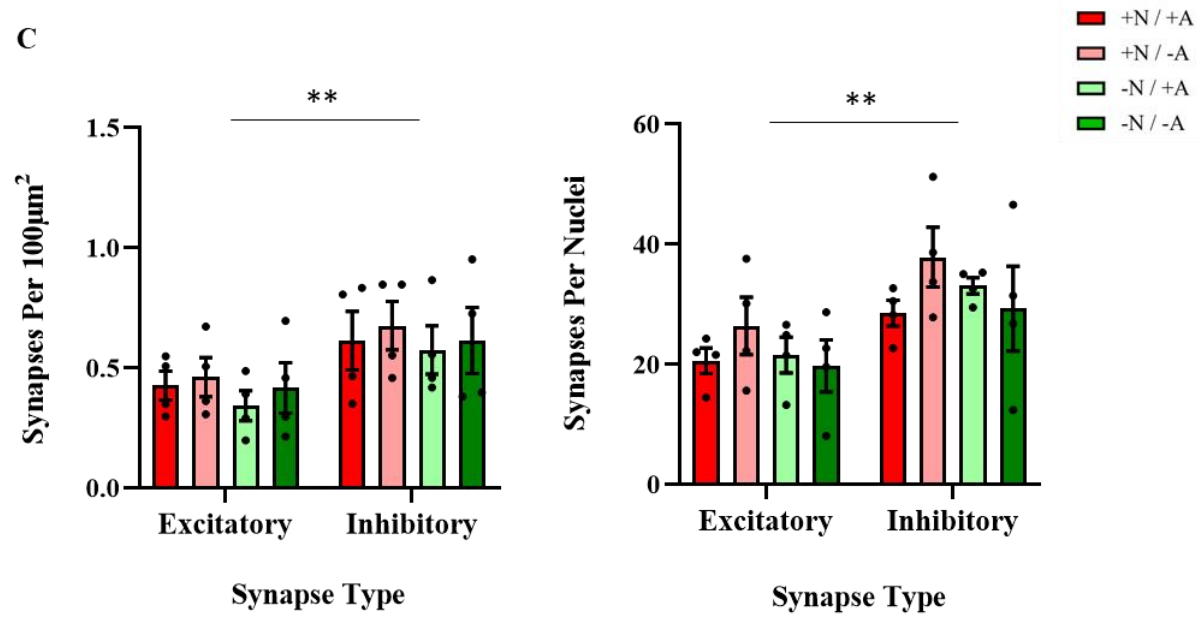
C
+N / +A
+N / -A
-N / +A
-N / -A
**
Synapses Per 100µm2
1.5
1.0
0.5
0.0
Excitatory
Inhibitory
Synapse Type
**
Synapses Per Nuclei
60
40
20
0
Excitatory
Inhibitory
Synapse Type

Figure 18: **A**) Example image of DIV 3W neuron in a $SOD1^{G93A}$ x PSD95-eGFP co-culture expressing synapsin, PSD95-eGFP and gephyrin. When zoomed, we see clear co-localisation of presynaptic and postsynaptic markers. **B**) Bar chart showing E:I ratios in co-cultures of 4 different combinations. + / - refers to the presence of the $SOD1^{G93A}$ mutation, N / A refers to the cell type referenced, either neurons or astrocytes, respectively (N=4 co-culture platedowns). **C**) Bar chart showing numbers of excitatory and inhibitory synapses normalised to area (N=4 co-culture plate downs). **D**) Bar chart showing numbers of excitatory and inhibitory synapses normalised to nuclei count (N=4 co-culture platedowns).

In order to determine if we saw no changes at all in numbers of synapses, or whether the E:I ratio was maintained due to a parallel increase or decrease in both types of transmission, we compared normalised excitatory and inhibitory synapse counts. First, we looked at synapse counts normalised to area (density per. 100µm^2). As expected, due to our previously mentioned <1 E:I ratio values, there was a significant main effect of synapse type, whereby there were consistently more inhibitory synapses than excitatory ones (F(1,24)=8.708, P=0.0070) (see Fig. 18C). However, multiple comparisons testing revealed no significant differences in excitatory vs inhibitory synapse density between individual genotype conditions (+N/+A: P=0.58, +N/-A: P=0.46, -N/+A: P=0.38 and -N/-A: P=0.54). Total synapse counts were consistent between genotype conditions (F(3,24)=0.4134, P=0.74), indicating that similar E:I ratios were not obscuring a scaled increase or decrease in synapse counts. Finally, as reflected in the lack of E:I differences, the degree of inhibitory bias was not dependent on the genotype (F(3,24)=0.01942, P=0.99).

Although useful, normalisation to area does not take into account variable numbers of neurons in the field of view between images. In order to account for this, synapse counts were also normalised to DAPI counts. To ensure that counts were normalised to the neural monolayer and not the underlying astrocyte layer, DAPI counts were taken from in-focus nuclei strictly in the focal plane of synaptic protein expression. When normalised to DAPI count, there was again a significant difference between synapse types, with more inhibitory than excitatory synapses being present (F(1,24)=12.09, P=0.0020). Again, multiple comparisons testing did not reveal individual differences between genotype conditions (+N/+A: P=0.59, +N/-A: P=0.22, -N/+A: P=0.21 and -N/-A: P=0.39). Consistently, there was also no difference in overall DAPI-normalised synapse counts between genotype conditions

($F(3,24)=1.510$, P=0.24), and no interaction of excitatory vs inhibitory synapse count and genotype condition ($F(3,24)=0.08735$, P=0.97).

As no bias in E:I ratio was found in our SOD1^{G93A} cultures, we next investigated this using our C9BAC500 model. Again, C9BAC500 $^{+/-}$ animals were bred with PSD95-eGFP $^{+/+}$ animals to produce C9BAC500 $^{+/-}$ PSD95-eGFP $^{+/-}$ and C9BAC500 $^{-/-}$ PSD95-eGFP $^{+/-}$ offspring. The experimental setup was replicated, again producing 4 genotype conditions. As can be seen in Fig. 19A, in cells derived from C9BAC500 x PSD95-eGFP crosses we see expression of our presynaptic marker synapsin, as well as postsynaptic markers PSD95-eGFP and gephyrin. Cropped images reveal clear co-localisation of pre- and postsynaptic markers, indicating the presence of large numbers of synapses. When E:I ratios were probed in these co-cultures, we again found no difference between our 4 genotype conditions ($F(3,21)=1.667$, P=0.20) (see Fig. 19B). Once more, there was a bias towards inhibitory synapse formation in these cultures, with a range of 0.61-0.78. When compared to our SOD1^{G93A} x PSD95-eGFP cultures, there was no difference in E:I ratios depending on ALS mouse model used ($F(1,33)=0.0006632$, P=0.94).

Again, to check that consistent E:I ratios between conditions were not masking a scaled increase or decrease in both synapse types, we looked at synapse counts normalised to area and cell count. Once again reflecting the <1 E:I ratio values observed, we found significantly more inhibitory synapses than excitatory ($F(1,42)=13.05$, P=0.0008) (see Fig. 19C). Multiple comparisons testing again failed to find differences between individual genotype conditions (+N/+A: P=0.08, +N/-A: P=0.25, -N/+A: P=0.76 and -N/-A: P=0.22). We also once again found no difference in total synapse counts between genotype conditions ($F(3,42)=2.245$,

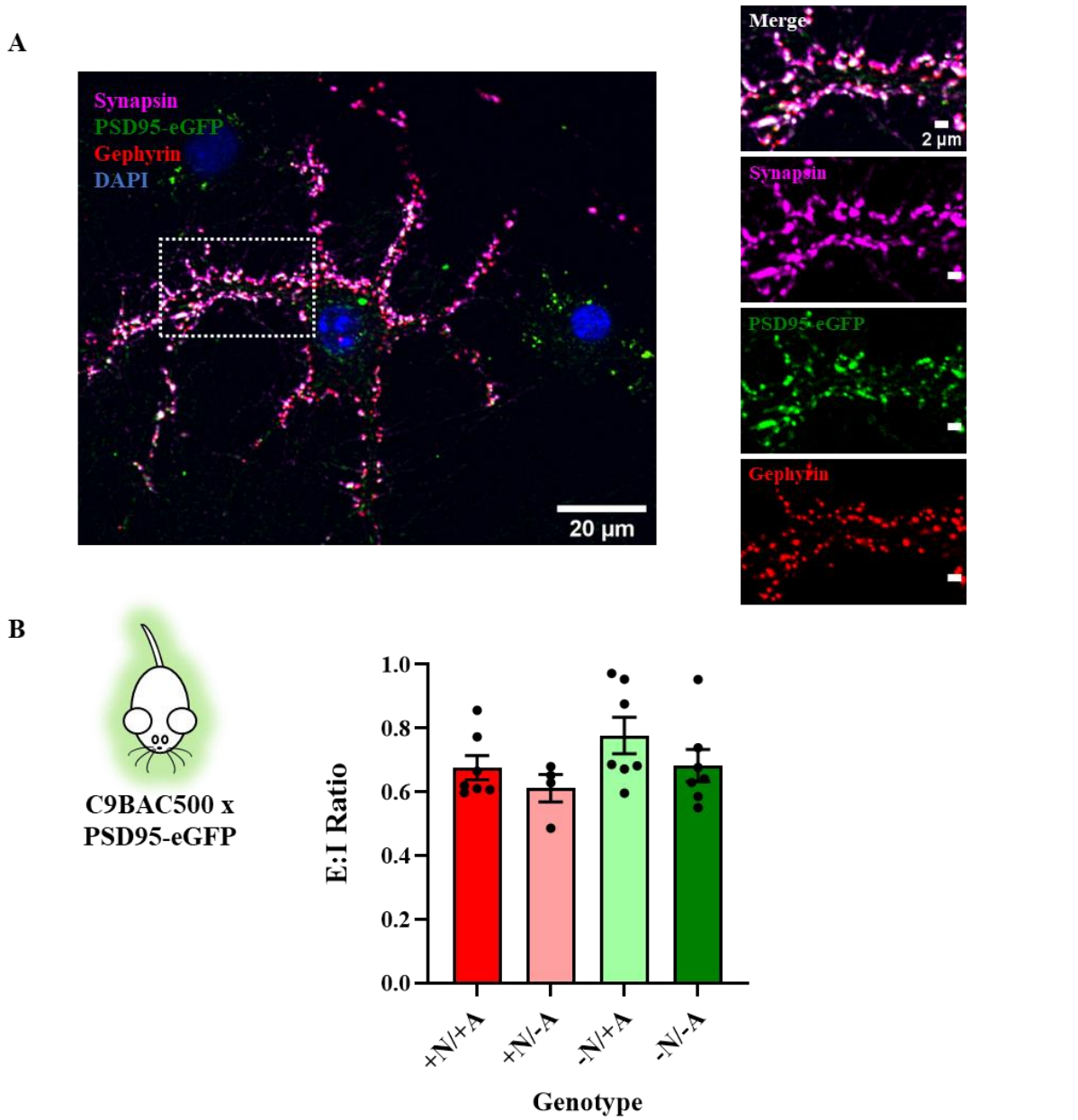
A
Synapsin
PSD95-eGFP
Gephyrin
DAPI
20 µm
Merge
2 µm
Synapsin
PSD95-eGFP
Gephyrin
B
C9BAC500 x
PSD95-eGFP
E:I Ratio
1.0
0.8
0.6
0.4
0.2
0.0
+N/+A
+N/-A
-N/+A
-N/-A
Genotype
C
***
**
+N / +A
+N / -A
-N / +A
-N / -A
Synapses Per 100µm2
1.5
1.0
0.5
0.0
Excitatory
Inhibitory
Synapse Type
Synapses Per Nuclei
60
40
20
0
Excitatory
Inhibitory
Synapse Type

Figure 19: **A**) Example image of DIV 3W neuron in a C9BAC500 x PSD95-eGFP co-culture expressing synapsin, PSD95-eGFP and gephyrin. When zoomed, we see clear co-localisation of presynaptic and postsynaptic markers, indicating significant synapse formation. **B**) Bar chart showing E:I ratios in co-cultures of 4 different combinations. + / - refers to the presence of the C9BAC500 mutation, N / A refers to the cell type, either neurons or astrocytes, respectively (N=4-7 co-culture platedowns). **C**) Bar chart showing numbers of excitatory and inhibitory synapses normalised to area (N=4-7 co-culture plate downs). **D**) Bar chart showing numbers of excitatory and inhibitory synapses normalised to nuclei count (N=4-7 co-culture platedowns).

P=0.10), showing no combination of genotypes significantly altered the total number of synapses formed. Finally, there was no significant interaction, indicating the degree of bias towards inhibitory transmission was not affected by genotype condition ($F(3,42)=0.3959$, P=0.76). Synapse numbers normalised to cell count showed the same effects, with an overall inhibitory transmission bias ($F(1,42)=9.532$, P=0.0036), consistent numbers of total synapses across genotype conditions ($F(3,42)=2.570$, P=0.07) and no effect of genotype on the degree of bias towards inhibitory synapse formation ($F(3,42)=0.3139$, P=0.82) (see Fig. 19C).

It appears to be the case therefore that in co-cultures generated from both $SOD1^{G93A}$ and C9BAC500 animals, there is no evidence that the presence of an ALS mutation causes a shift in the E:I ratio. Cells generated from both disease models have a bias towards inhibitory transmission, and neither the genotype of astrocytes nor neurons altered total numbers of synapses formed in culture. This remarkable consistency between mouse models gives us confidence that there is no structural evidence of non-cell autonomous E:I shifts *in vitro*.

2.3. Astrocytic Ephrin-B1 Expression Confirms Lack of Synaptogenic Changes in ALS Co-Culture Model

In order to further verify that we do not observe any non-cell autonomous effects on synaptogenesis as a result of an ALS mutation, we wanted to investigate the expression of a factor known to directly alter E:I ratios *in vivo*. As described in Chapter 1, ephrin-B1 expression appears to directly modulate the E:I balance during hippocampal synaptogenesis (Koeppen et al., 2018; Nguyen et al., 2020a; Nguyen et al., 2020b). It is involved in bi-directional communication via interaction with ephrin receptors on neurons in a contact-

dependent manner (Risher and Eroglu, 2020). Expression of astrocytic ephrin-B1 directly influences both excitatory and inhibitory synapse numbers, whereby reduced expression biases the system towards increased glutamatergic transmission and an increased E:I ratio (Nguyen et al., 2020b).

Therefore, in our co-culture system, a bias towards excitatory transmission would imply a downregulation of astrocytic ephrin-B1 expression. However, as we see no obvious non-cell autonomous effects on E:I ratios, we hypothesised no change of expression in astrocytes harbouring the $SOD1^{G93A}$ and C9BAC500 mutations. This would further support the lack of observed synaptogenesis perturbation seen in our co-culture model. To act as a positive control and to ascertain the expression pattern of ephrin-B1, we first immunohistochemically targeted this protein in spinal tissue, along with the classical astrocytic marker GFAP (see Fig. 20A). Similar to previous reports (Nguyen et al., 2020b), in tissue ephrin-B1 shows a widescale diffuse expression, punctuated by pronounced blob-like concentrations. Expression often co-localises with GFAP. Although GFAP is not expressed throughout the entire astrocyte, (Heller and Rusakov, 2015) there is clear astrocytic expression. As ephrin-B1 signalling is bidirectional, however, neurons in spinal tissue will also express ephrin-B1 (Nguyen et al., 2020b). Astrocytic expression is further confirmed in our validated enriched astrocyte cultures, whereby ephrin-B1 expression is abundant, appearing diffusely throughout the cell with high expression at putative cell boundaries (see Fig. 20B).

Ephrin-B1 is known to be abundantly expressed in postnatal week 2-3 in the hippocampus (Nguyen et al., 2020b), so in addition to looking at the effects of ALS mutations on expression, it was also interesting to investigate whether a similar developmental pattern of expression is seen at 2-6W *in vitro* . First, astrocytes harbouring the $SOD1^{G93A}$ mutation were

probed for putative effects on ephrin-B1 expression. Astrocytes were still dissociated from SOD1^{G93A} x PSD95-eGFP crosses, as although PSD95-eGFP expression was not seen due to a lack of neurons in culture, it allowed our findings to be directly comparable to our E:I co-culture datasets, which used these crosses and thus negated possible confounding variables as a result of different background strains. For clarity, cells not harbouring an ALS mutation are referred to simply as 'Control', as to avoid calling them 'non-transgenic' when they still express PSD95-eGFP $^{+/-}$. Ephrin-B1 expression was clear from DIV 2W, and this continued until the latest timepoint of DIV 6W (see Fig. 20C). Expression appeared to be highly variable in our SOD^{G93A} astrocyte cultures, although there was no overall statistical difference in expression as a result of the ALS mutation ($F(1,4)=1.928$, $P=0.24$). There were also no clear effects of time in culture, revealing no developmental trajectory of expression ($F(1.840, 7.359)=1.295$, $P=0.33$). Low Ns may account for this variability, however, there was still no clear evidence of disease related change. In our C9BAC500 cultures, there was considerably less variability, and expression was also clear at all time points measured (see Fig. 20D). Again, there was no effect of the presence of an ALS mutation on ephrin-B1 expression ($F(1,6)=0.4855$, $P=0.51$). There was a statistically significant effect of time ($F(2.192, 13.15)=4.237$, $P=0.0352$), however pairwise comparisons revealed no differences between individual time points.

Together, we see abundant expression of the contact-dependent, synaptogenic agent ephrin-B1 at all time points in our primary astrocyte cultures. Despite some variability, we see no clear evidence of changes in expression in SOD1^{G93A} or C9BAC500 astrocyte cultures, providing further evidence that our postnatal ALS astrocytes do not cause non-cell autonomous effects on E:I ratios in disease.

A

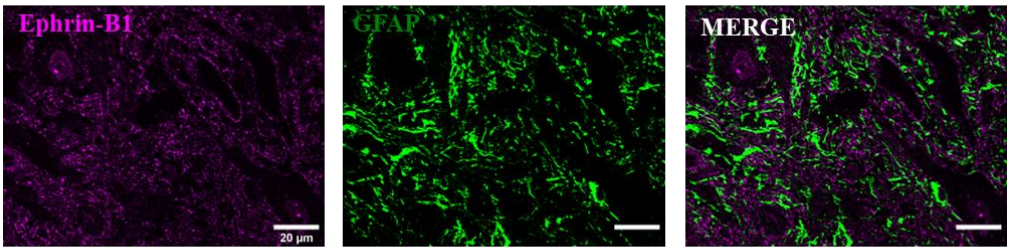
Ephrin-B1
GFAP
MERGE
20 µm

B

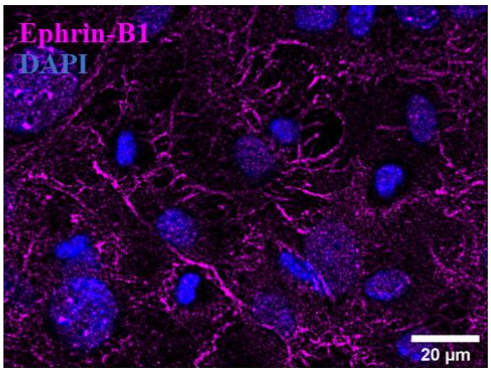
Ephrin-B1
DAPI
20 µm

C

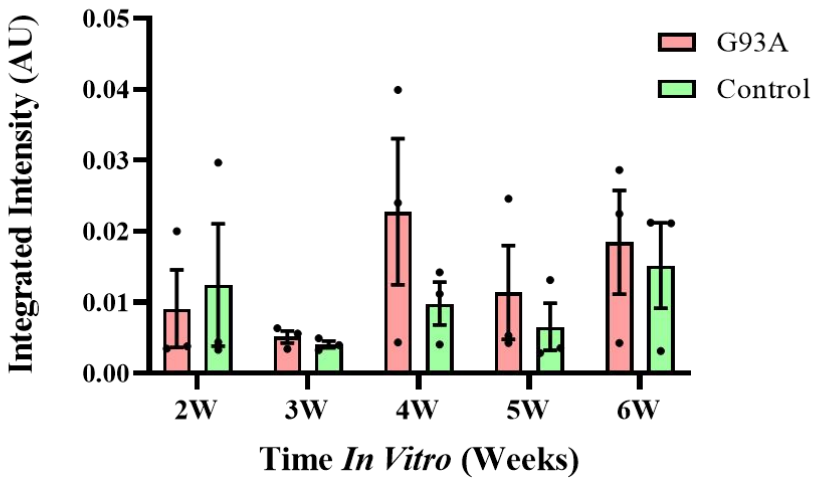
Integrated Intensity (AU)
0.05
0.04
0.03
0.02
0.01
0.00
G93A
Control
2W
3W
4W
5W
6W
Time *In Vitro* (Weeks)

D

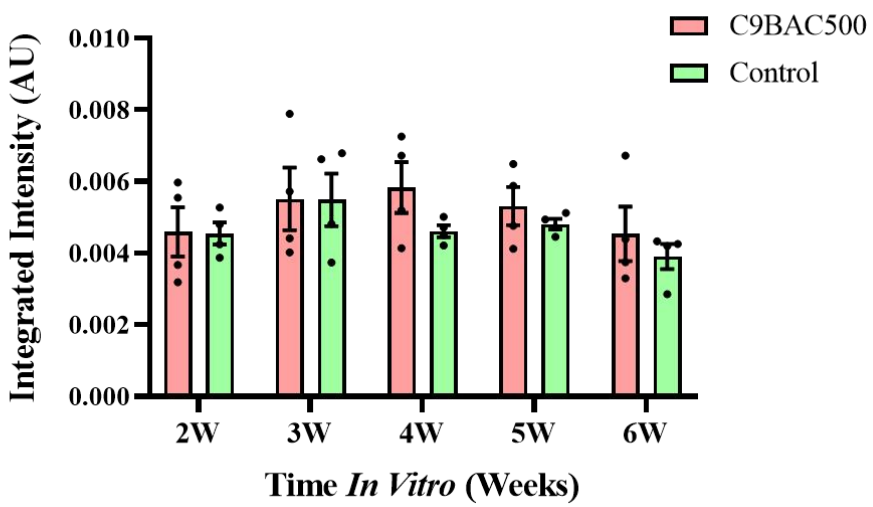
Integrated Intensity (AU)
0.010
0.008
0.006
0.004
0.002
0.000
C9BAC500
Control
2W
3W
4W
5W
6W
Time *In Vitro* (Weeks)

Figure 20: **A**) Positive control image of ephrin-B1 expression in P8 wild-type spinal tissue relative to astrocytic GFAP expression. **B**) Example image of ephrin-B1 expression in primary astrocyte culture. **C**) Expression of ephrin-B1 in primary astrocytes harbouring the $SOD1^{G93A}$ mutation. 'G93A' refers to cultures derived from $SOD1^{G93A\ +/-}$ PSD95-eGFP $^{+/-}$ animals, whilst 'Control' refers to cultures derived from $SOD1^{G93A\ -/-}$ PSD95-eGFP $^{+/-}$ animals (N=3 platedowns). **D**) Expression of ephrin-B1 in primary astrocytes harbouring the C9BAC500 mutation. 'C9BAC500' refers to cultures derived from C9BAC500 $^{+/-}$ PSD95-eGFP $^{+/-}$ animals, whilst 'Control' refers to cultures derived from C9BAC500 $^{-/-}$ PSD95-eGFP $^{+/-}$ animals (N=4 platedowns).

2.4. E:I Ratios Remain Unchanged in the Young SOD1^{G93A} Mouse Spinal Cord

As we observed no changes in E:I ratios when new synapses were being formed using our co-culture model, we wanted to verify this was also the case in the lumbar spinal cord of young SOD1^{G93A} mice. Given that postnatal development of the spinal circuitry undergoes major developmental changes from animals being relatively sessile in week 1, to developing basic weight bearing locomotion in week 2, to being able to produce complex motor behaviours similar to that of adults during week 3 (Sharples and Miles, 2021), week 3 was selected as an appropriate early time point. This provides an early presymptomatic timepoint whereby any biases in E:I ratios could be observed in the relatively 'mature' spinal cord avoiding these transient developmental changes. It is also a time point immediately after the peak of postnatal synaptogenesis in the spinal cord, allowing us to look at E:I ratios when this has largely concluded (Weber and Stelzner, 1980).

As has been discussed in depth previously, the observation that the pre-MN circuitry is hyperexcitable in ALS (van Zundert et al., 2008; Jiang et al., 2009) may be due to changes in E:I ratios throughout the grey matter, and not simply onto MNs. Therefore, we wanted to quantify E:I ratios broadly throughout the lumbar circuitry. In order to do this, we utilised SOD1^{G93A} x PSD95-eGFP crosses, and immunohistochemically targeted synapsin and gephyrin as before in our co-culture studies. Imaging was conducted at x63 magnification, however, stitches of 50-60 images were created to effectively capture an entire spinal cord hemi-section at high resolution. The images produced could then be delineated into Rexed's laminae. These are divisions of the grey matter described by Bror Rexed, who divided the grey matter into lamina 1-10 based on the neuronal cytoarchitecture (Watson et al., 2009).

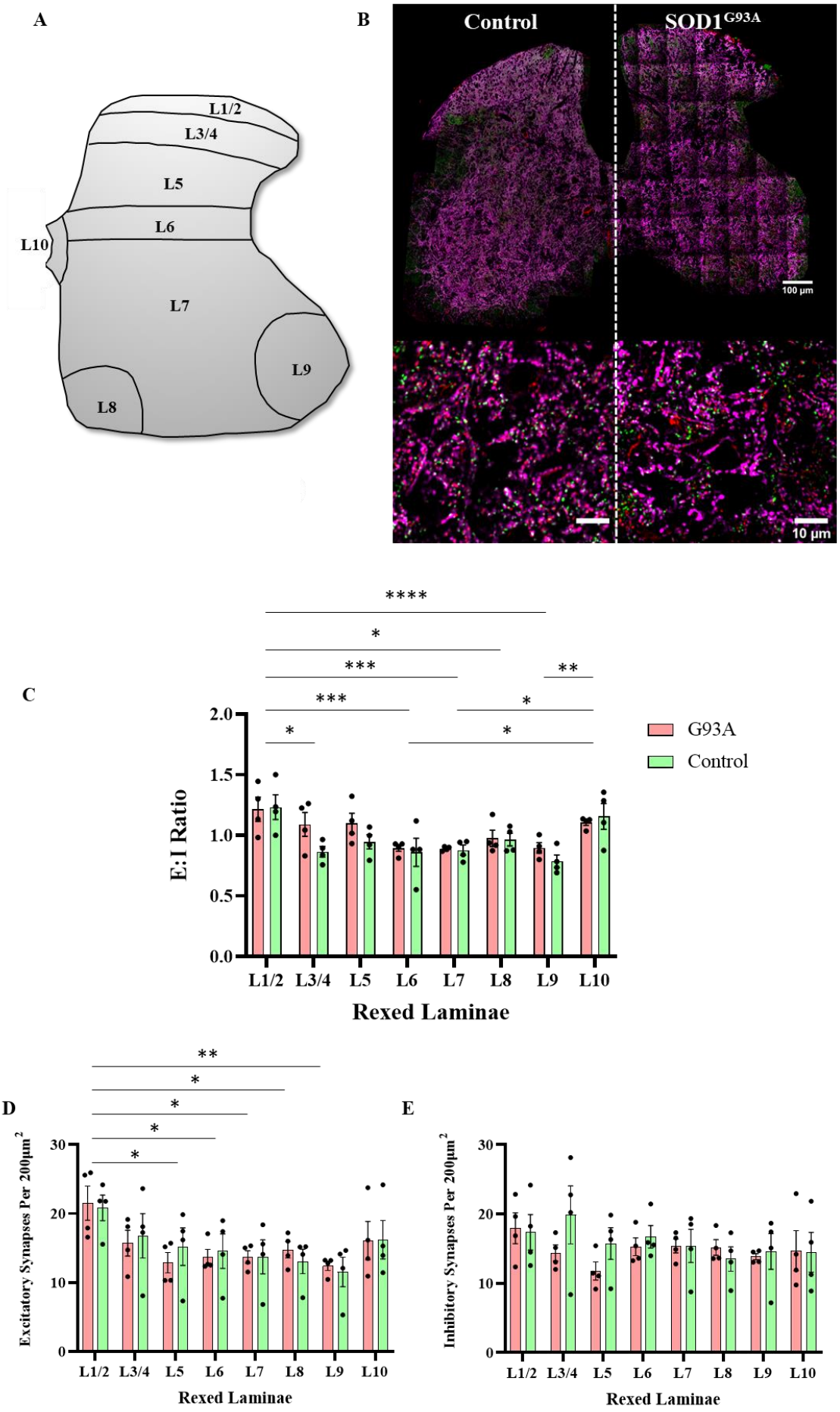
A
L1/2
L3/4
L5
L6
L10
L7
L9
L8
B
Control
SOD1G93A
100 µm
10 µm
C
****
*
***
**
***
*
*
*
G93A
Control
E:I Ratio
2.0
1.5
1.0
0.5
0.0
L1/2 L3/4 L5 L6 L7 L8 L9 L10
Rexed Laminae
D
**
*
*
*
*
Excitatory Synapses Per 200µm2
30
20
10
0
L1/2 L3/4 L5 L6 L7 L8 L9 L10
Rexed Laminae
E
Inhibitory Synapses Per 200µm2
30
20
10
0
L1/2 L3/4 L5 L6 L7 L8 L9 L10
Rexed Laminae

Figure 21: **A**) Schematic demonstrating the Rexed's laminae of the L3 lumbar spinal cord used to delineate E:I ratios in different parts of the grey matter (Watson et al., 2009). **B**) Example hemi-section scans of synapsin, PSD95-eGFP and gephyrin in a control spinal cord ($SOD1^{G93A\ -/-}$ $PSD95\text{-}eGFP^{+/-}$) and a $SOD1^{G93A}$ spinal cord ($SOD1^{G93A\ +/-}$ $PSD95\text{-}eGFP^{+/-}$), in addition to zoomed images revealing high resolution synaptic structures. **C**) Quantification of E:I ratios across spinal laminae in control versus $SOD1^{G93A}$ spinal slices (P16-P19, N= 4 for control and $SOD1^{G93A}$). **D**) Quantification of excitatory synapse density across spinal laminae in control versus $SOD1^{G93A}$ spinal slices (N=4 for control and $SOD1^{G93A}$). **E**) Quantification of inhibitory synapse density across spinal laminae in control versus $SOD1^{G93A}$ spinal slices (N=4 for control and $SOD1^{G93A}$). **NOTE:** Spinal tissue slices produced by Dr. Matthew Broadhead. Immunohistochemistry, imaging and analysis performed by Calum Bonthron.

Lamina 1 is the most dorsal, descending to lamina 8 and 9 which represent the medial and lateral MN pools, respectively (see Fig. 21A). The division of our spinal hemi-sections into laminae provided a tool with which to investigate putative region-specific alterations in E:I ratios.

Hemi-section scans were delineated using a standardised mouse spinal atlas (Watson et al., 2009), allowing for E:I ratio analysis to be compared within, and between, individual laminae. Examples of such hemi-sections can be seen in Fig. 21B, with zoomed images beneath showing that the resolution is maintained, allowing for clear observation of punctate synapsin, PSD95-eGFP and gephyrin expression. Our widescale mapping of E:I ratios across spinal laminae revealed no effect due to the presence of the $SOD1^{G93A}$ mutation (see Fig. 16C) ($F(1,48)=2.756$, $P=0.10$) (see Fig. 21C). Most laminae showed little variation between genotypes, with the exception being L3/4, which showed a trend towards a slightly higher E:I ratio in $SOD1^{G93A}$ animals versus controls. However, overall, this is consistent with the lack of E:I shift observed *in vitro*. There was, however, a strong effect of region on E:I ratio ($F(7,48)=6.740$, $P<0.0001$). In particular, L1/2 showed a stronger bias towards excitatory transmission compared to multiple other laminae (**L1/2 vs L3/4**: $P=0.0255$, **L1/2 vs L6**: $P=0.0004$, **L1/2 vs L7**: $P=0.0005$, **L1/2 vs L8**: $P=0.0189$ and **L1/2 vs L9**: $P<0.0001$). Lamina 10 surrounding the central canal also showed a higher E:I synaptic ratio compared to more ventral regions (**L10 vs L6**: $P=0.202$, **L10 vs L7**: $P=0.0258$ and **L10 vs L9**: $P=0.0048$). It therefore appears that different regions of the lumbar grey matter have differential biases in excitatory versus inhibitory transmission, presumably to facilitate the processing requirements of the local circuitry. Finally, there was a lack of more complex interactions between laminae and genotype ($F(7,48)=0.8583$, $P=0.55$).

In order to dissect changes in E:I ratios between regions, in addition to checking once again that there was no masked parallel change in both excitatory and inhibitory transmission, the density of both synapse types was quantified across laminae. Excitatory synapse density was not significantly different between $SOD1^{G93A}$ and control spinal cords ($F(1,48)=0.02050$, P=0.89), nor was there any interaction between genotype and region ($F(7,48)=0.1762$, P=0.99) (see Fig. 21D). There was, however, a difference in excitatory synapses between laminae ($F(7,48)=3.433$, P=0.0047), again revealing the most dorsal L1/2 region had significantly higher synapse density versus multiple other more ventral regions (**L1/2 vs L5**: P=0.0315, **L1/2 vs L6**: P=0.0337, **L1/2 vs L7**: P=0.0209, **L1/2 vs L8**: P=0.0264 and **L1/2 vs L9**: P=0.0019). Inhibitory synapse density was also not significantly different between $SOD1^{G93A}$ and control spinal cords ($F(1,48)=1.111$, P=0.30) (see Fig. 21E). Together with a lack of genotype effect in excitatory synapse numbers, it is clear that there is no masked parallel shift in excitatory and inhibitory synapse densities in $SOD1^{G93A}$ cords. Interestingly, there is no effect of region on inhibitory synapse density ($F(7,48)=0.8602$, P=0.54). This suggests therefore that region-specific differences in E:I ratios are mainly driven by changes in excitatory rather than inhibitory synapse formation.

Together, region-specific analysis of excitatory and inhibitory synapses in young $SOD1^{G93A}$ spinal cords does not reveal a disease-related E:I shift towards pathological excitation, and thus supports a lack of structural evidence for astrocyte-mediated synaptogenesis changes in ALS.

2.5. Human iPSC-Derived MN / Astrocyte Cultures Harbouring C9orf72 Mutations Show No Evidence of E:I Shifts

As we found no evidence of ALS-related E:I shifts in both our murine primary culture and spinal tissue models, we wanted to look for any evidence of excitability bias using human cells. Induced pluripotent stem-cell (iPSC)-derived MNs are a powerful tool, as they are electrophysiologcally active cells expressing MN markers such as ISL1/2 and SMI 32, and can be produced from patient skin fibroblasts (Devlin et al. 2015; Maury et al., 2015). This provides an effective way to study ALS in human cells *in vitro*. They can even be CRISPR-Cas9-corrected to remove pathogenic mutations, leaving otherwise genetically identical isogenic controls. These have been used to give powerful insights into ALS mechanisms, including the non-cell autonomous role of astrocytes (Devlin et al., 2015; Zhao et al., 2020). We therefore wanted to use them to look for evidence of E:I ratio changes outside of mouse models. We generated iPSC-derived cultures using a slightly modified protocol described by Selvaraj and colleagues (2018). This produces an enriched culture of neurons expressing MN marker Islet-1/2 (40-60%), with the rest presumably being uncharacterised spinal neurons. We, however, did not add anti-mitotic agent U/FDU to suppress astrocytes, allowing their proliferation to produce a mixed neuronal / astrocytic culture.

Interneuronal MN synapses have previously been shown to be entirely glutamatergic (excitatory) (Zhang et al., 2011), with evidence of robust PSD95 expression in other work using iPSC-derived MNs (Kim et al., 2020). In order to look at E:I ratios in this model, we

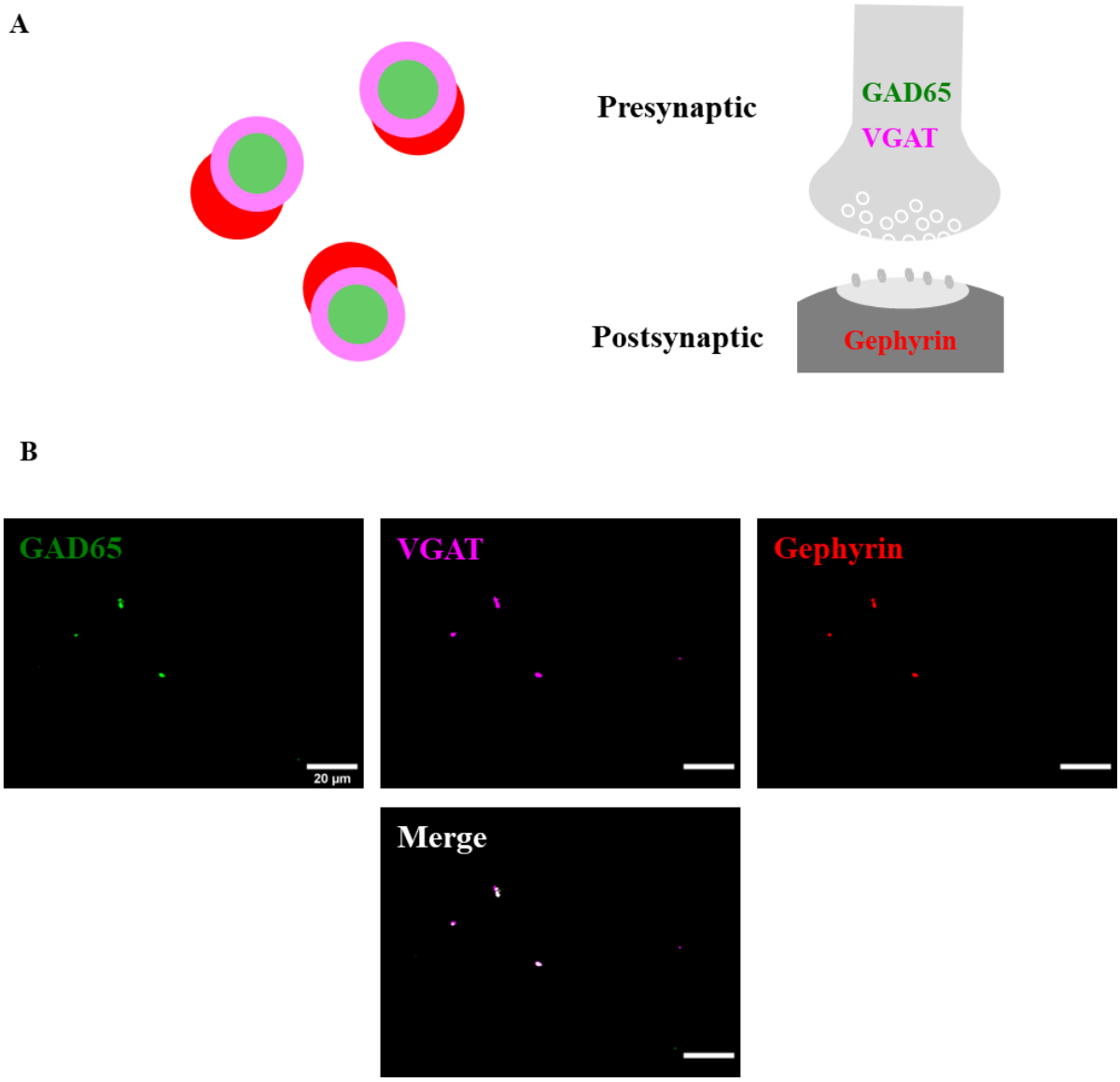

Figure 22: **A**) Schematic demonstrating expected location of GAD65, VGAT and gephyrin expression. **B**) Example image of co-localised presynaptic inhibitory markers GAD65 and VGAT, overlapping with postsynaptic marker gephyrin.

first had to validate that we had quantifiable inhibitory synapses. However, with the culture being enriched in MNs, and other iPSC-derived methodologies showing almost entirely excitatory transmission *in vitro* (Devlin et al., 2015), we first wanted to be sure that any infrequent inhibitory synapses we may see were genuine. To do this, we immunocytochemically targeted specific inhibitory presynaptic markers GAD65 and VGAT found at GABAergic and GABAergic / glycinergic presynaptic terminals, respectively (Saito et al., 2010; Walls et al., 2010). We looked for co-localisation of these markers in our iPSC-derived MN cultures with the postsynaptic marker gephyrin (see Fig. 22A). We found that gephyrin puncta were indeed very infrequent, and when they were observed they appeared as bright punctate structures, as expected. We found evidence of GAD65 and VGAT co-localisation, and these were opposed to gephyrin puncta (see Fig. 22B).

Confident that the limited inhibitory transmission we saw in our iPSC-derived MN cultures was genuine, we went on to quantify E:I ratios in multiple platedowns of MNs derived from an iPSC line harbouring a C9orf72 repeat expansion, along with a gene-corrected isogenic control line in which the hexanucleotide repeat sequence had been removed. This acts as the most ideal control when investigating the effects of an ALS mutation. Figure 23A demonstrates a representative image of our E:I markers in these iPSC-derived MN cultures. Synapsin and PSD95 are relatively abundant, showing an expected punctate expression and a significant degree of co-localisation, as can be seen in the zoomed panels. Gephyrin puncta are present, but very infrequent as described above. The infrequency of inhibitory transmission was found to limit the extent to which E:I ratios could be informative in this model (see Fig. 23B). Due to relatively few gephyrin puncta being present, small changes in inhibitory synapse counts caused large variations in E:I ratios between images, likely

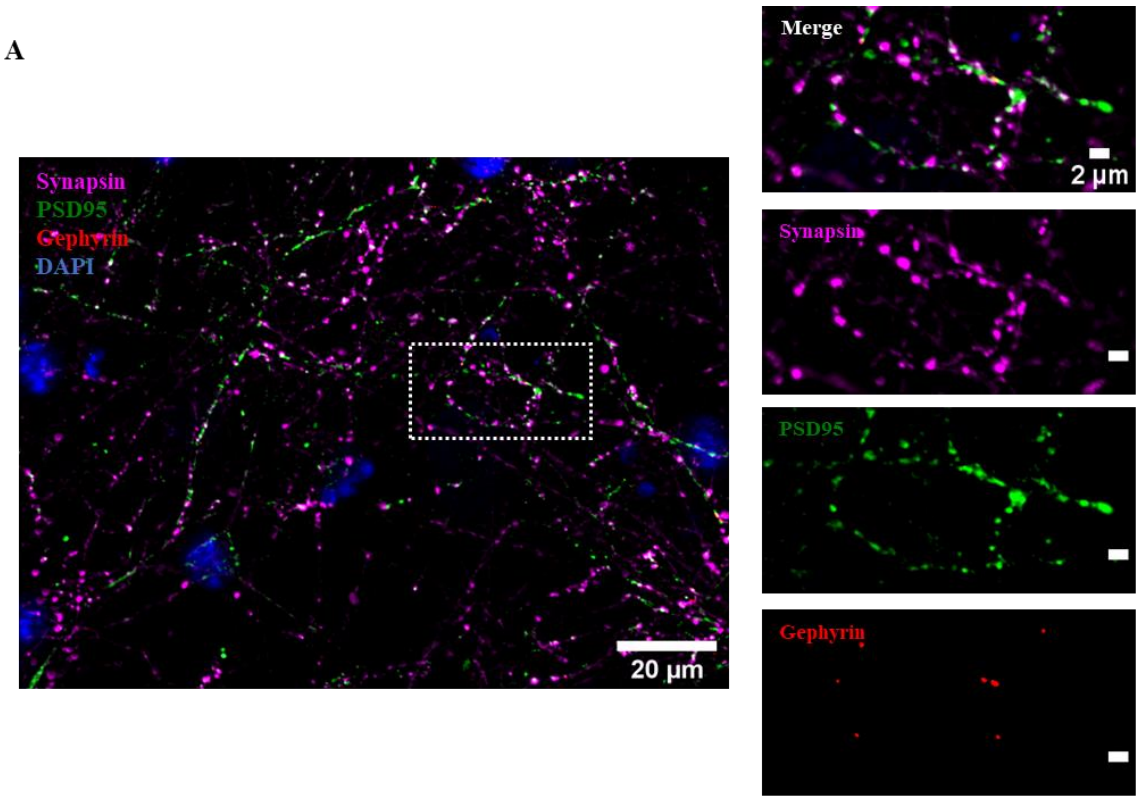
A
Synapsin
PSD95
Gephyrin
DAPI
20 µm
Merge
2 µm
Synapsin
PSD95
Gephyrin

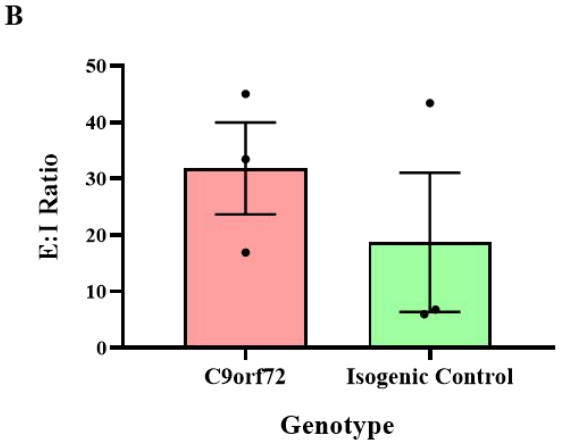
B
E:I Ratio
50
40
30
20
10
0
C9orf72
Isogenic Control
Genotype

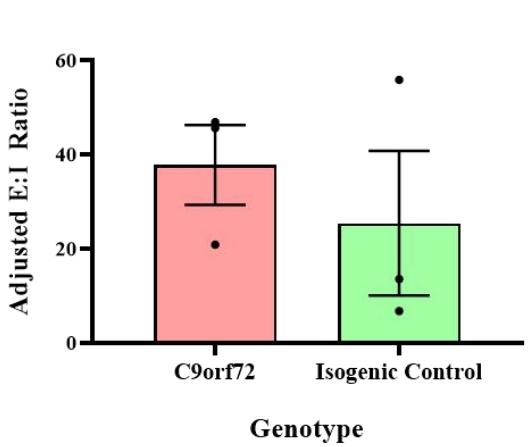
C
Adjusted E:I Ratio
60
40
20
0
C9orf72
Isogenic Control
Genotype

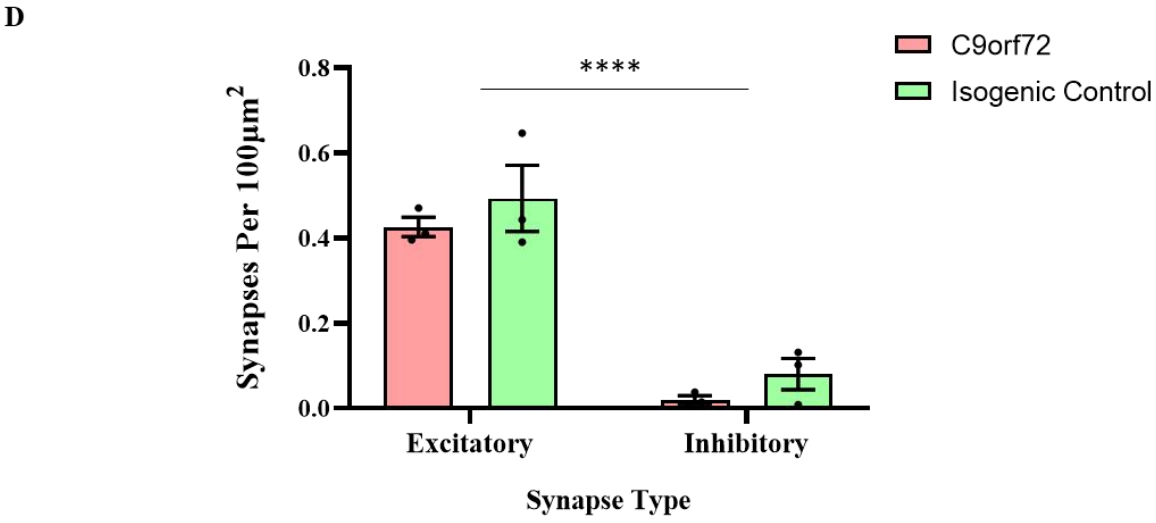
D
Synapses Per 100µm2
0.8
0.6
0.4
0.2
0.0
****
C9orf72
Isogenic Control
Excitatory
Inhibitory
Synapse Type

Figure 23: **A**) Example image of a DIV 4W iPSC-derived culture expressing synapsin, PSD95 and gephyrin. Zoomed panels on the right show large degree of synapsin-PSD95 co-localisation, with relatively few gephyrin puncta present. **B**) Quantification of E:I ratio in C9orf72 versus isogenic control cultures (DIV 4W, N=3 platedowns). **C**) Quantification of 'adjusted E:I ratio' in C9orf72 versus isogenic control cultures **D**) Quantification of excitatory vs inhibitory synapse densities in C9orf72 cultures vs isogenic controls. **NOTE**: Cells grown by Dr. Sarah Burley. Immunocytochemistry, imaging and analysis performed by Calum Bonthron.

accounting for the variability seen. Nonetheless, there was no statistically significant difference in E:I ratio between C9orf72 and isogenic control cultures ($t(4)=0.8854$, P=0.43). As it was very common for no obvious gephyrin puncta to be present in a single x63 magnification image, this caused many images to have an 'infinite' E:I ratio, due to the 'I' value = 0. Therefore, to attain the standard E:I ratio measurement, there was a large number of images rejected. In order to better represent all data captured, an 'adjusted E:I ratio' was also calculated, which simply artificially adds a value of '1' gephyrin synapse to images that lacked any inhibitory transmission at all. This prevents production of infinite values and resultant mass rejection of images. These values were also very noisy however, likely for the same reasons discussed earlier (see Fig. 23C). There was no statistically significant difference in adjusted E:I ratio between C9orf72 harbouring cultures and isogenic control cultures ($t(4)=0.7074$, P=0.52).

As a result of this issue, it was deemed more informative in this model to look at individual excitatory and inhibitory synapse densities to find whether there is any indication of a shift towards pathogenic excitation. This metric allowed a '0' density value of inhibitory synapses to be recorded without creating the issue of infinite values as seen in the E:I quantification, and likely gives a better idea of any synaptic changes. As expected, there was considerably more excitatory transmission in these cultures than inhibitory transmission ($F(1,8)=83.21$, P<0.0001) (see Fig. 23D). There was no significant difference in overall synapse counts between C9orf72 cultures and isogenic controls ($F(1,8)=2.041$, P=0.19). Importantly, the degree of bias towards excitatory synapse formation was not dependent on the genotype of the cells ($F(1,8)=0.006170$, P=0.94), indicating that the presence of the C9orf72 hexanucleotide repeat did not cause a pathological shift towards excitation. It should be noted, however, that iPSC-derived MN / astrocyte platedowns derive from differentiations of

one iPSC batch (as is common in the field). Therefore, to more definitely show that C9orf72 does not cause E:I shifts, more differentiations using this C9orf72 line, in addition to the use of more patient-derived lines would be required.

3. Discussion

We hypothesised that network-wide hyperexcitability in ALS could be, in part, caused by an early shift in the E:I ratio towards excitation, and that this reflected the perturbation of astrocytic synaptogenesis. To assess this, following validation of our ALS x PSD95-eGFP crosses which allowed for accurate tagging of glutamatergic postsynaptic densities, we grew combinations of ALS +ve and -ve neurons and astrocytes in our postnatal spinal co-cultures. When assessing the E:I ratios in these cultures with use of synapsin to tag presynaptic boutons, in addition to PSD95-eGFP and gephyrin to tag postsynaptic regions of excitatory and inhibitory synapses respectively, we found no difference between any combination of genotypes. This was the case in combinations of cells expressing both the $SOD1^{G93A}$ and C9BAC500 mutations. There was also no parallel change in the density of excitatory and inhibitory synapses. This lack of ALS-related E:I shift was mirrored in the expression of ephrin-B1, a known contact-dependent synaptogenic factor which controls E:I ratios. When the lumbar spinal cords of young $SOD1^{G93A}$ mice were compared to controls, they showed no difference in E:I ratios or densities of excitatory / inhibitory synapses across grey matter laminae. Finally in an iPSC-derived MN model containing astrocytes, we found no change in the density of excitatory synapses relative to inhibitory synapses as a result of a C9orf72 hexanucleotide repeat. Thus, we find no structural evidence of non-cell autonomous E:I ratio shifts across multiple ALS models.

The knock-in PSD95-eGFP mouse has been successfully used to investigate synaptic diversity and ultrastructure in the brain (Broadhead et al., 2016; Zhu et al., 2018) as well as the healthy spinal cord (Broadhead et al., 2020). It is a powerful genetic tool to reliably image postsynaptic densities. Thus, it was desirable to use in our study of synaptic changes in ALS.

We first wanted to verify that when bred with our ALS models, producing progeny that was now only heterozygous for PSD95-eGFP, that these cultures still showed detectable GFP signals. This could be worsened by gradual bleaching of GFP during the culturing period, with the photostability of GFP *in vitro* already being a known concern (Bogdanov et al., 2012). Our cultures, however, showed sufficient GFP signals, which strongly co-localised with a PSD95 antibody, giving us confidence that our GFP signal was being expressed at the desired postsynaptic site.

ALS x PSD95-eGFP crosses were therefore used to look at non-cell autonomous synaptogenic effects of astrocytes on E:I ratios. As primary culture protocols involve enzymatic digestion of tissue to isolate single neurons in suspension, their neurites are sheared thus so are their synapses (Katzenell et al., 2017). Therefore, plating neurons either +ve or -ve for $SOD1^{G93A}$ on top of +ve or -ve astrocytes produces a system whereby synapses are reformed and affected by the astrocytic factors discussed previously. We observed a bias towards inhibitory transmission in our co-cultures, with all conditions showing a E:I ratio below 1 which was not significantly different between $SOD1^{G93A}$ and C9BAC500 cultures, nor their respective controls. Our whole-cell patch-clamp data, however, suggested that the majority of active synapses *in vitro* were excitatory. There are a number of reasons why this may be the case. First, although downward deflections when held at -60mV are likely excitatory due to increased Ca^{2+} / Na^{+} permeability through glutamate-gated ion channels, the composition of the internal and external solutions may result in -60mV being *below* the Cl^{-} reversal potential instead of above, as assumed. Unlike when we are *above* the Cl^{-} reversal potential causing GABA / glycine-mediated Cl^{-} entry into the cell, if we are the *below* the reversal potential at -60mV, this would cause Cl^{-} to reverse in direction and leave the cell. This therefore would also create downward deflections in voltage clamp mode. This could be

checked by also looking at spontaneous postsynaptic currents when the cell is held at a value well above the Cl^- reversal potential, such as -40mV. In addition, electrophysiological synaptic quantification was done during validation of our neuronal monocultures, and as we know astrocytic presence directly modulates inhibitory synaptic formation (Cuevas et al., 2005; Diniz et al., 2012; Diniz et al., 2014), the astrocytic layer in our co-cultures may have preferentially increased inhibitory synaptogenesis. There is also the possibility that inhibitory synapses are structurally present but delayed in maturity versus excitatory ones. This is unlikely however, as there is physiological evidence in other primary co-culture models of mature inhibitory transmission by DIV 3W (Elmariah et al., 2005).

We did not note any astrocyte-driven effects on E:I ratios in our co-cultures, but we also did not see a difference in the E:I ratio between our purely +ve (+ve neurons and +ve astrocytes) and purely -ve cultures in both $SOD1^{G93A}$ and C9BAC500 cultures. Confirmation of this using multiple ALS mouse models is important, as although the C9BAC500 model has been criticised for its inconsistency in developing reliable phenotypes (Mordes et al., 2020; Nguyen et al., 2020), the lack of effect in the robustly phenotypic $SOD1^{G93A}$ model gives us confidence that this is not simply due to poor penetrance in one mouse model. Evidence of shifts towards excitation (usually only by quantifying a loss of inhibitory synapses) is found much later in disease progression than the P2/3 animals used in our cultures (Sunico et al., 2011; Chang and Martin, 2009; Qian et al., 2017). These studies often only look at inhibitory loss directly onto MNs, so it is possible a more nuanced effect of E:I shifts may be seen if MNs alone were investigated in our model. However, as previously mentioned, markers such as ChAT or VAChT fail to effectively stain all of the cell, making complete quantification of synaptic input challenging (Schutz, 2005; Chang and Martin, 2009). Even if we observed E:I ratio shifts of synaptic input onto MNs, hyperexcitability of the larger spinal network as a

whole has been recorded, so this would not explain this tendency for excessive excitability in spinal interneurons. It is also a possibility that the time point selected does not show any genotype-related effects on E:I ratios. Longer-term co-culture was found to be challenging, as a limitation in our model is the propensity for astrocytic layers to peel when in culture for longer than 6W (usually DIV 2-3W before neuronal plating), making this difficult to test.

We also found no clear changes in ephrin-B1 expression in both $SOD1^{G93A}$ and C9BAC500 astrocytes. In the hippocampus during a major period of synaptogenesis, ephrin-B1 can act to modulate E:I ratios. Downregulation causes boosted excitatory synapse formation as well as loss of inhibitory synapses, which appears to at least partially be due to parvalbumin +ve inhibitory neuron loss (Nguyen et al., 2020a; Nguyen et al., 2020b). This subtype of inhibitory interneuron is known to be populous in the spinal cord (Petitjean et al., 2015). In the brain, there is evidence of ALS-associated hypoexcitability of parvalbumin +ve interneurons, which directly modulate excitability of layer 5 primary motor cortex pyramidal cells (Khademullah et al., 2020). There is, however, no reported loss of these cells in $SOD1^{G93A}$ motor cortices (Clark et al., 2017), and although ubiquitinated aggregates are noted in parvalbumin +ve cells at 20W of age in a low-copy number $SOD1^{G93A}$ model (Hossaini et al., 2011), there is no evidence of early-stage loss which could contribute to an ephrin-B1-related shift in E:I ratios. This result provides further confidence in the conclusion that there are no ALS-related E:I shifts in our primary co-culture model.

In order to see if intact spinal circuitry shows alterations in E:I ratios in a mouse model of ALS, we utilised the same excitatory and inhibitory synaptic markers as in our *in vitro* study. We chose to compare $SOD1^{G93A}$ and control animals at week 3, immediately after major periods of synaptogenesis and maturation in order to assess if this early system may be

developmentally primed towards excess excitation. To our knowledge, this is the first instance of a complete synaptic map encompassing excitatory and inhibitory transmission across all lumbar laminae in ALS. We found region-specific differences in E:I ratios, finding that the most dorsal laminae L1/2 showed a greater bias towards excitation than more ventral regions. A high density of PSD95+ve PSDs has been noted previously in the superficial laminae of the dorsal horn (Broadhead et al., 2020). This is likely due to this area being a hub for somatosensory processing, with all primary afferents and a large majority of local interneurons being glutamatergic, increasing the relative amount of excitation in this region (Gutierrez-Mencinas et al., 2016). This was reflected when synapse densities were analysed separately, as we see significantly higher excitatory synapse densities in L1/2 compared to more ventral regions, whilst inhibitory synapses were not significantly different between laminae.

Presence of the $SOD1^{G93A}$ mutation had no effect on E:I ratios however, consistent with our *in vitro* dataset. Previous evidence of synaptic subtype loss throughout the grey matter is sparse, with most evidence measuring synapses directly onto MNs. Hossaini and colleagues (2011) noted GABAergic presynaptic loss at a symptomatic stage, and GABAergic / glycinergic loss at end stage in a low-copy number $SOD1^{G93A}$ mouse model. They used immunohistochemistry to look at intensity of staining throughout the grey matter. This timepoint is difficult to compare due to vastly different disease progression in these two models, but it appears to suggest that inhibitory loss is a late-stage phenomenon likely reflecting interneuron cell death, and not the developmental excitatory shift we hypothesised. Interestingly, we also observed no evidence of E:I shift in L8 and L9, which represent medial and lateral motor pools (and surrounding input), respectively. We did not see changes in MN input as reported by other groups described previously. Although this inconsistency may be

due to a different method of quantification (delineation of laminae vs direct quantification of synapses onto MNs) in addition to differential specificity of synapse subtype targeted, such changes have all been reported much later in disease progression (2-3 months of age), which is likely a factor in this discrepancy (Sunico et al., 2011; Chang and Martin. 2009).

Finally, as we saw no evidence of altered E:I ratios in our mouse models, we wanted to assess if this was the case in human cells. iPSC-derived MN cultures have been used to probe many mechanisms of disease, from excitability changes to non-cell autonomous MN death and mitochondrial impairment (Devlin et al., 2015; Mehta et al., 2021; Selvaraj et al., 2018). They provide a powerful tool with which to probe ALS disease mechanisms in human cells and in the process, hopefully aid translatability of knowledge. In our hands, we found that a large amount of intraneuronal MN synapses are glutamatergic *in vitro*, as has been previously shown (Zhang et al., 2011). We found evidence of infrequent inhibitory transmission in our cultures. As such, E:I values were highly variable due to this infrequency, whereby small changes in inhibitory synapse counts caused large differences in E:I ratios. Investigation of synapse densities alone was more informative, with no obvious pathological changes as a result of the C9orf72 mutation, although it is clear due to the low amount of inhibitory transmission in these cultures that quantifying the E-I balance is noisy. iPSC-derived MNs harbouring C9orf72 mutations have been shown to display some degree of excitatory synaptic loss previously (Catanese et al., 2021), however, this was seen in cultures grown for considerably longer (over twice the time DIV). Also, this quantification appears to have used a combination of iPSC-derived MN lines from healthy controls in addition to isogenic control lines in their comparison. This is not considered good practice, as the isogenic control for a single C9orf72 mutant line represents the best point of comparison. This is due to having an otherwise identical genetic profile, allowing the contribution of the mutation to be assessed

accurately. Although our data is informative in addition to results gathered from other models, more platedowns and patient derived iPSC lines would strengthen our argument, as admittedly N numbers are low for such a noisy quantification.

Overall, therefore, in our primary co-culture *in vitro* model, young SOD1^{G93A} spinal cords, and C9orf72-harbouring MN/astrocyte cultures, we see no structural evidence of early pathogenic E:I shifts in ALS. It is possible, however, that there are still early functional changes which may not have been picked up by anatomical analyses. One possibility is that although we see the same numbers of excitatory and inhibitory synapses between conditions, in ALS some may be dysfunctional as can be seen in Fragile X syndrome, where there appears to be an increase in synapses but not all are functional or mature (Pfeiffer and Huber, 2009). Alternatively, as hypothesised by Kiernan and colleagues (2019), a developmental shift towards hyperexcitability could be due to a delay in the GABAergic switch from excitatory to inhibitory transmission. This switch is a result of changes in KCC2 and NKCC1 expression during the early postnatal period (Furukawa et al., 2017). This helps alter the initially high intracellular chloride concentrations as neurons mature, resulting in a switch from GABAergic transmission causing depolarisation to hyperpolarisation (Kiernan et al., 2019; Schulte et al., 2018). Alterations in the balance of these transporters modulate intracellular Cl^- concentrations. Indeed, factors such as neonatal stress have been shown to downregulate KCC2 expression during development and cause a resultant delay in the GABAergic switch (Furukawa et al., 2017). It is conceivable therefore, that in ALS via an undefined mechanism, there is a downregulation of KCC2 expression that primes the system towards hyperexcitability *without* showing resultant changes in structural markers. Mòdol and colleagues (2014) observed no evidence of changes in KCC2 expression in the ventral lumbar spinal cord of SOD1^{G93A} mice at 8, 12 and 16 weeks of age. However, other authors

have noted downregulation of KCC2 mRNA transcripts at the symptomatic age of P120 in lumbar MNs, as well as presymptomatically (P80) in hypoglossal MNs (Fuchs et al., 2010). This was reflected in the qualitative assessment of KCC2 protein immunoreactivity in the ventral horn. NKCC1 mRNA levels were unaltered in the $SOD1^{G93A}$ spinal cord however (Fuchs et al., 2010). There is tentative evidence of possible KCC2-driven alterations in spinal network excitability therefore, however, a more thorough examination of the balance between KCC2 and NKCC1 at very early stages of the disease is necessary to ascertain if this is the case.

To conclude, there does not appear to be structural evidence of developmental shifts in E:I ratios in spinal networks in ALS. It is possible that we have failed to capture even earlier changes. However, evidence from young spinal tissue after the major period of postnatal synaptogenesis would suggest that if this is the case, it is transient and likely does not represent a major driver of later hyperexcitability. Astrocytes do not only modulate synaptogenesis, however. As discussed previously, they are important regulators of function at the tripartite synapse, where they have the capability to contribute to pathogenesis in a multitude of other ways. Investigation of their properties at these structures will be the next topic of investigation, in order to further elucidate the roles of astrocyte-synapse interactions in ALS.

Chapter 5

Investigating the Interaction of Astrocytes with Mature Synapses in ALS

Work within this chapter was completed with contribution from Dr. Matthew Broadhead and the NCM Lab. Elements are also published in the following papers:

- **Broadhead and Bonthron et al., 2020. Nanostructural Diversity of Synapses in the Mammalian Spinal Cord. *Scientific Reports*¸10, pp1-18**

- **Broadhead and Bonthron et al., 2022. Selective vulnerability of tripartite synapses in amyotrophic lateral sclerosis. *Acta Neuropathologica*, 143, pp471-486**

1. Introduction

Astrocytes do not only act to promote synaptogenesis early in development. They are responsible for a multitude of functions and interact with mature synapses at structures called 'tripartite synapses' (Allen and Eroglu, 2017). Envelopment of synapses by astrocytes appears to be a complex and dynamic process, whereby the degree of synaptic coverage is influenced by the activity of the surrounding neural network (Bernardinelli et al., 2014; Genoud et al., 2006). Synaptic envelopment involves very small protrusions (<100nm) budding off the astrocytes' complex branching structure. These are referred to as perisynaptic astrocytic processes (PAPs) and contain an enormous variety of proteins required for their function (Heller and Rusakov, 2015). These include metabotropic glutamate receptors, which are required for reacting to neuronal activity both via alteration of synaptic coverage and release of 'gliotransmitters' to modulate neuronal transmission (Bernardinelli et al., 2014; Broadhead and Miles, 2020; Lavialle et al., 2011; Witts et al., 2011). Also expressed at PAPs are glutamate transporters, including EAAT1 and EAAT2 (referred to GLAST and GLT-1 in humans, respectively), with EAAT2 appearing to be responsible for the majority of glutamate transport (Lehre and Danbolt, 1998; Pajarillo et al., 2019; Rothstein et al., 1996). Here they remove excess glutamate present in the synaptic cleft. This allows for the recycling of glutamate via the glutamate-glutamine cycle enabling sustained future synaptic activity (Uwechue et al., 2012; Tani et al., 2014), as well as the prevention of excitotoxicity (Rothstein et al., 1996).

Given that we found little evidence of astrocytic synaptogenic pathology during development, and considering the multitude of essential roles astrocytes fulfil at the mature synapse, perturbation of these interactions may also represent a mechanism of ALS pathogenesis.

Alterations of these roles in disease have indeed been reported. Amongst the most reported changes seen in ALS post-mortem tissue is the observation of dramatic EAAT2 loss (Rothstein et al., 1995). As discussed in Chapter 1 Section 3.4, multiple animal models reflect this loss, potentially presymptomatically (Bendotti et al., 2001; Bruijn et al., 1997; Howland et al., 2002). This may be the result of caspase-3-mediated cleavage of EAAT2, resulting in reduction of glutamate uptake (Boston-Howes et al., 2006). In addition, aberrant EAAT2 RNA processing has been shown to be present in sALS patients, producing translated proteins which undergo degradation (Lin et al., 1998). The only FDA-approved drug for ALS, Riluzole, adds credence to this disease mechanism whereby it appears to partially counter the effect of excitotoxicity (Rosenblum and Trotti, 2017). This is likely due to a number of factors including modulation of neuronal currents such as PIC_{Na}, however, there is also evidence that it may act to directly increase the activity of remaining EAAT2 transporters (Carbone et al., 2012; Rosenblum and Trotti, 2017).

Gliotransmission, the process by which astrocytes release factors in response to surrounding neuronal activity, might also be perturbed in ALS and could therefore represent another mechanism of tripartite dysfunction. Local glutamate release from the spinal CPG network activates metabotropic glutamate receptors on astrocytes, causing subsequent release of astrocytic ATP. This ATP is extracellularly degraded to adenosine, activating neuronal A_1 adenosine receptors which inhibit neuronal activity (Broadhead and Miles, 2020; Witts et al., 2011). Evidence of increased cerebrospinal adenosine levels (Yoshida et al., 1999), in addition to increased expression of the excitatory A_{2a} receptor in post-mortem ALS tissue (Ng et al., 2015), suggests such a system could be perturbed to promote excitotoxicity. This is further supported by evidence demonstrating that pharmacological inhibition of A_{2a} receptors delayed disease progression in $SOD1^{G93A}$ mice (Ng et al., 2015).

The interaction of astrocytes at mature synapses is therefore of interest, as tripartite synapses could represent a point of weakness in disease. In order to study them, however, we need a reliable way of visualising the fine astrocytic PAPs which envelope synapses. Astrocytes are complex cells, expressing a large number of markers that are not appropriate for such analysis. For example, GFAP, a classical marker regularly used to define astrocytic identity, is only expressed in the major processes of the cell, and not in the fine motile protrusions that are of interest (Heller and Rusakov, 2015). Multiple appropriate PAP protein targets have been suggested. One is glutamine synthetase, an abundantly expressed astrocytic marker which has been found at PAPs with the use of immunoelectron microscopy (Derouiche and Frotscher, 1991). Members of the ERM (ezrin, radixin and moesin) protein family are of interest due to their binding of actin at motile processes. Radixin was shown to be present in protruding 'filopodia' of cultured astrocytes, as was ezrin (Derouiche and Frotscher, 2001). Ezrin in particular is of interest, as later work suggested that its T567-phosphorylated active form (p-ezrin) is required for motility, where it links the actin skeleton to the plasma membrane (Bosk et al., 2011; Lavialle et al., 2011). Such motility is required at PAPs, with p-ezrin being found in motile filopodia, co-localising with glutamine synthetase and often being apposed to synaptic markers, providing strong evidence that p-ezrin is a selective marker for PAPs (Lavialle et al., 2011). Another favoured PAP protein candidate is EAAT2. Due to its role in clearing glutamate from the synaptic cleft, its perisynaptic location is required for its function. Its location at the PAP is supported by EM work (Melone et al., 2009).

Astrocytes therefore undergo a range of essential functions at the tripartite synapse. As discussed before, there is a large body of evidence reporting later-stage synaptic perturbations in ALS (Chang and Martin, 2009; Ince et al., 1995; Sunico et al., 2011; Zhang et al., 2005).

In addition, astrocytic dysfunction has been reported via a variety of different mechanisms (Valori et al., 2014). This includes dysfunction of proteins thought to reside at the tripartite synapse, such as EAAT2 (Howland et al., 2002). When taken together, it is conceivable that synaptic and astrocytic dysfunction are intrinsically linked, and that the tripartite synapse may represent a vulnerable fulcrum of disease in ALS. In order to test this hypothesis, we will look at tripartite synapse properties at multiple stages of ALS, from presymptomatic to symptomatic stages, in order to assess if tripartite synapses are at risk during the progression of disease.

2. Results

2.1. Validation of PAP Markers to Ensure Accurate Tripartite Visualisation

As previously mentioned, multiple markers have been suggested as appropriate protein targets for PAPs (Heller and Rusakov, 2015). Before being able to assess the interaction of astrocytes with mature synapses at the tripartite synapse, we first wanted to validate some of these suggested markers. The tripartite synapse is represented in a schematic in Figure 24A, whereby the presynaptic bouton releases glutamate which is detected at the PSD. The enveloping PAP, which is on average 50nm away from the pre- and postsynaptic membranes (Octeau et al., 2018), engulfs the synapse. Two markers were selected for further investigation: EAAT2 and T567-phosphorylated-ezrin (p-ezrin). As described earlier, EAAT2 expression at the astrocytic membrane facilitates the glutamate-glutamine cycle and prevention of excess glutamate retention, which could lead to excitotoxicity (Pajarillo et al., 2019; Stenovec et al., 2008; Uwechue et al., 2012). In order for this transporter to fulfil this role, it is logical for its expression to be located at PAPs, a hypothesis that is supported by EM work (Melone et al., 2009). P-ezrin, which has been shown to be expressed at astrocytic filopodia, is also a promising marker as it links the actin cytoskeleton to the plasma membrane at motile sections of the membrane (Bosk et al., 2011.; Derouiche and Frotscher, 2001). This therefore acts as a ‘structural marker’, whereby it should only be expressed at dynamic PAP membranes (Lavialle et al., 2011). Figure 24B provides a schematic of an astrocytic PAP, showing the locations of EAAT2 and p-ezrin.

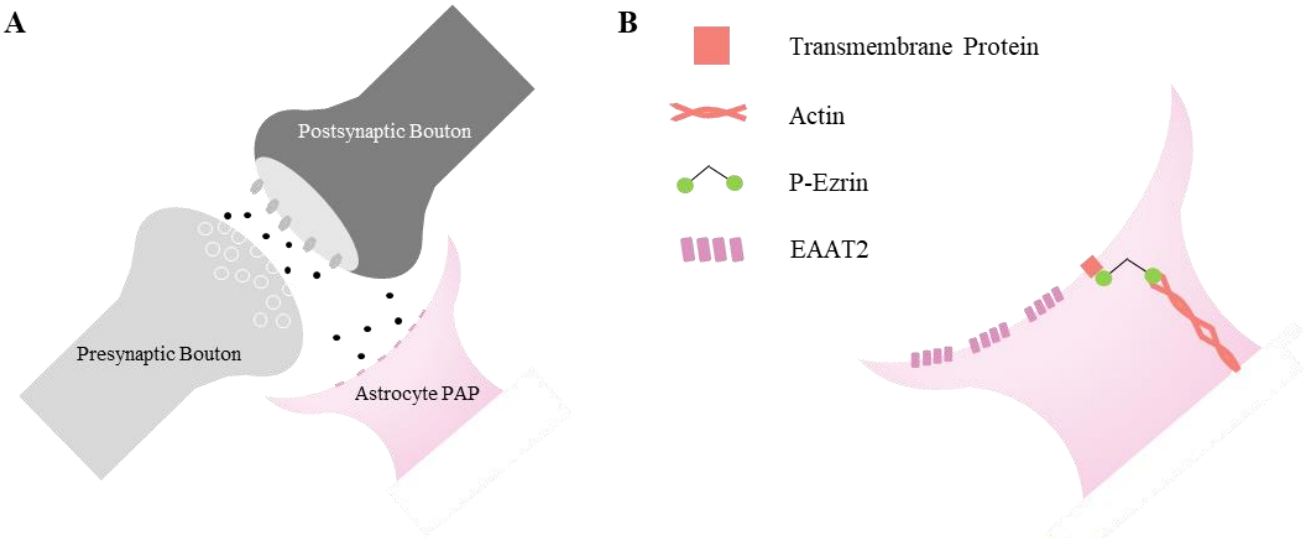
A
Postsynaptic Bouton
Presynaptic Bouton
Astrocyte PAP
B
Transmembrane Protein
Actin
P-Ezrin
EAAT2

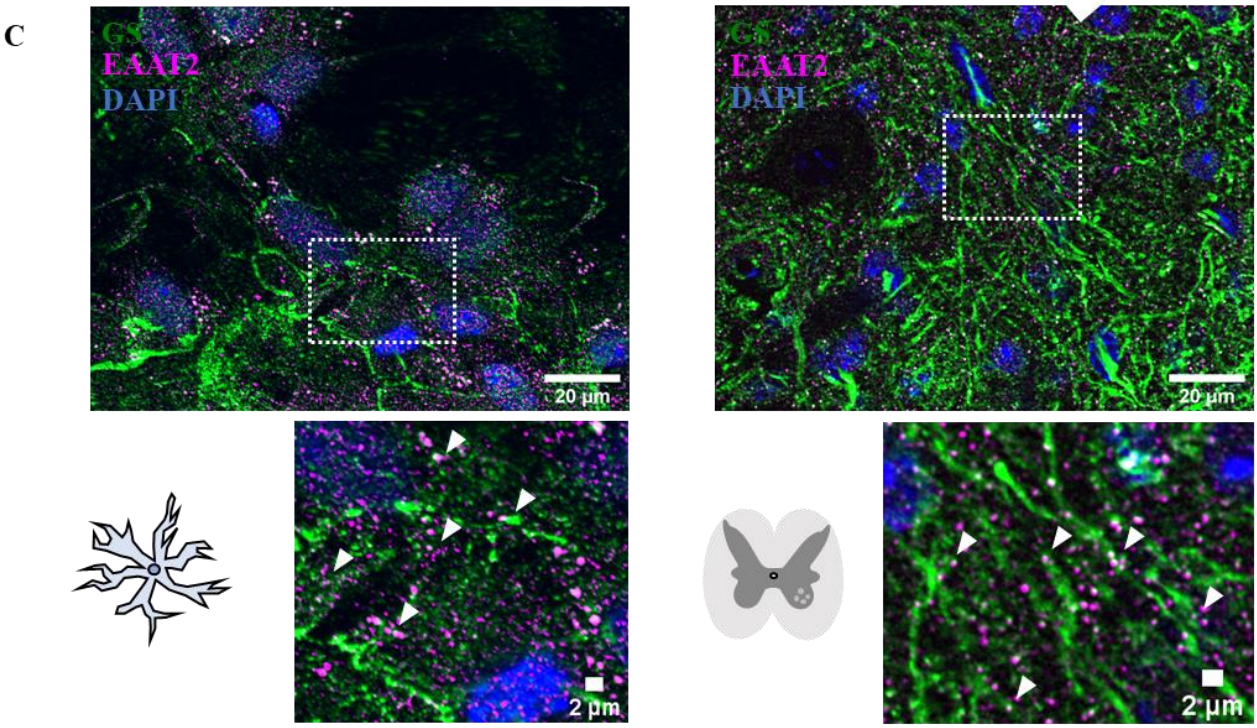
C
GS
EAAT2
DAPI
20 µm
2 µm

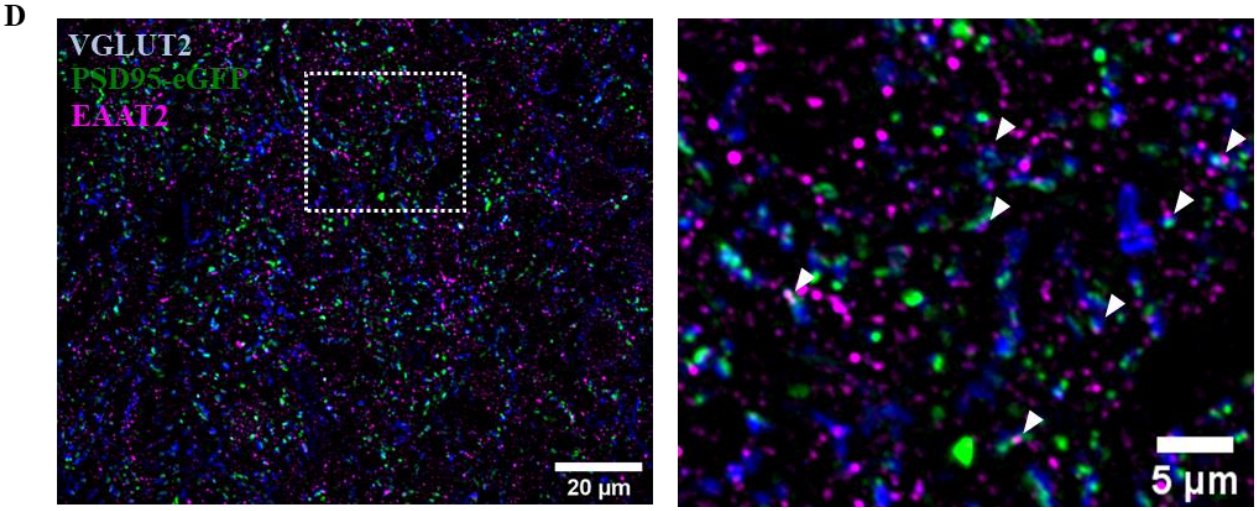
D
VGLUT2
PSD95-eGFP
EAAT2
20 µm
5 µm

Figure 24: **A**) Schematic demonstrating the organisation of the tripartite synapse, whereby excess glutamate (represented by ●) is transported into the astrocyte at the PAP. **B**) Molecular location of PAP markers EAAT2 and p-ezrin (Bosk et al., 2011; Stenovac et al., 2008). **C**) Expression of EAAT2 in primary culture astrocytes (*left*) and lumbar spinal cord tissue (*right*). EAAT2 regularly co-localises with astrocytic marker GS (white arrows). **D**) Example image demonstrating EAAT2 as a tripartite synapse marker in lumbar spinal tissue. EAAT2 partially co-localises with glutamatergic synapse markers VGLUT2 and PSD95-eGFP (white arrows).

In order to validate our markers, we wanted to examine their expression in a variety of models, including primary astrocyte cultures and lumbar spinal tissue. Figure 19C demonstrates expression of EAAT2 in primary astrocyte cultures, showing a refined, punctate appearance. This regularly co-localises with glutamine synthetase (GS). GS is a protein expressed throughout the astrocyte (Anlauf and Derouiche, 2013), has been confirmed at the PAP using EM work (Derouiche and Frotscher, 1991) and has been used previously to tag large areas of the cell including its fine processes (Lavialle et al., 2011). GS expression was similar to that in Chapter 3 and in previously described work (Anlauf and Derouiche, 2013). Importantly, EAAT2 puncta showed considerable co-localisation with GS, indicating that it is abundantly expressed in our primary astrocytes. In the lumbar spinal cord, GS is clearly expressed in astrocytic populations, revealing their long processes. EAAT2 again presents as fine puncta in the spinal cord, also showing clear localisation with GS +ve astrocytic processes (see Fig. 24C). Finally, in order to ascertain if this punctate expression is found in close association with synapses, we again used our PSD95-eGFP animals together with antibodies targeting the presynaptic glutamatergic marker VGLUT2 (Todd et al., 2003). VGLUT2 and PSD95-eGFP both showed expected dense punctate expression, often partially co-localising at putative synapses (see Fig. 24D). EAAT2 puncta showed regular apposition to both markers, and the 3 were often associated with one another. As EAAT2 is both expressed in GS +ve astrocytes and regularly associates with synapses, this provides convincing evidence that EAAT2 is an appropriate marker for visualising the tripartite synapse.

Next, we assessed the expression of our other putative PAP marker, p-ezrin. In order to assess expression at defined points of membrane extension where it is thought to reside, we first utilised super-resolution microscopy to look at p-ezrin. The resolution of conventional

microscopes is limited by Abbe's Diffraction Limit, which describes the maximum theoretical resolution of a point source of light (Huang et al., 2010). This is due to the diffraction of light when it passes thought a microscope objective, meaning even a point emitter will produce a wide intensity profile. This pattern of intensity is described as the point spread function (PSF). Therefore, if two identical emitters are separated by a distance less than the width of the PSF, they will be indistinguishable from one another and appear as a single object (Huang et al., 2010). Ultimately, this sets a resolution barrier dictated by diffraction, whereby conventional microscopy is limited to 200-250nm in the lateral direction (Wegel et al., 2016). Gated stimulated emission depletion (gSTED) microscopy is a method that can be used to overcome this and reach higher resolutions. It does this by utilising a high intensity red-shifted beam in a donut shape, which induces stimulated emission and confines fluorophores within this shape to the ground state for a limited time, transiently quenching them (Hernández et al., 2015; Vicidomini et al., 2014). Only fluorophores in a very small focal spot in the centre (which has a dimension below the diffraction limit) can fluoresce when excited by the non-STED laser, increasing resolution up to approximately 50nm (Wegel et al., 2016) (see Fig. 25).

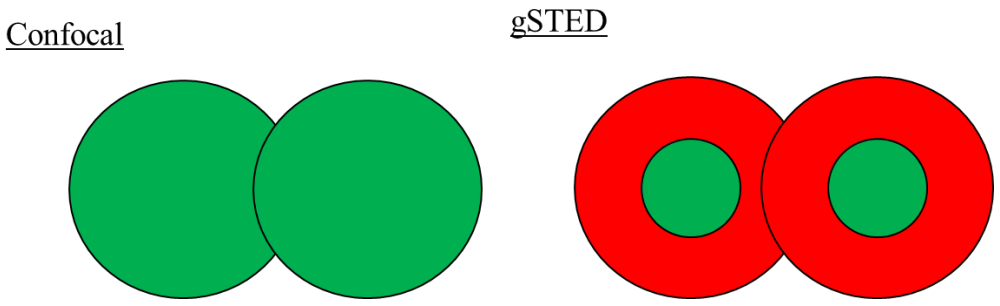

Figure 25: Schematic showing a 2D demonstration of PSFs in confocal vs gSTED microscopy. (*Left*) shows a 2 overlapping PSFs in confocal microscopy, meaning the 2 emitters are indistinguishable. (*Right*) shows 2 PSFs in gSTED microscopy, whereby the red circle represents the effective narrowing of the PSFs by the red-shifted gSTED beam, so the green PSFs are now far enough apart to be viewed as 2 separate emitters.

We utilised primary astrocytes labelled with p-ezrin and GFAP at x100 magnification using a gSTED microscope to reveal fine p-ezrin expression. GFAP showed expected fibrillar expression, with correlative confocal microscopy demonstrating the dramatic increase in resolution when using the STED laser (see Fig. 26A). P-ezrin had a heterogenous punctate expression, separated from the GFAP expression, likely representing the cell membrane which was not evident when observing GFAP alone. gSTED images show this membrane bound expression particularly clearly, with p-ezrin puncta presumably present at motile sections of astrocytic membrane. This was confirmed when looking at further astrocytic cultures, in which extending astrocytic processes showed large amounts of p-ezrin expression at the terminus of the process (see Fig. 26B, *left*). To confirm p-ezrin expression was similar in spinal tissue, we co-labelled p-ezrin with GS in tissue from the lumbar region of the spinal cord. P-ezrin was abundantly present, showing a similar punctate appearance. Importantly, it co-localised significantly with GS, particularly in what appeared to be more distal regions of the cell (see Fig. 26B, *right*). Again, expression was checked relative to glutamatergic pre- and postsynaptic markers VGLUT2 and PSD95-eGFP. P-ezrin puncta were regularly closely associated with VGLUT2-PSD95-eGFP +ve synapses (see Fig. 26C). Together, this provided evidence that p-ezrin was appropriately tagging PAP membranes. As a final piece of evidence that this was the case, we utilised dye-labelling of EAAT2 and p-ezrin primary antibodies to look at them simultaneously (as both were raised in the same animal). Importantly, both were strongly co-localised with one another, and appeared along GS +ve processes (see Fig. 26D). This indicates that both proteins are likely expressed in similar regions (i.e. at PAPs), and as such we were confident proceeding with their use as markers for imaging the tripartite synapse.

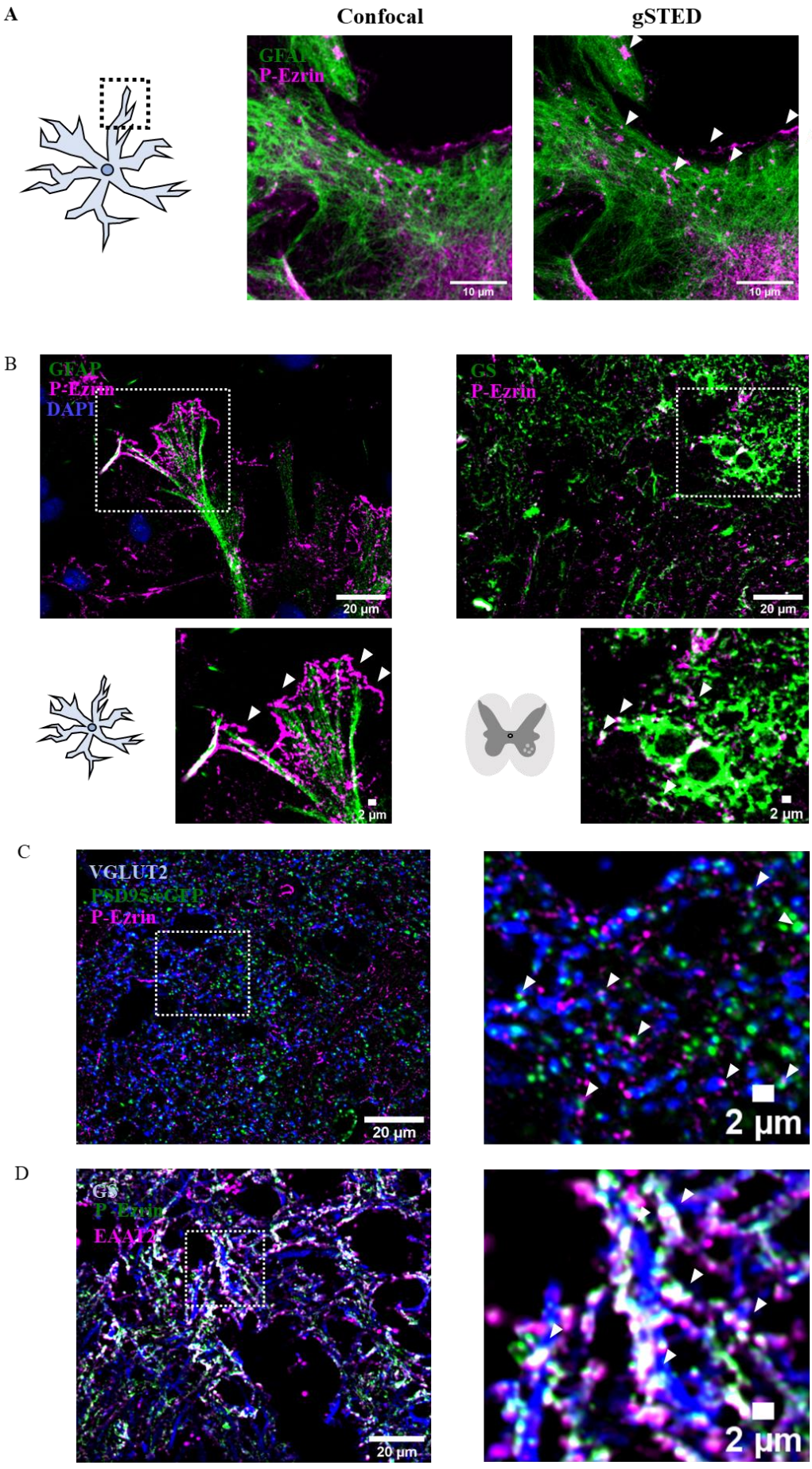
A
Confocal
gSTED
GFAP
P-Ezrin
10 µm
10 µm
B
GFAP
P-Ezrin
DAPI
20 µm
GS
P-Ezrin
20 µm
2 µm
2 µm
C
VGLUT2
PSD95-GFP
P-Ezrin
20 µm
2 µm
D
GS
P-Ezrin
EAAT2
20 µm
2 µm

Figure 26: **A**) Example images of correlative confocal and gSTED microscopy showing p-ezrin and GFAP expression in primary spinal astrocytes. White arrows indicate p-ezrin membrane expression. **B**) (*Left*) Example image showing p-ezrin expression at the terminus of an astrocytic process in primary spinal astrocytes. White arrows indicate p-ezrin expression. (*Right*) Example image demonstrating p-ezrin expression in lumbar spinal tissue, which co-localises with glutamine synthetase. White arrows indicate GS $^{+}$ve p-ezrin expression. **C**) Example image demonstrating p-ezrin is regularly associated with VGLUT2-PSD95 +ve synapses. White arrows point to tripartite synapses **D**) Example image showing dye-labelling of EAAT2 and p-ezrin primary antibodies, together with glutamine synthetase. This reveals significant co-localisation of both putative PAP markers along GS +ve processes (white arrows). **NOTE**: Dye-labelling performed by Dr. Matthew Broadhead and Maite Lopez.

2.2. Analysis of Tripartite Synapses in the Healthy Spinal Cord Reveals that Astrocytic Contact is Associated with Altered Postsynaptic Properties

After validation of our PAP markers, we first wanted to deploy them to assess tripartite properties in the healthy spinal cord. This enabled us to confirm whether we could use our methodology of conventional fluorescence tripartite imaging before utilising it in ALS studies. As there is evidence that astrocytic contact directly affects stability of dendritic spines (Bernardinelli et al., 2014), we wanted to probe whether postsynaptic properties varied depending on astrocytic contact. In order to do this, we used both EAAT2 and p-ezrin as PAP markers, in combination with VGLUT2 and PSD95-eGFP. Synapses were imaged in the ventral horn laminae L7-9 and divided into four groups: PSD95 only, PSD95 w. PAP marker (EAAT2 / p-ezrin), PSD95 w. VGLUT2 (i.e. non-tripartite synapses) and PSD95 w. VGLUT2 and PAP marker (i.e. tripartite synapses).

First, EAAT2 was abundantly expressed in the lumbar spinal cord. It also showed close association with VGLUT2 and PSD95, demonstrating the presence of many tripartite synapses (see Fig. 27A). We see isolated PSD95 +ve PSDs, likely because other VGLUT isoforms are expressed in the spinal cord and may be present at un-tagged presynaptic boutons (Alvarez et al., 2004), or their presynaptic partners may be on a different focal plane. However, VGLUT2 is the most densely and uniformly expressed isoform in the spinal cord (Todd et al., 2003). Taking advantage of our PSD95-eGFP model to accurately measure size and fluorescence intensity (1 GFP molecule per PSD95 molecule, therefore fluorescence intensity should linearly correlate with PSD95 expression (Chiu et al., 2001)), we analysed these postsynaptic properties across our 4 different synaptic subtypes. We observed a significant difference in PSD size between synaptic subtypes ($F(3)=224.7$, $P<0.0001$), with

A

EAAT2 Tripartite

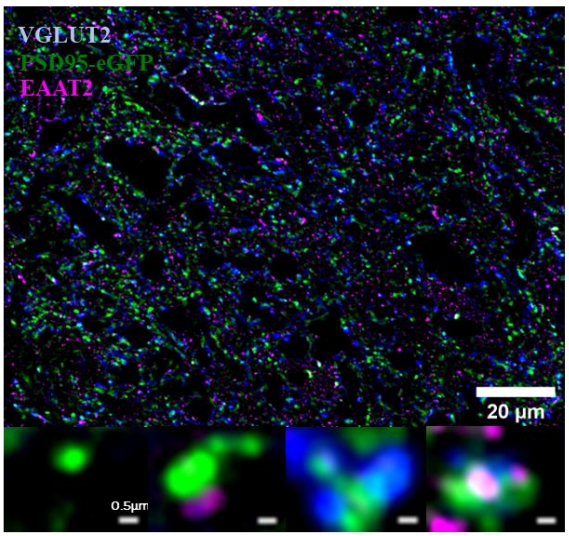

PSD95 Only | PSD95 w. EAAT2 | PSD95 w. VGLUT2 | Tripartite

B

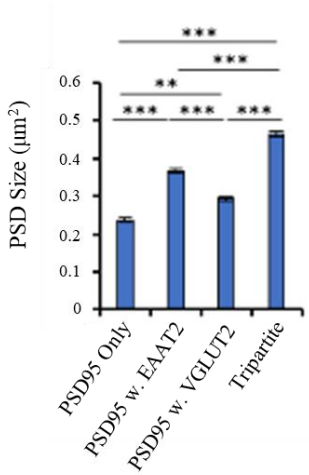

C

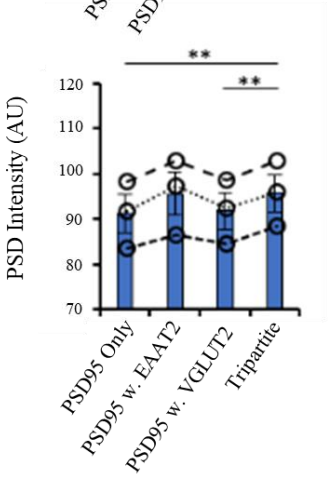

D

P-Ezrin Tripartite

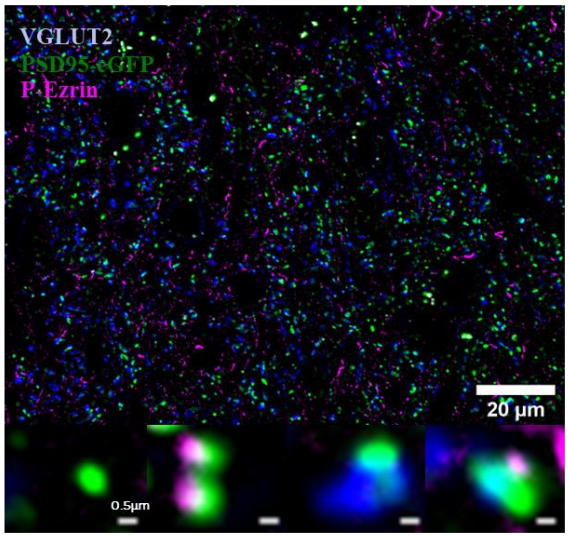

PSD95 Only | PSD95 w. p-Ezrin | PSD95 w. VGLUT2 | Tripartite

E

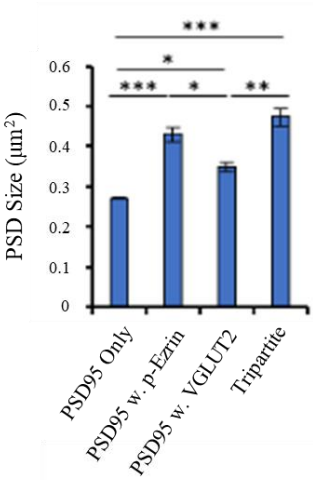

F

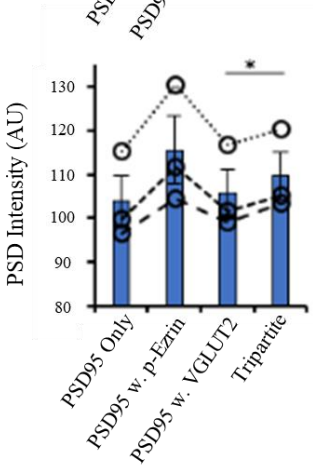

Figure 27: **A**) Example image showing tripartite imaging w. EAAT2 in 1-2 m.o. PSD95-eGFP$^{+/+}$ animals, including 4 analysed synaptic subtypes (PSD95 Only, PSD95 w. EAAT2, PSD95 w. VGLUT2 and Tripartite). **B**) Graph demonstrating PSD size in 4 synaptic subtypes w. EAAT2 as a PAP marker (N=3 animals). **C**) Graph demonstrating PSD intensity in 4 synaptic subtypes w. EAAT2 as a PAP marker (N=3 animals). **D**) Example image showing tripartite imaging w. p-ezrin in 1-2 m.o. PSD95-eGFP$^{+/+}$ animals, including 4 analysed synaptic subtypes (PSD95 Only, PSD95 w. p-ezrin, PSD95 w. VGLUT2 and Tripartite). **E**) Graph demonstrating PSD size in 4 synaptic subtypes w. p-ezrin as a PAP marker (N=3 animals). **F**) Graph demonstrating PSD intensity in 4 synaptic subtypes w. p-ezrin as a PAP marker (N=3 animals). **NOTE**: Tissue generation, method development and immunohistochemistry completed by Calum Bonthron and Dr. Matthew Broadhead. Analysis performed by Dr. Matthew Broadhead. Figure adapted from Broadhead and Bonthron et al., 2020).

PSDs that were part of tripartite synapses being up to 50% larger than uncontacted PSDs ($P<0.001$) (see Fig. 27B). Additionally, pairwise comparisons confirmed that tripartite synapses had significantly larger PSDs than non-tripartite synapses ($P<0.001$). We also noted a significant difference in PSD intensity between synaptic subtypes ($F(3,6)=35.0$, $P<0.0001$), with tripartite synapses being significantly brighter than PSDs alone ($P<0.01$) and non-tripartite ($P<0.01$) synapses (see Fig. 27C).

Next, postsynaptic properties were analysed with p-ezrin as our astrocytic PAP marker. Again, p-ezrin showed a heterogenous punctate appearance, which was regularly associated with glutamatergic synapses (see Fig. 27D). When we compared PSD size, we saw the same significant difference between synaptic subtypes ($F(3)=33.3$, $P<0.0001$). There was a strikingly similar increase in PSD size when part of a tripartite synapse compared to lone PSDs ($P<0.001$) when using p-ezrin as our PAP marker versus using EAAT2 (see Fig. 27E). Again, this was also the case when tripartite synapses were compared to non-tripartite synapses ($P<0.01$). Finally, a significant effect on PSD intensity was also noted when using p-ezrin as the PAP marker ($F(3,6)=17.1$, $P<0.01$) (see Fig. 27F), with pairwise comparisons confirming that PSDs at tripartite synapses were brighter than those at non-tripartite synapses ($P<0.05$).

Taking data utilising two different PAP markers together, we can conclude that astrocytic contact appears to be directly associated with differences in PSD structure, including PSD size and intensity (therefore molecular concentration of PSD95 at the PSD). The similarity between EAAT2 and p-ezrin datasets also further confirms they are tagging similar regions of the astrocyte, and therefore are appropriate to take forward for use in a comprehensive tripartite analysis in ALS.

2.3. Analysis of Tripartite Synapses in SOD1^{G93A} Mice Reveals Selective Loss Before MN Degeneration

Following the successful characterisation of tripartite synapses in the healthy spinal cord, we wanted to use our methodology to track tripartite synapses at different stages of disease. As previously mentioned, due to reported widescale synaptic changes in ALS (Ince et al., 1995), we wanted to quantify tripartite synapses throughout the grey matter of the lumbar spinal cord. In order to do this, we produced high magnification hemi-section scans of our tripartite markers EAAT2 / p-ezrin, VGLUT2 and PSD95-eGFP, again using SOD1^{G93A} x PSD95-eGFP crosses. We produced these at 3 different time points. These included a presymptomatic 8W time point, an early symptomatic 12W time point, and a later symptomatic 16W time point at which time the animals had undergone significant ALS-related weight loss (see Fig. 28A). 16W is still described as 'early symptomatic with weight loss', as late-stage disease or 'endpoint' can be up to 22-23 weeks of age (Kim et al., 2016). Our humane endpoint was well before this, defined as the emergence of gait abnormalities. This was selected together with our NACWO (Named Animal Care & Welfare Officer), as after this, animals can quickly progress to hind-limb dragging and begin to have difficulties eating. It also gives us insight into tripartite synapses during the early development of symptoms, which we were particularly interested in. Immediately before animals were transcardially perfused, the emergence of ALS motor phenotypes was assessed by checking for hind limb splay / tremors when lifted by the tail, which are the first observable signs of motor weakness in SOD1^{G93A} animals. Figure 28B shows the proportion of animals at each time point which showed this before death. At our 8W time point, no animals showed any signs of hind limb splay. At 12W, all males and 3/5 females showed early ALS phenotypes. A slight delay in female disease onset has been noted previously (Pfohl et al., 2015), and our

A

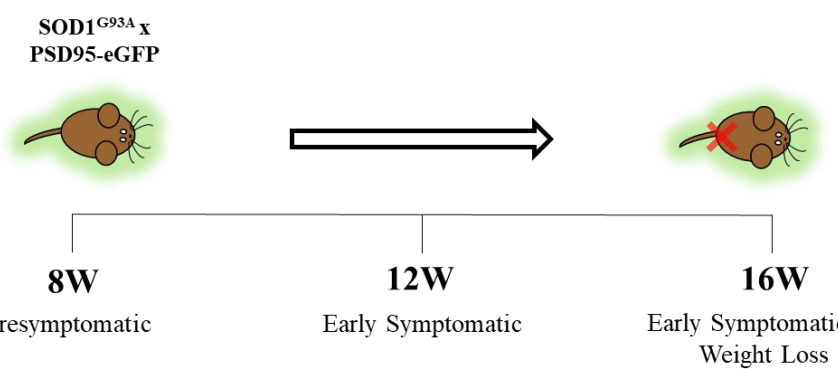

B

Timepoint	Sex	Proportion of Symptomatic Animals
8W	Male	0/5
	Female	0/5
12W	Male	5/5
	Female	3/5
16W	Male	6/6
	Female	5/5

C

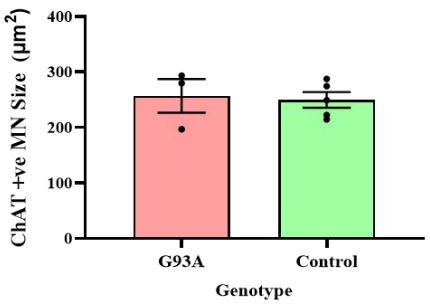

D

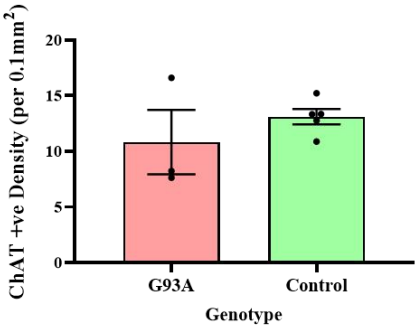

Figure 28: **A**) Schematic describing the time course in which tripartite synapses were assessed, from presymptomatic animals at 8W, to early symptomatic at 12W, and finally early symptomatic with weight loss at 16W. **B**) Table demonstrating the proportion of animals showing hind-limb tremors at each time point in male and female mice. **C**) Quantification of ChAT +ve MN size at 16W in SOD1^{G93A} animals (N=3) vs controls (N=5). **D**) Quantification of ChAT +ve MN density at 16W in SOD1^{G93A} animals (N=3) vs controls (N=5). **NOTE**: Tissue generation and phenotype monitoring performed by Calum Bonthron and Dr. Matthew Broadhead. MN quantification performed by Dr. Matthew Broadhead and William V. Smith. Figure adapted from Broadhead and Bonthron et al., 2022.

data is consistent with this. Finally, at 16W, all male and female animals showed clear hind limb splay in response to suspension by the tail. Finally, as another measure of disease progression, we measured ChAT +ve MNs at our latest time point of 16W. There was no significant difference in MN count at 16W ($t(6)=0.9903$, P=0.36) (see Fig. 28D) between $SOD1^{G93A}$ and control animals. There was also no difference in overall MN size ($t(6)=0.2461$, P=0.81) (see Fig. 28C), reflecting the fact that vulnerable, large F MNs were not yet being lost, which would have resulted in a decreased average MN area.

First, we utilised EAAT2 as our PAP marker and comprehensively mapped tripartite synapses in lumbar spinal hemi-sections at 8W, 12W and 16W in $SOD1^{G93A}$ males. Figure 29A demonstrates our high magnification scans in both control ($SOD1^{G93A\ -/-}$ PSD95-eGFP $^{+/-}$) and $SOD1^{G93A}$ ($SOD1^{G93A\ +/-}$ PSD95-eGFP $^{-/-}$) animals, along with zoomed images highlighting the association of EAAT2 puncta with VGLUT2 and PSD95-eGFP puncta. In order to assess whether astrocytic contact at the synapse is associated with any ALS-related changes, we separately quantified synapses not contacted by astrocytes (i.e. non-tripartite synapses) and those contacted by PAPs (i.e. tripartite synapses). At all time-points, we saw no significant differences in non-tripartite synapse density (8W: ($F(1,56) = <0.0001$, P=0.99), 12W: ($F(1,56)=1.37$, P=0.25) and 16W: $F(1,64)=2.40$, P=0.13)). Therefore, at all disease stages measured, non-tripartite synapse numbers were similar in $SOD1^{G93A}$ animals compared to controls (see Fig. 29B,C and D). When tripartite synapses were analysed, however, we noted there was a significant increase in EAAT2 tripartite synapse density in 8W $SOD1^{G93A}$ animals versus controls ($F(1,56)=7.21$, P=0.0095) (see Fig. 29B). Multiple comparisons testing found no significant differences between genotypes within individual laminae, however (P: L1/2 = 0.92, L3/4 = 0.97, L5 = 0.97, L6 = 0.82, L7 = 0.83, L8 = 0.99, L9 > 0.99 and L10 = 0.46). This was followed by a subtle but significant decrease in tripartite density

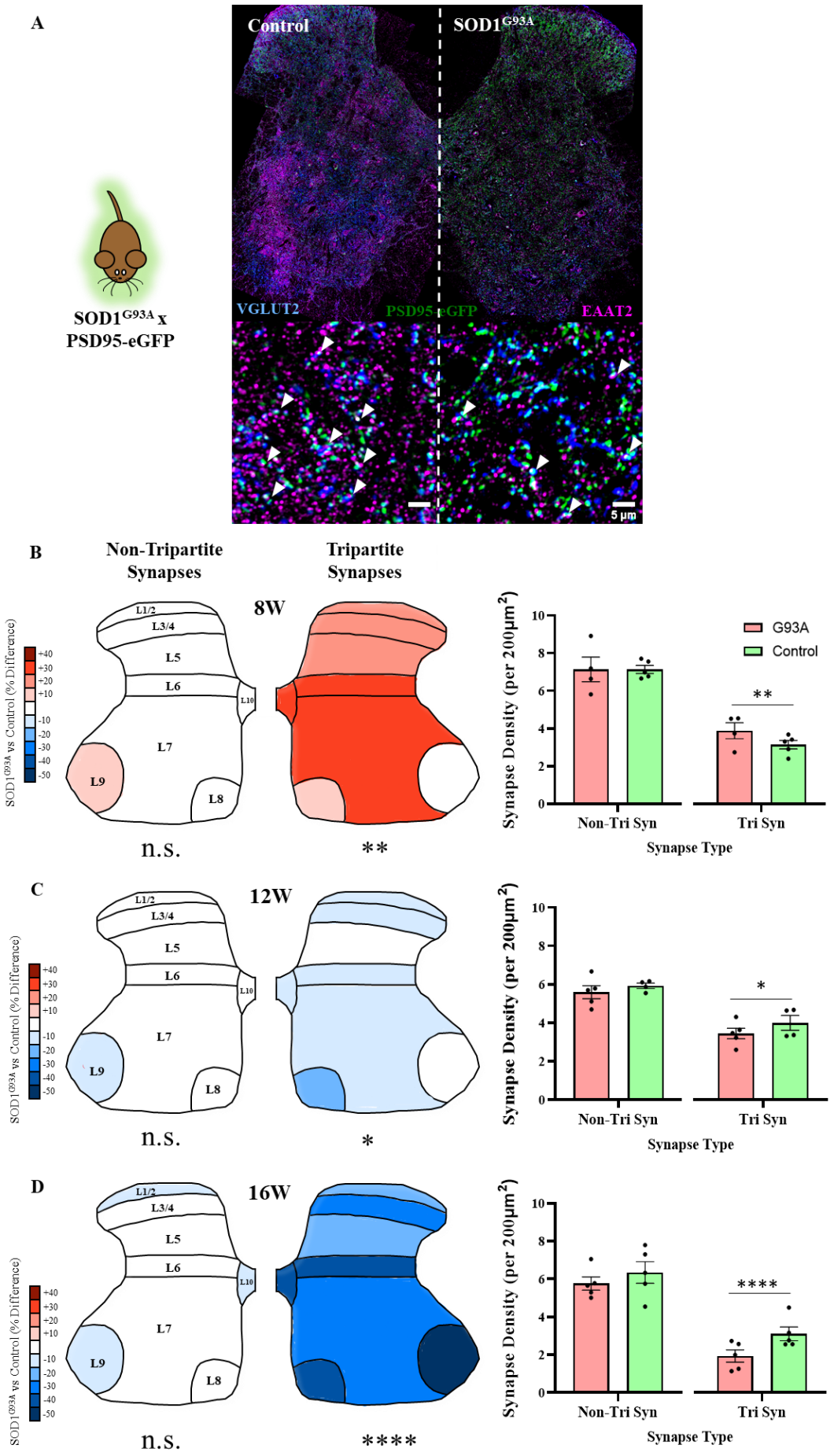
A
Control
SOD1G93A
SOD1G93A x
PSD95-eGFP
VGLUT2
PSD95-eGFP
EAAT2
5 µm
B
Non-Tripartite Synapses
Tripartite Synapses
8W
L1/2
L3/4
L5
L6
L10
L7
L9
L8
SOD1G93A vs Control (% Difference)
+40
+30
+20
+10
-10
-20
-30
-40
-50
n.s.
**
Synapse Density (per 200µm2)
G93A
Control
**
Non-Tri Syn
Tri Syn
Synapse Type
C
12W
n.s.
*
*
D
16W
n.s.
****
****

Figure 29: **A**) Example images of 16W EAAT2 tripartite hemi-sections from Control ($SOD1^{G93A\ -/-}$ PSD95-eGFP $^{+/-}$) and $SOD1^{G93A}$ ($SOD1^{G93A\ +/-}$ PSD95-eGFP $^{+/-}$) mice, along with zoomed sections. White arrows indicate tripartite synapses. **B**) Heat maps showing % change in density of non-tripartite (left) and tripartite (right) synapses in $SOD1^{G93A}$ animals relative to controls at 8W. Statistical significance is denoted below. Bar charts show the mean synapse density of non-tripartite and tripartite synapses at 8W, averaged across all laminae for simplicity (N=4 $SOD1^{G93A}$, N=5 Control). **C**) Heat maps showing % change in density of non-tripartite (left) and tripartite (right) synapses in $SOD1^{G93A}$ animals relative to controls at 12W. Statistical significance is denoted below. Bar charts show the mean synapse density of non-tripartite and tripartite synapses at 12W, averaged across all laminae for simplicity (N=5 $SOD1^{G93A}$, N=4 Control). **D**) Heat maps showing % change in density of non-tripartite (left) and tripartite (right) synapses in $SOD1^{G93A}$ animals relative to controls at 16W. Statistical significance is denoted below. Bar charts show the mean synapse density of non-tripartite and tripartite synapses at 16W, averaged across all laminae for simplicity (N=5 $SOD1^{G93A}$, N=5 Control). **NOTE**: Tissue generation, method development, immunohistochemistry and analysis performed by Calum Bonthron and Dr. Matthew Broadhead. Figure adapted from Broadhead and Bonthron et al., 2022.

by 12W (F(1,56)=4.774, P=0.0331) (see Fig. 29C). Again, this was not accompanied by any differences between genotypes within individual laminae when multiple comparisons testing was conducted (P: L1/2 = 0.99, L3/4 = 0.82, L5 > 0.99, L6 = 0.89, L7 = 0.99, L8 = 0.91, L9 > 0.99 and L10 = 0.99). Finally, at 16W, there was a greater reduction in EAAT2 tripartite synapses (F(1,64)=23.58, P<0.0001) (see Fig. 29D). Consistently, there were no differences in tripartite density between genotypes within individual laminae (P: L1/2 = 0.56, L3/4 = 0.45, L5 = 0.94, L6 = 0.33, L7 = 0.85, L8 = 0.67, L9 = 0.42 and L10 = 0.12). When female SOD1^{G93A} animals were assessed at 16W, we found the same selective loss of tripartite synapses (F(1,88)=8.42, P=0.0046) (N=6 control, N=7 SOD1^{G93A}). Non-tripartite synapses meanwhile remained similar to controls (F(1,88)=3.48, P=0.066). Taken together, we see an initial slight increase in tripartite synapse density, while at 16W we see a significant selective loss. At all time points, non-tripartite synapses remained similar in number to controls.

Although EAAT2 has been demonstrated to be a reliable PAP marker for visualising tripartite synapses, reported downregulation of the transporter protein (Bendotti et al., 2001; Howland et al., 2002) could represent a confounding variable when used to study the fate of tripartite synapses in ALS. In order to be further confident we are seeing loss of tripartite synapses and not just downregulation of EAAT2, we repeated our widescale tripartite mapping using the structural PAP marker p-ezrin. Once again in SOD1^{G93A} and control males, we produced high magnification hemi-sections that could be delineated into Rexed's laminae. P-ezrin showed an expected punctate expression, closely associating with VGLUT2-PSD95-eGFP synapses (see Fig. 30A). Again, we first assessed non-tripartite synapse densities in SOD1^{G93A} animals at 8W, 12W and 16W. At all recorded time points, there was once again no signficiant difference in synpase density versus controls (8W: (F(1,56)=2.236. P=0.14), 12W: (F(1,56)=0.5631, P=0.46), 16W: (F(1,48)=2.424, P=0.13)) (see Fig. 30B,C and D). When

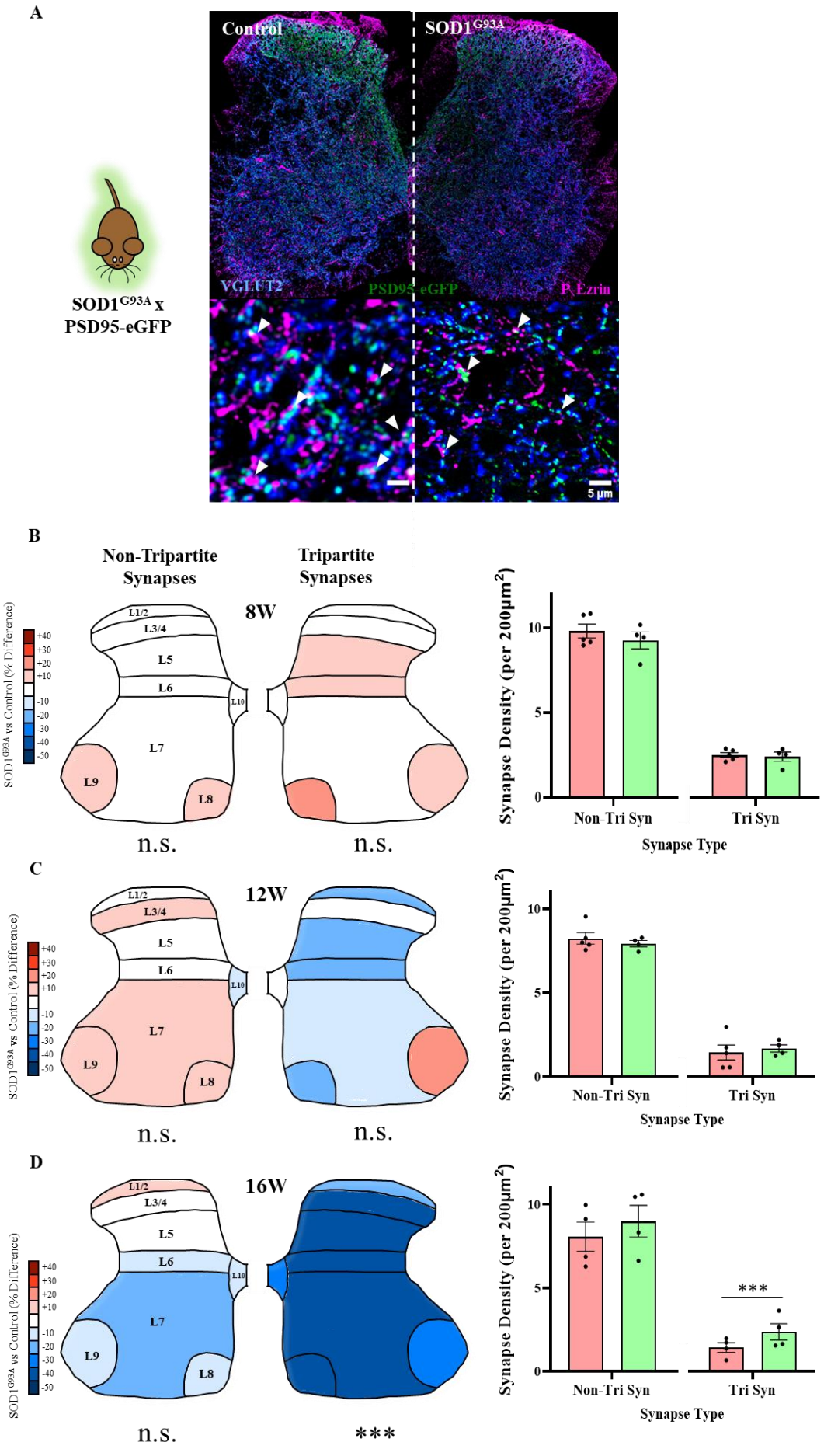
A
Control
SOD1G93A
SOD1G93A x
PSD95-eGFP
VGLUT2
PSD95-eGFP
P-Ezrin
5 µm
B
Non-Tripartite Synapses
Tripartite Synapses
8W
L1/2
L3/4
L5
L6
L10
L7
L9
L8
SOD1G93A vs Control (% Difference)
+40
+30
+20
+10
-10
-20
-30
-40
-50
n.s.
n.s.
Synapse Density (per 200µm2)
Non-Tri Syn
Tri Syn
Synapse Type
C
12W
n.s.
n.s.
D
16W
n.s.
***
***

Figure 30: **A**) Example images of 16W p-ezrin tripartite hemi-sections from Control ($SOD1^{G93A\ -/-}$ PSD95-eGFP $^{+/-}$) and $SOD1^{G93A}$ ($SOD1^{G93A\ +/-}$ PSD95-eGFP $^{+/-}$) mice, along with zoomed sections. White arrows indicate tripartite synapses. **B**) Heat maps showing % change in density of non-tripartite (left) and tripartite (right) synapses in $SOD1^{G93A}$ animals relative to controls at 8W. Statistical significance is denoted below. Bar charts show the mean synapse density of non-tripartite and tripartite synapses at 8W, averaged across all laminae for simplicity (N=5 $SOD1^{G93A}$, N=4 Control). **C**) Heat maps showing % change in density of non-tripartite (left) and tripartite (right) synapses in $SOD1^{G93A}$ animals relative to controls at 12W. Statistical significance is denoted below. Bar charts show the mean synapse density of non-tripartite and tripartite synapses at 12W, averaged across all laminae for simplicity (N=5 $SOD1^{G93A}$, N=4 Control). **D**) Heat maps showing % change in density of non-tripartite (left) and tripartite (right) synapses in $SOD1^{G93A}$ animals relative to controls at 16W. Statistical significance is denoted below. Bar charts show the mean synapse density of non-tripartite and tripartite synapses at 16W, averaged across all laminae for simplicity (N=4 $SOD1^{G93A}$, N=4 Control). **NOTE**: Tissue generation, method development, immunohistochemistry and analysis performed by Calum Bonthron and Dr. Matthew Broadhead. Figure adapted from Broadhead and Bonthron et al., 2022.

tripartite synapses were quantified using p-ezrin, we found no significant difference between SOD1^{G93A} and control animals at 8W (F(1,56)=0.2998, P=0.59) and 12W (F(1,56)=0.8332, P=0.37) (see Fig. 30B and C, respectively). However, consistent with our EAAT2 tripartite dataset, we see a signficiant loss of tripartite synapses at 16W (F(1,48)=14.59, P=0.0004) (see Fig. 30D). Again similar to our previous analysis, multiple comparisons testing revealed this loss appears to be widespread, rather than localised to specific anatomical regions (P: L1/2 = 0.55, L3/4 = 0.76, L5 = 0.93, L6 = 0.84, L7 = 0.79, L8 = 0.90, L9 = 0.98 and L10 = 0.38).

Finally, quantification of tripartite synapses in female SOD1^{G93A} animals at 16W also demonstrated selective tripartite loss when using p-ezrin as our tripartite marker (Non-Tri Syn: F(1,80)=0.19,P=0.66, Tri Syn: (F(1,80)=5.65, P=0.020) (N=6 control and SOD1^{G93A}). Our consistent results from both EAAT2 and p-ezrin datasets indicate that tripartite synapses appear to be selectively lost in SOD1^{G93A} animals, whilst non-tripartite synapses have similar densities relative to controls. Interestingly at 16W when this loss is observed, we observed a reduction in the density of both PAP markers (EAAT2: F(1,64)=11.31, P=0.0013, P-Ezrin = F(1,48)=8.828, P=0.0046). Although EAAT2 downregulation has been noted in ALS, concomitant loss of the structural marker p-ezrin suggests that PAPs themselves are being lost at this stage of disease. In addition, although after symptom onset, our observed selective tripartite vulnerability occurred before the overt loss of MNs.

2.4. Selective Tripartite Synapse Loss is Present in ALS Post-Mortem Spinal Tissue

Finally, we wanted to assess whether the selective vulnerability of tripartite synapses observed in the SOD1^{G93A} mouse model was also present in human ALS cases. Post-mortem cervical spinal cord sections were immunohistochemically labelled using PSD95 and p-ezrin to label PSDs and PAPs, respectively. Although not tagging all 3 components like previous experiments, autofluorescence issues in the GFP channel restricted staining to 2 channels (see Discussion). Therefore, this 2-channel stain was taken as a proxy for tripartite synapses. The human tissue analysed included 6 healthy controls and 9 ALS cases, which consisted of 4 cases harbouring SOD1 mutations and 5 harbouring *C9orf72* mutations. Controls and ALS patients were aged-matched, with the mean patient ages being 57.2 years for controls, 54 years for SOD1 cases and 57.6 years for *C9orf72* cases. PSD95 and p-ezrin, although slightly noisier due to the nature of immunohistochemistry in post-mortem tissue, showed expected punctate expression patterns, which frequently partially co-localised with one another and were interpreted as tripartite synapses (see Fig. 31A). When PSD density was assessed, we observed a significant decrease in ALS cases compared to control cases ($t(13)=2.6$, P=0.021) (see Fig. 31B). As different genetic mutations have been linked to differences in disease severity and survival, as well as SOD1 cases not showing classical TDP-43 pathology unlike the vast majority of other cases (Mackenzie et al., 2007; Swinnen and Robberecht, 2014), we also chose to separately analyse our SOD1 and *C9orf72* tissue. When this was done, we found that only *C9orf72* cases showed significantly lower PSD densities compared to controls ($F(2,12)=5.4$, P=0.0214) (Control vs *C9orf72*: P=0.0167, Control vs SOD1: P=0.42).

A

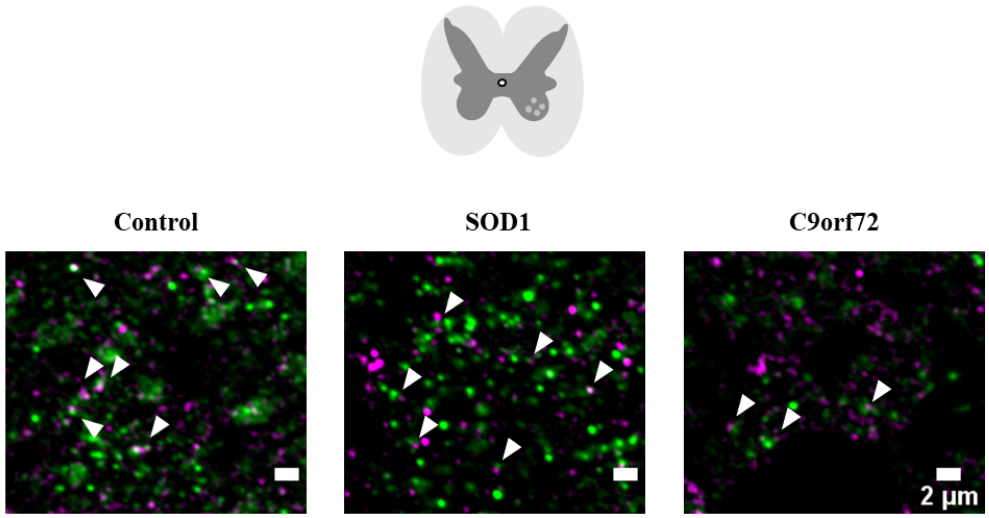
Control
SOD1
C9orf72
2 µm

B

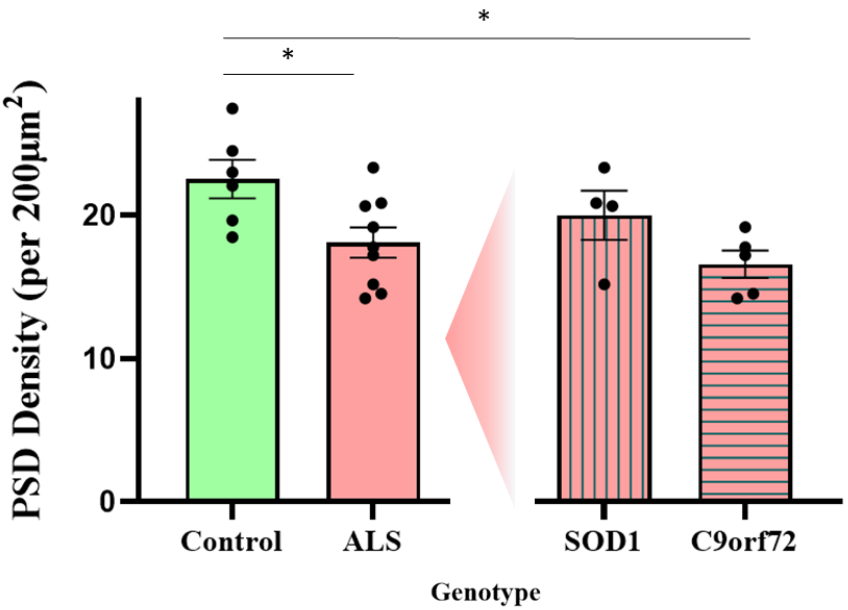
*
*
PSD Density (per 200µm2)
20
10
0
Control
ALS
SOD1
C9orf72
Genotype

C

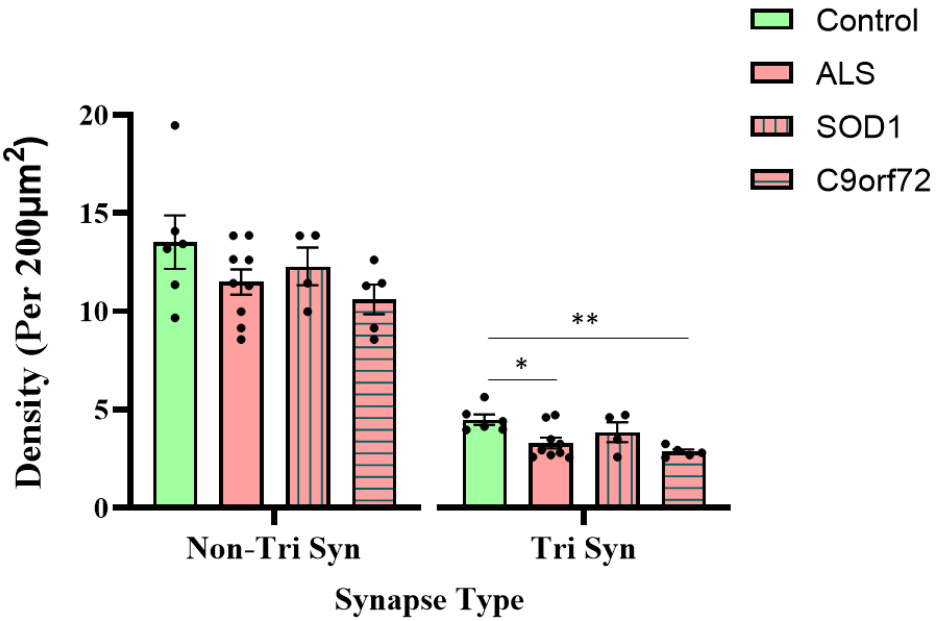
Control
ALS
SOD1
C9orf72
Density (Per 200µm2)
20
15
10
5
0
**
*
Non-Tri Syn
Tri Syn
Synapse Type

Figure 31: **A**) Example images of PSD95 and p-ezrin in post-mortem lumbar cervical spinal cord sections. White arrows indicate association of PSDs and PAPs, interpreted as tripartite synapses. **B**) Bar graph showing comparison of PSD density in control and ALS cases, then divided into SOD1 and C9orf72 cases alone (Control: N=6, ALS: N=9, SOD1: N=4 and C9orf72: N=5). **C**) Bar graph showing comparisons of non-tripartite synapse (PSD95 alone) and tripartite synapse (PSD95 + p-ezrin) densities in control vs ALS spinal tissue (Control: N=6, ALS: N=9, SOD1: N=4 and C9orf72: N=5). **NOTE**: Method development conducted by Calum Bonthron and Dr. Matthew Broadhead, adapted from Curran et al., 2021. Immunohistochemistry and analysis performed by Dr. Matthew Broadhead. Figure adapted from Broadhead and Bonthron et al., 2022.

Next, we separately analysed non-tripartite synapse (PSD95 alone) and tripartite synapse (PSD95 + p-ezrin) densities. Consistent with our SOD1^{G93A} mouse dataset, non-tripartite synapse densities were not different between control, SOD1 and *C9orf72* cases ($F(2,12)=1.787$, P=0.21). However, we did again see a selective loss of tripartite synapses, with *C9orf72* cases showing a significant reduction in density compared to controls ($F(2,12)=8.163$, P=0.0058) (Control vs *C9orf72*: P=0.0044) (see Fig. 31C). SOD1 cases once again did not show this difference (Control vs SOD1: P=0.34).

3. Discussion

As we found no evidence of pathological astrocytic modulation of synaptogenesis, we hypothesised that astrocytes may instead have perturbed interactions with mature synapses at the tripartite synapse. Widescale astrocytic dysfunction (Valori et al., 2014) including involvement of proteins expressed at the tripartite synapse (Howland et al., 2002), in addition to a large body of evidence demonstrating synaptic dysfunction (Hossaini et al., 2011; Ince et al., 1995; Sasaki and Iwata, 1995) make investigating their interaction at the mature tripartite synapse essential. In order to do this, we first had to reliably visualise the fine astrocytic processes that envelope synapses, PAPs. Analysis of glutamate transporter EAAT2 at high resolution in primary astrocyte cultures and spinal tissue showed a dense punctate expression, which regularly associated with glutamatergic synapses. Another putative PAP marker, actin-binding protein p-ezrin, was found at the cell membrane when visualised using gSTED microscopy, as expected due to its reported expression only at fine motile membrane extensions. P-ezrin was also regularly associated with synapses, and dye-labelling of EAAT2 and p-ezrin primary antibodies revealed substantial co-localisation of both markers, giving us confidence that we were targeting PAPs. To validate this methodology of tripartite visualisation, we used these markers to first characterise tripartite synapses in the healthy spinal cord, revealing that astrocytic contact was associated with both larger PSDs and greater GFP intensities at the PSD. This methodology could then be used to comprehensively characterise tripartite synapses in ALS. We found that at 16W, $SOD1^{G93A}$ animals had a selective loss of tripartite synapses using both EAAT2 and p-ezrin as PAP markers, whilst non-tripartite synapse densities remained similar to controls. Finally in ALS patient post-mortem tissue, this selective vulnerability of tripartite synapses was also observed, suggesting this is a conserved characteristic of ALS-related neurodegeneration.

Both utilised PAP markers demonstrated astrocytic expression, as indicated by co-localisation with glutamine synthetase and close association with glutamatergic synapse markers VGLUT2 and PSD95. Not all synapses are contacted by astrocytes, however, with 56% of synapses observed being tripartite when imaged with EAAT2. PAPs dynamically envelope and detach from synapses influenced by the activity of surrounding local circuitry (Bernardinelli et al., 2014; Genoud et al., 2006). Other groups have found approximately similar amounts of synaptic coverage by PAPs, reporting around 60% in the rat hippocampus (Lavialle et al., 2011; Ventura and Harris, 1999), whilst in the cerebellum over 70% synaptic coverage has been observed (Špaček, 1985). A number of factors affect estimations of tripartite synapse frequency. There appears to be true biological variability between CNS regions imaged, as well as variability as a result of the technique used to quantify them (EM vs. immunohistochemistry). Such differences may even highlight differential expression levels of certain PAP markers, for example, the proportion of synapses that were tripartite when tagged with p-ezrin was approximately 14%. However, it should be noted that the stringent criteria (binarised objects above certain intensity and size cut-offs) used to define co-localisation in our analyses may have resulted in the exclusion of 'true' tripartite synapses. This could be facilitated by variability of marker expression between individual PAP structures. Irrespective of this, we noted, using dye-labelling of primary ABs, that EAAT2 and p-ezrin showed considerable co-localisation, giving us confidence that we were imaging the same structures. This is supported by previous reports of both markers being closely apposed to synapses (Lavialle et al., 2011; Melone et al., 2009).

We next utilised our method of tripartite visualisation to initially characterise these structures in the healthy spinal cord. Previous work heavily utilised EM to visualise tripartite synapses (Lehre and Rusakov, 2002; Witcher et al., 2010), and led to many important findings

including estimations of glial coverage in different CNS regions and preferential envelopment of spines with certain size characteristics (Heller and Rusakov, 2017). However, the laborious and time-consuming nature of EM limits the ability to image large numbers of tripartite synapses. It is therefore much more practical to utilise other imaging methods, such as fluorescence microscopy, to quantify large numbers of tripartite synapses and enable characterisation across entire regions of the grey matter. This was desired, as ultimately, we hoped to use our method to compare tripartite characteristics across anatomical regions in ALS.

This initial utilisation of our tripartite imaging method led to the discovery that PSDs, quantified using our PSD95-eGFP mouse, were both structurally larger and had an increased GFP fluorescence intensity when contacted by PAPs. Fluorescence intensity of our GFP tag is expected to linearly correlate with expression of PSD95, as each PSD95 molecule expresses 1 GFP tag (see Chapter 4, Fig. 12) (Chiu et al., 2001). This increase in intensity therefore reflects an increase in PSD95 concentration at the PSDs which are part of tripartite synapses. As PSD95 is required for recruitment and binding of NMDARs and AMPARs via intermediate proteins (Hafner et al., 2015), it is conceivable that increasing PSD95 concentration at the PSD could lead to increased synaptic strength. In addition, we noted a clear association between PSD size and synapse subtype, with tripartite synapses having larger PSDs. Previous EM work supports this, showing larger, more complex PSDs are associated with increased astrocytic envelopment (Ventura and Harris, 1999). At a nanoscale level, PSD95 is actually organised into subdomains called nanoclusters (NCs), which are conserved in size, with larger synapses simply consisting of increased numbers of NCs (Broadhead et al., 2016). This is important, as synaptic size and therefore NC count, is correlated with synaptic strength (Liu et al., 2017). Therefore, astrocytic contact at the

synapse is associated with larger PSDs, which likely means tripartite synapses are greater in strength, containing NCs of increased PSD95 concentration. It is unclear whether astrocytes cause structural alterations of the PSD, or simply preferentially envelope larger synapses. There is evidence, however, that the astrocyte-secreted protein hevin (involved in synaptogenesis as described earlier), can directly influence expression of key PSD proteins, including PSD95 and postsynaptic receptor subunits (Farhy-Tselnicker and Allen, 2018). Together with evidence that the presence of PAPs at developing synapses is key for postsynaptic alteration and maturation (Risher and Eroglu, 2020), in addition to astrocytes' proposed involvement in cortical LTP induction, which involves significant postsynaptic plasticity (Ota et al., 2013), it is conceivable that astrocytes may be able to directly modulate postsynaptic structure.

Following its use in characterisation of tripartite synapses in the healthy spinal cord, we next deployed our visualisation strategy to comprehensively analyse tripartite synapses in the $SOD1^{G93A}$ model. We opted not to continue with the use of the C9BAC500 model in our tripartite analyses. As discussed previously, several other groups have reported a lack of observable phenotypes in their C9BAC500 colonies (Mordes et al., 2020; Nguyen et al., 2020), possibly as the result of housing environment affecting phenotypic penetrance. At no point did we observe any motor symptoms in either our C9BAC500 or C9BAC500 x PSD95-eGFP animals, even when kept well into the 20-40W timeframe when 'acute' disease was expected to develop (Liu et al., 2016). Early pilot data suggested a lack of any observable synaptic phenotypes in C9BAC500 mice (data not shown), which are not exclusive to the $SOD1^{G93A}$ model and have been observed in others such as the $TDP\text{-}43^{A315T}$ model (Jiang et al., 2019). Together, it was decided that the C9BAC500 model failed to appropriately recapitulate ALS and was excluded from future work.

Our SOD1^{G93A} colony did not show any evidence of drift in the time of symptom onset, indicating that our transgene copy number was likely kept consistent. Such a reduction is a concern in ALS studies, as copy number directly correlates to disease severity (Alexander et al., 2004). Quantification of MN number revealed no loss at our latest 16W time point, a finding that is consistent with other reports of MN loss in the SOD1^{G93A} model (Feeney et al., 2001). Mice are clearly phenotypic at this late stage however, as other contributors to muscle dysfunction, such as NMJ degeneration, have been shown to occur much earlier than overt MN death (Alhindi et al., 2021).

Tripartite mapping of SOD1^{G93A} PSD95-eGFP spinal cords revealed a selective loss of tripartite synapses at an early symptomatic timepoint of 16W, with evidence of loss in our EAAT2 dataset beginning at 12W. This 16W loss was consistent when using both EAAT2 and p-ezrin as PAP markers. This is important, as the use of p-ezrin helps to mitigate concerns over loss of EAAT2 expression being a confound in disease, and provides convincing evidence that the PAPs themselves appear to be lost in ALS. This is interesting, as it could imply that the reported downregulation of EAAT2, thought to be due in part to pathological cleavage of the functional transporter (Boston-Howes et al., 2006), may also partially be due to loss of PAPs where this transporter is expressed.

This specific tripartite loss, however, was not focussed in ventral regions as may be expected. Analysis of laminae-by-laminae tripartite densities indicated that there were small decreases across all laminae rather than large decreases in specific anatomical regions. Due to the N numbers that were practical to generate in a large-scale study, an overall decrease across all regions was detected statistically, whereas small differences within laminae were not detected

in multiple comparisons testing, likely due to α-value adjustment. Although some previous work in post-mortem tissue has reported a bias towards ventral synaptic loss (Matsumoto et al., 1996), widespread loss has also been noted (Ince et al., 1995). A lack of specific loss in the medial and lateral motor pools (L8 and L9, respectively) is of particular interest, as a number of papers report synaptic disruption directly onto MNs (Chang and Martin, 2009; Schultz et al., 2005; Sunico et al., 2011). It may be the case that analysis of larger delineated laminae, instead of specifically MNs, may have masked such an effect when looking at tripartite synapses. However, as has been discussed before, disagreement in the field renders MN synaptic changes inconclusive. We do not observe tripartite loss presymptomatically, as has been the case with other synapse types such as NMJ degeneration (Alhindi et al., 2021). Instead, this may represent a later consequence of disease progression that worsens the function of spinal circuitry with age. Equally, there may be finer changes in tripartite synapses that occur presymptomatically that we cannot detect with the use of our GFP tag. Evidence of preferential astrocytic contact according to dendritic spine size (Heller and Rusakov, 2017), in addition to previously noted spine abnormalities in ALS (Fogarty et al., 2016), demonstrates that ultrastructural changes in tripartite synapses could occur in disease that require higher resolution imaging techniques beyond the use of the PSD95-eGFP tag. Also, it should be noted that this work specifically studies VGLUT2 +ve glutamatergic tripartite synapses. Circuitry using other VGLUT isoforms, such as VGLUT1 +ve mechanoreceptive afferents (Todd et al., 2003), should be further explored to see if tripartite synapse loss is conserved. In addition, comparatively, inhibitory tripartite synapses receive less research attention (Ishibashi et al., 2019), and further work to map their numbers throughout disease progression would be informative to find out if this is a universal phenomenon for all astrocyte-contacted synapses in ALS.

Finally, we found that the selective vulnerability of tripartite synapses was also observed in spinal sections from human ALS patients. Difficulties in human CNS immunohistochemistry have long been reported (Waldvogel et al., 2006). These include preservation delays compromising tissue quality, and the prevalence of lipofuscin-based autofluorescence. This study utilised a PSD marker (PSD95) and a PAP marker (p-ezrin), and omitted the use of a presynaptic marker. This was due to autofluorescence issues encountered in our post-mortem spinal tissue, particularly when using fluorophores within the GFP excitation spectrum, as they appear especially bright (Teuscher and Ewald, 2018). We therefore decided to use fluorophores with longer wavelength excitation spectra to reduce this issue, limiting us to two markers.

Interestingly, we only observed this tripartite loss in patients harbouring *C9orf72* mutations, and not those harbouring SOD1 mutations. Previous ALS frontal cortex work found no differences in synaptic loss between *C9orf72* and SOD1 cases (Henstridge et al., 2018). However, it was suggested that more severe synaptic loss was associated with TDP-43 pathology, which SOD1 cases are known to lack. On the surface there is an apparent conflict in our datasets, in which $SOD1^{G93A}$ mice show selective tripartite loss, whilst in post-mortem tissue *C9orf72* patients display this but SOD1 patients do not. However, limitations of the $SOD1^{G93A}$ model have long demonstrated that there are differences between mouse lines expressing exogenous ALS mutations, and the human cases they are attempting to recapitulate. For example, TDP-43 pathology in $SOD1^{G93A}$ mice has been reported at end-stage (Shan et al., 2009), while human SOD1 cases are known to lack this (Mackenzie et al., 2007). $SOD1^{G93A}$ mice also show a rapid rate of disease onset, which does not align with human $SOD1^{G93A}$ cases which display a relatively slow progression (Picher-Martel et al., 2016). It is clear therefore, that directly correlating mouse models with human cases

harbouring similar mutations should be done with care. This does not render the $SOD1^{G93A}$ mouse model useless, as its contribution to the understanding of ALS mechanisms is substantial.

Although our mouse model and human cases show mutations associated with fALS, *C9orf72* mutations are the most common genetic mutation found in both fALS *and* sALS. Together with the fact that 3 / 5 of our *C9orf72* patients had confirmed cases of sALS, our findings of selective tripartite loss may be applicable to both forms of ALS. More data in a larger cohort of specifically sALS patients would enable our results to be further extrapolated.

Although the mechanism behind tripartite loss is unknown, it could be the result of a number of factors. First, as regularly reported, EAAT2 expression is reduced around symptom onset (Bendotti et al., 2001; Howland et al., 2002). This has been suggested to be due to aberrant RNA processing (Lin et al., 1998), as well as cleavage of the translated protein (Boston-Howes et al., 2006). Loss of functional glutamate transporters at tripartite synapses could specifically leave them vulnerable to excitotoxicity, synapse degeneration and subsequent cell death. Observed tripartite loss also roughly coincides with previous observations of EAAT2 loss in the $SOD1^{G93A}$ mouse model (Bendotti et al., 2001; Bruijn et al., 1997). As our study in healthy spinal tissue demonstrates, astrocytes are more likely to contact synapses with larger PSDs, which ultrastructural work suggests are also functionally stronger (Liu et al., 2017). These large, particularly active synapses which experience EAAT2 loss in disease progression may be particularly vulnerable to degeneration. The effect of excess glutamate present in the spinal circuitry could also be exacerbated by perturbed gliotransmission. As discussed previously, elevated adenosine in the cerebrospinal fluid of ALS patients (Yoshida et al., 1999), in combination with alterations in the excitatory A_{2A} adenosine receptor (Ng et

al., 2015), could worsen excitotoxicity. In such a scenario, lower EAAT2 expression causes excess glutamate retention in the synaptic cleft, which subsequently promotes further excitability via astrocyte-to-neuron bidirectional communication, ultimately causing synapse loss and cell death. Our study points towards a potential target for therapeutic intervention, therefore. As mentioned previously, upregulation of EAAT2 has shown some promising results in ALS mouse models (Ganel et al., 2006; Rothstein et al., 2005). If these synapses could be preserved, possibly through modulation of excitotoxicity, it could help reduce degeneration of synaptic networks and thus improve function in early symptomatic ALS.

To conclude, we find a robust, selective loss of tripartite synapses in both our SOD1^{G93A} mouse model and ALS patient post-mortem tissue. Astrocytic interaction with mature synapses is therefore implicated in ALS pathogenesis, which could be the result of a number of mechanisms including exacerbation of excitotoxicity, resulting in tripartite synaptic loss. We conclude therefore that the tripartite synapse is a vulnerable fulcrum of disease in ALS, and should be a target of future work to slow or prevent spinal circuit degeneration.

Concluding Statements

Astrocytes are becoming increasingly implicated in neurodegenerative disease. In ALS, multiple astrocytic disease mechanisms have been discussed. Secretion of toxic factors, ROS production and a decrease in glutamate clearance are thought to induce MN death (Valori et al., 2014; Zhao et al., 2020). In addition, there is a huge body of evidence demonstrating synaptic pathology at different stages of disease progression and in different models of ALS (Chang and Martin, 2009; Hossaini et al., 2011; Ince et al., 1995; Sunico et al., 2011; Zang et al., 2005). We were therefore interested in looking at how astrocytes interact with synapses in ALS, with the suggestion that their disease mechanisms may be intrinsically linked as a result of the multiple ways glia and synapses interact.

First, as one of the prominent roles of astrocytes is their ability to promote synaptogenesis (Risher and Eroglu, 2020), this represented the first way in which aberrant astrocyte-synapse interactions may contribute to ALS. Spinal network hyperexcitability has been reported (Jiang et al., 2009; Van Zundert et al. 2008), with the source of such excitability changes being up for debate. One idea is that a shift in the ratio of excitatory : inhibitory synapses (E:I ratio) throughout the pre-MN networks during development results in a 'priming' towards excitation, which later facilitates excitotoxic cell death. Due to the synaptogenenic role of astrocytes and their reported involvement in ALS, we wanted to investigate whether perturbed synaptogenesis could drive E:I ratio shifts in disease.

To do this, we developed a novel postnatal primary co-culture system of spinal astrocytes and neurons. This allowed us to investigate whether the genotype of astrocytes and neurons had an effect on E:I ratios in a system where all synapses were severed during dissociation and allowed to reform. Our methodology had several key advantages over classical

embryonically-derived culture protocols. This included reducing animal usage, avoiding anaesthetic administration which can alter electrophysiological output (De Sousa et al., 2000), is fast and simple, and allows neurons to be maintained for weeks enabling their use in time course studies. We believe our validated methodology will be of use to the ALS field as a whole. This is due to neurons being maintainable *in vitro* for weeks and the validation that our cultures contain a subset of putative SMI 32 +ve MNs. Our model represents a good alternative to embryonically derived protocols, where cells are intrinsically less mature at the point of dissociation.

We next deployed our methodology using both $SOD1^{G93A}$ x PSD95-eGFP and C9BAC500 x PSD95-eGFP crosses, whereby the genotype of both astrocytes and neurons were controlled in order to assess the role of each in generating putative E:I ratio shifts. Combined with synapsin and gephyrin as presynaptic and inhibitory postsynaptic markers, respectively, we looked at E:I ratios across our genotype conditions. We found no structural evidence of E:I ratio changes, irrespective of the genotype combination in our co-cultures. This was not masking any parallel increases or decreases in excitatory / inhibitory synapse numbers, either. In addition, $SOD1^{G93A}$ PSD95-eGFP spinal cords immediately after the main peak of postnatal spinal synaptogenesis showed no evidence of E:I ratio shifts compared to controls. Finally, in iPSC-derived MN / astrocyte cultures harbouring C9orf72 hexanucleotide repeat expansions, we found no evidence of E:I ratio shifts or changes in the number of excitatory synapses formed.

Together, we concluded there was no structural evidence that astrocytes drive non-cell autonomous changes in synaptogenesis and cause E:I ratio changes early in ALS. Such a developmental bias towards increased excitatory synapse numbers may present in a way not

visible using our anatomical quantification methods, however. GABAergic transmission switches from excitatory to inhibitory during the first-to-second postnatal week (Furukawa et al., 2017; Jean-Xavier et al., 2007). Delays in the GABAergic switch could cause an early E:I ratio shift, which would not be detectible in our studies. A future comprehensive analysis looking at GABAergic reversal potentials, mEPSCs / mIPSCs and KCC2 / NKCC1 expression in early SOD1^{G93A} spinal cords would reveal whether such a delay exists and whether it is driving pathogenic excitability shifts in early ALS.

Astrocytes do not only interact with synapses during their formation, but they also interact with mature synapses at the tripartite synapse. Astrocytes participate in a multitude of functions at these structures, including glutamate clearance (Tani et al., 2014) and gliotransmission (Broadhead and Miles, 2020). Considering these essential functions, in addition to the knowledge that there is dysfunction at the tripartite synapse in ALS (Bendotti et al., 2001; Howland et al., 2002), we aimed to investigate these structures throughout the grey matter at different stages of disease. After validating 2 PAP markers (EAAT2 and p-ezrin), we first used them to characterise tripartite synapses in the healthy spinal cord. Interestingly during this process, we noted using PSD95-eGFP mice that PSDs which were part of tripartite synapses were both structurally larger and had a greater concentration of PSD95 at the synapse (increased intensity).

We next deployed our tripartite synaptic imaging process on SOD1^{G93A} x PSD95-eGFP crosses at different stages of disease progression. This included at 8W (presymptomatic), 12W (early symptomatic) and 16W (early symptomatic w. weight loss). At all time points, we saw no changes in non-tripartite synapse density in SOD1^{G93A} spinal cords. Interestingly, however, we consistently noted tripartite synapse loss throughout the grey matter at 16W,

using both EAAT2 and p-ezrin as our PAP markers. This implied that the decreased number of these structures was not just reflecting EAAT2 loss, but instead likely demonstrated loss of tripartite synapses and their associated PAPs. Such loss occurred before overt MN loss. This effect was replicated in ALS patient post-mortem spinal tissue, although interestingly only in *C9orf72* patients.

We conclude therefore that tripartite synapses may represent a vulnerable fulcrum of disease in ALS. Previous studies looking at synaptic pathology failed to look at the interaction of astrocytes at synapses, and our work demonstrates that future studies should consider the tripartite sub-population in their analyses. As demonstrated in healthy spinal tissue, astrocytes tend to associate with larger PSDs, which ultrastructural work suggests are also functionally stronger (Liu et al., 2017). It may be that large, particularly active synapses that experience EAAT2 loss are particularly vulnerable to degeneration, and thus are those which are lost during disease progression. In addition, potential perturbations in gliotransmission (Ng et al., 2015; Yoshida et al., 1999), which acts to modulate the surrounding CPG network, could exacerbate excitotoxic events.

Future work should consider tripartite synapses as a possible site of intervention to slow neurodegeneration. Regulation of EAAT2 expression has shown some promising results in mice (Ganel et al., 2006; Rothstein et al., 2005), however, as of the time of writing has not successfully been translated to humans. These findings hopefully provide a starting point to further explore the mechanisms behind tripartite synapse loss, and how interventions may prevent this.

References

Acevedo-Arozena, A., Kalmar, B., Essa, S., Ricketts, T., Joyce, P., Kent, R., Rowe, C., Parker, A., Gray, A., Hafezparast, M., Thorpe, J.R., Greensmith, L. and Fisher, E.M. (2011). A comprehensive assessment of the SOD1^{G93A} low-copy transgenic mouse, which models human amyotrophic lateral sclerosis. *Disease Models & Mechanisms*, 4(5), pp686-700

Ackerley, S., Grierson, A.J., Brownlees, J., Thronhill, P., Anderton, B.H., Leigh, P.N., Shaw, C.E. and Miller, C.C.J. (2000). Glutamate Slows Axonal Transport of Neurofilaments in Transfected Neurons. *The Journal of Cell Biology*, 150(1), pp165-175

Agalave, N.M., Lane, B.T., Mody, P.H., Szabo-Pardi, T.A. and Burton, M.D. (2020). Isolation, culture and downstream characterization of primary microglia and astrocytes from adult rodent brain and spinal cord. *Journal of Neuroscience Methods*, 340, pp1-8

Alčaz, S., Jarebinski, M., Pekmezović, T., Stević-Marinković, Z., Pavlović, S. and Apostolski, S. (1996). Epidemiological and clinical characteristics of ALS in Belgrade, Yugoslavia. *Acta Neurologica Scandinavica*, 94(4), pp264-268

Al-Chalabi, A., Andersen, P.M., Linsson, P., Chioza, B., Andersson, J.L., Russ, C., Shaw, C.E., Powell, J.F. and Leigh, P.N. (1999). Deletions of the heavy neurofilament subunit tail in amyotrophic lateral sclerosis. *Human Molecular Genetics*, 8(2), pp157-164

Alexander, G.M., Erwin, K.L., Byers, N., Deitch, J.S., Augelli, B.J., Blankenhorn, E.O. and Heiman-Patterson, T.D. (2004). Effect of transgene copy number on survival in the G93A SOD1 transgenic mouse model of ALS. *Molecular Brain Research*, 130, pp7-115

Alhindi, A., Boehm, I. and Chaytow, H. (2021). Small junction, big problems: Neuromuscular junction pathology in mouse models of amyotrophic lateral sclerosis (ALS). *Journal of Anatomy*, 00, pp1-19

Ali, Y.O., Kitay, B.M. and Zhai, R.G. (2010). Dealing with Misfolded Proteins: Examining the Neuroprotective Role of Molecular Chaperones in Neurodegeneration. *Molecules*, 15(10), pp6859-6887

Allen, N.J., Bennett, M.L., Foo, L.C., Wang, G.X., Chakraborty, C., Smith, S.J. and Barres, B.A. (2012). Astrocyte glypicans 4 and 6 promote formation of excitatory synapses via GluA1 AMPA receptors. *Nature*, 486(7403), pp410-414

Allen, N.J. and Eroglu, C. (2017). Cell Biology of Astrocyte-Synapse Interactions. *Neuron*, 96(3), pp697-708

Allodi, I., Montañana-Rosell, R., Selvan, R., Löw, P. and Kiehn, O. (2021). Locomotor deficits in a mouse model of ALS are paralleled by loss of V1-interneuron connections onto fast motor neurons. *Nature Communications*, 12(1), pp1-18

Almad, A.A., Doreswamy, A., Gross, S.K., Richard, J.P., Huo, Y., Haughey, N. and Maragakis, N.J. (2016). Connexin 43 in Astrocytes Contributes to Motor Neuron Toxicity in Amyotrophic Lateral Sclerosis. *Glia*, 64(7), pp1154-1169

Almad, A.A., Taga, A., Joseph, J., Gross, S.K., Welsh, C., Patankar, A., Richard, J.P., Rust, K., Pokharel, A., Plott, C., Lillo, M., Dastgheyb, R., Eggan, K., Haughey, N., Contreras, J.E. and Maragakis, N.J. (2022). Cx43 hemichannels contribute to astrocyte-mediated toxicity in sporadic and familial ALS. *PNAS*, 119(13), pp1-12

Alsultan, A.A., Waller, R., Heath, P.R. and Kirby, J. (2016). The genetics of amyotrophic lateral sclerosis: current insights. *Degenerative Neurological and Neuromuscular Disease*, 6, pp49-64

Amaral, A., Hadera, M.G., Tavares, J.M., Kotter, M.R.N. and Sonnewald, U. (2016). Characterization of Glucose-Related Metabolic Pathways in Differentiated Rat Oligodendrocyte Lineage Cells. *Glia*, 64, pp21-34

Anderson, P.M., Restagno, G., Stewart, H.G. and Chiò, A. (2004). Disease Penetrance in Amyotrophic Lateral Sclerosis Associated with Mutations in the SOD1 Gene. *Annals of Neurology*, 55(2), pp298-299

Anlauf, E. and Derouiche, A. (2013). Glutamine synthetase as an astrocytic marker: its cell type and vesicle localization. *Frontiers in Endocrinology*, 4, pp1-5

Apolloni, S., Amadio, S., Montilli, C., Volonté, C. and D'Ambrosi, N.D. (2013). Ablation of P2X7 receptor exacerbates gliosis and motoneuron death in the SOD1-G93A mouse model of amyotrophic lateral sclerosis. *Human Molecular Genetics*, 22(20), pp4102-4116

Apolloni, S., Amadio, S., Parisi, C., Matteucci, A., Potenza, R.L., Armida, M., Popoli, P., D'Ambrosi, N. and Volonté, C. (2014). Spinal cord pathology is ameliorated by P2X7 antagonism in a SOD1-mutant mouse model of amyotrophic lateral sclerosis. *Disease Models & Mechanisms*, 7, pp1101-1109

Arai, T., Hasegawa, M., Akiyama, H., Ikeda, K., Nonaka, T., Mori, H., Mann, D., Tsuchiya, K., Yoshida, M., Hashizume, Y. and Oda, T. (2006). TDP-43 is a component of ubiquitin-positive tau-negative inclusions in frontotemporal lobar degeneration and amyotrophic lateral sclerosis. *Biochemical and Biophysical Research Communications*, 351(3), pp602-611

Avossa, D., Grandolfo, M., Mazzarol, F., Zatta, M. and Ballerini, L. (2006). Early Signs of Motoneuron Vulnerability in a Disease Model System: Characterization of Transverse Slice Cultures of Spinal Cord Isolated from Embryonic ALS Mice. *Neuroscience*, 138(4), pp1179-1194

Bai, G., Wang, Y. and Zhang, M. (2021). Gephyrin-mediated formation of inhibitory postsynaptic density sheet via phase separation. *Cell Research*, 31(3), pp312-325

Balendra, R. and Isaacs, A.M. (2019). C9orf72-mediated ALS and FTD: multiple pathways to disease. *Nature Reviews Neurology*, 14(9), pp544-558

Bame, M., Pentiak, P.A., Needleman, R. and Brusilow, W.S.A. (2012). Effect of Sex on Lifespan, Disease Progression, and the Response to Methionine Sulfoximine in the SOD1 G93A Mouse Model for ALS. *Gender Medicine*, 9(6), pp524-535

Bannwarth, S., Ait-El-Mkadem, S., Chaussenot, A., Genin, E.C., Lacas-Gervais, S., Fragaki, K., Berg-Alonso, L., Kageyama, Y., Serre, V., Moore, D.G., Verschueren, A., Rouzier, C., Le Ber, I., Augé, G., Cochaud, C., Lespinasse, F., N'Guyen, K., Septenville, A.D., Brice, A., Yu-Wai-Man, P., Sesaki, H., Pouget, J. and Paquis-Flucklinger, V. (2014). A mitochondrial origin for frontotemporal dementia and amyotrophic lateral sclerosis through CHCHD10 involvement. *Brain*, 137(8), pp2329-2345

Barber, S.C., and Shaw, P.J. (2010). Oxidative stress in ALS: Key role in motor neuron injury and therapeutic target. *Free Radical Biology and Medicine*, 48(5), pp629-641

Barres, B.A., Jacobson, M.D., Schmid, R., Sendtner, M. and Raff, M.C. (1993). Does oligodendrocyte survival depend on axons? *Current Biology*, 3(8), pp489-497

Barthelme, D., Jauregui, R. and Sauer, R.T. (2015). An ALS disease mutation in Cdc48/p97 impairs 20S proteasome binding and proteolytic communication. *Protein Science*, 24(9), pp1521-1527

Beaudet, M.J., Yang, Q., Cadau, S., Blais, M., Bellenfant, S., Gros-Louis, F. and Berthod, F. (2015). High yield extraction of pure spinal motor neurons, astrocytes and microglia from single embryo and adult mouse spinal cord. *Scientific Reports*, 5, pp1-12

Beers, D.R., Henkel, J.S., Zhao, W., Wang, J. and Appel, S.H. (2008). CD4+ T cells support glial neuroprotection, slow disease progression, and modify glial morphology in an animal model of inherited ALS. *PNAS*, 105(40), pp15558-15563

Beers, D.R., Henkel, J.S., Zhao, W., Wang, J., Huang, A., Wen, S., Liao, B. and Appel, S.H. (2011). Endogenous regulatory T lymphocytes ameliorate amyotrophic lateral sclerosis in mice and correlate with disease progression in patients with amyotrophic lateral sclerosis. *Brain*, 134, pp1293-1314

Beers, D., Zhao, W., Wang, J., Zhang, X., Wen, S., Neal, D., Thonhoff, J., Alsuliman, A., Shpall, E., Rezvani, K. and Appel, S. (2017). ALS patients' regulatory T lymphocytes are dysfunctional, and correlate with disease progression rate and severity. *Journal of Clinical Investigation Insight*, 2(5), pp1-15

Behrouzi, R., Liu, X., Wu, D., Robinson, A.C., Tanaguchi-Watanabe, S., Rollinson, S., Shi, J., Tian, J., Hamdalla, H.H.M., Ealing, J., Richardson, A., Jones, M., Pickering-Brown, S., Davidson, Y.S., Strong, M.J., Hasegawa, M., Snowden, J.S. and Mann, D.M.A. (2016). Pathological tau deposition in Motor Neurone Disease and frontotemporal lobar degeneration associated with TDP-43 proteinpathy. *Acta Neuropathologica Communications*, 4, pp1-16

Bendotti, C., Tortarolo, M., Suchak, S.K., Calvaresi, N., Carvelli, L., Bastone, A., Rizzi, M., Rattray, M. and Mennini, T. (2001). Transgenic SOD1 G93A mice develop reduced GLT-1 in spinal cord without alterations in cerebrospinal fluid glutamate levels. *Journal of Neurochemistry*¸79(4), p737-746

Bennett, M.L., Bennett, F.C., Liddelow, S.A., Ajami, B., Zamanian, J.L., Fernhoff, N.B., Mulinyawe, S.B., Bohlen, C.J., Adil, A., Tucker, A., Weissman, I.L., Chang, E.F., Li, G., Grant, G.A., Gephart, M.G.H. and Barres, B.A. (2016). New tools for studying microglia in the mouse and human CNS. *PNAS*, 113(12), pp1738-1746

Bennett, S.A., Tanaz, R., Cobos, S.N. and Torrente, M.P. (2019). Epigenetics in Amyotrophic Lateral Sclerosis: A Role for Histone Post Translational Modifications in Neurogenerative Disease. *Translational Research*, 204, pp19-30

Bergles, D.E. and Richardson, W.D. (2016). Oligodendrocyte Development and Plasticity. *Cold Spring Harbor Perspectives in Biology*, 8(2), pp1-27

Bernardinelli, Y., Randall, J., Janett, E., Nikonenko, I., König, S., Jones, E.V., Flores, C.E., Murai, K.K., Bochet, C.G., Holtmaat, A. and Muller, D. (2014). Activity-Dependent Structural Plasticity of Perisynaptic Astrocytic Domains Promotes Excitatory Synapse Stability. *Current Biology*, 24(15), pp1679-1688

Bogdanov, A.M., Kudryavtseva, E.I. and Lukyanov, K.A. (2012). Anti-Fading Media for Live Cell GFP Imaging. *PLoS ONE*¸7(12), pp1-4

Boivin, J.R. and Nedivi, E. (2018). Functional implications of inhibitory synapse placement on signal processing in pyramidal neuron dendrites. *Current Opinion in Neurobiology, 51, pp16-22*

Booker, S. and Wyllie, D.J.A. (2017). Parvalbumin interneurons in the dorsal horn: it's not all about GABA. *Journal of Physiology*, 595(23), pp7019-7020

Bosco, D.A., Morfini, G., Karabacak, N.M., Song, Y., Gros-Louis, F., Pasinelli, P., Goolsby, H., Fontaine, B.A., Lemay, N., McKenna-Yasek, D., Frosch, M.P., Agar, J.N., Julien, J.P., Brady, S.T. and Brown Jr., R.H. (2010). Wild-type and mutant SOD1 share an aberrant conformation and a common pathogenic pathway in ALS. *Nature Neuroscience*, 13(11), pp1396-1403

Bosk, S., Braunger, J.A., Gerke, V. and Steinem, C. (2011). Activation of F-Active Binding Capacity of Ezrin: Synergism of PIP_2 Interaction and Phosphorylation. *Biophysical Journal*, 100(7), pp1708-1717

Boston-Howes, W., Gibb, S.L., Williams, E.O., Pasinelli, P., Brown Jr., R.H. and Trotti, D. (2006). Caspase-3 Cleaves and Inactivates the Glutamate Transporter EAAT2. *Journal of Biological Chemistry*, 281(20), pp14076-14084

Bott, N.T., Radke, A., Stephens, M.L. and Kramer, J.H. (2016). Frontotemporal dementia: diagnosis, deficits and management. *Neurodegenerative Disease Management*, 4(6), pp439-454

Braems, E., Swinnen, B. and Bosch, L.V.D. (2020). C9orf72 loss-of-function: a trivial, stand alone or additive mechanism in C9 ALS/FTD? *Acta Neuropathologica*, 140, pp625-643

Broadhead, M.J., Bonthron, C., Arcinas, L., Bez, S., Zhu, F., Goff, F., Nylk, J., Dholakia, K., Gunn-Moore, F., Grant, S.G.N. and Miles, G.B. (2020). Nanostructural Diversity of Synapses in the Mammalian Spinal Cord. *Scientific Reports*, 10, pp1-18

Broadhead, M.J., Bonthron, C., Waddington, J., Smith, W.V., Lopez, M.F., Burley, S., Valli, J., Zhu, F., Komiyama, N.H., Smith, C., Grant, S.G.N. and Miles, G.B. (2022). Selective

vulnerability of tripartite synapses in amyotrophic lateral sclerosis. *Acta Neuropathologica*, 143, pp471-486

Broadhead, M.J., Horrocks, M.H., Zhu, F., Muresan, L., Benavides-Piccione, R., DeFelipe, J., Fricker, D., Kpanitsa, M.V., Duncan, R.R., Klenerman, D., Komiyama, N.H., Lee, S.F. and Grant, S.G.N. (2016). PSD95 nanoclusters are postsynaptic building blocks in hippocampus circuits. *Scientific Reports*, 6, pp1-14

Broadhead, M.J. and Miles, G.B. (2020). Bi-Directional Communication Between Neurons and Astrocytes Modulates Spinal Motor Circuits. *Frontiers in Cellular Neuroscience*¸14, pp1-14

Bronstein, J.M., Popper, P., Micevych, P.E. and Farber, D.B. (1996). Isolation and characterisation of a novel oligodendrocyte-specific protein. *Neurology*, 47(3), pp772-778

Brown, R.H. and Al-Chalabi, A. (2017). Amyotrophic Lateral Sclerosis. *The New England Journal of Medicine*, 377(2), pp162-172

Brown, A.L., Wilkins, O.G., Keuss, M.J., Hill, S.E., Zanovello, M., Lee, W.C., Bampton, A., Lee, L.C.Y., Masino, L., Qi, Y.A., Bryce-Smith, S., Gatt, A., Hallegger, M., Fagegaltier, D., Phatnani, H, Newcombe, J., Gustavsson, E.K., Seddighi, S., Reyes, J.F., Coon, S.L., Ramos, D., Schiavo, G., Fisher, E.N.C., Raj, T., Secrier, M., Lashley, T., Ule, J., Buratti, E., Humphrey, J., Ward, M.E. and Fratta, P. (2022). TDP-43 loss and ALS-risk SNPs drive mis-splicing and depletion of UNC13A. *Nature*, 603, pp131-137

Bruijn, L.I., Becher, M.W., Lee, M.K., Anderson, K.L., Jenkins, N.A., Copeland, N.G., Sisodia, S.S., Rothstein, J.D., Borchelt, D.R., Price, D.L. and Cleveland, D.W. (1997). ALS-Linked SOD1 Mutant G85R Mediates Damage to Astrocytes and Promotes Rapidly Progressive Disease with SOD1-Containing Inclusions. *Neuron*, 18(2), pp327-338

Butti, Z. and Patten, S.A. (2019). RNA Dysregulation in Amyotrophic Lateral Sclerosis. *Frontiers in Genetics*, 10(712), pp1-18

Carbone, M., Duty, S. and Rattray, M. (2012). Riluzole elevates GLT-1 activity and levels in striatal astrocytes. *Neurochemistry International*, 60(1), pp31-38

Carriedo, S.G., Yin, H.Z. and Weiss, J.H. (1996). Motor Neurons Are Selectively Vulnerable to AMPA/Kainate Receptor-Mediated Injury *In Vitro*. *Journal of Neuroscience*, 16(13), pp4069-4079

Catanese, A., Rajkumar, S., Sommer, D., Freisem, D., Wirth, A., Aly, A., Massa-López, D., Olivieri, A., Torelli, F., Ioannidis, V., Lipecka, J., Guerrera, I.C., Zytnicki, D., Ludolph, A., Kabashi, E., Mulaw, M.A., Roselli, F. and Böckers, T.M. (2021). Synaptic disruption and CREB-regulated transcription are restored by K^+ channel blockers in ALS. *EMBO Molecular Medicine*, 13(7), pp1-16

Chang, Q. and Martin, L.J. (2009). Glycinergic Innervation of Motoneurons Is Deficient in Amyotrophic Lateral Sclerosis Mice. *American Journal of Pathology*, 174(2), pp574-585

Chang, Q. and Martin, L.J. (2011). Glycine Receptor Channels in Spinal Motoneurons Are Abnormal in a Transgenic Mouse Model of Amyotrophic Lateral Sclerosis. *Journal of Neuroscience*, 31(8), pp2815-2827

Chen, Y., Balasubramaniyan, V., Peng, J., Hurlock, E.C., Tallquist, M., Li, J. and Lu, Q.R. (2007). Isolation and culture of rat and mouse oligodendrocyte precursor cells. *Nature Protocols*, 2(5), pp1044-1051

Chen, Z., Jalabi, W., Hu, W., Park, H.J., Gale, J.T., Kidd, G.J., Bernatowicz, R., Gossman, Z.C., Chen, J.T., Dutta, R. and Trapp, B.D. (2014). *Nature Communications*, 5, pp1-12

Chiò, A., Calvo, A., Moglia, C., Mazzini, L., Mora, G., PARALS study group (2011). Phenotypic heterogeneity of amyotrophic lateral sclerosis: a population based study. *Journal of Neurology, Neurosurgery and Psychiatry*, 82, pp740-746

Chiu, I.M., Chen, A., Zheng, Y., Kosaras, B., Tsiftsoglou, S.A., Vartanian, T.K., Brown Jr., R.H. and Carroll, M.C. (2008). T lymphocytes potentiate endogenous neuroprotective inflammation in a mouse model of ALS. *PNAS*, 105(46), pp17913-17918

Chiu, C.S., Kartalov, E., Unger, M., Quake, S. and Lester, H.A. (2001). Single-molecular measurements calibrate green fluorescent protein surface densities on transparent beads for use with 'knock-in' animals and other expression systems. *Journal of Neuroscience Methods*, 105, pp55-63

Choi, S. and Lovinger, D.M. (1997). Decreased Frequency But Not Amplitude of Quantal Synaptic Responses Associated with Expression of Corticostriatal Long-Term Depression. *Journal of Neuroscience*, 17(21), pp8613-8620

Christopherson, K.S., Ullian, E.M., Stokes, C.C.A., Mullowney, C.E., Hell, J.W., Agah, A., Lawler, J., Mosher, D.F., Bornstein, P. and Barres, B.A. (2005). *Cell*, 120, pp421-433

Chung, W.S., Allen, N.J. and Eroglu, C. (2015). Astrocytes Control Synapse Formation, Function, and Elimination. *Cold Spring Harbor Perspectives in Biology*, 7(9), pp1-19

Clark, R.M., Blizzard, C.A., Young, K.M., King, A.E. and Dickson, T.C. (2017). Calretinin and Neuropeptide Y interneurons are differentially altered in the motor cortex of the $SOD1^{G93A}$ mouse model of ALS. *Scientific Reports*, 7, pp1-13

Corcia, P., Tauber, C., Vercoullie, J., Arlicot, N., Prunier, C., Praline, J., Nicolas, G., Venel, Y., Hommet, C., Baulieu, J.L., Cottier, P., Roussel, C., Kassiou, M., Guilloteau, D. and Ribeiro, M.J. (2012). Molecular Imaging of Microglia Activation in Amyotrophic Lateral Sclerosis. *PLoS ONE*, 7(12), pp1-7

Couratier, P., Corcia, P., Lautrette, G., Nicol, M., Preux, P.M. and Marin, B. (2016). Epidemiology of amyotrophic lateral sclerosis: A review of literature. *Ravue Neurologique*, 172(1), pp37-45

Cuevas, M.E, Carrasco, M.A., Fuentes, Y., Castro, P., Nualart, F., Roa, J. and Aguayo, L.G. (2005). The presence of glia stimulates the appearance of glycinergic synaptic transmission in spinal cord neurons. *Molecular and Cellular Neuroscience*, 28(4), pp770-778

Curran, O.E., Qiu, Z., Smith, C. and Grant, S.G.N. (2020). A single-synapse resolution survey of PSD95-positive synapses in twenty human brain regions. *European Journal of Neuroscience*, 54, pp6864-6881

Delestrée, N., Manuel, M., Iglesias, C., Elbasiouny, S.M., Heckman, C.J. and Zytnicki, D. (2014). Adult spinal motoneurones are not hyperexcitable in a mouse model of inherited amyotrophic lateral sclerosis. *Journal of Physiology*, 592(7), pp1687-1703

Deng, H.X., Chen, W., Hong, S.T., Boycott, K.M., Gorrie, G.H., Siddique, N., Yang, Y., Fecto, F., Shit, Y., Zhai, H., Jiang, H., Hirano, M., Rampersaud, E., Jansen, G.H., Donkervoot, S., Bigio, E.H., Brooks, B.R., Ajroud, K., Sufit, R.L., Haines, J.L., Mugnaini, E., Pericak-Vance, M. and Siddique, T. (2011). *Nature*, 477(7362), pp211-215

Derouiche, A. and Frotscher, M. (1991). Astroglial processes around identified glutamatergic synapses contain glutamine synthetase: evidence for transmitter degradation. *Brain Research*, 552(2), pp346-350

Derouiche, A. and Frotscher, M. (2001). Peripheral Astrocyte Processes: Monitoring by Selective Immunostaining for the Actin-Binding ERM Proteins. *Glia*, 36(3), pp330-341

De Sousa, S.L.M., Dickinson, R., Lieb, W.R. and Franks, N.P. (2000). Contrasting Synaptic Actions of the Inhalation General Anesthetics Isoflurane and Xenon. *Anesthesiology*, 92(4), pp1055-1066

Devlin, A.C., Burr, K., Borooah, S., Foster, J., Cleary, E.M., Geti, I., Vallier, L., Shaw, C.E., Chandran, S. and Miles, G.B. (2015). Human iPSC-derived motoneurons harbouring TARDBP or C9ORF72 ALS mutations are dysfunctional despite maintaining viability. *Nature Communications*, 6, pp1-12

De Vos, K.J., Chapman, A.L., Tennant, M.E., Manser, C., Tudor, E.L., Lau, K.F., Brownless, J., Ackerley, S., Shaw, P.J., McLoughlin, M., Shaw, C.E., Leigh, P.N., Miller, C.C.J. and Grierson, A.J. (2007). Familial amyotrophic lateral sclerosis-linked SOD1 mutants perturb fast axonal transport to reduce axonal mitochondria content. *Human Molecular Genetics*, 16(22), pp2720-2728

De Vos, K.J. and Hafezparast, M. (2017). Neurobiology of axonal transport defects in motor neuron diseases: Opportunities for translation research? *Neurobiology of Disease*, 105, pp283-299

Dharmadasa, T. and Kiernan, M.C. (2018). Riluzole, disease stage and survival in ALS. *The Lancet Neurology*, 17(5), pp385-386

Díaz-Villanueva, J.F., Díaz-Molina, R. and García-González, V. (2015). Protein Folding and Mechanisms of Proteostasis. *International Journal of Molecular Sciences*, 16(8), pp17193-17230

Diniz, L.P., Almeida, J.C., Tortelli, V., Lopes, C.V., Setti-Perdigão, Stipursky, J., Kahn, S.A., Romão, L.F., de Miranda, J., Alvea-Leon, S.V., de Souza, J.M., Castro, N.G., Panizzutti, R. and Gomes, F.C.A. (2012). Astrocyte-induced Synaptogensis Is Mediated by Transforming

Growth Factor β Signaling through Modulation of D-Serine Levels in Cerebral Cortex Neurons. *The Journal of Biological Chemistry*, 287(49), pp41432-41445

Diniz, L.P., Tortelli, V., Garcia, M.N., Araújo, A.P.B., Melo, H.M., da Silva, G.S.S., De Delice, F.G., Alves-Leon, S.V., de Souza, J.M., Ramão, L.F., Castro, N.G. and Gomes, F.C.A. (2014). Astrocyte Transforming Growth Factor Beta 1 Promotes Inhibitory Synapse Formation via CaM Kinase II Signaling. *Glia*, 62(12), pp1917-1931

Dong, X.X., Wang, Y. and Qin, Z.H. (2009). Molecular mechanisms of excitotoxicity and their relevance to pathogenesis of neurodegenerative diseases. *Acta Pharmacologica Sinica*, 30(4), pp379-387

Donnelly, C.J., Zhang, P.W., Pham, J.T., Heusler, A.R., Mistry, N.A., Vidensky, S., Daley, E.L., Poth, E.M., Hoover, B., Fines, D.M., Maragakis, N., Tienari, P.J., Petrucelli, L., Traynor, B.J., Wang, J., Rigo, F., Bennett, C.F., Blackshaw, S., Sattler, R. and Rothstein, J.D. (2013). RNA Toxicity from the ALS/FTD C9ORF&" Expansion Is Mitigated by Antisense Intervention. *Neuron*, 80(2), pp415-428

Eldeiry, M., Yamanaka, K., Reece, T.B. and Aftab, M. (2017). Spinal Cord Neurons Isolation and Culture from Neonatal Mice. *Journal of Visualized Experiments*, 2017(125), pp1-9

Elmariah, S.B., Oh, E.J., Hughes, E.G. and Balice-Gordon, R.J. (2005). Astrocytes Regulate Inhibitory Synapse Formation via Trk-Mediated Modulation of Postsynaptic $GABA_A$ Receptors. *Journal of Neuroscience*, 25(14), pp3638-3650

Eroglu, C., Allen, N.J., Susman, M.W., O'Rourke, N.A., Park, C.Y., Özkan, E., Chakraborty, C., Mulinyawe, S.B., Annis, D.S., Huberman, A.D., Green, E.M., Lawler, J., Dolmetsch, R., Garcia, K.C., Smith, S.J., Luo, Z.D., Rosenthal, A., Mosher, D.F. and Barress, B.A. (2009). Gabapentin Receptor α2δ-1 Is a Neuronal Thrombospondin Receptor Responsible for Excitatory CNS Synaptogenesis. *Cell*, 139(2), pp380-392

Farhy-Tselnicker, I. and Allen, N.J. (2018). Astrocytes, neurons, synapses: a tripartite view on cortical circuit development. *Neural Development*, 13, pp1-12

Feeney, S.J., McKelvie, P.A., Austin, L., Jean-Francois, M.J.B., Kaspa, R., Tombs, S.M. and Byrne, E. (2001). Presymptomatic Motor Neuron Loss and Reactive Astrocytosis in the SOD1 Mouse Model of Amytrophic Lateral Sclerosis. *Muscle and Nerve*, 24(11), pp1510-1519

Fernández, E., Collins, M.O., Uren, R.T., Kopanitsa, M.V., Komiyama, N.H., Croning, M.D.R., Zografos, L., Armstrong, J.D., Choudhary, J.S. and Grant, S.G.N. (2009). Targeted tandem affinity purification of PSD-95 recovers core postsynaptic complexes and schizophrenia susceptibility proteins. *Molecular Systems Biology*, 5, pp1-17

Ferraiuolo, L., Meyer, K., Sherwood, T.W., Vick, J., Likhite, S., Frakes, A., Miranda, C.J., Brain, L., Heath, P.R., Pineda, R., Beattie, C.E., Shaw, P.J., Askwith, C.C., McTigue, D. and Kaspar, B.K. (2016). Oligodendrocytes contribute to motor neuron death in ALS via SOD1-dependent mechanism. *PNAS*, 113(42), pp6496-6505

Ferrari, R., Kapogiannis, D., Huey, E.D., Momeni, P. (2011). FTD and ALS: a tale of two disease. *Current Alzheimer Research*, 8(3), 273-294

Figlewicz, D.A., Krizus, A., Martinoli, M.G., Meininger, V., Dib, M., Rouleau, G.A. and Julien, J.P. (1994). Variants of the heavy neurofilament subunit are associated with the development of amyotrophic lateral sclerosis. *Human Molecular Genetics*, 3(10), pp1757-1761

Fogarty, M.J., Klenowski, P.M., Lee, J.D., Drieberg-Thompson, J.R., Bartlett, S.E., Ngo, S.T., Hilliard, M.A., Bellingham, M.C. and Noakes, P.G. (2016). Cortical synaptic and dendritic spine abnormalities in a presymptomatic TDP-43 model of amyotrophic lateral sclerosis. *Scientific Reports*, 6, pp1-13

Fogarty, M.J., Noakes, P.G. and Bellingham, M.C. (2015). Motor Cortex Layer V Pyramidal Neurons Exhibit Dendritic Regression, Spine Loss and Increased Synaptic Excitation in the Presymptomatic hSOD1^{G93A} Mouse Model of Amyotrophic Lateral Sclerosis. *Journal of Neuroscience*, 35(2), pp643-647

Freeman, K.A., Fullerton, D.A., Foley, L.S., Bell, M.Y., Cleveland, J.C., Weyant, M.J., Mares, J., Meng, X., Puskas, F. and Reece, T.B. (2015). Spinal cord protection via alpha-2-agonist-mediated increase in glial cell-line-derived neurotrophic factor. *Journal of Thoracic and Cardiovascular Surgery*, 149(2), pp578-586

Fritz, E., Izaurieta, P., Weiss, A., Mir, F.R., Rojas, P., Gonzalez, D., Rojas, F., Brown Jr., R.H., Madrid, R. and van Zundert, B. (2013). Mutant SOD1-expressing astrocytes release toxic factors that trigger motoneuron death by inducing hyperexcitability. *Journal of Neurophysiology*, 109(11), pp2803-2814

Fuchs, A., Ringer, C., Bilkei-Gorzo, A., Weihe, E., Roeper, J. and Schütz, B. (2010). Downregualtion of the Potassium Chloride Cotransporter KCC2 in Vulnerable Motoneurons in the SOD1-G93A Mouse Model of Amyotrophic Lateral Sclerosis. *Journal of Neuropathology and Experimental Neurology*, 69(10), pp1057-1070

Fünfschilling, U., Supplie, L.M., Mahad, D., Boretius, S., Saab, A.S., Edgar, J., Brinkmann, B.G., Kassmann, C.M., Tzvetanova, I.D., Möbius, W., Diaz, F., Meijer, D., Suter, U., Hamprecht, B., Sereda, M.W., Moraes, C.T., Frahm, J., Goebbels, S. and Nave, K.A. (2012). Glycolytic oligodendrocytes maintain myelin and long-term axonal integrity. *Nature*, 485(7399), pp517-521

Furukawa, M., Tsukahara, T., Tomita, K., Iwai, H., Sonomura, T., Miyawaki, S. and Sato, T. (2017). Neonatal maternal separation delays the GABA excitatory-to-inhibitory functional switch by inhibiting KCC2 expression. *Biochemical and Biophysical Research Communications*, 493(3), pp1243-1249

Gamlin, C.R., Yu, W.Q., Wong, R.O.L. and Hoon, M. (2018). Assembly and maintenance of GABAergic and Glycinergic circuits in the mammalian nervous system. *Neural Development*, 13(1), pp1-17

Ganel, R., Ho, T., Maragakis, N.J., Jackson, M., Steiner, J.P. and Rothstein, J.D. (2006). Selective up-regulation of the glial Na^+-dependent glutamate transporter GLT1 by a

neuroimmunophilin ligan results in neuroprotection. *Neurobiology of Disease*, 21(3), pp556-567

Garrett, A.M. and Weiner, J.A. (2009). Control of CNS synapse development by γ-protocadherin-mediated astrocyte-neuron contact. *Journal of Neuroscience*, 29(38), pp11723-11731

Garruto, R.M., Yanagihara, R. and Gajdusek, D.C. (1985). Disappearance of high-incidence amyotrophic lateral sclerosis and parkinsonism-dementia on Guam. *Neurology*, 35(2), pp193-198

Geevasinga, N., Menon, P., Scherman, D.B., Simon, N., Yiannikas, C., Henmderson, R.D., Kiernan, M.C. and Vucic, S. (2017). Diagnostic criteria in amyotrophic lateral sclerosis. *Neurology*, 88(7), pp719-726

Gendron, T.F. and Petrucelli, L. (2018). Disease Mechanisms of C9ORF72 Repeat Expansions. *Cold Spring Harbor Perspective in Medicine*, 8(4), pp1-21

Genoud, C., Quairiaux, C., Steiner, P., Hirling, H., Welker, E. and Knott, G.W. (2006). Plasticity of Astrocytic Coverage and Glutamate Transporter Expression in Adult Mouse Cortex. *PLoS Biology*, 4(11), pp2057-2064

Gibb, S.L., Boston-Howes, W., Lavina, Z.S., Gustincich, S., Brown Jr., R.H., Pasinelli, P. and Trotti, D. (2007). A Caspase-3 cleaved Fragment of the Glial Glutamate Transporter EAAT2 is Sumoylated and Targeted to Promyelocytic Leukemia Nuclear Bodies in Mutant SOD1-linked Amyotrophic Lateral Sclerosis. *Journal of Biological Chemistry*, 282(42), pp32480-32490

Gijselinck, I., Mossevelde, S.V., van der Zee, J., Sieben, A., Engelborghs, S., De Bleecker, J., Ivanoiu, A., Deryck, O., Edbauer, D., Zhang, M., Heeman, B., Bäumer, V., Van den Broeck, M., Mattheijssens, M., Peeters, K., Rogaeva, E., De Jonghe, P., Cras, P., Martin, J.J., de Deyn, P.P., Cruts and M., Van Broeckhoven, C. (2016). The C9orf72 repeat size correlates with onset age of disease, DNA methylation and transcriptional downregulation of the promoter. *Molecular Psychiatry*, 21(8), pp1112-1124

Glantz, L.A., Gilmore, J.H., Hamer, R.M., Lieberman, J.A. and Jarskog, L.F. (2007). Synaptophysin and PSD-95 in the human prefrontal cortex from mid-gestation into early adulthood. *Neuroscience*, 149(3), pp582-591

Gordon, P.H., Mehal, J.M., Holman, R.C., Rowland, L.P., Rowland, A.S. and Cheek, J.E. (2013). Incidence of Amyotrophic Lateral Sclerosis Among American Indians and Alaska Natives. *JAMA Neurology*, 70(4), pp476-480

Gortiz, C., Mauch, D.H. and Pfrieger, F.W. (2005). Multiple mechanisms mediate cholesterol-induced synaptogenesis in a CNS neuron. *Molecular and Cellular Neuroscience*, 29(2), pp190-201

Guirado, R., Carceller, H., Castillo-Gómez, E., Castrén, E. and Nacher, J. (2018). Automated analysis of images for molecular quantification in immunohistochemistry. *Heliyon*, 4(6), pp1-16

Guo, H., Lai, L., Butchbach, M.E.R. and Lin, C.L.G. (2002). Human Glioma Cells and Undifferentiated Primary Astrocytes That Express Aberrant EAAT2 mRNA Inhibit Normal EAAT2 Protein Expression and Prevent Cell Death. *Molecular and Cellular Neuroscience*, 21, pp546-560

Gurney, M.E., Pu, H., Chiu, A.Y., Dal Canto, M.C., Polchow, C.Y., Alexander, D.D., Caliendo, J., Hentati, A., Kwon, Y.W., Deng, H.X., Chen, W., Zhai, P., Sufit, R.L. and Siddique, T. (1994). Motor Neuron Degeneration in Mice That Express a Human Cu,Zn Superoxide Dismutase Mutation. *Science*, 264(5166), pp1772-1775

Gutierrez-Mencinas, M., Kuehn, E.D., Abraira, V.E., Polgár, E., Watanabe, M. and Todd, A.J. (2016). Immunostaining for Homer Reveals the Majority of Excitatory Synapses in Laminae I-III of the Mouse Spinal Dorsal Horn. *Neuroscience*, 329, pp171-181

Haeusler, A.R., Donnelly, C.J., Periz, G., Simko, E.A.J., Shaw, P.G., Kim, M.S., Maragakis, N.J., Troncoso, J.C., Pandey, A., Sattler, R., Rothstein, J.D. and Wang, J. (2014). C9orf72 nucleotide repeat structures initiate molecular cascades of disease *Nature*, 507(7491), pp195-200.

Hafner, A.S., Penn, A.C., Grillo-Bosch, D., Retailleau, N., Poujol, C., Philippat, A., Coussen, F., Sainlos, M., Opazo, P. and Choquet, D. (2015). Lengthening of the Stargazin Cytoplasmic Tail Increases Synaptic Transmission by Promoting Interaction to Deeper Domains of PSD-95. *Neuron*, 86(2), pp475-489

Hama, H., Hara, C., Yamaguchi, K. and Miyawaki, A. (2004). PKC Signaling Mediates Global Enhancement of Excitatory Synaptogenesis in Neurons Triggered by Local Contact with Astrocytes. *Neuron*, 41, pp405-415

Hardiman, O., Al-Chalabi, A., Chio, A., Corr, E.M., Logroscino, G., Robberecht, W., Shaw, P.J., Simmons, Z., van der Berg, L.H. (2017). Amyotrophic Lateral Sclerosis. *Nature Reviews Disease Primers*, 3(17071), pp1-19

Hayashi, H., Suga, M., Satake, M. and Tsubaki, T. (1981). Reduced Glycine Receptor in the Spinal Cord in Amyotrophic Lateral Sclerosis. *Annals of Neurology*, 9(3), pp292-294

Heiman-Patterson, T.D., Sher, R.B., Blankenhorn, E.A., Alexander, G., Deitch, J.S., Kunst, C.B., Maragakis, N. and Cox, G. (2011). Effect of genetic background on phenotype variability in transgenic mouse models of amyotrophic lateral sclerosis: A window of opportunity in the search for genetic modifiers. *Amyotrophic Lateral Sclerosis*, 12(2), pp79-88

Heller, J.P. and Rusakov, D.A. (2015). Morphological plasticity of astroglia: Understanding synaptic microenvironment. *Glia*, 63(12), pp2133-2151

Heller, J.P. and Rusakov, D.A. (2017). The Nanoworld of the Tripartite Synapse: Insights from Super-Resolution Microscopy. *Frontiers in Cellular Neuroscience*, 11, pp1-14

Henneberger, C., Bard, L., Panatier, A., Reynolds, J.P., Kpach, O., Medvedev, N.I., Minge, D., Herde, M.K., Anders, S., Kraev, I., Heller, J.P., Rama, S., Zheng, K., Jensen, T.P.,

Sanchez-Romero, I., Jackson, C.J., Janovjak, H., Ottersen, O.P., Nagelhus, E.A>, Oliet, S.H.R., Stewart, M.G., Nägerl, U.V. and Rusakov, D.A. (2020). LTP Induction Boots Glutamate Spillover by Driving Withdrawal of Perisynaptic Astroglia. *Neuron*, 108(5), pp919-936

Henstridge, C.M., Sideris, D.I., Carroll, E., Rotariu, S., Salomonsson, S., Tzioras, M., McKenzie, C.A., Smith, C., von Arnim, C.A.F., Ludolph, A.C., Lulé, D., Leighton, D., Warner, J., Cleary, E., Newton, J., Swingler, R., Chandran, S., Gillingwater, T.H., Abrahams, S. and Spires-Jones, T.L. (2018). Synapse loss in the prefrontal cortex is associated with cognitive decline in amyotrophic lateral sclerosis. *Acta Neuropathologica*, 135(2), pp213-226

Henstridge, C.M., Tzioras, M. and Paolicelli, R.C. (2019). Glial Contribution to Excitatory and Inhibitory Synapse Loss in Neurodegeneration. *Frontiers in Cellular Neuroscience*, 13, pp1-26

Hernández, I.C., Buttafava, M., Boso, G., Diaspro, A., Tosi, A. and Vicidomini, G. (2015). Gated STED microscopy with time-gated single-photon avalanche diode. *Biomedical Optics Express*, 6(6), pp2258-2267

Higgins, C.M.J., Jung, C. and Xu, Z. (2004). ALS-associated mutant $SOD1^{G93A}$ causes mitochondrial vacuolation by expansion of the intermembrane space and by involvement of SOD1 aggregation and peroxisomes. *BMC Neuroscience*, 4(16), pp1-14

Hochstim, C., Deneen, B., Lukaszewicz, A., Zhou, Q., and Anderson, D.J. (2008). The spinal cord contains positionally distinct astrocyte subtypes whose identities are specified by a homeodomain transcriptional code. *Cell*, 133(3), pp510-522

Hol, E.M. and Pekny, M. (2015). Glial fibrillary acidic protein (GFAP) and the astrocyte intermediate filament system in disease of the central nervous system. *Current Opinion in Cell Biology*, 32, pp121-130

Hook, E.B. and Regal, R.R. (1995). Capture-Recapture Methods in Epidemiology: Methods and Limitations. *Epidemiologic Reviews*, 17(2), pp243-264

Hossaini, M., Cano, S.C., van Dis, V., Haasdijk, E.D., Hoogenraad, C.C., Holstege, J.C. and Jaarsma, D. (2011). Spinal Inhibitory Interneuron Pathology Follows Motor Neuron Degeneration Independent of Glial Mutant Superoxide Dismutase 1 Expression in SOD1-ALS Mice. *Journal of Neuropathology and Experimental Neurology*, 70(8), pp662-677

Howland, D.S., Liu, J., She, Y., Goad, B., Maragakis, N.J., Kim, B., Erickson, J., Kulik, J., DeVito, L., Psaltis, G., DeGennaro, L.J., Cleveland, D.W. and Rothstein, J.D. (2002). *PNAS*, 99(3), pp1604-1609

Huang, B., Babcock, H. and Zhuang, X. (2010). Breaking the Diffraction Barrier: Super-Resolution Imaging of Cells. *Cell*, 143(7), pp1047-1058

Hughes, E.G., Kang, S.H., Fukaya, M. and Bergles, D.E. (2013). Oligodendrocyte progenitors balance growth with self-repulsion to achieve homeostasis in the adult brain. *Nature Neuroscience*, 16(6), pp668-679

Hui, C.W., Zhang, Y. and Herrup, K. (2016). Non-Neuronal Cells Are Required to Mediate the Effects of Neuroinflammation: Results from a Neuron-Enriched Culture System. *PLoS ONE*¸11, pp1-17

Ince, P.G., Slade, J., Chinnery, R.M., McKenzie, J., Royston, C., Roberts, G. and Shaw, P.J. (1995). Quantitative Study of Synaptophysin Immunoreactivity of Cerebral Cortex and Spinal Cord in Motor Neuron Disease. *Journal of Neuropathology and Experimental Neurology*, 54(5), pp673-679

Ince, P.G., Tomkins, J., Slade, J.Y., Thatcher, N.M., and Shaw, P.J. (1998). Amyotrophic Lateral Sclerosis Associated with Genetic Abnormalities in the Gene Encoding Cu/Zn Superoxide Dismutase: Molecular Pathology of Five New Cases, and Comparison with Previous reports and 73 Sporadic Cases of ALS. *Journal of Neuropathology and Experimental Neurology*, 57(10), pp895-904

Ishibashi, M., Egawa, K. and Fukuda, A. (2019). Diverse Actions of Astrocytes in GABAergic Signaling. *International Journal of Molecular Sciences*, 20(12), pp1-18

Ishiura, H., Takahashi, Y., Mitsui, J., Yoshida, S., Kihira, T., Kokubo, Y., Kuzuhara, S., Ranum, L.P.W., Tamaoki, T., Ichikawa, Y., Date, Hidetoshi, Goto., J. and Tsuji, S. (2012). C9ORF72 Repeat Expansion in Amyotrophic Lateral Sclerosis in the Kii Peninsula of Japan. *Archives of Neurology*, 69(9), pp1154-1158

Jean-Xavier, C., Mentis, G.Z., O'Donovan, M.J., Cattaert, D. and Vinay, L. (2007). Dual personality of GABA/glycine-mediated depolarisations in immature spinal cord. *PNAS*, 104(27), pp11477-11482

Jiang, M.C., Adimula, A., Birch, D. and Heckman, C.J. (2017). Hyperexcitability in synaptic and firing activities of spinal motoneurons in an adult mouse model of amyotrophic lateral sclerosis. *Neuroscience*, 362, pp33-46

Jiang, T., Handley, E., Brizuela, M., Dawkins, E., Lewis, K.E.A., Clark, R.M., Dickson, T.C. and Blizzard, C.A. (2019). Amyotrophic lateral sclerosis mutant TDP-43 may cause synaptic dysfunction through altered dendritic spine function. *DMM Disease Models and Mechanisms*, 12, pp1-11

Jiang, M., Schuster, J.E., Fu, R., Siddique, T. and Heckman, C.J. (2009). Progressive Changes in Synaptic Inputs to Motoneurons in Adult Sacral Spinal Cord of a Mouse Model of Amyotrophic Lateral Sclerosis. *Journal of Neuroscience*, 29(48), pp15031-15038

Jiang, Z.G. and Smith, R.A. (1993). Effects of Nerve Growth Factor on the Survival of Primary Culutred Adult and Aged Mouse Sensory Neurons. *Journal of Neuroscience Research*, 35(1), pp29-37

Joensen, P. (2012). Incidence of amyotrophic lateral sclerosis in the Faroe Islands. *Acta Neurologica Scandinavica*, 126(1), pp62-66

Ju, J.S., Fuentealba, R.A., Miller, S.E., Jackson, E., Piwnica-Worms, D., Baloh, R.H. and Weihl, C.C. (2009). Valosin-containing protein (VCP) is required for autophagy and is disrupted in VCP disease. *Journal of Cell Biology*, 187(6), pp875-888

Juge, N., Muroyama, A., Hiasa, M., Omote, H. and Moriyama, Y. (2009). Vesicular Inhibitory Amino Acid Transporter Is a Cl^- / γ-Aminobutyrate Co-Transporter. *Journal of Biological Chemistry*, 284(50), pp35073-35078

Kang, S.H., Li, Y., Fukaya, M., Lorenzini, I., Cleveland, D.W., Ostrow, L.W., Rothstein, J.D. and Bergles, D.E. (2013). Degeneration and impaired regeneration of gray matter oligodendrocytes in amyotrophic lateral sclerosis. *Nature Neuroscience*, 16(5), 571-579

Katzenell, S., Cabrera, J.R., North, B.J. and Leib, D.A. (2017). Isolation, Purification, and Culture of Primary Murine Sensory Neurons. *Methods in Molecular Biology*, 1656, pp229-251

Kehl, L.J., Fairbanks, C.A., Laughlin, T.M. and Wilcox, G.L. (1997). Neurogenesis in Postnatal Rat Spinal Cord: A study in Primary Culture. *Science*, 276, pp586-589

Keith, D. and El-Husseini, A. (2008). Excitation control: balancing PSD-95 function at the synapse. *Frontiers in Molecular Neuroscience*, 1, pp1-12

Kerstetter, A.E. and Miller, R.H. (2012). Isolation and Culture of Spinal Cord Astrocytes. *Methods in Molecular Biology*, 814, pp93-104

Khademullah, C.S., Aqrabawi, A.J., Place, K.M., Dargaei, Z., Liang, X., Pressey, J.C., Bedard, S., Yang, J.W., Garand, D., Keramidis, I., Gasecka, A., Côte, D., De Koninck, Y., Keith, J., Zinman, L., Robertson, J., Kim, J.C. and Woodin, M.A. (2020). Cortical interneuron-mediated inhibition delays the onset of amyotrophic lateral sclerosis. *Brain*, 143, pp800-810

Kiernan, M.C., Ziemann, U. and Eisen, A. (2019). Amyotrophic Lateral Sclerosis: Origins Traced to Impaired Balance Between Neural Excitation and Inhibition in the Neonatal Period. *Muscle & Nerve*, 60(3), pp232-235

Kim, R.B., Irvin, C.W., Tilva, K.R. and Mitchell, C.S. (2016). State of the field: An informatics-based systematic review of the SOD1-G93A amyotrophic lateral sclerosis transgenic mouse model. *Amyotrophic Lateral Sclerosis and Frontotemporal Degeneration*, 17(1-2), pp1-14

Kim, B.W., Ryu, J., Jeong, Y.E., Kim, J. and Martin, L.J. (2020). Human Motor Neurons With SOD1-G93A Mutation Generated From CRISPR/Cas9 Gene-Edited iPSCs Develop Pathological Features of Amyotrophic Lateral Sclerosis. *Frontiers in Cellular Neuroscience*, 14, pp1-16

Koeppen, J., Nguyen, A.Q., Nikolakopoulou, A.M., Garcia, M., Hanna, S., Woodruff, S., Figueroa, Z., Obenause, A. and Ethell, I.M. (2018). Functional Consequences of Synapse Remodelling Following Astrocyte-Specific Regulation of Ephrin-B1 in the Adult Hippocampus. *Journal of Neuroscience*, 38(25), pp5710-5726

Koerner, D.R. (1952). Amyotrophic lateral sclerosis on Guam: a clinical study and review of the literature. *Annals of Internal Medicine*, 37(6), pp1204-1220

Kucukdereli, H., Allen, N.J., Lee, A.T., Feng, A., Ozlu, M.I., Conatser, L.M., Chakraborty, C., Workman, G., Weaver, M., Sage, E.H., Barres, B.A. and Eroglu, C. (2011). *PNAS*, 108(32), pp440-449

Kumar, D.R., Aslinia, F., Yale, S.H. and Mazza, J.J. (2011). Jean-Martin Charcot: The Father of Neurology. *Clinical Medicine & Research*, 9(1), pp46-49

Kumar, V., Hasan, G.M. and Hassan, M.I. (2017). Unraveling the Role of RNA Mediated Toxicity of C9orf72 repeats in C9-FTD/ALS. *Frontiers in Neuroscience*, 11(711), pp1-10

Kuo, J.J., Schonewille, M., Siddique, T., Schults, A.N.A., Fu, R., Bär, P.R., Anelli, R., Heckman, C.J. and Kroese, A.B.A. (2004). Hyperexcitability of Cultured Spinal Motoneurons From Presynaptic ALS Mice. *Journal of Neurophysiology*, 91(1), pp571-575

Kuo, J.J., Siddique, T., Fu, R. and Heckman, C.J. (2005). Increased persistent Na^+ current and its effect on excitability in motoneurones cultured from mutant SOD1 mice. *Journal of Physiology*, 563(3), pp843-854

Lagier-Tourenne, C., Baughn, M., Rigo, F., Sun, S., Liu, P., Li, H.R., Jiang, J., Watt, A.T., Chun, S., Katz, M., Qiu, J., Sun, Y., Ying, S.C., Zhu, Q., Polymenidou, M., Drenner, K., Artates, J.W., McAlonis-Downes, M., Markmiller, S., Hutt, K.R., Pizzo, D.P., Cady, j., Harms, M.B., Baloh, R.H., Vandenberg, S.R., Yeo, G.W., Fu, X.D., Bennett, C.F., Cleveland, D.W. and Ravits, J. (2013). Targeted degradation of sense and antisense C9orf72 RNA foci as therapy for ALS and frontotemporal degeneration. *PNAS*, 110(47), pp1-10

Lamas, N.J., Johnson-Kerner, B., Roybon, L., Kim, Y.A., Garcia-Diaz, A., Wichterle, H. and Henderson, C.E. (2014). Neurotrophic Requirements of Human Motor Neurons Defined Using Amplified and Purified Stem Cell-Derived Cultures. *PLoS ONE*, 9(10), pp1-13

Lasiene, J. and Yamanaka, K. (2011). Glial Cells in Amyotrophic Lateral Sclerosis. *Neurology Research International*, 2011, pp1-7

Lavialle, M., Aumann, G., Anlauf, E., Pröls, F., Arpin, M. and Derouiche, A. (2011). Structural plasticity of perisynaptic astrocyte processes involves ezrin and metabotropic glutamate receptors. *PNAS*, 108(31), pp12915-12919

Lee, S. and Huang, E.J. (2017). Modeling ALS and FTD with iPSC-derived neurons. *Brain Research*, 1656, pp88-97

Lee, Y., Morrison, B.M., Li, Y., Lengacher, S., Farah, M.H., Hoffman, P.N., Liu, Y., Tsingalia, A., Jin, L., Zhnag, P.W., Pellerin, L., Magistretti, P.J. and Rothstein, J.D. (2012). Oligodendroglia metabolically support axons and contribute to neurodegeneration. *Nature*, 487(7408), pp443-448

Lehre, K.P. and Danbolt, N.C. (1998). The Number of Glutamate Transporter Subtype Molecules at Glutamatergic Synapses: Chemical and Stereological Quantification in Young Adult Rat Brain. *Journal of Neuroscience*¸18(21), pp8751-8757

Lehre, K.P. and Rusakov, D.A. (2002). Asymmetry of Glia near Central Synapses Favors Presynaptically Directed Glutamate Escape. *Biophysical Journal*, 83, pp125-134

Leroy, F., d'Incamps, B.L., Imhoff-Manuel, R.D. and Zytnicki, D. (2014). Early intrinsic hyperexcitability does not contribute to motoneuron degeneration in amyotrophic lateral sclerosis. *eLife*, 3, pp1-25

Liayw, J., Hoang, S., Choi, M., Eroglu, C., Choi, M., Sun, G.H., Percy, M., Wildman-Tobriner, B., Bliss, T., Guzman, R.G., Barres, B.A. and Steinberg, G.K. (2008). Thrombospondins 1 and 2 are necessary for synaptic plasticity and functional recovery after stroke. *Journal of Cerebral Blood Flow and Metabolism*, 28(10), pp1722-1732

Liddelow, S.A. and Barres, B.A. (2017). Reactive Astrocytes: Production, Function, and Therapeutic Potential. *Immunity*, 46(6), pp957-967

Lillo, P. and Hodges, J.R. (2009). Frontotemporal dementia and motor neurone disease: Overlapping clinic-pathological disorders. *Journal of Clinical Neuroscience*, 16(9). 1131-1135

Lin, C.L.G., Bristol, L.A., Jin, L., Dykes-Hoberg, M., Crawford, T., Clawson, L. and Rothstein, J.D. (1998). Aberrant RNA Processing in a Neurodegenerative Disease: the Cause for Absent EAAT2, a Glutamate Transporter, in Amyotrophic Lateral Sclerosis. *Neuron*, 20(3), pp589-602

Ling, S.C., Polymenidou, M. and Cleveland, D.W. (2013). Converging mechanisms in ALS and FTD: Disrupted RNA and protein homeostasis. *Neuron*, 79(3), pp416-438

Liu, W., Cui, Y., Wei, J., Sun, J., Zheng, L. and Xie, J. (2020). Gap junction-mediated cell-to-cell communication in oral development and oral disease: a concise review of research progress. *International Journal of Oral Science*, 12, pp1-9

Liu, Y., Pattamatta, A., Zu, T., Reid, T., Bardhi, O., Borchelt, D.R., Yachnis, A.T. and Ranum, L.P.W. (2016). C9orf72 BAC Mouse Model with Motor Deficits and Neurodegenerative Features of ALS/FTD. *Neuron*, 90(3), pp521-534

Liu, J. and Wang, F. (2017). Role of Neuroinflammation in Amyotrophic Lateral Sclerosis: Cellular Mechanisms and Therapeutic Implications. *Frontiers in Immunology*, 8(1006), pp1-12

Longinetti, E. and Fang, F. (2019). Epidemiology of amyotrophic lateral sclerosis: an update of recent literature. *Current Opinion in Neurology*, 32(5), pp771-776

Lopez-Gonzalez, R., Lu, Y., Gendron, T.F., Karydas, A., Tran, H., Yang, D., Petrucelli, L., Miller, B.L., Almedia, S. and Gao, F.B. (2016). Poly(GR) in C9ORF72-Related ALS/FTD Compromises Mitochondrial Function and Increases Oxidative Stress and DNA Damage in iPSC-Derived Motor Neurons. *Neuron*, 92(2), pp383-391

LoRusso, E., Hickman, J.J. and Guo, X. (2019). Ion channel dysfunction and altered motoneuron excitability in ALS. *Neurological Disorders and Epilepsy Journal*, 3(2), pp1-13

Lundström, Y., Lundström, P., Popova, S.N., Lindbolm, R.P.F. and Alafuzoff, I. (2019). Detection of Changes in Immunohistochemical Stains Caused by Postmortem Delay and Fixation Time. *Applied Immunohistochemistry and Molecular Morphology*, 3, pp238-245

Ma, X.R., Prudencio, M., Koike, Y., Vatsavayai, S.C., Kim, G., Harbinski, F., Briner, A., Rodriguez, C.M., Guo, C., Akiyama, T., Schmidt, H.B., Cummings, B.B., Wyatt, D.W., Kurulo, K., Miller, G., Mekhoubad, S., Sallee, N., Mekonnen, G., Ganser, L., Rubien, J.D., Jansen-West, K., Cook, C.N., Pickles, S., Oskarsson, B., Gradd-Radford, N.R., Boeve, B.F., Knopman, D.S., Petersen, R.C., Dickson, D.W., Shorter, J., Myong, S., Green, E.M., Seeley, W.W., Petrucelli, L. and Gitler, A.D. (2022). TDP-43 represses cryptic inclusion in the FRD-ALS gene UNC1A. *Nature*, 603, pp124-130

Mackenzie, I.R.A., Bigio, E.H., Ince, P.G., Geser, F., Neumann, M., Cairns, N.J., Kwong, L.K., Forman, M.S., Ravits, J., Stewart, H., Eisen, A., McClusky, L., Kretzschmar, H.A., monoranu, C.M., Highly, J.R., Kirby, J., Siddique, T., Shaw, P.J., Lee, V.M.Y., Trojanowski, J.Q. (2007). Pathological TDP-43 Distinguishes Sporadic Amyotrophic Lateral Sclerosis from Amyotrophic Lateral Sclerosis with SOD1 Mutations. *Annals of Neurology*, 61(5), pp427-434

Mackenzie, I.R.A. and Rademakers, R. (2010). The role of TDP-43 in amyotrophic lateral sclerosis and frontotemporal dementia. *Current Opinion in Neurology*, 21(6), pp693-700

Magrané, J., Cortez, C., Gan, W.B. and Manfredi, G. (2014). Abnormal mitochondrial transport and morphology are common pathological denominators in SOD1 and TDP43 ALS mouse models. *Human Molecular Genetics*, 23(6), pp1413-1424

Martin, L.J. and Chang, Q. (2012). Inhibitory Synaptic Regulation of Motoneurons: A New Target of Disease Mechanisms in Amyotrophic Lateral Sclerosis. *Molecular Neurobiology*, 45(1), pp30-42

Martínez-Silva, M.D.L., Imhoff-Manuel, R.D., Sharma, A., Heckman, C.J., Shneider, N.A., Roselli, F., Zytnicki, D. and Maniel, M. (2018). Hypoexcitability precedes denervation in the large fast-contracting motor units in two unrelated mouse models of ALS. *eLife*, 7, pp1-26

Matejuk, A. and Ransohoff, R.M. (2020). Crosstalk Between Astrocytes and Microglia: An Overview. *Frontiers in Immunology*, 11, pp1-11

Mathis, S., Goizet, C., Soulages, A., Vallat, J.M and Le Masson, G. (2019). Genetics of amyotrophic lateral sclerosis: A review. *Journal of the Neurological Sciences*, 399, pp217-226

Matos, M., Bosson, A., Riebe, I., Reynell, C., Vallée, Laplante, I., Panatier, A., Robitaille, A., Lacaille, J.C. (2018). Astrocytes detect and upregulate transmission at inhibitory synapses of somatostatin interneurons onto pyramidal cells. *Nature Communications*, 9(1), pp1-14

Matsumoto, S., Goto, S., Kusaka, H., Ito, H. and Imai, T. (1996). Synaptic pathology of spinal anterior horn cells in amyotrophic lateral sclerosis: an immunohistochemical study. *Acta Neuropathologica*, 91(6), pp603-607

Mattson, M.P. (2019). *Stress: Physiology, Biochemistry, and Pathology, Chapter 11: Excitotoxicity.* Elsevier, London UK

Maury, Y., Côme, J., Piskorowski, R.A., Salah-Mohellibi, N, Chevaleyre, V., Peschanski, M., Martinant, C. Nedelec, S. (2015). Combinatorial analysis of developmental cues efficiently converts human pluripotent stem cells into multiple neuronal subtypes. *Nature Biotechnology*, 33(1), pp89-96

McQuin, C., Goodman, A., Chernyshev, V., Kamentsky, L., Cimini, B.A., Karhohs, K.W., Doan, M., Ding, L., Rafelski, S.M., Thirstrup, D., Wiegraebe, W., Singh, S., Becker, T., Caicedo, J.C. and Carpenter, A.E. (2018). Cell Profiler 3.0: Next-generation image processing for biology. *PLoS Biology*, 16(7), pp1-17

Medinas, D.B., Valenzuela, V. and Hetz, C. (2017). Proteostasis disturbance in amyotrophic lateral sclerosis. *Human Molecular Genetics*, 26(2), pp91-104

Mehta, A.R., Gregory, J.M., Dando, O., Carter, R.N., Burr, K., Nanda, J., Story, D., McDade, K., Smith, C., Morton, N.M., Mahad, D.J., Hardingham, G.E., Chandran, S. and Selvaraj, B.T. (2021). Mitochondrial bioenergetic deficits in C9orf72 amyotrophic lateral sclerosis motor neurons cause dysfunctional axonal homeostasis. *Acta Neuropathologica*, 141, pp257-279

Mejzini, R., Flynn, L.L., Pitout, I.L., Fletcher, S., Wilton, S.D. and Akkari, P.A. (2019). ALS Genetics, Mechanisms and Therapeutics: Where Are We Now? *Frontiers in Neuroscience*, 13(1310), pp1-27

Melone, M., Bellesi, M. and Conti, F. (2009). Synaptic Localization of GLT-1a in the Rat Somatic Sensory Cotex. *Glia*, 57(1), pp108-117

Michalski, D., Keck, A.L., Grosche, J., Martens, H. and Härtig, W. (2018). Immunosignals of Oligodendrocyte Masrkers and Myeline-Associated Proteins Are Critically Affected after Experimental Stroke in Wild-Type and Alzheimer Modelling Mice of Different Ages. *Frontiers in Cellular Neuroscience*, 12, pp1-14

Michalski, J.P. and Kothary, R. (2015). Oligodendrocytes in nutshell. *Frontiers in Cellular Neuroscience*, 9(340), pp1-11

Mikhailova, M.M., Bolshakov, A.P., Chaban, E.A., Paltsev, M.A. and Panteleyev, A.A. (2019). Primary culture of mouse embryonic spinal cord neurons: cell composition and suitability for axonal regeneration studies. *International Journal of Neuroscience*, 129(9), pp762-769

Millecamps, S. and Julien, J.P. (2013). Axonal transport deficits and neurodegenerative disease. *Nature Reviews Neuroscience*, 14(3), pp161-176

Milligan, C. and Gifondorwa, D. (2011). Isolation and Culture of Postnatal Spinal Motoneurons. *Molecular Neurodegeneration*, 6(1), pp77-85

Mirza, F.J. and Zahid, S. (2018). The Role of Synapsins in Neurological Disorders. *Neuroscience Bulletin*, 34(2), pp349-358

Mòdol, L., Mancuso, R., Alé, A., Francos-Quijorna, F. and Navarro, X. (2014). Differential effects on KCC2 expression and spasticity of ALS and traumatic injuries to motoneurons. *Frontiers in Cellular Neuroscience*, 8, pp1-11

Moore, N.J., Bhumbra, G.S., Foster, J.D. and Beato, M. (2015). Synaptic Connectivity between Renshaw Cells and Motoneurons in the Recurrent Inhibitory Circuit of the Spinal Cord. *Journal of Neuroscience*, 35(40), pp13663-13686

Mordes, D.A., Morrison , B.M., Ament, X.H., Cantrell, C., Mok, J., Eggan, P., Xue, C., Wang, J.Y., Eggan, K. and Rothstein, J.D. (2020). Absence of Survival and Motor Deficits in 500 Repeat C9orf72 BAC Mice. *Neuron*, 108(4), pp775-783

Morgan, S. and Orrell, R.W. (2016). Pathogenesis of amyotrophic lateral sclerosis. *British Medical Bulletin*, 119, pp87-97

Mori, K., Weng, S.M., Arzberger, T., May, S., Rentzsch, K., Kremmer, E., Schmid, B., Kretzschmar, H.A., Cruts, M., Van Broeckhoven, C., Haass, C. and Edbauer, D. (2013). The C9orf72 GGGGCC Repeat Is Translated in Aggregating Dipeptide-Repeat Proteins in FTLD/ALS. *Science*, 339(6125), pp1335-1338

Mórotz, G.M., De Vos, K.J., Vagnoni, A., Ackerley, S., Shaw, C.E. and Miller, C.C.J. (2012). Amyotrophic lateral sclerosis-associated mutant VAPBP56S perturbs calcium homeostasis to disrupt axonal transport of mitochondria. *Human Molecular Genetics*, 21(9), pp1979-1988

Murphy, N.A., Arthur, K.C., Tienari, P.J., Houlden, H., Chiò, A and Traynor, B.J. (2017). Age-related penetrance of the C9orf72 repeat expansion. *Scientific Reports*, 7(1), pp1-7

Nagai, M., Re, D.B., Nagata, T., Chalazonitis, A., Jessell, T.M., Wichterle, H. and Przedborski, S. (2007). Astrocytes expressing ALS-linked mutated SOD1 release factors selectively toxic to motor neurons. *Nature Neuroscience*, 10(5), pp615-622

Nahar, L., Delacroix, B.M. and Nam, H.W. (2021). The Role of Parvalbumin Interneurons in Neurotransmitter Balance and Neurological Disease. *Frontiers in Psychiatry*, 12, pp1-14

Nelson, S.B. and Valakh, V. (2015). Excitatory / Inhibitory balance and circuit homeostasis in Autism Spectrum Disorders. *Neuron*, 87(4), pp684-698

Ng, S.K., Higashimori, H., Tolman, M. and Yang, Y. (2015). Suppression of adenosine 2a receptor ($A_{2a}R$)-mediated adenosine signaling improves disease phenotypes in a mouse model of amyotrophic lateral sclerosis. *Experimental Neurology*, 267, pp115-122

Nguyen, H.P., Broeckhoven, C.V. and van der Lee, J. (2018). ALS Genes in the Genomic Era and their Implications for FTD. *Trends in Genetics*, 34(6), pp404-423

Nguyen, A.Q., Koeppen, J., Woodruff, S., Mina, K., Figueroa, Z. and Ethell, I.M. (2020a). Astrocyte Ephrin-B1 Controls Synapse Formation in the Hippocampus During Learning and Memory. *Frontiers in Synaptic Neuroscience*, 12, pp1-18

Nguyen, L., Laboissonniere, L.A., Guo, S., Pilotto, F., Scheidegger, O., Oestmann, A., Hammond, J.W., Li, H., Hyysalo, A., Peltola, R., Pattamatta, A., Zu, T., Voutilainen, M.J., Gelbard, H.A., Saxena, S. and Ranum, L.P.W. (2020). Survival and Motor Phenotypes in FVB c9-500 ALS/FTS BAC Transgenic Mice Reproduced by Multiple Labs. *Neuron*, 108(4), pp784-796

Nguyen, A.Q., Sutley, S., Koeppen, J., Mina, K., Woodruff, S., Hanna, S., Vengala, A., Hickmott, P.W., Obenaus, A. and Ethell, I.M. (2020b). Astrocytic Ephrin-B1 Controls Excitatory-Inhibitory Balance in Developing Hippocampus. *Journal of Neuroscience*, 40(36), pp6854-6871

Octeau, J.C., Chai, H., Jiang, R., Bonanno, S.L., Martin, K.C. and Khakh, B.S. (2018). An Optical Neuron-Astrocyte Proximity Assay at Synaptic Distance Scales. *Neuron*, 98(1), pp49-66

Ota, Y., Zanetti, A.T. and Hallock, R.M. (2013). The Role of Astrocytes in the Regulation of Synaptic Plasticity and Memory Function. *Neural Plasticity*, 2013, pp1-11

Pajarillo, E., Rizor, A., Lee, J., Aschner, M. and Lee, E. (2019). The role of astrocytic glutamate transporters GLT-1 and GLAST in neurological disorders: Potential targets for neurotherapeutics. *Neuropharmacology*, 161, pp1-29

Pannasch, U., Derangeon, M., Chever, O. and Rouach, N. (2012). Astroglial gap junctions shape neuronal network activity. *Communicative and Integrative Biology*, 5(3), pp248-254

Paolicelli, R.C., Jawaid, A., Henstridge, C.M., Valeri, A., Merlini, M., Robinson, J.L., Lee, E.B., Rose, J., Appel, S., Lee, V.M.Y., Trojanowski, J.Q., Spires-Jones, T., Schulz, P.E. and Rajendran, L. (2017). TDP-43 Depletion in Microglia Promotes Amyloid Clearance but Also Induces Synapse Loss. *Neuron*, 95(2), pp208-308

Paré, B., Lehmann, M., Beaudin, M., Nordström, U., Saikali, S., Julien, J.P., Gilthorpe, J.D., Marklund, S.L., Cashman, N.R., Andersen, P.M., Forsberg, K., Dupré, N., Gould, P., Brännstroöm and Gros-Louis, F. (2018). Misfolded SOD1 pathology in sporadic Amyotrophic Lateral Sclerosis. *Scientific Reports*, 8(14223), pp1-13

Petitjean, H., Pawlowski, S.A., Fraine, S.L., Sharif, B., Hamad, D., Fatima, T., Berg, J., Brown, C.M., Jan, L.Y., Ribeiro-da-Silvaq, A., Braz, J.M., Basbaum, A.I., Sharif-Naeini, R. (2015). Dorsal Horn Parvalbumin Neurons Are Gate-Keepers of Touch-Evoked Pain after Nerve Injury. *Cell Reports*, 13(6), pp1246-1257

Pfeiffer, B.E. and Huber, K.M. (2009). The State of Synapses in Fragile X Syndrome. *Neuroscientist*, 15(5), pp549-567

Pfohl, S.R., Halicek, M.T. and Mitchell, C.S. (2015). Characterization of the Contribution of Genetic Backgroun and Gender to Disease Progression in the SOD1 G93A Mouse Model of Amyotrophic Lateral Sclerosis: A Meta-Analysis. *Journal of Neuromuscular Diseases*, 2(2), pp137-150

Pfrieger, F.W. and Barres, B.A. (1997). Synaptic Efficacy Enhanced by Glial Cells in Vitro. *Science*, 277(5332), pp1684-1687

Philips, T. and Robberecht, W. (2011). Neuroinflammation in amyotrophic lateral sclerosis: role of glial activation in motor neuron disease. *Lancet Neurology*, 10, pp253-263

Philips, T. and Rothstein, J.D. (2015). Rodent Models of Amyotrophic Lateral Sclerosis. *Current Protocols in Pharmacology*, 69, 1-21

Picher-Martel, V., Valdmanis, P.N., Gould, P.V., Julien, J.P. and Dupré, N. (2016). From animal models to human disease: a genetic approach for personalized medicine in ALS. *Acta Neuropathologica Communications*, 4, pp1-29

Polymenidou, M., Lagier-Tourenne, C., Hutt, K.R., Huelga, S.C., Moran, J., Liang, T.Y., Ling, S.C., Sun, E., Wancewicz, E., Mazur, C., Kordasiewicz, H., Sedaghat, Y., Donohue, J.P., Shinue, L., Bennett, C.F., Yeo, G.W. and Cleveland, D.W. (2011). Long pre-mRNA depletion and RNA missplicing contribute to neuronal vulnerability from loss of TDP-43. *Nature Neuroscience*, 14(4), pp459-468

Purves, D., Augustine, G.J., Fitzpatrick, D., Hall, W.C., LaMantia, A.S., McNamara, J.O. and Williams, S.M. (2011). *Neuroscience 3rd Ed.* Sinauer Associates, Massachusetts USA

Qian, K., Huang, H., Peterson, A., Hu, B., Maragakis, N.J., Ming, G.L., Chen, H. and Zhang, S.C. (2017). Sporadic ALS Astrocytes Induce Neuronal Degeneration In Vivo. *Stem Cell Reports*, 8(4), pp843-855

Quinlan, K.A., Schuster, J.E., Fu, R., Siddique, T. and Heckman, C.J. (2011). Altered postnatal maturation of electrical properties in spinal motoneurons in a mouse model of amyotrophic lateral sclerosis. *Journal of Physiology*, 589(9), pp2245-2260

Rakowicz, W.P., Staples, C.S., Milbrandt, J., Brunstrom, J.E. and Johnson Jr., E.M. (2002). Glial Cell Line-Derived Neurotrophic Factor Promotes the Survival of Early Postnatal Spinal Motor Neurons in the Lateral and Medial Motor Columns in Slice Culture. *Journal of Neuroscience*, 22(10), pp3953-3962

Ramírez-Jarquín, U.N., Rojas, F., van Zundert, B. and Tapia, R. (2017). Chronic infusion of $SOD1^{G93A}$ astrocyte-secreted factors induces spinal motoneuron degeneration and neuromuscular dysfunction in healthy rats. *Journal Of Cellular Physiology*, 232(10), pp2610-2615

Ransom, B.R., Neale, E., Henkart, M., Bullock, P.N. and Nelson, P.G. (1977). Mouse Spinal Cord in Cell Culture. I. Morphology and Intrinsic Neuronal Electrophysiological Properties. *Journal of Neurophysiology*, 40(5), pp1132-1150

Raynor, E.M. and Shefner, J.M. (1994). Recurrent inhibition is decreased in patients with amyotrophic lateral sclerosis. *Neurology*¸ 44(11), pp2148-2153

Renton, A.E., Chiò, A.and Traynor, B.J. (2014). State of play in amyotrophic lateral sclerosis genetics. *Nature Neuroscience*, 17(1), pp17-23

Retamal, M.A., Alcayaga, J., Verdugo, C.A., Bultynck, G., Leybaert, L., Sáez, P.J., Fernández, R., León, L.E. and Sáez, J.C. (2014). Opening of pannexin- and connexin-based

channels increases the excitability of nodose ganglion sensory neurons. *Frontiers in Cellular Neuroscience*, 8, pp1-12

Reth, M. (2013). Matching cellular dimensions with molecular sizes. *Nature Immunology*, 14(8), pp765-767

Risher, W.C. and Eroglu, C. (2012). Thrombospondins as key regulators of synaptogenesis in the central nervous system. *Matrix Biology*, 31(3), pp170-177

Risher, W.C. and Eroglu, C. (2020). *Synapse Development and Maturation*. Elsevier, London

Risher, W.C., Patel, S., Kim, I.H., Uezu, A., Bhagat, S., Wilton, D.K., Pilaz, L.J., Alvarado, J.S., Calhan, O.Y., Silver, D.L., Stevens, B., Calakos, N., Soderling, S.H. and Eroglu, C. (2014). Astrocytes refine cortical connectivity at dendritic spines. *eLife*, 3, pp1-24

Rosen, D.R., Siddique, T., Patterson, D., Figlewicz, D.A., Sapp, P., Hentati, A., Donaldson, D., Goto, J., O'Regan, J.P., Deng, H.X., Rahmani, Z., Krizus, A., McKenna-Yasek, D., Cayabyab, A., Gatson, S.M., Berger, R., Tanzi, R.E., Halperin, J.J., Herzfeldt, B., Van den Bergh, R., Hung, W.Y., Bird, T., Deng, G., Mulder, D.W., Smyth, C., Laing, N.G., Soriano, E., Pericak-Vance, M.A., Haines, J., Rouleau, G.A., Guseella, J.S., Horvitz, H.R. and Brown, R.H. Jr. (1993). Mutations in Cu/Zn superoxide dismutase gene are associated with familial amyotrophic lateral sclerosis. *Nature*, 362, pp59-62

Rosenblum, L.T. and Trotti, D. (2017). EAAT2 and the molecular signature of amyotrophic lateral sclerosis. *Advances in Neurobiology*, 16, pp117-136

Rothstein, J.D., Jin, L., Dykes-Hoberg, M. and Kuncl, R.W. (1993). Chronic inhibition of glutamate uptake produces a model of slow neurotoxicity. *PNAS*, 90(14), pp6591-6595

Rotherstein, J.D., Dykes-Hoberg, M., Pardo, C.A., Bristol, L.A., Jin, L., Kuncl, R.W., Kanai, Y., Hediger, M.A., Wang, Y., Schielke, J.P. and Welty, D.F. (1996). Knockout of Glutamate Transporters Reveals a Major Role for Astroglial Transport in Excitotoxicity and Clearance of Glutamate. *Neuron*, 16(3), pp675-686

Rothstein, J.D., Patel, S., Regan, M.R., Haenggell, C., Huang, Y.H., Bergles, D.E., Jin, L., Dykes-Hoberg, M., Vidensky, S., Chung, D.S., Toan, S.V., Bruijn, L.I., Su, Z.Z., Gupta, P. and Fisher, P.B. (2005). B-Lactam antibiotics offer neuroprotection by increasing glutamate transporter expression. *Nature*, 433(7071), pp73-77

Rothstein, J.D., Van Kammen, M., Levey, A.I., Martin, L.J. and Kuncl, R.W. (1995). Selective Loss of Glial Glutamate Transporter GLT-1 in Amyotrophic Lateral Sclerosis. *Annals of Neurology*, 38(1), pp73-84

Ruegsegger, C. and Saxena, S. (2016). Proteostasis impairment in ALS. *Brain Research*, 1648, pp571-579

Saba, L., Viscomi, M.T., Caioli, S., Pignataro, A., Bisicchia, E., Pieri, M., Molinari, M., Ammassari-Teule, M. and Zona, C. (2015). Altered Functionality, Morphology and Vesicular Glutamate Transporter expression of Cortical Motor Neurons from Presymptomatic Mouse Model of Amyotrophic Lateral Sclerosis. *Cerebral Cortex*, 26(4), pp1512-1528

Sabatelli, M., Madia, F., Conte, A., Luigetti, M., Zollino, M., Mancuso, I., Lo Monaco, M., Lippi, G. and Tonali, P. (2008). Natural history of young-adult amyotrophic lateral sclerosis. *Neurology*, 71(12), pp876-881

Saberi, S., Stauffer, J.E., Schulte, D.J. and Ravits, J. (2015). Neuropathology of amyotrophic lateral sclerosis and its variants. *Neurologic Clinics*, 33(4), pp855-876

Saito, K., Kakizaki, T., Hayashi, R., Nishimaru, H., Furukawa, T., Nakazato, Y., Takamori, S., Ebihara, S., Uematsu, M., Mishina, M., Miyazaki, J.I., Yokoyama, M., Konishi, S., Inoue, K., Fukuda, A., Fukumoto, M., Nakamura, K., Obata, K. and Yanagawa, Y. (2010). The physiological roles of vesicular GABA transporter during embryonic development: a study using knockout mice. *Molecular Brain*, 3, pp1-13

Sasaki, S. and Iwata, M. (1995). Synaptic loss in the proximal axon of anterior horn neurons in motor neuron disease. *Acta Neuropathologica*, 90(2), pp170-175

Sasaki, S., Maruyama, S., Yamane, K., Sakuma, H. and Takeishi, M. (1990). Ultrastructure of swollen proximal axons of anterior horn neurons in motor neuron disease. *Journal of the Neurological Sciences*, 97(2-3), pp233-240

Sasaki, S. and Maruyuma, S. (1994). Decreased synaptophysin immunoreactivity of the anterior horns in motor neuron disease. *Acta Neuropathologica*, 87(2), pp125-128

Schindelin, J., Arganda-Carreras, I., Frise, E., Kaynig, V., Longair, M., Pietzsch, T., Preibisch, S., Rueden, C., Saalfeld, S., Schmid, B., Tinevez, J.Y., White, D.J., Hartenstein, V., Eliceiri, K., Tomancak, P. and Cardona, A. (2012). Fiji: an open-source platform for biological-image analysis. *Nature Methods*, 9, pp676-682

Schulte, J.T., Wierenga, C.J. and Bruining, H. (2018). Chloride transporters and GABA polarity in developmental, neurological and psychiatric conditions. *Neuroscience and Biobehavioural Reviews*, 90, pp250-271

Schütz, B. (2005). Imbalanced excitatory to inhibitory synaptic input precedes motor neuron degeneration in an animal model of amyotrophic lateral sclerosis. *Neurobiology of Disease*, 20(1), pp131-140

Selvaraj, B.T., Livesey, M.R., Zhao, C., Gregory, J.M., James, O.T., Cleary, E.M., Chouhan, A.K., Gane, A.B., Perkins, E.M., dando, O., Lillico, S.G., Lee, Y.B., Nishimura, A.l., Poreci, U., Thankmony, S., Pray, M., Vasistha, N.A., Magnani, S., Borooah, S., Burr, K., Story, D., McCampbell, A., Shaw, C.E., Kind, P.C., Aitman, T.J., Whitelaw, C.B.A., Wilmut, I., Smith, C., Miles, G.B., Hardingham, G.E., Wyllie, D.J.A. and Chandran, S. (2018). C9ORF72 repeat expansion causes vulnerability of motor neurons to Ca^{2+}-permeable AMPA receptor-mediated excitotoxicity. *Nature Communications*, 9, pp1-14

Shan, X., Vocadlo, D. and Krieger, C. (2009). Mislocalization of TDP-43 in G93A mutant SOD1 transgenic mouse models of ALS. *Neuroscience Letters*, 458(2), pp70-74

Sharples, S.A. and Miles, G.B. (2021). Maturation of persistent and hyperpolarization-activated inward currents shapes the differential activation of motoneuron subtypes during postnatal development. *eLife*, 10, pp1-30

Shellikeri, S., Karthikeyan, V., Martino, R., Black, S.E., Zinman, L., Keith, J. and Yunosova, Y. (2017). *Neuroscience & Biobehavioural Reviews*, 75, pp378-392

Shen, Y., Qin, H., Chen, J., Mou, L., He, Y., Yan, Y., Zhou, H., Lv, Y., Chen, Z., Wang, J. and Zhou, Y.D. (2016). Postnatal activation of TLR4 in astrocytes promotes excitatory synaptogenesis in hippocampal neurons. *Journal of Cell Biology*, 5, pp719-734

Smith, E.F., Shaw, P.J. and De Vos, K.J. (2019). The role of mitochondria in amyotrophic lateral sclerosis. *Neuroscience Letters*, 710, pp1-17

Sofroniew, M.V. (2015). Astrogliosis. *Cold Spring Harbor Perspectives in Biology*, 7(2), pp1-16

Sofroniew, M.V. and Vinters, H.V. (2010). Astrocytes: biology and pathology. *Acta Neuropathologica*, 119(1), pp7-35

Sommer, D., Rajkumar, S., Seidel, M., Aly, A., Ludolph, A., Ho, R., Boeckers, T.M. and Catanese, A. (2022). Aging-Dependent Altered Transcriptional Programs Underlie Activity Impairments in Human C9orf72-Mutant Motor Neurons. *Frontiers in Molecular Neuroscience*, 15, pp1-17

Špaček, J. (1985). Three-dimensional analysis of dendritic spines. III Glial sheath. *Anatomy and Embryology*, 171(2), pp245-252

Spiegel, J., Adhikari, S. and Balasubramanian, S. (2020). The Structure and Function of DNA G-Quadruplexes. *Trends in Chemistry*, 2(2), pp123-136

Stenovec, M., Kreft, M., Grilc, S., Pangršič and Zorec, R. (2008). EAAT2 density at the astrocyte plasma membrane and Ca^{2+}-regulated exocytosis. *Molecular Membrane Biology*, 25(3), pp203-215

Strong, M.J., Volkening, K., Hammond, R., Yang, W., Strong, W., Leystra-Lantz, C. and Shoesmith, C. (2007). TDP43 is a human low molecular weight neurofilament (hNFL) mRNA-binding protein. *Molecular and Cellular Neuroscience*, 35(2), pp320-327

Strong, M.J. (2010). The evidence for altered RNA metabolism in amyotrophic lateral sclerosis. *Journal of the Neurological Sciences*, 288(1-2), pp1-12

Suk, T.R. and Rousseaux, M.W.C. (2020). The role of TDP-43 mislocalization in amyotrophic lateral sclerosis. *Molecular Degeneration*, 15(1), pp1-16

Sullivan, K.F. (1988). Structure and Utilization of Tubulin Isotypes. *Annual Review of Cellular Biology*, 4, pp687-716

Sunico, C.R., Domínguez, G., García-Verdugo, J.M., Osta, R., Montero, F., and Moreno-glatzLópez, B. (2011). Reduction in the Motoneuron Inhibitory / Excitatory Synaptic Ratio in

an Early-Symptomatic Mouse Model of Amyotrophic Lateral Sclerosis. *Brain Pathology*, 21(1), pp1-15

Sun, D. and Jakobs, T.C. (2012). Structural Remodelling of Astrocytes in the Injured CNS. *Neuroscientist*, 28(6), pp567-588

Swinnen, B. and Robberecht, W. (2014). The phenotypic variability of amyotrophic lateral sclerosis. *Nature Reviews Neurology*, 10(11), pp661-670

Tabata, H. (2015). Diverse subtypes of astrocytes and their development during corticogenesis. *Frontiers in Neuroscience*, 9, pp1-7

Tan, W., Su, P.Y.P., Leff, J., Gao, X., Chen, J., Guan, A.K., Kalyanasundaram, G., Ma, A. and Guan, Z. (2022). Distinct phases of adult microglia proliferation: a *Myc*-mediated early phase and a *Tnfaip3*-medaited late phase. *Cell Discovery*, 8, pp1-18

Tang, Y. and Le, W. (2016). Differential Roles of M1 and M2 Microglia in Neurodegenerative Diseases. *Molecular Neurobiology*, 53(2), pp1181-1194

Tani, H., Dulla, C.G., Farzampour, Z., Taylor-Weiner, A., Huguenard, J.R. and Reimer, R.J. (2014). A Local Glutmate-Glutamine Cycle Sustains Synaptic Excitatory Transmitter Release. *Neuron*, 81(4), pp888-900

Taylor, J.P., Brown Jr., R.H. and Cleveland, D.W. (2016). Decoding ALS: From Genes to Mechanism. *Nature*, 539(7628), pp197-206

Teuscher, A.C. and Ewald, C.Y. (2018). Overcoming Autofluorescence to Assess GFP Expression During Normal Physiology and Aging in *Caenorhabditis elegans*. *Bio-Protocol*, 8(14), pp1-23

Todd, A.J., Polgár, H.E., Nagy, G.G., Mackie, M., Ottersen, O.P. and Maxwell, D.J. (2003). The expression of vesicular glutamate transporters VGLUT1 and VGLUT2 in neurochemically defined axonal populations in the rat spinal cord with emphasis on the dorsal horn. *European Journal of Neuroscience*, 17(1), pp13-27

Trias, E., Barbeito, L. and Yamanaka, K. (2018). Phenotypic heterogeneity of astrocytes in motor neuron disease. *Clinical and Experimental Neuroimmunology*, 8, pp225-234

Tsang, Y.M., Chiong, F., Kuznetsov, D., Kasarskis, E. and Geula, C. (2000). Motor neurons are rich in non-phosphorylated neurofilaments: cross-species comparison and alterations in ALS. *Brain Research*, 861, pp45-58

Turner, M.R., Al-Chalabi, A., Chio, A., Hardiman, O., Kiernan, M.C., Rohrer, J.D., Rowe, J., Seeley, W. and Talbot, K. (2017). Genetic screening in sporadic ALS and FTD. *Journal of Neurology, Neurosurgery and Psychiatry*, 88(12), pp1042-1044

Tyagarajan, S.K. and Fritschy, J.M. (2014). Gephyrin: a master regulator of neuronal function. *Nature Reviews Neuroscience*, 15(3), pp141-156

Ullian, E.M., Sapperstein, S.K., Christopherson, K.S. and Barres, B.A. (1997). Control of Synapse Number by Glia. *Science*, 291(5504), pp657-661

Umoh, M.E., Fournier, C., Li, Y., Polak, M., Shaw, L., Landers, J.E., Hu, W., Gearing, M. and Glass, J.D. (2016). Comparative analysis of C9orf72 and sporadic disease in an ALS clinic population. *Neurology*, 87(10), pp1024-1030

Uwechue, N.M., Marx, M.C., Chevy, Q. and Billups, B. (2012). Activation of glutamate transport evokes rapid glutamine release from perisynaptic astrocytes. *Journal of Physiology*, 590(10), pp2317-2331

Valori, C.F., Brambilla, L., Martorana, F. and Rossi, D. (2014). The multifaceted role of glial cells in amyotrophic lateral sclerosis. *Cellular and Molecular Life Sciences*, 71(2), pp287-297

Vande Velde, C., McDonald, K.K., Boukhedimi, Y., McAlonis-Downes, M., Lobsiger, C.S., Hadj, S.B., Zandona, A., Julien, J.P., Shah, S.B., Cleveland, D.W. (2011). Misfolded SOD1 Associated with Motor Neuron Mitochondria Alters Mitochondrial Shape and Distribution Prior to Clinical Onset. *PLoS ONE*, 6(7), pp1-11

Van Den Bosch, L., Van Damme, P., Bogaert, E. and Robberecht, W. (2005). The role of excitotoxicity in the pathogenesis of amyotrophic lateral sclerosis. *Biochimica et Biophysica Acta*, 1762, pp1068-1082

Van Zundert, B., Peuscher, M.H., Hynynen, M., Chen, A., Neve, R.l., Brown Jr, R.H., Constantine-Paton, M. and Bellingham, M.C. (2008). Neonatal Neuronal Circuitry Shows Hyperexcitable Disturbance in a Mouse Model of the Adult-Onset Neurodegenerative Disease Amyotrophic Lateral Sclerosis. *Journal of Neuroscience*, 28(43), pp10864-10874

Vasile, F., Dossi, E. and Rouach, N. (2017). Human astrocytes: structure and functions in the healthy brain. *Brain Structure and Function*, 222(5), pp2017-2029

Ventura, R. and Harris, K.M. (1999). Three-Dimensional Relationships between Hippocampal Synapses and Astrocytes. *Journal of Neuroscience*, 19(16), pp6897-6909

Waldvogel, H.J., Curtis, M.A., Baer, K., Rees, M.I. and Faull, R.L.M. (2007). Immunohistochemical staining of *post-mortem* adult human brain sections. *Nature Protocols*, 1(6), pp2719-2732

Walls, A.B., Nilsen, L.H., Eyjolfsson, E.M., Vestergaard, H.T., Hansen, S.L., Schousboe, A., Sonnewald, U. and Waagepetersen, H.S. (2010). GAD65 is essential for synthesis of GABA destined for tonic inhibition regulating epileptiform activity. *Journal of Neurochemistry*, 115(6), pp1398-1408

Wang, P., Deng, J., Dong, J., Liu, J., Bigio, E.H., Mesulam, M., Wang, T., Sun, L., Wang, L., Lee, A.Y.L., McGee, W.A., Chen, X., Fushimi, K., Zhu, L. and Wu., J.Y. (2019). TDP-43 induces mitochondrial damage and activates the mitochondrial unfolded protein response. *PLoS Genetics*, 15(5), pp1-32

Wang, D.D. and Kriegstein, A.R. (2009). Defining the role of GABA in cortical development. *Journal of Physiology*, 587(9), pp1873-1879

Wang, W., Wang, L., Lu, J., Siedlak, S.L., Fujioka, H., Liang, J., Jiang, S., Ma, X., Jiang, Z., da Rocha, E.L., Sheng, M., Choi, H., Lerou, P.H. and Wang, X. (2016). The inhibition of TDP-43 mitochondrial localization blocks its neuronal toxicity. *Nature Medicine*, 22(8), pp869-878

Watson, C., Paxinos, G. and Kayalioglu, G. (2009). *The Spinal Cord, 1st Ed.* Elsevier, London

Weber, E.D. and Stelzner, D.J. (1980). Synaptogenesis in the Intermediate Gray Region of the Lumbar Spinal Cord in the Postnatal Rat. *Brain Research*¸185, pp17-37

Webster, C.O., Smith, E.F., Bauer, C.S., Moller, A., Hautbergue, G.M., Ferraiuolo, L., Myszczynska, M.A., Higginbottom, A., Walsh, M.J., Whitworth, A.J., Kaspar, B.K., Meyer, K., Shaw, P.J., Grierson, A.J. and De Vos, K.J. (2016). The C9orf72 protein interacts with Rab1a and the ULK1 complex to regulate initiation of autophagy. *The EMBO Journal*, 35(15), pp1656-1676

Webster, C.P., Smith, E.F., Shaw, P.J. and De Vos, K.J. (2017). Protein Homeostasis in Amyotrophic Lateral Sclerosis: Therapeutic Opportunities? *Frontiers in Molecular Neuroscience*, 10(123), pp1-22

Wegel, E., Göhler, A., Lagerholm, B.C., Wainman, A., Uphoff, S., Kaufmann, R. and Dobbie, I.M. (2016). Imaging cellular structures in super-resolution with SIM, STED and Localisation Microscopy: A practical comparison. *Scientific Reports*, 6, pp1-13

Varini, K., Benzaria, A., Taïeb, N., Di Scala, C., Azmi, A., Graoudi, S. and Maresca, M. (2012). Mislocalization of the excitatory amino-acid transports (EAATs) in human astrocytoma and non-astrocytoma cancer cells: effect of the cell confluence. *Journal of Biomedical Sciences*, 19, pp1-11

Vicidomini, G., Hernández, I.C., d;Amora, M., Zanacchi, F.C., Bianchini, P. and Disapro, A. (2014). Gated CW-STED microscopy: A versatile tool for biological nanometer scale investigation. *Methods*, 66(2), pp124-130

Wiedemann, F.R., Manfredi, G., Mawrin, C., Beal, M.F. and Schon, E.A. (2002). Mitochondrial DNA and respiratory chain function in spinal cords of ALS patients. *Journal of Neurochemistry*, 80(4), pp616-625

Wijesekera, L.C. and Leigh, P.N. (2009). Amyotrophic lateral sclerosis. *Orphanet Journal of Rare Diseases*, 4(3), pp1-22

Witcher, M.R., Park, Y.D., Lee, M.R., Sharma, S., Harris, K.M. and Kirov, S.A. (2010). Three-Dimensional Relationships Between Perisynaptic Astroglia and Human Hippocampal Synapses. *Glia*, 58(5), pp572-587

Witts, E.C., Panetta, K.M. and Miles, G.B. (2011). Glial-derived adenosine modulates spinal motor networks in mice. *Journal of Neurophysiology*, 107(7), pp1925-1934

Wootz, H., FitzSimons-Kantamneni, E., Larhammar, M., Rotterman, T.M., Enjin, A., Patra, K., Andrew, E., van Zundert, B., Kullander, K. and Alvarez, F.J. (2013). Alterations in the motor neuron-Renshaw cell circuity in the Sod1^{G93A} mouse model. *Journal of Comparative Neurology*, 30, pp311-328

Xing, L., Yang, T., Cui, S. and Chen, G. (2019). Connexin Hemichannels in Astrocytes: Role in CNS Disorders. *Frontiers in Molecular Neuroscience*, 12, pp1-10

Yang, J., Cheng, X., Shen, J., Xie, B., Zhao, X., Zhang, Z., Cao, Q., Shen, Y. and Qiu, M. (2016). A Novel Approach for Amplification and Purification of Mouse Oligodendrocyte Progenitor Cells. *Frontiers in Cellular Neuroscience*, 10, pp1-10

Yang, Y., Higashimori, H. and Morel, L. (2013). Developmental maturation of astrocytes and pathogenesis of neurodevelopmental disorders. *Journal of Neurodevelopmental Disorders*, 5(1), pp1-8

Yeo, L., Lynch, C. and Hardiman, O. (2010). Validating population-based registers for ALS: how accurate is death certification? *Journal of Neurology*, 257(8), pp1235-1239

Yoshida, Y., Une, F., Utatsu, Y., Nomoto, M., Furukawa, Y., Maruyama, Y., Machigashira, N., Matsuzaki, T. and Osame, M. (1999). Adenosine and Neopterin Levels in Cerebrospinal Fluid of Patients with Neurological Disorders. *Internal Medicine*, 38(2), pp133-139

Young, J.J., Lavakumar, M., Tampi, D., Balachandran, S., Tampi, R.R. (2018). Frontotemporal dementia: latest evidence and clinical implications. *Therapeutic Advances in Psychopharmacology*, 8(1), pp33-48

Yunusova, Y., Plowman, E.K., Green, J.R., Barnett, C. and Bede, P. (2019). Clinical Measures of Bulbar Dysfunction in ALS. *Frontiers in Neurology*, 10(106), pp1-11

Zhang, Y.J., Jansen-West, K., Xu, Y.F., Gendron, T.F., Bieniek, K.F., Lin, W.L., Sasaguri, H., Caulfield, T., Hubbard, J., Daughrity, L., Chew, J., Belzil, V.V., Prudencio, M., Stankowski, J.N., Castanedes-Casey, M., Whitelaw, E., Ash, P.E.A., DeTure, M., Rademakers, R., Boylan, K.B., Dickson, D.W. and Petrucelli, L. (2014). Aggregation-prone c9FTD/ALS poly(GA) RAN-translated proteins cause neurotoxicity by inducing ER stress. *Acta Neuropathologica*, 128(4), pp505-524

Zhang, D.W., Lopes, E.C. and Cheema, S.S. (2005). Loss of Synaptophysin-Positive Boutons on Lumbar Motor Neurons Innervating the Medial Gastrocnemius Muscle of the SOD1$^{G93A\ G1H}$ Transgenic Mouse Model of ALS. *Journal of Neuroscience Research* 79(5), pp694-699

Zhang, H., Wu, Z.Y., Wang, W. and Harrington, M.A. (2011). Interneuronal synapses formed by motor neurons appear to be glutamatergic. *Neuroreport*, 22(16), pp809-813

Zhao, C., Devlin, A.C., Chouhan, A.K., Selvaraj, B.T., Stavrou, M., Burr, K., Brivio, V., He, X., Mehta, A.R., Story, D., Shaw, C.E., Dando, O., Hardingham, G.E., Miles, G.B. and Chandran, S. (2020). Mutant C9orf72 human iPSC-derived astrocytes cause non-cell autonomous motor neuron pathophysiology. *Glia*, 68(5), pp1046-1064

Zhu, F., Cizeron, M., Qiu, Z., Benavides-Piccione, R., Kpanitsa, M.V., Skene, N.G., Koniaris, B.DeFelope, J., Fransén, E., Komiyama, N.H. and Grant, S.G.N. (2018). Architecture of the Mouse Brain Synaptome. *Neuron*, 99(4), pp781-799

Zhu, Y.B. and Sheng, Z.H. (2011). Increased Axonal Mitochondrial Mobility Does Not Slow Amyotrophic Lateral Sclerosis (ALS)-like Disease in Mutant SOD1 Mice. *The Journal of Biological Chemistry*, 286(26), pp23432-23440

Zuber, B., Nikonenko, I., Klauser, P., Muller, D. and Dubochet, J. (2005). The mammalian central nervous synaptic cleft contain a high density of periodically organized complexes. *PNAS*, 102(52), pp19192-19197